

M0016997TP

Experimental and Modelling Studies of Electronic Packaging Interconnections formed with Lead-free Materials

Md. Jahir Rizvi

Centre for Numerical Modelling and Process Analysis

School of Computing and Mathematical Sciences

University of Greenwich

London, UK



A thesis submitted in partial fulfilment of the requirements of the University of
Greenwich for the Degree of Doctor of Philosophy

November 2007

Abstract

Both the experimental and the modelling techniques have been investigated and used to investigate factors that influence the formation, quality and reliability of electronic packaging interconnections formed using solder alloys and anisotropic conductive films (ACFs).

The wetting behaviours of new lead-free solders (i.e. Sn-2.8Ag-0.5Cu-1.0Bi and Sn-0.7Cu-0.3Ni) have been evaluated using the wetting balance test. This assessment has been performed for three soldering temperatures with three different types of fluxes. The results have been compared with the conventional Sn-Pb, Sn-Ag-Cu and Sn-Cu solders. It has been found that the wettability of the lead-free solders is not as good as that of the Sn-Pb solder. The additions of Bi into the Sn-Ag-Cu solder and Ni into the Sn-Cu solder improve the wettability that is strongly dependent on the type of the flux and the soldering temperature. In general, NC-flux is suitable for Cu-substrate whereas WS-flux is suitable for Ni substrate, but for the Sn-2.8Ag-0.5Cu solder on Ni substrate, good wettability has been observed with both the NC and the R-type fluxes. Computational modelling of this test has revealed that the increase in the depth and the radius of the solder bath has little effect on the wetting force, but the meniscus height decreases when the bath radius exceeds 14 mm.

Dissolution of solid metals into liquid solders has been investigated through experiments and computer modelling. Microstructural studies have been carried out and the growth behaviours of the intermetallic compounds (IMCs) during wetting, solidification and isothermal ageing have been investigated. It has been found that the addition of Bi into the Sn-Ag-Cu solder reduces the consumptions of the substrates and suppresses the growth of IMCs during wetting and ageing. Similarly, the addition of Ni into the Sn-Cu solder reduces both the consumptions of the substrates and the

growth of IMCs during wetting and short term ageing but enhances the growth of IMCs during long term ageing.

Experimental and computer modelling techniques have been used to measure the temperature in the ACF during bonding. The temperature in an ACF joint becomes very close to the required maximum bonding temperature within the first 1 s of bonding time. The impact of this temperature on the cure process and on the ACF physical properties such as loss modulus, storage modulus, and glass transition temperature has been investigated. It has been found that the higher the bonding temperature the more the curing degree of ACF is. Rapid changes occur in the physical properties of ACF at temperatures above the glass transition point. When the ACF is cured for a long time at a high temperature, the physical properties may degrade. The adhesion strength of ACF joint increases as the curing degree increases. However, when the ACF joint undergoes a thermal aging treatment, the adhesion strength increases for the samples bonded at lower temperatures, but decreases for the samples bonded at higher temperatures. The rate of increase in the contact resistance is dramatically higher for the samples bonded at lower temperatures than for those bonded at higher temperatures. Computer modelling of the isothermal ageing of ACF joint confirms that the thermal load causes the expansion of the adhesive matrix and generates high stresses on the conductive particle. This may result in the permanent damage of the outermost conductive metallic layers as well as electrical failure.

The effect of external bending loads on the electrical reliability of ACF-based interconnection has also been studied through computer modelling. The analysis reveals that ACF thickness increases at the corners of the chip-ACF joint more than that of the middle position. This causes a gap between the chip and the substrate results in the failure of the electrical interconnections.

Acknowledgements

I would like to thank my supervisor Prof. Chris Bailey who has given me the opportunity to pursue this PhD study. His enthusiasm of this PhD work and his support has helped me through my studies. Thanks are also given to my other supervisor Dr. Hua Lu who was always very helpful. His patience, expertise and valuable guidance have greatly helped me overcome many of the technical obstacles faced during my research.

I am grateful to my parents and my younger brothers who always pray for my success.

A special thank you is also given to my beloved wife who has sacrificed her desires and demands for my research work and who has encouraged me whenever I felt frustrated with my work.

I do express my thanks to my adorable son who has always missed his dad due to this PhD work.

Many thanks also go to Prof. Y.C. Chan (City University of Hong Kong) who guided my early career as a researcher, introduced me to the University of Greenwich, and has continued to provide valuable guidance and support during my time in the UK.

I also acknowledge the EPA Centre of City University of Hong Kong for providing support to enable me to undertake my experimental work. I also extend my thanks to ASM Assembly Automation (Hong Kong) Ltd for supporting part of this PhD work.

Nomenclature

AA	Area Array
ACA	Anisotropic Conductive Adhesive
ACF	Anisotropic Conductive Film
Ag	Silver
Al	Aluminum
BGA	Ball Grid Array
Bi	Bismuth
C	Instantaneous concentration of the diffusing substance
CC	Chip Carrier
Cd	Cadmium
Cr ⁶⁺	Hexavalent Chromium
c_s	Saturation concentration of the diffusing substance
CSP	Chip Scale Package
CTE	Coefficients of Thermal Expansion
Cu	Copper
C_0	Initial concentration of the diffusing substance
C_l	Constant concentration of the diffusing substance
$C(x)$	Concentration distribution of the diffusing substance
D	Diffusion coefficient
DIP	Dual-in-line Package
DMA	Dynamic Mechanical Analyzer
DSC	Differential Scanning Calorimeter
EC	European Commission
ECA	Electrically Conductive Adhesive
EDX	Energy Dispersive X-ray spectrometer
erf	Error Function
$erfc$	Complement of Error Function
EU	European Union
F	Rate of transfer per unit area of the interfacial section
FC	Flip Chip
F_w	Wetting force
g	Acceleration due to the gravity

Hg	Mercury
ICA	Isotropically Conductive Adhesive
IC	Integrated Circuits
IMCs	Intermetallic Compounds
In	Indium
I/O	Input/Output
ISP	Integral Substrate Package
J	Joule
k	IMC growth rate constant
K	Kelvin
kg	Killogram
M_t	total mass loss of diffusing substance
mm	Mili-meter
min	Minute
μm	Micro-meter
mN	Milli-Newton
μN	Micro-Newton
n	Time exponent
N	Newton
NC	No-Clean
NCA	Non Conductive Adhesive
Ni	Nickel
P	Perimeter of the submerged substrate
Pb	Lead
PBB	Polybrominated Biphenyl
PBDE	Polybrominated Diphenyl Ether
PCB	Printed Circuit Board
QFP	Quad Flat Package
Q_r	Total exothermic heat of the uncured ACF
Q_R	Residual heat of the cured ACF sample
R	Non-activated
RoHS	Restriction of certain Hazardous Substances
s	Second
s	Surface area
Sb	Antimony
SEM	Scanning Electron Microscope
SMT	Surface Mount Technology
Sn	Tin
SOP	Small-out-line Package
t	Time
THT	Through-Hole Technology
T_g	Glass transition temperature
V, v	Volume
W	Watt
WLP	Wafer Level Package

WS	Water Soluble
wt%	Weight percentage
x	Space coordinate measured normal to the interfacial section
Y	Thickness of the IMC layer at time t
Y_0	Initial thickness of the IMC layer
Zn	Zinc
γ_{LF}	Surface energy of the liquid solder/flux
γ_{SF}	Surface energy of the substrate/flux
γ_{SL}	Surface energy of the substrate/liquid solder interfacial area
θ_c	Contact angle
Δh	Dissolved thickness
α	Degree of curing
ρ	Density

Contents

Nomenclature.....vi

List of Figures.....xv

List of Tables.....xxiv

Chapter 1: Introduction

1.1 Electronic Packaging..... 1

 1.1.1 The Definition 2

 1.1.2 The Functions..... 3

 1.1.3 The Applications 3

1.2 A History of Electronic Packaging Technology..... 4

1.3 Descriptions of Some Electronic Packages..... 4

 1.3.1 Area Array (AA) Package 5

 1.3.2 Ball Grid Array (BGA) Package 5

 1.3.3 Wafer Level Package (WLP) 7

 1.3.4 Flip Chip (FC) Package..... 7

1.4 Interconnect Methods for Electronic Packages..... 9

 1.4.1 Soldering Method..... 9

 1.4.2 Non-Soldering Method..... 10

1.5 Interconnect Materials for Electronic Packages 11

 1.5.1 Soldering Materials 11

 1.5.2 Non-soldering Materials..... 11

1.6	Pb-based Interconnect Materials.....	11
1.6.1	Pb-based Materials-The Issues.....	12
1.6.2	Pb-based Materials-The Legislations.....	14
1.7	Pb-free Interconnect Materials for Electronic Packages.....	15
1.7.1	Pb-free Materials – The Real Definitions.....	15
1.7.2	Pb-free Materials – The Problems.....	15
1.8	Motivation for this PhD Work.....	17
1.9	Outlines of this PhD Work.....	18
1.10	Originality and Novelty of this PhD Work.....	18
1.11	Industrial Benefits from this PhD Work.....	19
1.12	Publications Resulted from this PhD Work.....	20

Chapter 2: Review of Electronic Packaging Interconnections

2.1	Review of Solder Interconnections.....	22
2.1.1	Solder Materials.....	22
2.1.2	General Criteria to Select a Solder Alloy.....	23
2.1.3	Alloys as Green Solders.....	23
2.1.4	Soldering Methods.....	24
2.1.4.1	Reflow Soldering.....	24
2.1.4.2	Wave Soldering.....	26
2.1.5	Issues associated with Soldering.....	28
2.1.5.1	Solderability and Wettability.....	28
2.1.5.2	Wetting, Non-wetting and Dewetting.....	28
2.1.5.3	Intermetallic Compounds (IMCs).....	29
2.1.5.4	Circuit Board Surface Finish.....	30
2.1.5.5	Voids in Solder Joints.....	32
2.2	Review of Adhesive Interconnections.....	33
2.2.1	Adhesive Materials.....	33
2.2.2	Types of Adhesives.....	34
2.2.2.1	Isotropic Conductive Adhesives (ICAs).....	34
2.2.2.2	Anisotropic Conductive Adhesives (ACAs).....	35

2.2.2.3	Non-Conductive Adhesives (NCAs).....	36
2.2.3	Applications of Adhesives	37
2.2.4	Bonding with Adhesives	38
2.2.5	Curing of Adhesives.....	39
2.3	Closure.....	40

Chapter 3: Review of Computer Modelling of Electronic Packaging

Interconnections

3.1	Introduction	41
3.2	Techniques of Computer Modelling	42
3.3	Tools of Computer Modelling	43
3.4	Computer Modelling for Electronic Packaging Interconnections.....	44
3.4.1	Computer Modelling of Solder-based Interconnections	44
3.4.2	Computer Modelling for Adhesive-based Interconnections	48
3.5	Closure.....	50

Chapter 4: Study of Interconnections formed with Lead-free Solder

Alloys

4.1	The Background and the Objectives of this Work.....	51
4.2	Experimental Procedures	56
4.2.1	The Measurement of Contact Angle and Wetting Force.....	56
4.2.2	Substrate Preparation.....	59
4.2.3	Solders and Fluxes	59
4.2.4	Analysis of Microstructures	59
4.2.5	Dissolution of Substrates into Solder during Wetting.....	60
4.2.6	The Growth of IMC Layer during Isothermal Aging.....	60
4.3	Computer Modelling Procedures.....	60
4.3.1	Wetting Balance Tests.....	60
4.3.2	Dissolution of Substrates into Molten Solders during Wetting Balance Tests	61

4.4	Results and Discussions	63
4.4.1	Wetting Behaviours of Pb and Pb-free Solders on Cu and Ni Substrates	63
4.4.1.1	Wetting Behaviours of Sn-2.8Ag-0.5Cu-1.0Bi Lead-free Solder and Sn-37Pb Solder on Cu and Ni Substrates	63
4.4.1.2	Wetting Behaviours of Sn-2.8Ag-0.5Cu and Sn-2.8Ag-0.5Cu-1.0Bi Solders on Cu and Ni Substrates.....	68
4.4.1.3	Wetting Behaviours of Sn-0.7Cu and Sn-0.7Cu-0.3Ni Solders on Cu and Ni Substrates	77
4.4.1.4	Discussions.....	82
4.4.2	Reactions of Cu and Ni Substrates with Solders during the Wetting Balance Tests.....	84
4.4.2.1	Dissolution of Substrates into Molten Solders.....	84
4.4.2.1.1	Dissolution of Cu and Ni Substrates into Sn-37Pb Solder.....	86
4.4.2.1.2	Dissolution of Cu and Ni Substrates into Sn-2.8Ag-0.5Cu and Sn-2.8Ag-0.5Cu-1.0Bi Solders.....	87
4.4.2.1.3	Dissolution of Cu and Ni Substrates into Sn-0.7Cu and Sn-0.7Cu-0.3Ni Solders.....	89
4.4.2.2	IMC formations of Sn-Pb and Pb-free Solders on Cu and Ni Substrates during Wetting.....	91
4.4.2.2.1	IMC formations of Sn-37Pb Solder on Cu and Ni Substrates.....	91
4.4.2.2.2	IMC formations of Sn-2.8Ag-0.5Cu and Sn-2.8Ag-0.5Cu-1.0Bi Solders on Cu and Ni Substrates	93
4.4.2.2.3	IMC formations of Sn-0.7Cu and Sn-0.7Cu-0.3Ni Solders on Cu and Ni Substrates.....	98
4.4.2.3	Modelling the Dissolution of Cu Substrate into Sn-37Pb and Sn-0.7Cu Solders during the Wetting Balance Tests	104
4.4.2.3.1	Mathematics of Diffusion.....	104
4.4.2.3.2	Calculation of Diffusion Coefficients from the Data obtained from the Wetting Balance Tests.....	107
4.4.2.3.3	Modelling Results and Discussions	108

4.4.3	Growth Behaviours of IMC Layers on Cu-Substrate during Isothermal Aging of Pb-free Solders.....	112
4.4.3.1	IMC Layer formations in Sn-2.8Ag-0.5Cu and Sn-2.8Ag-0.5Cu-1.0Bi Solders.....	112
4.4.3.2	IMC Layer formations in Sn-0.7Cu and Sn-0.7Cu-0.3Ni Solders	120
4.5	Closure.....	126

Chapter 5: Study of Interconnections formed with Anisotropic Conductive Films

5.1	The Background and the Objectives of this Work.....	128
5.2	Experimental Procedures	132
5.2.1	Materials Selection.....	132
5.2.1.1	The chip.....	132
5.2.1.2	Flexible Substrate.....	133
5.2.1.3	Glass Substrate	133
5.2.1.4	FR-4 Substrate.....	134
5.2.1.5	Anisotropic Conductive Films (ACFs)	134
5.2.2	Bonding Process.....	135
5.2.3	Experimental Setup	137
5.2.3.1	Bonding Temperature Measurement in the ACF	137
5.2.3.2	Dynamic Mechanical Analysis (DMA) of ACF	138
5.2.3.3	Differential Scanning Calorimeter (DSC) tests of ACF	138
5.2.3.4	Adhesion Strength Measurement	139
5.2.3.5	Thermal Ageing Tests of ACF Joints.....	140
5.2.3.6	Contact Resistance Measurement.....	140
5.2.3.7	3-point Bending Tests of ACF Joints.....	141
5.2.3.8	Failure Analysis.....	142
5.3	Computer Modelling Procedures.....	142
5.3.1	Bonding Temperature Measurement in the ACF	142
5.3.2	Thermal Ageing Tests of ACF Joints.....	144
5.3.3	3-point Bending Tests of ACF Joints.....	145

5.4	Results and Discussions	149
5.4.1	Measurement of Temperature in the ACF during Bonding	149
5.4.2	The Effect of Bonding Temperature and Time on the Physical Properties of the ACF	151
5.4.3	The Effect of Temperatures on the Curing of ACF	159
5.4.4	The Effect of Curing on the Performance of ACF Joints after Thermal Ageing	161
5.4.4.1	Adhesion Strength of the ACF Joints after Thermal Ageing	161
5.4.4.2	Contact Resistance of ACF Joints after Thermal Ageing	163
5.4.5	The Effect of Ageing Temperature on the Contact Resistance of ACF Joints with Various Curing Degrees	169
5.4.6	Modelling the Effect of Isothermal Ageing on ACF Joints Delamination	173
5.4.7	The Effect of Mechanical Loading on the Performance of ACF Joint during 3-point Bending	177
5.5	Closure.....	183

Chapter 6: Results Summary and Future Work

6.1	Results Summary.....	185
6.1.1	Study of Interconnections formed with Lead-free Solder Alloys	187
6.1.2	Study of Interconnections formed with Anisotropic Conductive Films .	190
6.2	Future work	193
6.2.1	The Effects of Bonding/Soldering Time	193
6.2.2	The Effects of the Surface Roughness	193
6.2.3	Prediction of the Fatigue Life of ACF/Solder Joints under Thermal Loads .	194
6.2.4	Numerical Modelling of the Growth Kinetics of IMC Layers.....	194

List of Figures

		<i>Page</i>
Figure 1-1	Schematic of electronic package	2
Figure 1-2	Pin Grid Array Packages.....	5
Figure 1-3	Plastic Ball Grid Array (PBGA) Package	6
Figure 1-4	Ceramic Ball Grid Array (CBGA) Package	6
Figure 1-5	Wafer Level Package (WLP).....	7
Figure 1-6	Flip Chip (FC) Packages.....	8
Figure 1-7	Flip Chip (FC) interconnection through conductive adhesive.....	10
Figure 1-8	Transmission of Pb to human being from electronic packaging interconnections.....	13
Figure 2-1	Flip chip solder joint: (a) before reflow, (b) after reflow.....	25
Figure 2-2	Wave soldering process. (Figure reproduced from the ref. [37])...	27
Figure 2-3	Wetting states: (a) wetting, (b) nonwetting and (c) dewetting.....	29
Figure 2-4	Void in solder.....	32
Figure 2-5	Schematic representation of an ICA joint.....	35
Figure 2-6	Schematic representation of (a) metal particle, (b) metal coated particle, (c) metal coated particle with insulation layer and (d) a complete ACA joint.....	36
Figure 2-7	Schematic representation of a NCA joint.....	37

Figure 2-8	Thermo-compression bonding of a flip chip on the circuit board with NCA: (a) before bonding, (b) after bonding.....	39
Figure 2-9	Time-temperature-transformation (TTT) diagram of adhesive materials during curing. (Figure reproduced from the reference [51]).....	40
Figure 3-1	The process flow chart for computer modelling.....	42
Figure 3-2	Schematic of the stencil printing used for computer analysis in [71].....	45
Figure 3-3	Wetting behaviour of a solder alloy.....	46
Figure 3-4	Schematic of the chip scale package assembly used in [76] to analyze the solidification process of solder.....	47
Figure 3-5	Temperature distribution (°C) in the adhesive-based flip chip assembly.....	48
Figure 3-6	Computer grids show the one-quarter of the conductive particle before and after bonding.....	49
Figure 3-7	Thermo-mechanical analysis of ACF-based flip chip assembly; (a) computer model of the package and (b) stress distribution in the package.....	49
Figure 4-1	The test configuration for the wetting balance technique and modelling.....	57
Figure 4-2	A typical force-time curve for the wetting balance test.....	58
Figure 4-3	The solution of the computer model showing the meniscus height at the solder-substrate interface due to the surface tension.....	61
Figure 4-4	Computer mesh used in the analysis of dissolution of Cu into solder during wetting balance tests.....	62
Figure 4-5	Wetting forces as a function of solder bath temperatures for Cu-substrate with (a) NC- flux (b) R-type flux and (c) WS-flux.....	64
Figure 4-6	Wetting forces as a function of solder bath temperatures for Ni-substrate with (a) NC- flux (b) R-type flux and (c) WS-flux.....	65
Figure 4-7	Dependency of estimated wetting force and meniscus height on the substrate perimeter with SnAgCuBi-solder.....	67

Figure 4-8	Effect of immersion depth on the estimated wetting force for SnAgCuBi solder	67
Figure 4-9	Force-time curve for (a) Cu and (b) Ni substrates with NC-flux. Immersion depth = 3 mm, immersion speed = 21mm/sec, immersion time = 10 s and solder bath temperature = 255 °C.....	69
Figure 4-10	Contact angle-time curve for (a) Cu and (b) Ni substrates with NC-flux. Immersion depth = 3 mm, immersion speed = 21mm/sec, immersion time = 10 s and solder bath temperature = 255 °C.....	70
Figure 4-11	Modelling results showing the conditions of (a) wetting (contact angle = 10°) and (b) non-wetting (contact angle = 120°).....	71
Figure 4-12	Contact angles as a function of solder bath temperatures for Cu-substrate with (a) NC-flux, (b) R-flux and (c) WS-flux.....	72
Figure 4-13	Contact angles as a function of solder bath temperatures for Ni-substrate with (a) NC-flux, (b) R-flux and (c) WS-flux.....	73
Figure 4-14	Wetting force and meniscus height versus contact angle.	76
Figure 4-15	Modelling results showing meniscus heights with contact angles (a) 0°, (b) 20°, (c) 40°, (d) 60°, (e) 80° and (f) 120°.....	76
Figure 4-16	Wetting force and meniscus height versus solder bath radius.....	77
Figure 4-17	Wetting forces as a function of solder bath temperatures for Cu-substrate with (a) NC-flux, (b) R-flux and (c) WS-flux.....	79
Figure 4-18	Wetting forces as a function of solder bath temperatures for Ni-substrate with (a) NC-flux, (b) R-flux and (c) WS-flux.....	80
Figure 4-19	Comparative contact angle formations on Cu-substrate.....	81
Figure 4-20	Comparative contact angle formations on Ni-substrate.....	81
Figure 4-21	Single side dissolutions of Cu and Ni substrates into molten Sn-Pb solder during the wetting balance test with NC-flux.....	86
Figure 4-22	Single side dissolution of (a) Cu and (b) Ni substrates into molten SnAgCu and SnAgCuBi solders during the wetting balance test with NC-flux.....	88
Figure 4-23	Single side dissolution of (a) Cu and (b) Ni substrates into molten	

	SnCu and SnCuNi solders during the wetting balance test with NC-flux.....	90
Figure 4-24	SEM images showing the wetting reactions at 255 °C between: (a) Sn-Pb and Cu, (b) Sn-Pb and Ni.....	92
Figure 4-25	Solder-Cu interfaces after dipping into (i) SnAgCu, (ii) SnAgCuBi solders at a) 255 °C, b) 275 °C and c) 295 °C.....	94
Figure 4-26	Solder-Ni interfaces after dipping into (i) SnAgCu, (ii) SnAgCuBi solders at a) 255 °C, b) 275 °C and c) 295 °C.....	95
Figure 4-27	Formation of IMCs after dipping (i) Cu and (ii) Ni-substrates into the molten Sn-Ag-Cu-Bi solder bath. Bath temperatures: (a) 255 °C, (b) 275 °C and (c) 295 °C.....	96
Figure 4-28	Formation of IMCs after dipping (i) Cu and (ii) Ni-substrates into the molten Sn-Ag-Cu solder bath. Bath temperatures: (a) 255 °C, (b) 275 °C and (c) 295 °C.....	97
Figure 4-29	Solder-Cu interfaces after dipping into (i) Sn-Cu, (ii) Sn-Cu-Ni solders at a) 255 °C, b) 275 °C and c) 295 °C.....	99
Figure 4-30	Formation of IMCs after dipping Cu-substrate into the molten (i) Sn-Cu, (ii) Sn-Cu-Ni solders bath. Bath temperatures: (a) 255 °C, (b) 275 °C and (c) 295 °C.....	100
Figure 4-31	Solder-Ni interfaces after dipping into (i) Sn-Cu, (ii) Sn-Cu-Ni solders at a) 255 °C, b) 275 °C and c) 295 °C.....	101
Figure 4-32	Formation of IMCs after dipping Ni-substrate into the molten (i) Sn-Cu, (ii) Sn-Cu-Ni solder baths. Bath temperatures: (a) 255 °C, (b) 275 °C and (c) 295 °C.....	102
Figure 4-33	Diffusion path of the Cu atoms into liquid solder. C_o is the initial concentration of the diffusing substance in the solder; C_l is the constant concentration at the solder-Cu interface and $C(x)$ is the concentration distribution of Cu in the solder.....	105
Figure 4-34	Cu-Sn phase diagram.....	108
Figure 4-35	Dissolution of Cu substrate after 10 s of reaction with (a) Sn-37Pb and (b) Sn-0.7Cu solders (colour bars represent Cu concentrations in wt%).....	109
Figure 4-36	Concentration of Cu over reaction time (near interface).....	110

Figure 4-37	Concentration of Cu over reaction time (in the bulk of solders).....	110
Figure 4-38	Cu concentration at various distances from the solder-Cu interface towards the bulk of the solder.....	111
Figure 4-39	SEM images showing the solder-Cu interfaces after 2 days of aging for a) Sn-2.8Ag-0.5Cu and b) Sn-2.8Ag-0.5Cu-1.0Bi solders.....	113
Figure 4-40	SEM images showing the solder-Cu interfaces after 6 days of aging for a) Sn-2.8Ag-0.5Cu and b) Sn-2.8Ag-0.5Cu-1.0Bi solders.....	114
Figure 4-41	SEM images showing the solder-Cu interfaces after 14 days of aging for a) Sn-2.8Ag-0.5Cu and b) Sn-2.8Ag-0.5Cu-1.0Bi solders.....	114
Figure 4-42	Thickness of IMC layer as a function of square root of the aging time.....	116
Figure 4-43	Cu-consumptions in solders as functions of the aging time.....	118
Figure 4-44	Formation of IMCs in the bulk of a) Sn-2.8Ag-0.5Cu and b) Sn-2.8Ag-0.5Cu-1.0Bi solders after aging at 150 °C for i) 2 days, ii) 6 days iii) 10 days and iv) 14 days.....	119
Figure 4-45	Growth of IMC layer after 2 days of aging. (a) Sn-0.7Cu solder and (b) Sn-0.7Cu-0.3Ni solder.....	120
Figure 4-46	Growth of IMC layer after 6 days of aging. (a) Sn-0.7Cu solder and (b) Sn-0.7Cu-0.3Ni solder.....	121
Figure 4-47	Growth of IMC layer after 10 days of aging. (a) Sn-0.7Cu solder and (b) Sn-0.7Cu-0.3Ni solder.....	122
Figure 4-48	Growth of IMC layer after 14 days of aging. (a) Sn-0.7Cu solder and (b) Sn-0.7Cu-0.3Ni solder.....	123
Figure 4-49	IMC formations in the bulk of (a) Sn-0.7Cu and (b) Sn-0.7Cu-0.3Ni solders with Cu substrate during aging for (i) 2 days, (ii) 6 days, (iii) 10 days and (iv) 14 days.....	124
Figure 4-50	Average IMC layer thickness versus square root of aging time.....	125
Figure 5-1	A typical flip chip joint with anisotropic conductive film.....	130

Figure 5-2	Schematic of a flip chip with daisy-chained bump groups.....	133
Figure 5-3	Cross-sectional view of ACF of the type A.....	134
Figure 5-4	Cross-sectional view of ACF of the type B.....	135
Figure 5-5	Schematic of the ACF flip chip bonding process; (a) placement of ACF on the substrate, (b) pre-bonding, (c) alignment between chip and substrate, (d) final bonding.....	136
Figure 5-6	Typical flip chip joints through anisotropic conductive films with (a) Au-bump flip chip, (b) bumpless flip chip	136
Figure 5-7	Experimental setup to measure the real-time temperature in ACF; (a) Position of thermocouple on the stage; (b) Computer-controlled data logger setup to grab the temperature in fractions of seconds...	137
Figure 5-8	A schematic diagram of the shear test.....	139
Figure 5-9	Typical flip chip assembly with ACF.....	140
Figure 5-10	Circuitry of contact resistance measurement using four-point probe method.....	140
Figure 5-11	Experimental setup of 3-point bending tests.....	141
Figure 5-12	Computer model to simulate the heat transfer during bonding of chip-on-glass assembly.....	143
Figure 5-13	(a) A slice model of chip-on-flex assembly with ACF; (b) close view of ACF joint.....	144
Figure 5-14	General configuration of the chip on board assembly (top view-chip side).....	146
Figure 5-15	SEM photograph of undeformed (inset) and deformed ACF particle.....	147
Figure 5-16	A schematic model of 3-point bending.....	148
Figure 5-17	The temperature in the ACF. The bonding time is 10 s, the bonding temperature is 170 °C and the bonding pressure is 80 N....	149
Figure 5-18	The temperature in the ACF. The bonding time is 10 s, the bonding temperature is 190 °C and the bonding pressure is 80 N....	150

Figure 5-19	The temperature in the ACF. The bonding time is 10 s, the bonding temperature is 210 °C and the bonding pressure is 80 N...	150
Figure 5-20	The loss modulus of the ACF samples cured at 170, 190 and 210 °C for 3 s.....	152
Figure 5-21	The loss modulus of the ACF samples cured at 170, 190 and 210 °C for 10 s.....	152
Figure 5-22	The appearance of (a) the uncured (raw) ACF and cured (b) at 170 °C, (c) at 190 °C and (d) at 210 °C. (Optical pictures, magnification = 20 X).....	154
Figure 5-23	The storage modulus of the ACF samples cured at 170, 190 and 210 °C for 3 s.....	155
Figure 5-24	The storage modulus of the ACF samples cured at 170, 190 and 210 °C for 10 s.....	155
Figure 5-25	The displacement of the ACF samples cured at 170, 190 and 210 °C for 3 s.....	156
Figure 5-26	The displacement of the ACF samples cured at 170, 190 and 210 °C for 10 s.....	156
Figure 5-27	The strain (%) of the ACF samples cured at various temperatures for 3 s.....	157
Figure 5-28	The strain (%) of the ACF samples cured at various temperatures for 10 s.....	158
Figure 5-29	DSC scans for ACFs cured at different bonding temperatures.....	160
Figure 5-30	Curing degree of ACF samples bonded at different temperatures...	160
Figure 5-31	Adhesion strength of the ACF assembly before and after thermal ageing.....	162
Figure 5-32	SEM image showing uncured regions of the ACF when bonded at 160 °C.....	162
Figure 5-33	Increase in contact resistance of samples which underwent thermal ageing.....	164
Figure 5-34	SEM images of ACF joints; (a) before thermal ageing and (b-f) after thermal ageing for the samples bonded at (b) 160 °C, (c) 180	

	°C, (d) 200 °C, (e) 220 °C and (f) 240 °C.....	165
Figure 5-35	Open joint occurred due to thermal ageing.....	166
Figure 5-36	SEM image showing deformations of the Au-bump and the conductive particles.....	167
Figure 5-37	ACF interconnection through conductive particles; (a) before thermal ageing, (b) after thermal ageing.....	168
Figure 5-38	Maximum recovery of the deformed particle after thermal ageing...	168
Figure 5-39	Increase in contact resistance of samples underwent ageing at 60 °C.....	169
Figure 5-40	Increase in contact resistance of samples underwent ageing at 100 °C.....	170
Figure 5-41	Increase in contact resistance of samples underwent ageing at 140 °C.....	170
Figure 5-42	Contact resistances after 10 hours of isothermal ageing.....	171
Figure 5-43	ACF joints aged at (a) 60 °C and (b) 100 °C.....	172
Figure 5-44	ACF joints aged at 140 °C.....	173
Figure 5-45	Computer modelling shows the ACF joints after isothermal ageing at 150 °C; (a) stress in x-direction; (b) stress in y-direction.....	174
Figure 5-46	Computer modelling shows the ACF joints after isothermal ageing at 150 °C for 10 hours; (a) resultant deformation with stress in x- direction and (b) resultant deformation with stress in y-direction...	175
Figure 5-47	Stresses along the particle-pad interface after 10 hours of aging at 150 °C.....	176
Figure 5-48	Shear stresses along the particle-pad interface at various aging temperatures.....	176
Figure 5-49	Front view of deformed flip chip assembly.....	177
Figure 5-50	Zoom view of deformed ACF (inner edge).....	178
Figure 5-51	Increase in ACF thickness at the corner position of ACF-chip joint.....	178

Figure 5-52	The possible three cases of ACF joint failure are shown in (a), (b) and (c).....	180
Figure 5-53	Deformed solder joint under mechanical loading.....	181
Figure 5-54	Deformed ACF joint under mechanical loading.....	181

List of Tables

	<i>Page</i>
Table 2-1: Advantages and limitations of various reflow methods.....	25
Table 4-1: Wettability evaluation based on the contact angles (θ_c).....	71
Table 4-2: Growth of IMC layer during soldering of SnAgCu and SnAgCuBi solders.....	93
Table 4-3: Growth of IMC layer during soldering of SnCu and SnCuNi solders.....	100
Table 5-1: Bonding parameters.....	135
Table 5-2: Dimensions and thermal properties used in the modeling.....	143
Table 5-3: Material properties used in the simulation.....	145
Table 5-4: Dimensions of the model geometry in mm.....	147
Table 5-5: Mechanical properties of materials used in modeling.....	148

Chapter 1

Introduction

1.1 Electronic Packaging

In recent years, electronic devices require more and more resistors, transistors or diodes on a single semiconductor chip or die. All those discrete circuit components are embedded in or on the chip and need to be connected to the printed circuit board. The establishment of the interconnections for all these tiny components can be achieved through various technologies. When the device is in operation, large amount of heat may be generated in the electric circuit and this heat has to be removed so that the device can perform its functions. Further more, semiconductor chips are fragile and require a coat of 'armour' to protect from mechanical, chemical and other environmental damage. Hence, the concept of "electronic packaging" has been introduced to describe the manufacturing process or the hardware that provide the electrical connections, the removal of excessive heat and the protection from environmental damage [1].

1.1.1 The Definition

According to Martin B. Miller (author of the Electronic Packaging, Microelectronics and Interconnection Dictionary), electronic packaging is the combination of engineering and manufacturing technologies required to convert an electronic circuit into a manufactured assembly where the engineering technologies include electrical, mechanical, thermal, chemical, materials, components and others [2].

Electronic packaging is a cost-effective and reliable science based engineering solution to the problems facing the electronics manufacturing industry. It establishes the interconnections ranging from zero level packages to first, second and third level packages [1]. Here, the zero level packages represent the chip-level connections such as the gold and solder bumps on the chip whereas the first level packages include single or multichip modules. The second and the third level packages consist of printed circuit boards (PCB) and motherboards respectively. These levels of electronics packaging are illustrated in Figure 1-1.

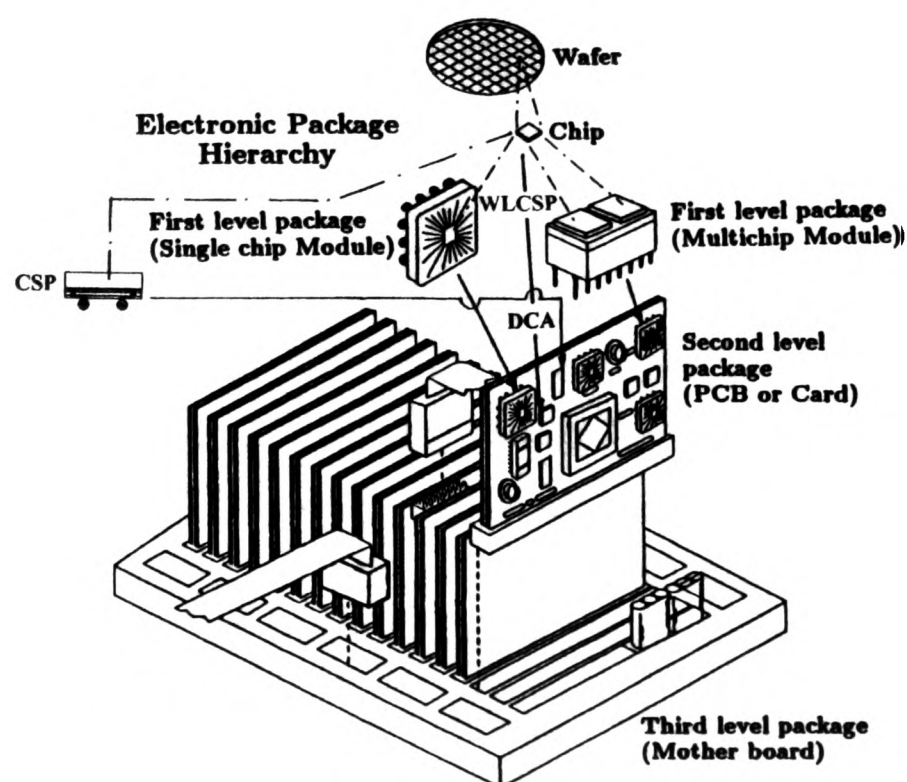


Figure 1-1: Schematic of electronic package [1].

1.1.2 The Functions

A typical electronic device consists of a few integrated circuits (IC), some discrete resistors, capacitors and other components. These components are mounted on a printed circuit board to provide suitable and effective environment for the electronic product. The main functions of the electronic packaging are [3][4]

- Distribution of signal lines leading to and from the ICs. Topological and electromagnetic considerations are the major issues for this function.
- Distribution of power lines to the circuits on the chip. This involves electromagnetic, structural and material issues.
- Dissipation of heats generated by the circuits. Materials and structural considerations are important.
- Provision of protection to the bare chip, the discrete components and the interconnections against mechanical, chemical and electromagnetic damage.

1.1.3 The Applications

The electronic packaging assemblies are broadly used in the following areas [3]:

- Computers and Business Equipment: Calculators, desktop computers, printers, notebooks, photocopiers, personal digital assistants, workstations, servers, high performance computers etc.
- Communications: Cellular phones, handsets, line cards, LAN cards and switches, pagers, modems, fax machines, routers, main switches etc.
- Automotive Electronics: Engine control and management systems, transmission controllers, cruise controllers, braking controllers, traction controllers, suspension controllers, steering controllers, lighting, wipers, air conditioning and heating systems, electronic dashboard and mirrors, safety, convenience and entertainment systems etc.

- Consumer Electronics: VCR, compact audio systems, music CD players, game systems and cartridges, watches, portable audio players, camcorders, smart cards, microwave ovens, TV sets etc.
- Industrial and Medical Systems: Test and measuring devices and instruments, calibrators, process control systems, motor controls, uninterruptible power systems, NC controls, vision systems, robotics, hearing aids, ECGs, implants medical imaging systems etc.
- Military Electronics: Mobile communications, fire control systems, missiles, avionics radar, satellite links land-based radar and communication systems etc.

1.2 A History of Electronic Packaging Technology

In order to achieve high I/O counts, more reliable and complex functional products, and miniaturized electronics products, various types of electronic packages have been developed over the last few decades. In the early 1960s, there were two types of packages namely the “simple plastic package” and the “metal package”. These packages suffered from standardization, costs and assembly difficulties. To overcome those difficulties “Flatpack” and “Dual-in-line Package (DIP)” were developed in the late 1960s. Then, over time the size of the packages has decreased and “Integral Substrate Package (ISP)”, “Chip Carrier (CC) Package”, “Small-out-line Package (SOP)”, “Quad Flat Package (QFP)”, “Area Array (AA) Package” etc. have been developed. Now the size of the packages has reduced even further but the functions have increased tremendously and the configurations of the packages have become more and more complex. The modern complex packages include the “Ball Grid Array (BGA) Package”, the “Chip Scale Package (CSP)”, the “Wafer Level Package (WLP)”, and the “Flip Chip (FC) Package” etc.

1.3 Descriptions of Some Electronic Packages

Before getting into the discussions about the electronic packaging interconnection technologies, the interconnection materials and other issues, it will be useful to get some

ideas about the configurations of some typical electronic packages. The following sections provide descriptions of several types of electronic packages, their advantages and the disadvantages.

1.3.1 Area Array (AA) Package

The Area Array package contains leads around the periphery and the bottom surface areas of the component. The AA packages that contain solder pads on the bottom surfaces are called the Lid Grid Array (LGA) package and that contain small solder columns are called the Column Grid Array (CGA) package. Another type of AA package that contain pins on the bottom surfaces are known as the Pin Grid Array (PGA) package. The main advantages of PGA and LGA packages are the varieties in the grid sizes and in the grid densities. These advantages help to fulfill the ICs input/output requirements. Insufficient direct visual inspectability and rework difficulties are the disadvantages of these packages [2][5]. Several types of PGA packages are shown in Figure 1-2.

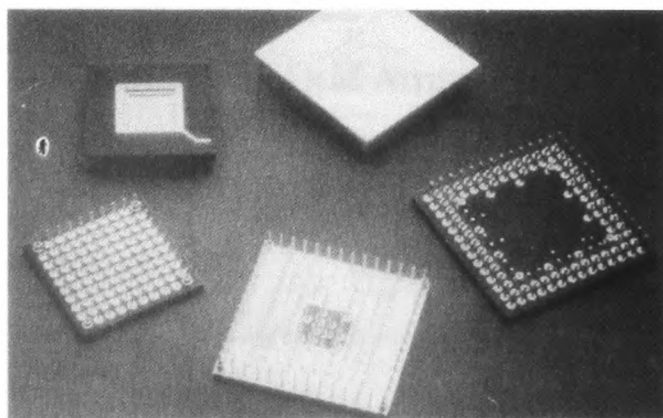


Figure 1-2: Pin Grid Array Packages [5].

1.3.2 Ball Grid Array (BGA) Package

BGA package is a low-cost, leadless package that can be soldered directly to the substrate. This type of package ensures high number of I/Os and offers maximum space efficiency in board with excellent thermal and electrical performance. The main disadvantage of this package is that it's not easy to inspect the solder joints as they are kept hidden [2]. Depending on the substrate type, BGA packages can be classified as

Chapter-1: Introduction

Plastic Ball Grid Array (PBGA), Ceramic Ball Grid Array (CBGA), Tape-automated bonding Ball Grid Array (TBGA), Metal Ball Grid Array (MBGA), Dimple Ball Grid Array (DBGGA) etc [6][7]. The schematics of a PBGA and a CBGA packages are shown in Figure 1-3 and 1-4 respectively. The differences between the two packages are clearly shown in these two figures.

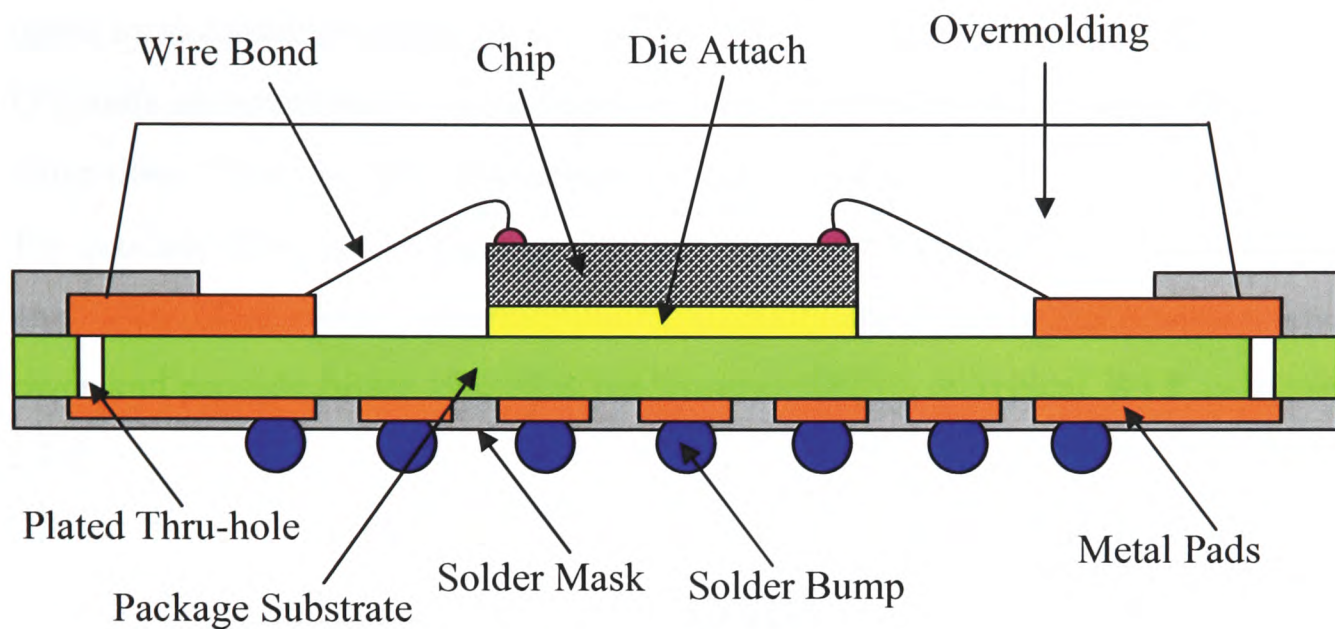


Figure 1-3: Plastic Ball Grid Array (PBGA) Package.

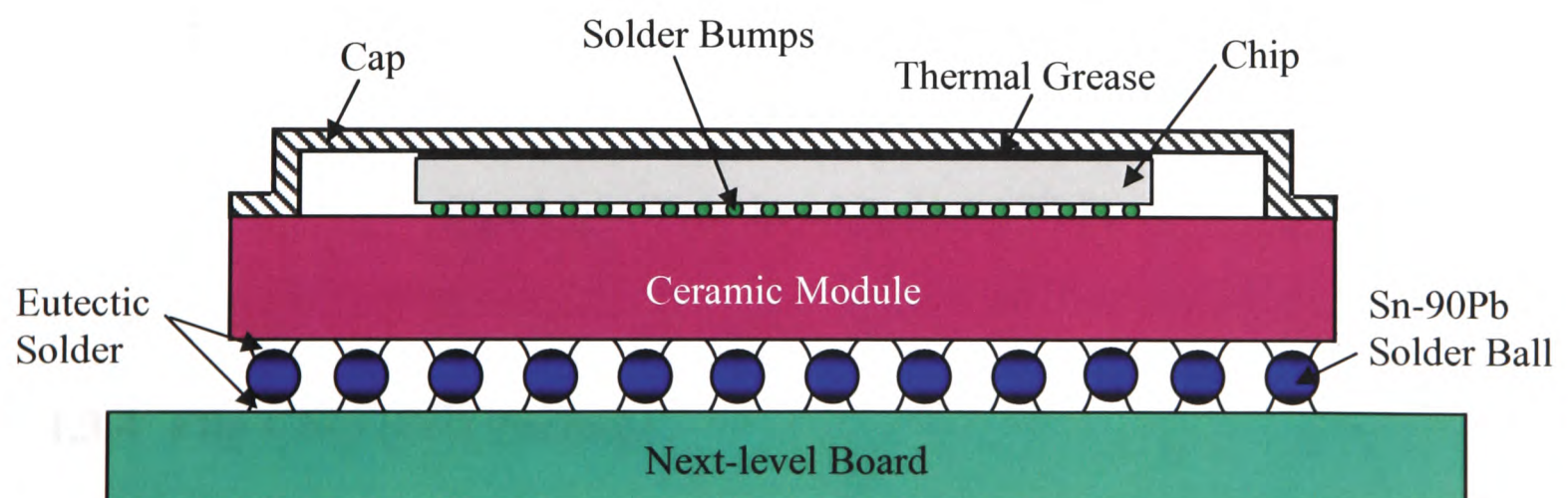


Figure 1-4: Ceramic Ball Grid Array (CBGA) Package.

1.3.3 Wafer Level Package (WLP)

Wafer Level Package (WLP) is an Integrated Circuit (IC) package and is completely fabricated on the wafer at the wafer level prior to the dicing, interconnection and test functions of the IC devices are carried out at the wafer level. WLPs are used in small and the reliable semiconductor packages such as cell phones and other portable devices where low I/O counts are required. Au-Sn solders are very suitable for the requirements of WLP interconnections. Due to the limitations in the Surface Mount Technology (SMT) assembly process, this type of package can not be used for high I/O counts. WLPs with their small sizes offer several advantages. They can maximize the use of boards, consume less power and provide better electrical performance [8][9]. A typical WLP is shown in Figure 1-5.

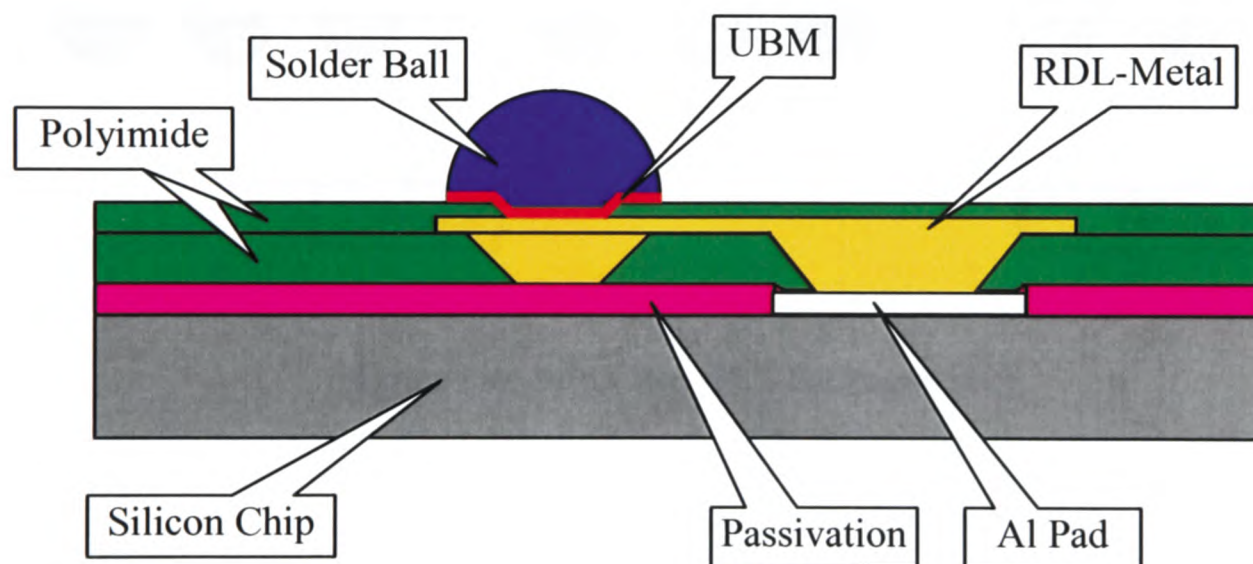


Figure 1-5: Wafer Level Package (WLP).

1.3.4 Flip Chip (FC) Package

In a Flip Chip (FC) package, the chip is directly mounted on the printed circuit board (PCB) through solder and/or non-solder materials. FC packages are also known as the

Chapter-1: Introduction

face bonding package or controlled-collapse chip connection package because the chip is flipped or faced down to make the interconnection. Several types of FC packages are shown in Figure 1-6.

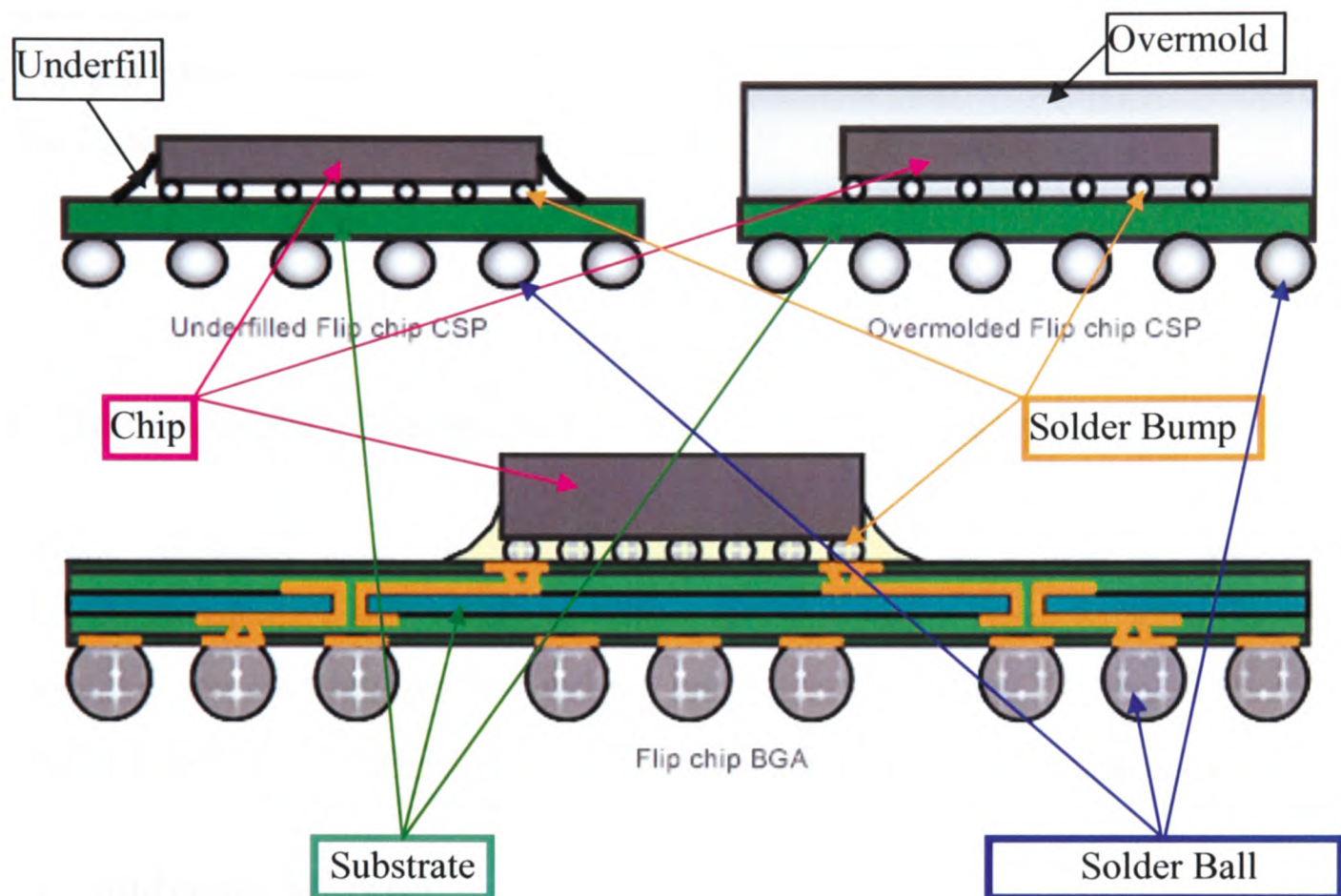


Figure 1-6: Flip Chip (FC) Packages [10].

In the early stages of the flip chip technology, small solder-coated copper balls were placed between the chip termination lands and the substrate pads. The package was then heated at an elevated temperature to form the interconnections. This process was difficult and was not cost-effective. At present, in order to avoid those problems, solid solder bumps are attached on the chip termination lands. The bumps of the chip are then aligned with the pad of the substrate prior to the heating at a temperature higher than the melting point of the solder bumps. During heating, solder bumps melt and form permanent chip-to-package interconnections. As the FC package doesn't need any wire bonding, it reduces the size, height and weight of the package. This package also increases the I/O

counts, provides fine pitch interconnections and delivers low inductance, capacitance and resistance. Moreover, this type of package generally doesn't contain any mould or encapsulant so that it can dissipate heats very efficiently from the back side of the chip. Despite of these advantages, FC packages have some disadvantages. For example, it is difficult to inspect the solder joints in the package and hard to rework. The availability of the bumped chips is limited and needs extra care to handle the bare chips. The package can be made reliable in the long term only when an underfill material is used in the gaps of the solder joints [2][7].

1.4 Interconnect Methods for Electronic Packages

Electronic packages must be interconnected to the circuit boards to realize the functionalities of electronic products. There are two major types of interconnection methods, i.e. the soldering method and the non-soldering method. Details of these two methods are described below.

1.4.1 Soldering Method

Soldering is a process that uses solder alloys to make permanent physical, metallurgical, and electrical connections of an electronic package to the PCB. Soldering is performed at a temperature above the melting point of a solder alloy so that the alloy can melt and wet the PCB surfaces (details will be discussed in Chapter 2). Both the surface-mount technology (SMT) and the through-hole technology (THT) generally use soldering technology because it offers a wide range of advantages such as (1) it requires low energy to provide a sustainable and reliable joint, (2) it is cost-effective, (3) the joints are easy to rework, (4) the joints can be formed at various melting temperatures by using a selection of solder alloys with different melting points. Figure 1-6 shows an FCP where soldering method has been used to join the chip to the substrate (circuit board).

1.4.2 Non-Soldering Method

Soldering method can only be used where two metals to be joined together. When substrates are made of non-solderable materials such as glass or plastic, adhesives are used to join the electronic packages to the substrates. Another reason of using adhesive is that it helps to miniaturize electronic products. Adhesively joined packages reduce the thickness and weight of a product. Adhesives are suitable for using in portable electronic devices like mobile phones, personal digital assistant (PDA), MP3 players, and notebook computers. Figure 1-7 shows an FC Package where conductive adhesive has been used to joint the chip to the substrate. The details of this interconnection method will be discussed in Chapter 2.

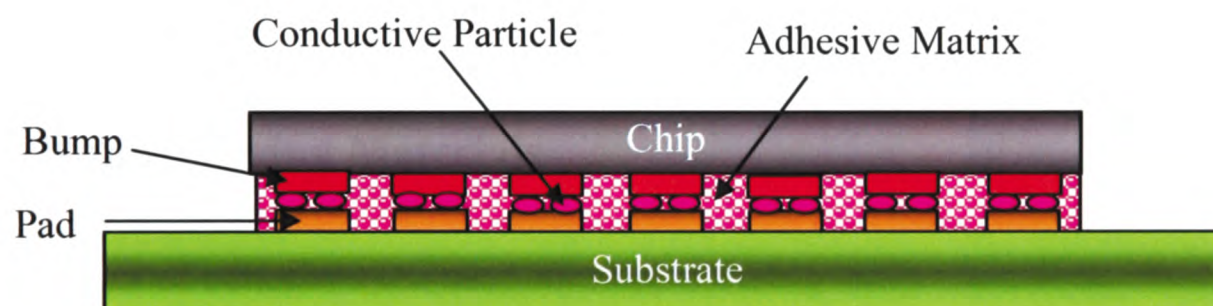


Figure 1-7: Flip Chip (FC) interconnection through conductive adhesive.

Non-soldering method offers several advantages over soldering method. Compared to the soldering, adhesive technology requires lower processing temperature. As adhesive is made from polymeric material, it reduces the possibility of stress cracking in the package interconnection. Furthermore, adhesive doesn't cause any chemical and metallurgical reaction; hence any unexpected reaction species can not be formed. In spite of these advantages, adhesives have a number of challenges. For example, oxidation and galvanic corrosion take place in the adhesive interconnections under high temperature and high humidity condition. As a result electrical conductivity drops.



1.5 Interconnect Materials for Electronic Packages

Based on the interconnection methods, the interconnect materials can be classified as (a) soldering materials and (b) non-soldering materials.

1.5.1 Soldering Materials

There are a range of solder alloys that are used for soldering interconnections. These solders are basically alloys of tin (Sn) and one or more of the following metallic elements [2]: lead (Pb), silver (Ag), bismuth (Bi), indium (In), antimony (Sb), cadmium (Cd), zinc (Zn), copper (Cu), nickel (Ni) etc. If a solder alloy's solidus and liquidus temperatures are identical it called a eutectic solder alloy, otherwise it is a non-eutectic solder alloy. Commercially available solder alloys are in solid form, paste form or powder form.

1.5.2 Non-soldering Materials

Several types of adhesives are used for non-soldering interconnections. These adhesives are classified as the anisotropic conductive adhesive (ACA), the isotropically conductive adhesive (ICA), the electrically conductive adhesive (ECA), and the non-conductive adhesive (NCA). These are available in the market either as film or as paste. The processing temperatures of adhesives are low compared to the solder alloys. Therefore, adhesives can be used to interconnect an electronic package to the substrate when the assembly is designed to work at low temperatures.

1.6 Pb-based Interconnect Materials

The trend in the miniaturization of consumer electronic products has led to the adoption of the flip chip technology which ensures a huge number of input/output interconnections in a small die footprint [11]. Soldering (as discussed above) is one of the effective

methods to interconnect flip chips and organic substrates. This method has been used in the electronic packaging industries extensively for decades. The soldering alloys include 5Sn-95Pb, 10Sn-90Pb, 25Sn-75Pb, 30Sn-70Pb, 40Sn-60Pb, 50Sn-50Pb, 60Sn-40Pb, 63Sn-37Pb, and 70Sn-30Pb. The reasons behind this loyalty to Sn-Pb solders in the electronic packaging industries are these solders' favourable physical, mechanical and metallurgical properties that ensure the long-term reliability of flip chip interconnects [12][13]. However, in spite of the advantages of Sn-Pb solders, environmental concerns have led the world to restrict the broad usage of these solders because Pb is a toxic substance [14][15]. The details of this issue are discussed below.

1.6.1 Pb-based Materials-The Issues

Although the excellent performance and reliability of Pb-based electronic packaging interconnections, the toxicity of Pb has caused some concerns. When a person is contaminated with Pb, it may cause the following effects [16][17]:

- Immediate effects:
 - Vomiting, diarrhoea, convulsions etc.
 - Appetite loss, abdominal pain, constipation etc.
 - Sleeplessness, irritability and headache etc.
- Ultimate effects:
 - Continuous exposure to Pb-environment can damage the kidney, liver, brain
 - Pb causes the osteoporosis (a disease that makes the bone brittle)
 - Excessive exposure to Pb can cause seizures, mental retardation, behavioural disorders, anaemia, high blood pressure etc.
 - In the last trimester of pregnancy, Pb can cross the placenta and can affect the unborn child
 - Female workers who are in contact with high level Pb can suffer from miscarriages and stillbirths
 - A small amount of Pb can harm the intellectual development, behaviour, size and hearing of infants

Chapter-1: Introduction

Pb can also cause damaging effects to the earth's ecosystem in general. When the earth or the environment becomes contaminated with Pb,

- wild and domestic animals can consume Pb while grazing and can experience the same effects as human being
- Pb can enter into the water from sewage or by the industrial wastes thrown in the water, or from the landfill of Pb-containing electronic products. The contaminated water then damages the aquatic life and causes the neurological changes in the fish and other water-based species

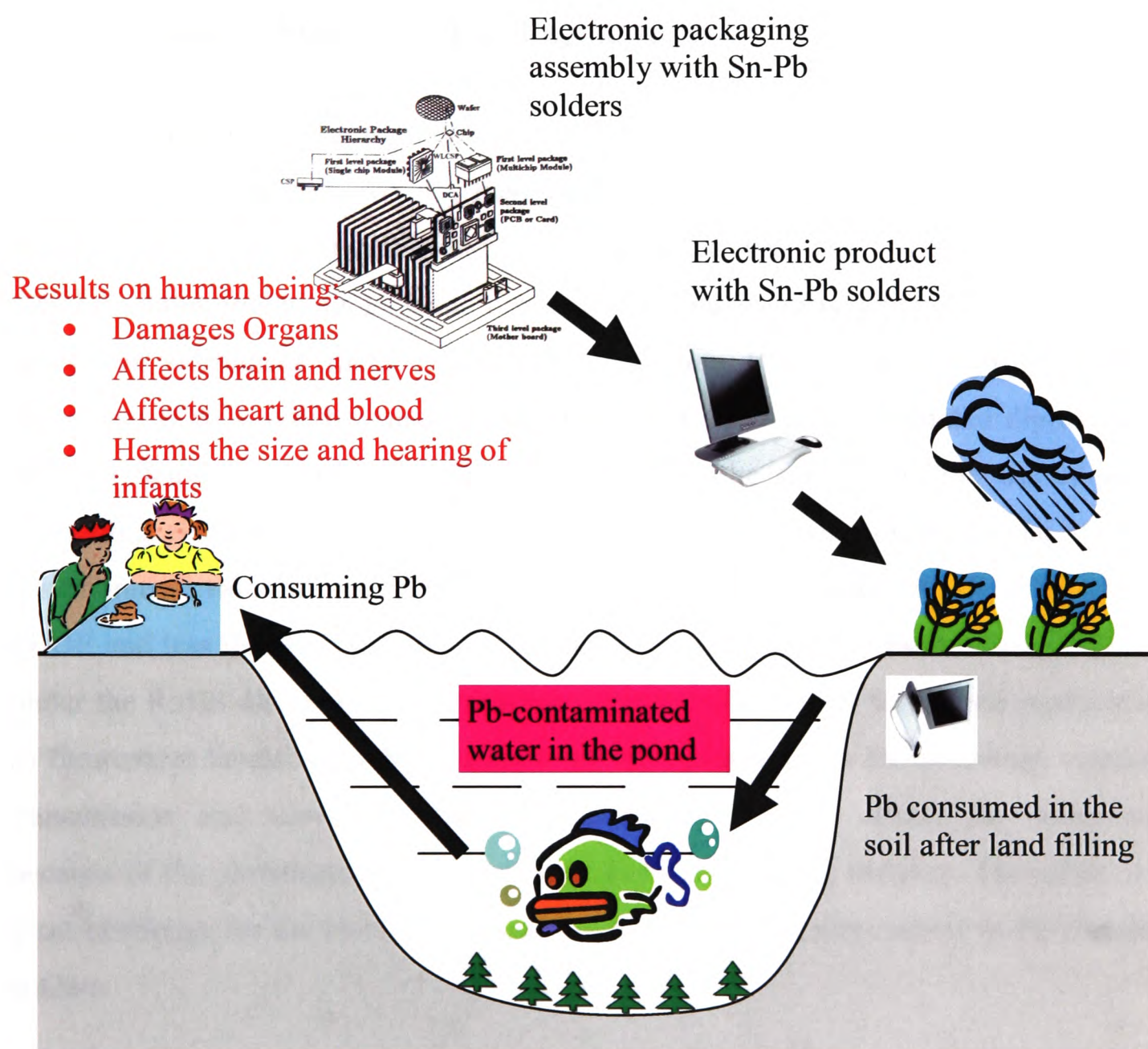


Figure 1-8: Transmission of Pb to human being from electronic packaging interconnections.

Figure 1-8 demonstrates how a Pb-containing electronic product can cause harm to the environment and indirectly put the human health in danger. This figure shows that an electronic product bears Pb when a Pb-containing solder alloy is used to connect electronic packages to the circuit boards of that product. At the end of the life cycle, that electronic product is thrown away into the soil. Eventually, the soil absorbs the Pb from that electronic product and becomes contaminated. This poisonous soil then affects trees, water, hydras and fish. When people eat those contaminated fish or drink the Pb contained water, indirectly they take Pb into their bodies and get affected.

1.6.2 Pb-based Materials-The Legislations

Concerned about the long term effects of poisonous elements used in electronic products, the European Commission (EC) has set up a directive on the Restriction of certain Hazardous Substances (RoHS) which is implemented in all the 25 European Union (EU) member states including Iceland, Liechtenstein and Norway since 1st July 2006. The hazardous substances include lead (Pb), cadmium (Cd), mercury (Hg), hexavalent chromium (Cr6⁺), polybrominated biphenyl (PBB), and polybrominated diphenyl ether (PBDE) flame retardants [18]. The directive bans the supply and the use of the Pb-containing electronic and electrical products in the European markets. The maximum concentration value in materials should be less than 0.1wt% for Pb, Hg, Cr6⁺, PBB or PBDE and less than 0.01wt% for Cd. Although a broad range of electronics products are under the RoHS directive, there are some exemptions of RoHS for certain products such as fluorescent lamps and tubes, cathode ray tubes, equipments for switching, signalling, transmission and telecommunication. The RoHS directive affects the entire world because of the globalization of the electronics manufacturing industry. Therefore, it is a great challenge for the electronic industries to find suitable alternatives to Pb-containing solders.

1.7 Pb-free Interconnect Materials for Electronic Packages

Electronic packages need interconnect materials to provide electrical path to the PCB and the Pb-based materials have been used for many decades for this purpose. Due to the implementation of the RoHS directive, electronic industries have to search for alternatives of Pb-based materials. The interconnect materials that do not contain the hazardous “Pb” are generally referred to as Pb-free materials.

1.7.1 Pb-free Materials – The Real Definitions

Although a Pb-free material means a material without Pb, a material with a trace of Pb can also be considered as a Pb-free material. According to the RoHS directive, an interconnecting material can be treated as “green” or “Pb-free” if it contains less than 0.1wt% lead. Furthermore, ISO 9453 standard allows less than 0.05-0.10 wt% Pb but ASTM B32-96 standard accepts less than 0.1 wt% Pb generally and 0.2 wt% Pb for especial cases to define the material as Pb-free [19].

1.7.2 Pb-free Materials – The Problems

Moving from the Pb to the Pb-free technology requires massive changes from the production lines to the applications. The problems are mainly associated with (1) manufacturing, (2) application and (3) reliability issues [19][20]. The transition from Pb containing solder to Pb-free solder may cause the following problems.

1. **Increase in Production Costs:** It has been stated earlier that the acceptable amount of Pb in Pb-free solder is 0.1 wt%. It is very difficult to control the Pb-contamination and to maintain such amount of Pb during manufacturing of Pb-free materials. The alloy bath can easily be contaminated by the air, the production floor, the handling or by the equipments. Therefore, Pb-free

production requires special enclosed system/area that increases the production costs of Pb-free materials.

- 2. Increase in Process Temperature:** Sn-Pb solders consist of Sn and Pb. The melting points of these two metals are 231 °C and 327 °C respectively. The elements that replace lead (Pb) are either silver (Ag), aluminium (Al), copper (Cu), or zinc (Zn). All of them possess higher melting temperatures (961 °C for Ag, 660 °C for Al, 1083 °C for Cu, 420 °C for Zn) than that of lead (Pb). As a result Pb-free solder alloys have higher melting points and this means that the furnace temperature has to be increased. Therefore, when a Pb-free alloy is used, the assembly process of an electronic package with a PCB is performed at a relatively high temperature. As a result, the components and the devices used in the Sn-Pb assembly process may not withstand with the increased processing temperature. Improvements of all the components and the devices are necessary to make them compatible with the increased processing temperature.
- 3. Degradation of Joint Reliability:** Apart from the processing temperature, wetting difficulties, higher consumptions of metallization and formations of thick intermetallic layer are the well-known problems for Pb-free materials. All these problems are detrimental to the package lifetime. Because when a Pb-free alloy consumes all the metallization, spalling of intermetallic layer takes place and the package interconnection fails. For these reasons, the use of Pb-free solders is questionable in the sectors where high interconnection reliability is required.

Adhesives are also Pb-free green materials and have been proven to be successful electronic packaging interconnection materials. The process temperatures of adhesives are far lower than the Pb-free alloys and actually they are even lower than the Pb-based alloys. However, adhesives absorb moisture very quickly and the properties are very sensitive to temperature changes. Therefore, the use of adhesives is restricted and their performance can be erratic when exposed to high temperature and humidity.

1.8 Motivation for this PhD Work

In order to gather the experiences of using various lead-free solders instead of Sn-Pb solders, a study has been carried out by “elfnet” (European Lead-free Soldering NETWORK) in 2004 [20] on the electronic industries from Finland, Norway, Italy, the Netherlands, Germany, the United Kingdom and Poland. The results of that study have revealed that 56% of the industries think quality and reliability are the most important technological problems for Pb-free materials. 33 % of them face problems with the processing temperature and 11 % are in trouble with the wetting behaviours of Pb-free materials. D.A. Fazekus [21] has also pointed out that two-thirds of the total defects found in the electronic packages are associated with the wetting problems. The microstructures and the compositions of the reaction species that are formed during wetting reaction determine the solder joint quality and the integrity. The elemental composition of a Pb-free solder dominates the physical behaviours of that solder. Therefore, it is necessary to find out the answers of the following questions:

1. Is there any means to improve the wetting behaviour?
2. Which parameters influence the wetting phenomena?
3. How the changes in the elemental composition of a solder affects the formation of the reaction species?
4. How does temperature influence the reaction?

For the adhesive interconnecting material, the properties are very sensitive to the temperature. Delamination in the adhesive matrix occurs when the adhesive-based interconnections are subjected to an elevated temperature for a while [22]. The effects of moisture on the reliability of adhesive-based interconnection has been studied by Lin et al [23] and it has been found that the adhesive absorbs considerable amount of moisture and degrades the joint strength. Therefore, it is clear that adhesives are very sensitive to temperature and humidity. Now the question is

1. Which factors dominate the physical properties of adhesives?
2. How and which factors degrade the joint integrity?
3. Is there any means to improve the performance of an adhesive joint?

1.9 Outlines of this PhD Work

This PhD work has been carried out to investigate the problems related to Pb-free interconnect materials described in the previous section. In order to find out the possible solutions of those problems a series of experiments and computer modelling work have been carried out. The results are presented and discussed in Chapter 4 and Chapter 5. The contents of each chapter are described below.

In Chapter 4 the research work on Pb-free solders is described. The effects of elemental compositions of solders on the wetting, on the reaction and on the growth behaviour of intermetallic compounds (IMCs) with Cu and Ni metal substrates have been investigated. The effects of soldering temperatures and fluxes on the wetting of the solders are also investigated here. This chapter also contains the computer modelling results of the wetting and diffusion behaviours of solders.

Chapter 5 presents the research on adhesives. The parameters (such as bonding temperature and time) that influence the changes in the physical properties of adhesives and affect the reliability of the interconnections have been studied here. Computer modelling has also been carried out to identify the effects of mechanical or thermal loads on the electrical and mechanical performance of the adhesive interconnections and the results are presented in this chapter.

1.10 Originality and Novelty of this PhD Work

To the author's best knowledge, the followings are the original contributions of this PhD work as presented in Chapter 4 and Chapter 5:

1. Wetting data has been generated for two completely new Pb-free solders (Sn-2.8Ag-0.5Cu-1.0Bi and Sn-0.7Cu-0.3Ni).

2. The qualification of three types of fluxes (NC, R and WS) has been justified for three different temperatures (255, 275 and 295 °C), for two types of substrates (Cu and Ni) and for the two above mentioned new Pb-free solders along with the well-known Sn-Ag-Cu and Sn-Cu solders.
3. The growth rate constants of the IMCs have been calculated for these new solders
4. Computer model has been developed to verify the experimental wetting data.
5. Computer modelling technique has been used to study the dissolution behaviour of metal substrates into solders and results have been compared with experimental observations.
6. The physical properties of an adhesive have been measured as a function of temperature and time.
7. The relationship among the bonding temperature, the curing degree of the adhesive matrix, the adhesion strength and the electrical performance of the interconnection has been established.
8. The possible failure mechanisms of the electrical conduction path during the isothermal ageing of the adhesive joints have been proposed.
9. Computer modelling techniques have been used to establish the correlation between electrical failure and external bending load.

1.11 Industrial Benefits from this PhD Work

The electronic packaging industries can use the results obtained in this PhD work as a reference guidelines in the ways:

1. Based on the wetting data the industries can decide which solder should use with which flux for which particular metallization.
2. Based on the substrate consumption data the industry can chose a right solder alloy when the preservation of a too thin metallization thickness is the main concern.

3. The data provided for the growth rate of IMCs can be used to warn the industries of the consequences of keeping a solder interconnection at a relatively high temperature for a long time.
4. The industries can use the computer modelling technique to carry out the parametric studies about the wetting behaviour of solders.
5. The data provided here for the curing of adhesives can be used by the industries to optimize the bonding conditions.
6. The industries can be informed about the consequences of exposing an adhesive-based package to the elevated temperatures for prolonged time.

1.12 Publications Resulted from this PhD Work

Seven journal papers and one conference paper have been published so far from this PhD work:

1. Computer modelling of adhesive-based interconnection under bending condition presented in section 5.4.7 has been published in the Journal of Microelectronics Reliability [24].
2. The curing of adhesive matrix and its effects on the mechanical and the electrical performance of adhesive-based interconnection presented in sections 5.4.4 has been published in the Journal of Soldering & Surface Mount Technology [25].
3. The wetting behaviour of the newly developed Sn-2.8Ag-0.5Cu-1.0Bi solder on Cu and Ni substrates presented in section 4.4.1.1 and section 4.4.1.2 has been published in the Journal of Electronic Materials [26].
4. The growth behaviour of IMCs of the newly developed Sn-2.8Ag-0.5Cu-1.0Bi solder during soldering and isothermal aging presented in section 4.4.2.2.2 and section 4.4.3.1 has been published in the Journal of Alloys and Compounds [27].
5. The wetting behaviour of newly developed Sn-0.7Cu-0.3Ni solder on Cu and Ni substrates has been published in the Journal of Alloys and Compounds [28].

6. The growth of IMC layer for the newly developed Sn-0.7Cu-0.3Ni solder during wetting and aging presented in section 4.4.2.2.3 and section 4.4.3.2 has been published in the Journal of Alloys and Compounds [29].
7. The effect of heating time and temperature on the changes in the physical properties of adhesive presented in section 5.4.1 and section 5.4.2 has been accepted for publication in the Journal of Microelectronic Engineering [30].
8. Comparative wetting behaviour of Sn-0.7Cu and Sn-0.7Cu-0.3Ni solders on Cu and Ni substrates has been presented in the 1st Electronics System Integration Technology Conference (ESTC), Dresden, Germany, on 5th -7th September of 2006 [31].

Chapter 2

Review of Electronic Packaging Interconnections

2.1 Review of Solder Interconnections

2.1.1 Solder Materials

Solder materials are fusible alloys that possess melting temperatures below 400 °C [32]. Lead-free solders usually contain a high proportion of Sn (more than 90 wt %). Small amount of other elements like Ag, Bi, In, Cu, Ni, Cd, Sb, Mg are added to produce binary, ternary or quaternary eutectic or near-eutectic alloys. The melting point of a solder alloy is very important as the electronic package contains a number of active and passive components on the FR4, glass or flexible substrates and these components have certain temperature tolerance levels.

Solder materials can also be found in powder form which is made using chemical reduction, electrolytic deposition, mechanical processing of solid particles or atomization of liquid alloys. Another form of lead-free solder materials is paste which is a homogeneous and kinetically stable mixture of solder alloy powder, flux and vehicle. The “vehicle” of the solder paste holds the alloy powders and flux. In this case, the particle size of the alloy powder is very important. Reducing the size of the particles in the alloy powder increases not only the number particle density but also the surface area and this means that higher fluxing activity is required and this eventually increases the production cost. Moreover, fine powder alloy causes solder balling during the soldering, therefore, solder pastes with coarse alloy powder perform better and they are more cost-effective than pastes with fine powder.

2.1.2 General Criteria to Select a Solder Alloy

To select a solder alloy, the following criterion [32] should be checked out:

- it should have a melting range that is suitable for the service temperature range
- it should have mechanical properties that are compatible with service conditions
- it should be metallurgically compatible with surrounding metallization
- it should have a reasonably low rate of intermetallic compounds (IMCs) formation at the service temperature
- it should have an acceptable wettability on surrounding metallization
- it should be stable in the ambient environment

2.1.3 Alloys as Green Solders

There are numerous choices of lead-free solders in the market. It's really very hard to pick one of them as the standard soldering material. At present the most widely used lead-free solders are Sn-Cu and Sn-Ag-Cu alloys. The melting temperatures of these two solders are 227 °C and 218 °C respectively. Lower cost is the most significant advantage

of the Sn-Cu solder over the Sn-Ag-Cu solder and some other solders. Also, this solder consumes less copper in the coating process and produces comparatively stable IMC layer along the bond line and shows almost similar reliability performances to the Sn-Pb solders. However, the high melting temperature of this solder prevents it from being used in some soldering processes [33][34]. Adding Ag into the Sn-Cu solder results in a decrease of about 5-10 °C in the melting temperature and an increase in the cost by about 2.18 times compared to the Sn-Cu solder [34]. Although the solderability of Sn-Ag-Cu solder is better than Sn-Cu solder, it is still not as good as the Sn-Pb solder. The Sn-Zn alloy has a melting temperature of 198 °C which is close to that of the Sn-Pb solder (183 °C). While there are benefits of using this solder as a lead-free alternative because of its low melting point, there are also some serious problems with this solder. The most important shortcoming of this solder is that the zinc in the alloy causes excessive oxidization and this causes severe drossing in soldering pots. Moreover wettability of this solder is very inferior compared to the Sn-Pb solder and other lead-free solders. Bismuth (Bi) is often added to the Sn-Zn solders to reduce the liquidus temperature, to improve the wetting and corrosion behaviours [34].

2.1.4 Soldering Methods

There are two major types of widely used soldering methods in the electronic packaging industry: reflow soldering and wave soldering.

2.1.4.1 Reflow Soldering

Reflow soldering as described in ANSI/IPC-T-50E Standard [35] is the joining of mating surfaces that have solder between them, placing them together, heating them until the solder fuses, and allowing them to cool in the joined position. Reflow soldering requires a few steps. The first step is to place the flux and the solder alloy (in the form of bar, sphere or disc) on the surfaces to be soldered. The second step is the placement of components on the placed solder. The third step is the heating and then the cooling of the assembly. During the heating stage, the solder melts and spreads over the surfaces.

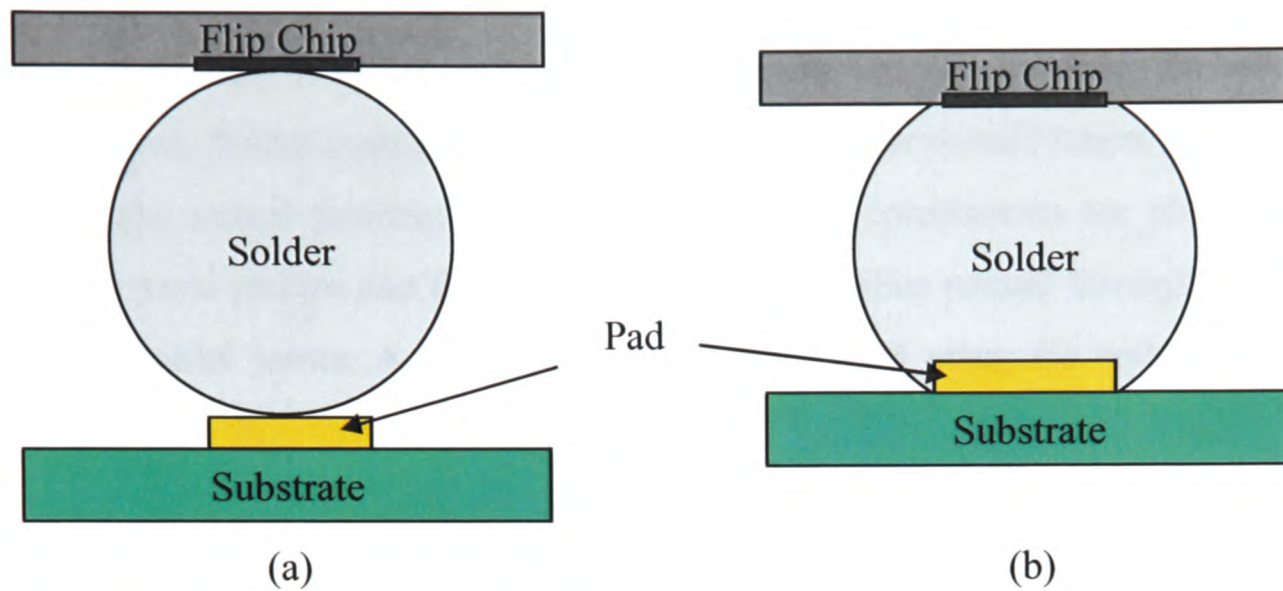


Figure 2-1: Flip chip solder joint: (a) before reflow, (b) after reflow.

Table 2-1: Advantages and limitations of various reflow methods [1]

Reflow Methods	Advantages	Limitations
Conduction	Low equipment capital, rapid temperature changeover, visibility during reflow	Planar surface and single side attachment requirement, limited surface area
Infrared	High throughput, versatile temperature profiling and processing parameters, easier zone separation	Mass, geometry dependence
Vapour phase condensation	Uniform temperature, geometry independence, high throughput, consistent reflow profile	Difficult to change temperature, temperature limitation, relatively high operating cost
Hot gas	Low cost, fast heating rate, localized heating	Temperature control, low throughput
Convection	High throughput, versatility	Slower heating, higher demand for flux activity
Induction	Fast heating rate, high temperature capacity	Applicability to nonmagnetic metal parts only
Laser	Localized heating with high intensity, short reflow time, superior solder joint, package crack prevention	High equipment capital, specialized paste equipment, limit in mass soldering
Focused Infrared	Localized heating, suitable for rework and repair	Sequential heating, limit in mass soldering
White beam	Localized heating, suitable for rework and repair	Sequential heating, limit in mass soldering
Vertical reflow	Floor space saving, maintenance of desired throughput	Often more costly

During cooling, molten solder solidifies and solder joints form. The last step is to clean the residues of the flux. If solder pastes, instead of solder bars etc. are used, the soldering steps are different. Solder pastes can be placed directly on the metallization on the circuit boards using the stencil printing method. After that, the components are placed on the printed solder paste pattern and the assembled boards are then passed through the reflow oven to form solder joints. A typical flip chip solder joint using the reflow soldering method is shown in the Figure 2-1.

In the reflow soldering process, there are quite a few different heating methods that can be used. These include conduction, infrared, vapour phase, hot gas, convection, induction, laser, focused infrared, white beam, and vertical reflow methods. Each of these methods has advantages and limitations as listed in Table 2-1.

2.1.4.2 Wave Soldering

Wave soldering is completely different from reflow soldering. In this method, the printed circuit board (PCB) assembly passes over a continuous wave of solders. The crest of the liquid solder wave touches and wet the exposed metallization of the assembly and solder-joints form upon cooling. The wave soldering process is shown in Figure 2-2. The steps of wave soldering are described bellows as suggested in [36].

1. Automatic insertion of leads of through-hole components into the holes in the printed circuit board.
2. Dispensing of adhesives at the locations of surface mount components to be placed throughout the printed circuit board.
3. Placements of surface mount components over the dispensed adhesive.
4. Curing of adhesive to make a temporary bond so that components can be hung beneath the circuit board.

5. Manual insertion of leads of through-hole components through holes in the printed circuit board.
6. Application of flux at the locations to be soldered by foam, wave or spray.
7. Preheating of the circuit board so that solvent of the flux can be evaporated and the flux can be activated, pre-heating also minimizes the thermal shock of the board during soldering.
8. Passing the circuit board assembly over the wave of molten solder so that required locations can be soldered.
9. Cooling of the circuit board assembly so that the solder can solidify to make the joint.
10. Cleaning of the flux residues.

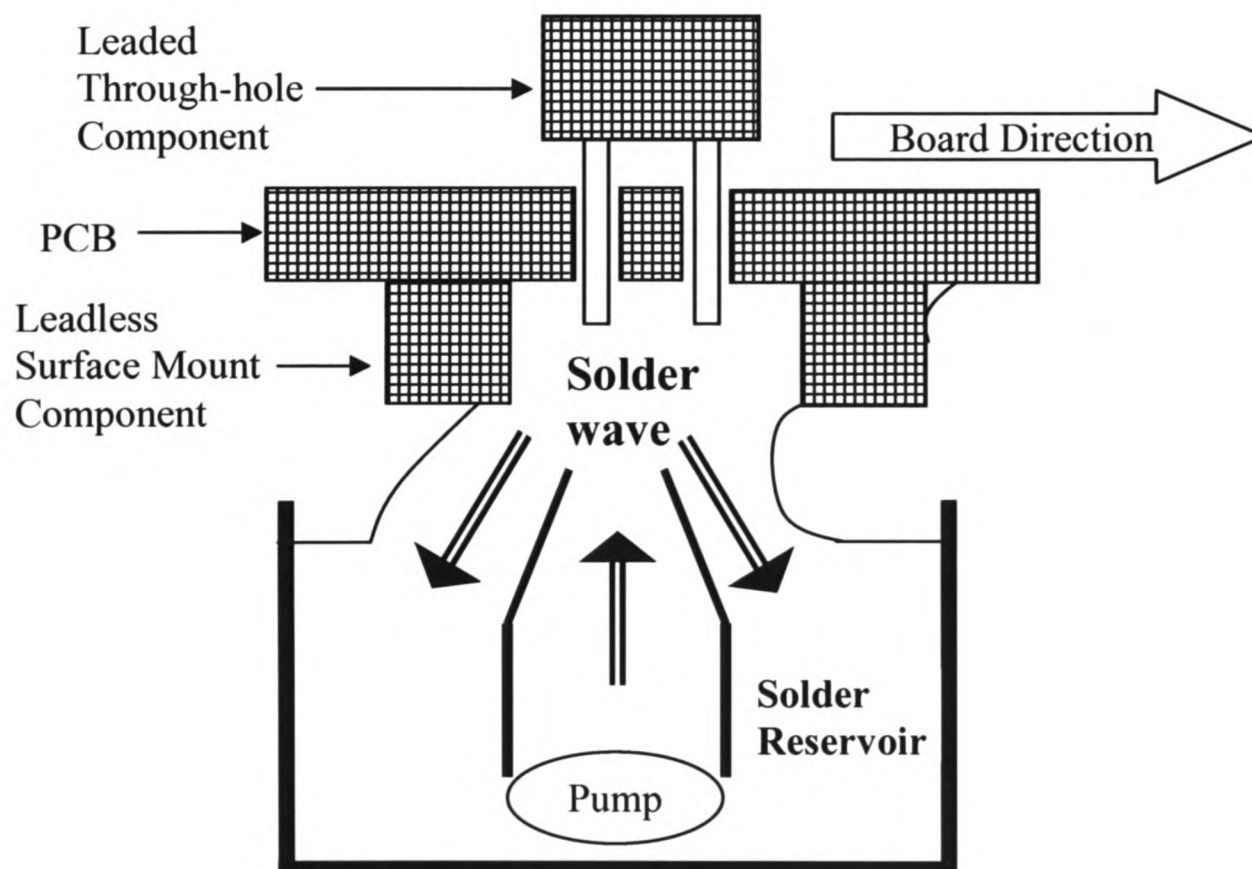


Figure 2-2: Wave soldering process. (Figure reproduced from the ref. [37]).

The success and the reliability of the wave-soldered joint depend on the wettability of the solder used because the solder has to travel through the holes in the PCB. Therefore, the selection of the type of solder alloy is very important. Also the type of flux, the solder bath temperature and the dwell time of soldering are important factors in providing good quality solder joints.

2.1.5 Issues associated with Soldering

2.1.5.1 Solderability and Wettability

Solderability is the ability to achieve a clean metallic surface on which a molten solder can wet properly [32]. In other words solderability is the ability of a surface to be wet by a molten solder [38]. Solderability depends on the several factors such as the type of flux, the type of solder and the type of surface finish on which soldering will be performed.

The word wettability is basically the same as solderability but it is often used as a quantitative measure of solderability. The parameters such as the contact angle, the meniscus rise, the capillary penetration depth etc. that can be obtained in solderability tests are often used as measures of the wettability of solders [38]. Wettability is very important as the success of soldering depends on the wettability of the solder. Inappropriate wettability raises the possibility of a rework to correct the visible solder joint defects and the rework not only increases the production costs but also increases the risk to the solder joint reliability.

2.1.5.2 Wetting, Non-wetting and Dewetting

According to C. A. Harper [32], wetting can only be achieved when a smooth, uniform and continuous solder coating is formed on the substrate surface without any pinholes. Nonwetting is defined as “the phenomenon of molten solder not adhering to the substrate

surface, thereby leaving the substrate surface exposed” [32]. The term “dewetting” is related to the solderability and it can be defined as “the phenomenon of molten solder receding after it has coated the surface, leaving a rough and irregular surface with thick mounds of solder connected by thin solder film” [32]. These three wetting states are shown in Figure 2-3.

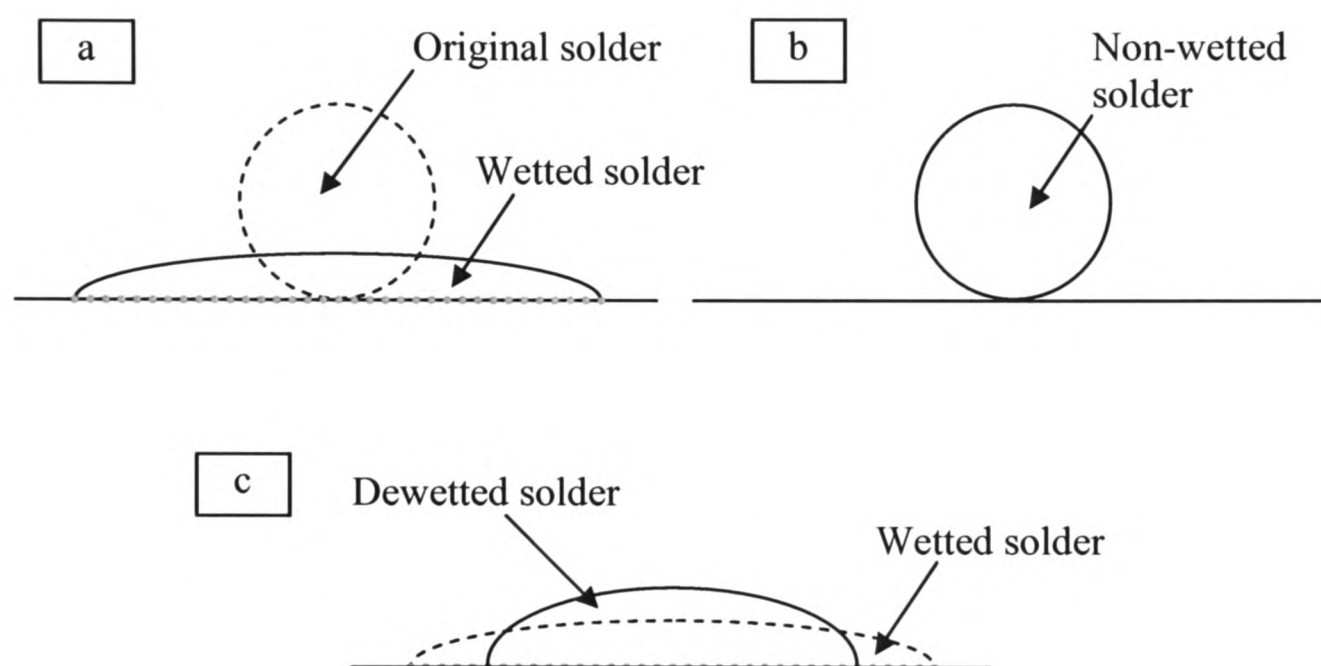


Figure 2-3: Wetting states: (a) wetting, (b) nonwetting and (c) dewetting.

2.1.5.3 Intermetallic Compounds (IMCs)

When a liquid solder alloy spreads over a metal surface during soldering, chemical and metallurgical reaction takes place at the solder-metal interfaces. The reaction products are called intermetallic compounds (IMCs) which are often seen at the interfaces and in the bulk of the solder alloys. From the metallurgical point of view, IMCs are considered as solid phases those contain two or more metallic elements and whose structural properties are completely different than that of any of the constituent elements. The assembly is under one or more of the following conditions an IMC may form [32][38].

1. When the electronic components are soldered to the substrate.
2. If the solder has certain compositions such as 96Sn-4Ag which creates inborn IMCs in the bulk of solder.
3. When the assembly is subjected to environmental stress conditions such as thermal cycling or aging.

It is believed that the formation of IMCs at the interfaces during the soldering of two dissimilar materials is a common mechanism for the creation of permanent bond. However, the acceptable thickness of the IMC layer ranges from 1 to 5 μm [32][38]. When the IMC layer is less than 1 μm , solder joint is prone to receding and when it is more than 5 μm thick it can be detrimental to the solder joint [32][38]. IMCs are basically crystal structured and brittle in nature. The thicker the IMC layer the easier it is for brittle fracture to happen. It has been observed in experiments that cracks are often found around the thick IMC layer under stressful conditions. Another damaging effect that a thick IMC layer may have is the deterioration of the reliability caused by the formation of a weaker IMC layer within the thick IMC layer.

In the situation where IMCs form in the bulk of a solder material, the solder joint's strength may increase. However, if the size of the IMCs is very large or the shape is needle-like, the mechanical properties of the solder joint's strength may decrease.

2.1.5.4 Circuit Board Surface Finish

Solderability and thereafter the solder joint integrity depends partly on the surface finish of the circuit board to be soldered. In the electronic packaging assembly, copper is a common metal that is widely used in the circuit board as a conductor through which electrical signal passes from the integrated circuits to other components on the board. Usually the Sn from the solder and the Cu from the substrate have great affinity to each other and this results in the formation of Cu-Sn IMCs. It is possible that excessive

amount of Cu reacts with the Sn (as can be seen from the Cu-Sn phase diagram shown in Figure 4-34) supplied from the solder such that the remaining Cu conductor becomes very thin. This may put the reworking and the reliability of the assembly at risk. Ni coating on Cu is often used as a diffusion barrier to overcome this problem. This works because Sn has to react with Ni first and only after Ni is consumed Sn can react with Cu. In this case Ni-Sn, Cu-Sn and Cu-Ni-Sn IMCs can be found in the solder joint. However, Ni is prone to oxidize and possesses less wettability than Cu. It has also been found that compared to the original metal, the metal oxides have poorer thermal and electrical conductivities [38]. Oxides are considered a barrier to the heat transfer during soldering and, therefore, delay the fusion of solder coating. Moreover, solders can not wet and spread over the oxide layer. When an oxide layer forms during soldering, dewetting can take place. To eliminate these problems, a coating of an inert material such as Au is used on the conductors of the electronic packaging system. Au-coated copper also shows better wetting and spreading than the pure copper [32]. During soldering, Au dissolves very quickly into the solder matrix. The rate of the dissolution of the Au-coating depends on the soldering time, the temperature, and the solder compositions. Diffused Au-atoms then react with the Sn in the solder and form Au-Sn IMCs. After the Au layer is consumed, the base material comes in contact with the solder and reacts to form IMCs. The presence of Au in the solder matrix alters the microstructures and the appearance of the solder joints and hence, the physical and the mechanical properties of the joints are affected. The shear strength of a solder joint slowly drops when the concentration of Au in the solder matrix is beyond 3 wt%. Furthermore, the ductility of a solder joint drops rapidly when the Au concentration exceeds 7 wt%. However, a concentration of Au below 10 wt% doesn't affect solder's electrical and thermal conductivities. High Au concentration in solders causes premature solder joint fracture due to the gold embrittlement, void creation and microstructure coarsening [32]. The electronics packaging industries have to make great effort to control the concentration of surface coating materials in the solder matrix. Therefore, it is obligatory to have the proper knowledge about the consumption of the surface coating materials by molten solders.

2.1.5.5 Voids in Solder Joints

Solder joints not only connect the package assembly electrically to the circuit board but also provide mechanical strength. The formation of a small void in a solder joint may not be too detrimental to the performance of the solder joint but the role of a large void as seen in Figure 2-4 is questionable.

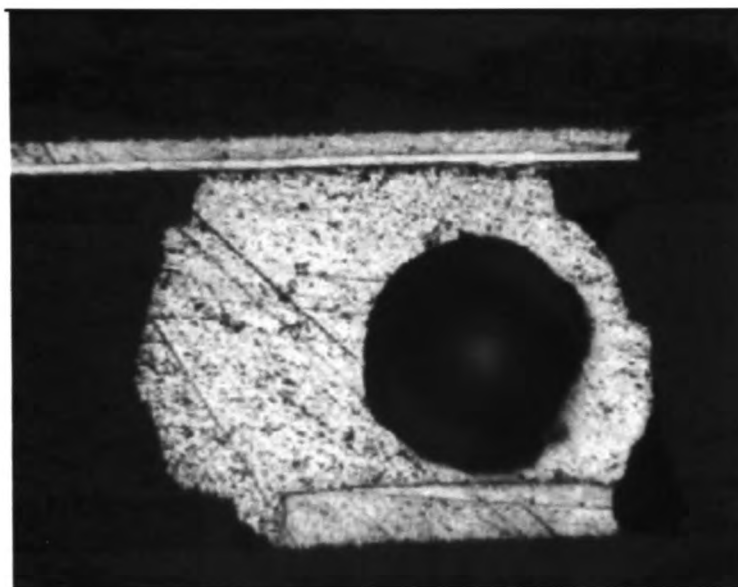


Figure 2-4: Void in solder [44].

Previous studies [39][40] have shown that voids in solders can form either due to manufacturing flaws or thermal-mechanical cycling. The voids reduce the solder joint cross-sectional area and affect the heat dissipation. As a result, the increase in the local current density and in the resistance may cause catastrophic failures [41][42]. Lin et al [43] have found that an increase in the current density by a factor of two has significant effects on the Joule heating and the temperature can rise above the melting point of eutectic SnPb solder. If a solder joint melts it may collapse and causing electrical failure. Voids also affect the thermo-mechanical reliability of solder joints as reported by Yunus et al [44]. These researchers have found that a solder joint with a void that occupies more than 50% of the solder joint area suffered from a 25-50 % reduction in the solder joint life time. In contrast, Kim et al [45] recently has reported that the effect of void formation on the fatigue life of solder joints is too small and can be neglected. Possibly the sizes and

numbers of voids discovered by Kim et al are not as large as the voids found by other researchers. There are a number of factors that affect the formation of voids during soldering. These factors include the wettability of the soldering system, the contamination of the substrate surface, the duration of soldering, and the cooling rate etc. [32][46]. The outgasing of the substrate or the solder materials is another factor that affects the formation of voids in solder joints. In this PhD work, the voids are also noticed in the solder joints because of the outgasing of the substrates. The exact causes of voids formation, the solutions of this problem, and the effects of voids on the quality and the reliability of solder joints are research areas where thorough studies are needed.

2.2 Review of Adhesive Interconnections

2.2.1 Adhesive Materials

Adhesives in paste or film forms are being used for the electronic packaging interconnections as an alternative to the lead-free solders. Whenever fine pitch is required, adhesives are the solution. While solders are inherently electrical conductors, conductive fillers (such as silver-based conductors, copper, nickel, carbon, metal-coated particles etc.) have to be added to a polymer binder to convert the adhesives to electrical conductors. Therefore, adhesives used in the electronic packaging assemblies are complex in structure and the types of binder used in an adhesive dominate the chemical and the mechanical properties of that particular adhesive.

There are two types of epoxy polymers that can be used as binders to make interconnect adhesives: the thermoplastic and thermosetting polymers. Thermoplastics can be melted or softened with heat without changing their intrinsic properties whereas thermosets are cross-linked polymer with three-dimensional molecular structure that can be softened to some degree but can not be melted or reshaped at elevated temperatures [47]. The advantages of thermoplastic epoxy based adhesives are

- Fast processing and easy to rework
- Chemically non-reactive
- Takes less than a second to transform from solid to flowable form
- Infinite shelf life
- Can be stored in room temperature

The disadvantages are

- Can be melted or softened with high heat application
- Limited in service temperature performance
- Can flow under mechanical force
- Forms weak adhesive bond

The thermosetting epoxy-based adhesives offer the following advantages

- Non-deformable and mechanically stable
- Forms strong and durable bonds
- Can wet out a surface for complete bonding

and the following disadvantages

- Undergoes true chemical reactions for several hours
- Limited shelf or pot life
- Lower temperature thermosets must be kept frozen to prevent premature hardening

2.2.2 Types of Adhesives

2.2.2.1 Isotropic Conductive Adhesives (ICAs)

Isotropic conductive adhesives are composite in nature and contain non-conductive thermoset epoxy-based binder and conductive fillers. The fillers are dispersed randomly in the binder and provide the conductivity equally in all directions. Silver flakes are used as fillers due to their cost effectiveness [48]. A typical conduction path through ICA-joint is shown in Figure 2-5.

The fundamental properties of ICAs depend on the geometric properties of the fillers [49]. Other than flakes, fillers can also be mono-sized spheres, bi-modal spheres or coated spheres [47]. The total number of the fillers in the ICAs depends on the shape, the distribution and the orientation of the particles [49].

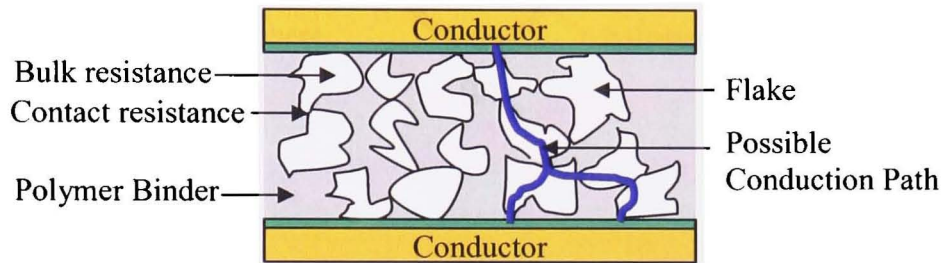


Figure 2-5: Schematic representation of an ICA joint.

2.2.2.2 Anisotropic Conductive Adhesives (ACAs)

Anisotropic conductive adhesives (ACAs) are also composite materials that contain thermoplastic or thermosetting epoxy polymers as binders and randomly dispersed conductive spheres. The properties of ACAs are mainly dominated by the type of binder that is used. Some ACA materials possess hybrid properties that combine both the properties of thermoplastic and the thermosetting polymers. Unlike the isotropic conductive adhesives, anisotropic conductive adhesives are electrically conductive only in the Z-axis direction (inter-plane connection). Even if the conductive particles come in contact with the conductor surfaces, a conduction path doesn't establish unless heat and pressure are applied. The details of the interconnection technique using this type of adhesive will be discussed in Chapter-5. The conductive particles of an ACA are either solid metals or metal coated polymer particles. Sometimes, there is an insulation layer on the outermost surface of the particle to prevent the electrical bridging. With the applied pressure, insulation layer breaks and exposes the conductive particles to the conductor planes. A schematic of conductive particles and a typical ACA-joint is shown in Figure 2-6.

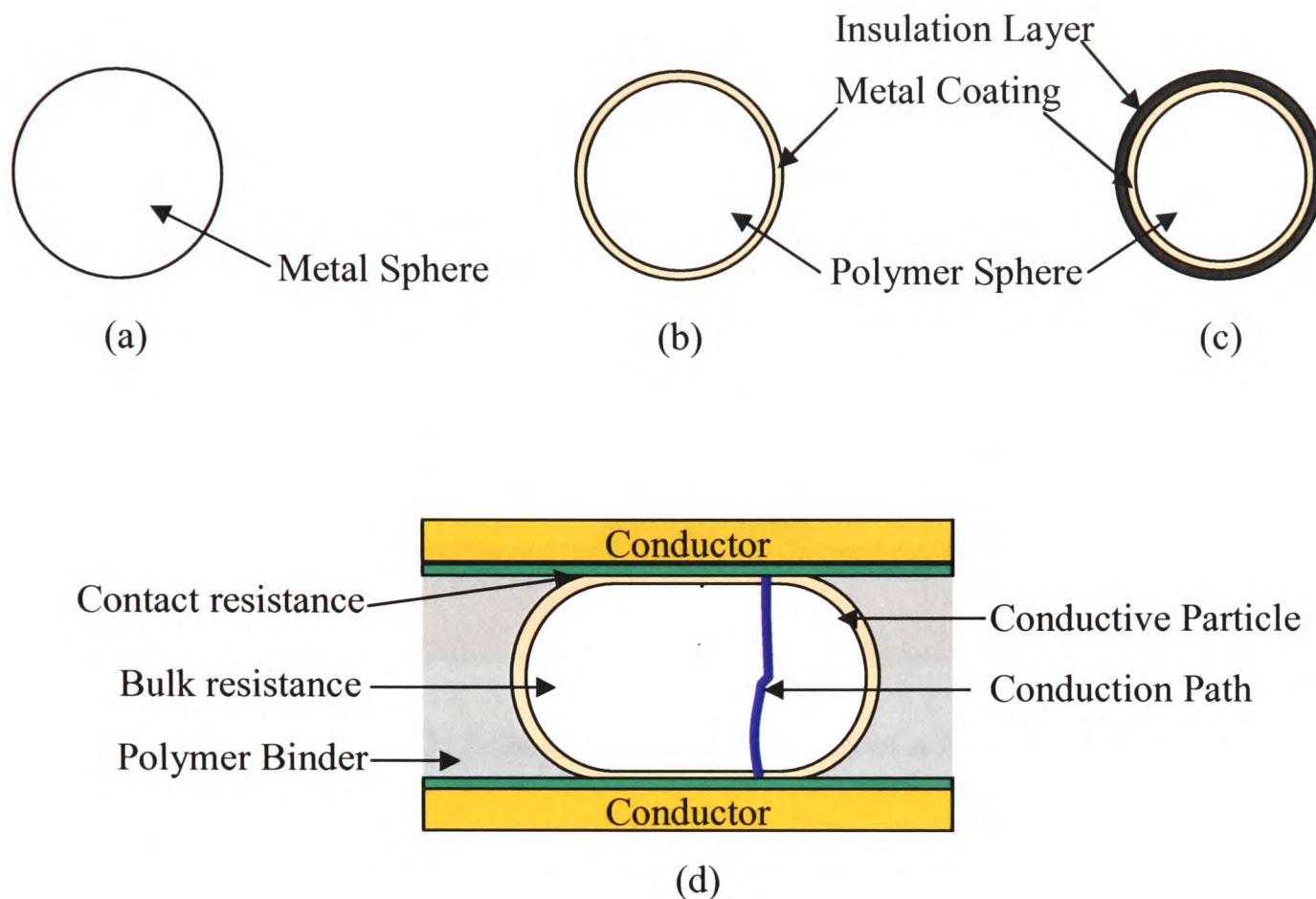


Figure 2-6: Schematic representation of (a) metal particle, (b) metal coated particle, (c) metal coated particle with insulation layer and (d) a complete ACA joint.

2.2.2.3 Non-Conductive Adhesives (NCAs)

Non-conductive adhesives (NCAs) contain polymer resin and a hardener (curing agent) [50]. Although NCA does not contain any conductive particles, it creates a mechanical tension to provide forces between opposing conductors so that direct metallic conductivity can be achieved [47]. In order to form the interconnections, sufficient pressures are required so that NCA material can be squeezed out of the contact areas for the electrical conduction. With the application of heat, NCA material cures and shrinks and generates compressive stress to hold the two conductive parts together.

NCA materials have been used successfully for the circuit-to-circuit and the bare die-to-circuit interconnections. Compared to the ACA interconnections, NCA provides more contact area as the whole conductor areas come in contact as seen in Figure 2-7. The only disadvantage of this material is the reliability of the joints. As the bond strength of this material depends only on the mechanical contact, polymer relaxation over time can weaken the bond.

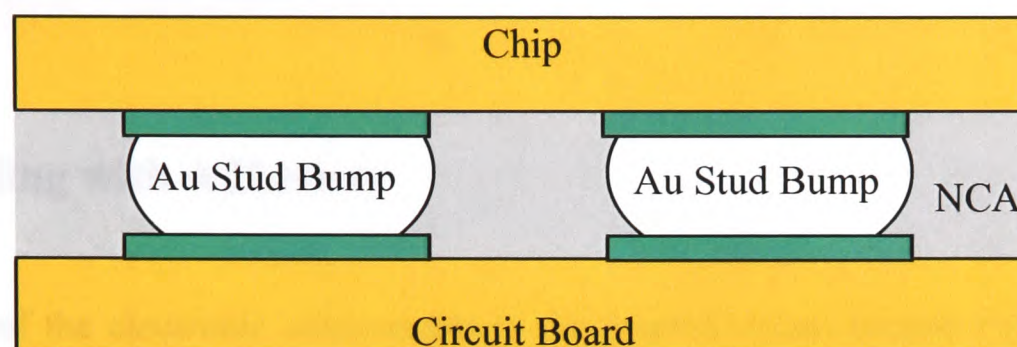


Figure 2-7: Schematic representation of a NCA joint.

2.2.3 Applications of Adhesives

The use of adhesives in the electronic packaging helps to produce miniaturized products because adhesives make it possible to attach the die directly to the printed circuit board. Moreover, the advantages of adhesives are very prominent in areas where low processing temperature is the key requirement. Adhesives are being used successfully in the following ways [47].

- Anisotropic conductive films are used in the flat panel displays or in the liquid crystal displays
- Adhesives are used to connect the chips and the components on the Polyester-based flexible circuits and on the moulded circuits.
- Isotropic conductive adhesives are used in the membrane switch and in the low-cost flexible circuit industries where processing temperature must be kept below 150 °C.

- Adhesives are used in the flip chip assembly to connect the flip chips to the organic circuit boards.
- Adhesives are used in the case where soldering is not possible to connect the glass and the vacuum deposited conductors.
- Anisotropic adhesives are used for bonding the flexible circuits and the Tape Automated Bonding (TAB) devices to the panels.
- Patterned array imposers use adhesives to make multilayer circuits.

2.2.4 Bonding with Adhesives

The bonding of the electronic components to the printed circuit boards with an adhesive requires the thermo-compression method where both the heat and the pressure are applied simultaneously. In order to achieve maximum bond strength, the adhesive matrix should be perfectly cured with the applied heat and pressure. During the thermo-compression bonding, adhesive melts with the heat and wets the required bonding areas. As the wetting of the adhesive is non-reactive, the viscosity of the adhesive plays an important role in wetting and filling the gaps between the parts being joined together. The pressure helps to squeeze and to achieve an even distribution of the adhesive matrix. However, pressure serves different purposes for different types of adhesives. The silver flakes in the isotropic conductive adhesives come in physical contact with each other and with the conductors when a pressure is applied. The conductive spheres of the anisotropic conductive adhesives can be deformed only with a pressure to provide effective contact areas for the electrical conduction. The details of the bonding technique using an anisotropic conductive adhesive are discussed in Chapter 5. In the case of nonconductive adhesives, pressure helps the stud bumps to penetrate the adhesive matrix, to squeeze out the adhesives from between the contact parts, to deform and to establish the direct metallic contacts with sufficient effective areas for the electrical conduction. This bonding process is schematically shown in Figure 2-8.

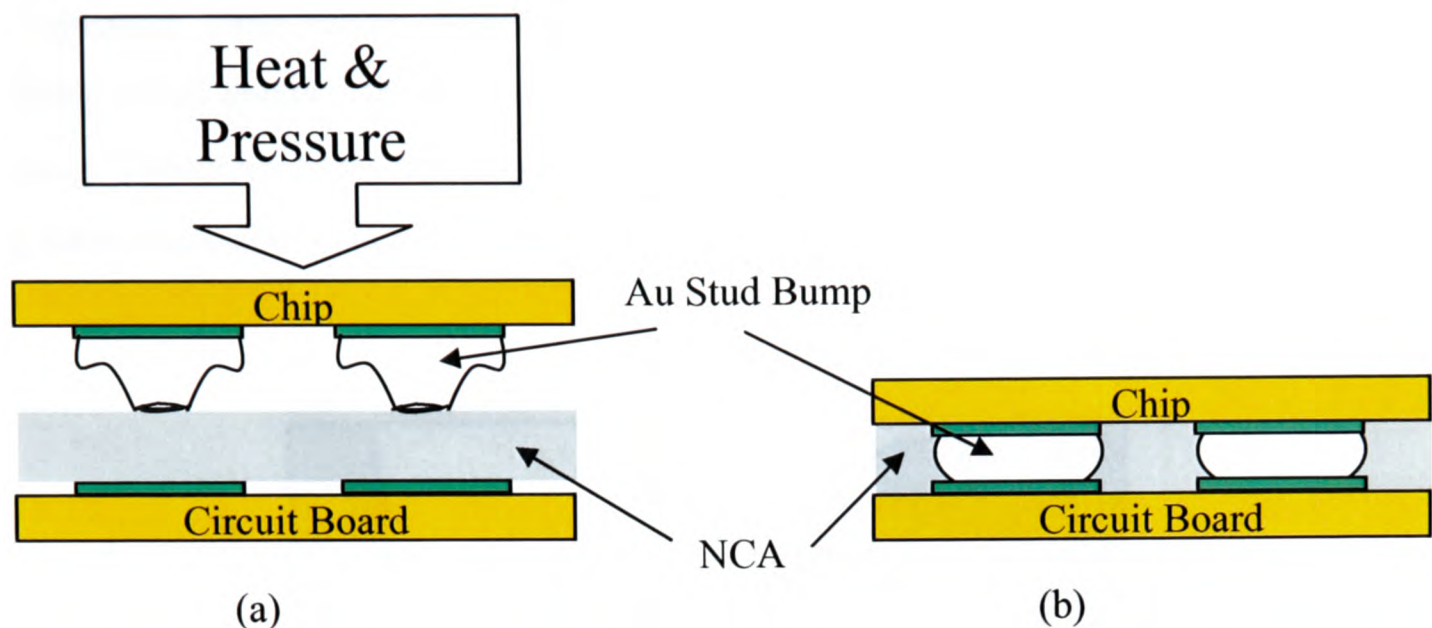


Figure 2-8: Thermo-compression bonding of a flip chip on the circuit board with NCA:
(a) before bonding, (b) after bonding.

2.2.5 Curing of Adhesives

As adhesives are made from epoxy based polymers, the curing of the polymers is the most important part of the adhesives interconnection formation process. The curing of an adhesive means the formation and the linear growth of the polymeric chains in the adhesive matrix and the branching and cross-linking of the polymeric chains. The higher the cross-linking density, the higher the degree of curing is [51]. The degree of curing of the adhesive matrix determines the adhesion strength of that particular adhesive.

Figure 2-9 represents the four states of the epoxy materials during curing. Here, T_{c0} is the melting temperature of the epoxy mixture. At temperatures above T_{c0} the polymeric reaction takes place and below this temperature the reaction is in solid state and reaction rate is slow. $T_{c, gel}$ is the cure temperature at which both the vitrification and the gelation occur simultaneously. Gelation is the sudden and irreversible transformation from a viscous liquid to an elastic gel. After gelation, epoxy remains in the rubbery state. Vitrification is the transformation from a viscous liquid or an elastic gel to the glass state. However, gelation precedes vitrification and a cross-linked rubbery network forms between the $T_{c\infty}$ and the $T_{c, gel}$ temperatures. The reaction becomes quenched when the

glass transition temperature coincides with the cure temperature. In order to get a completely cured epoxy, vitrification must be avoided because it causes an abrupt halt to the curing. Therefore, fully cured epoxy and its ultimate properties can be achieved when curing takes place above $T_{c\infty}$.

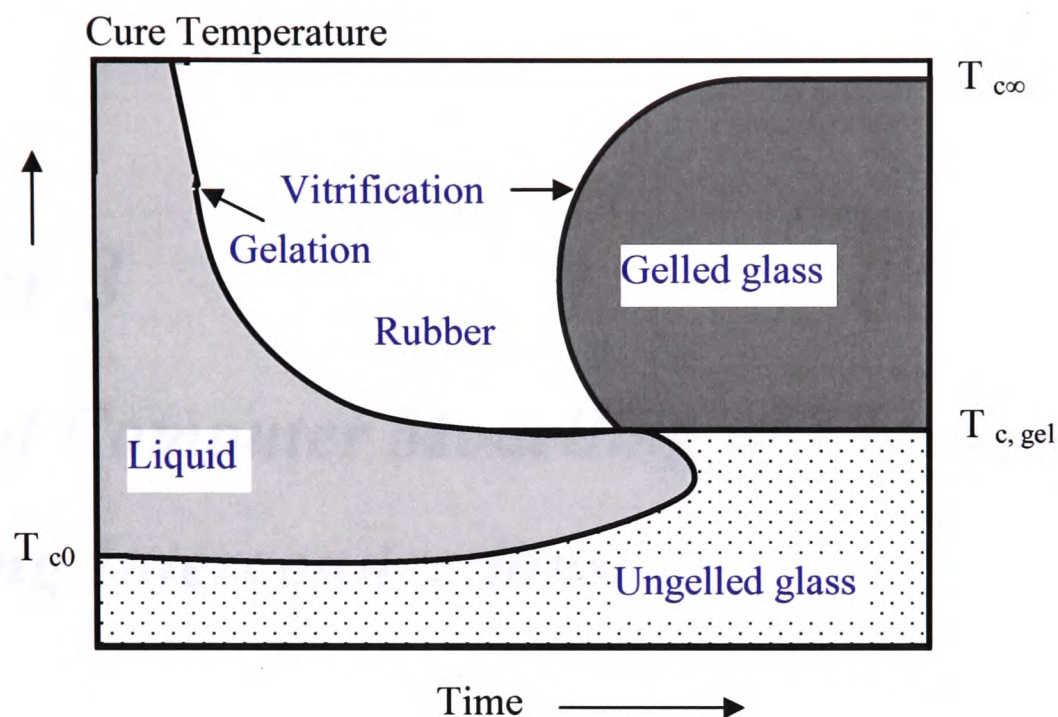


Figure 2-9: Time-temperature-transformation (TTT) diagram of adhesive materials during curing. (Figure reproduced from the reference [51]).

2.3 Closure

This chapter describes the interconnection technologies that are used in the electronic packaging, the interconnection materials and the problems associated with the use of those materials. It is understood that solders are the most common interconnection medium and sometimes adhesives are used as an alternative to the solders. When a solder alloy is used for the electronic packaging interconnections, the wettability of the solder, voids formation in the solder, the reactions and the IMCs formations of the solder with different circuit board surface finishes etc. dominate the solder joint quality and the integrity. When an adhesive is used as the interconnection medium, the bonding parameters and the curing of the adhesive determine the functionality and the reliability of the adhesive joint.

Chapter 3

Review of Computer Modelling of Electronic Packaging Interconnections

3.1 Introduction

“A computer model is a computer program that attempts to simulate an abstract model of a particular system [52]”. In other words, a computer modelling is basically a mathematical modelling that is implemented and solved using a computer in order to predict the behaviours of the model. In the last few decades computer modelling has been used very efficiently and fruitfully in the fields of electronic packaging interconnections to predict thermal, mechanical, thermo-mechanical behaviours and their ultimate effects on the reliability of electronic devices [53][54][55][56]. In this work, computer modelling has been used as an effective tool in the analysis of a range of phenomena that have been observed in the study of solder and adhesives interconnect. In this chapter some of the computer modelling techniques and successful examples are reviewed.

3.2 Techniques of Computer Modelling

Computer modelling solves a model of a system that is described in the form of partial differential equations. The three most widely used numerical techniques are the finite element (FE) method, the finite difference method and the boundary element method. Among these techniques the FE method is the very popular method for solving the structural problems [57] and it has been used successfully to solve steady state and transient problems in linear and non-linear regions with one, two or three-dimensional domains [58].

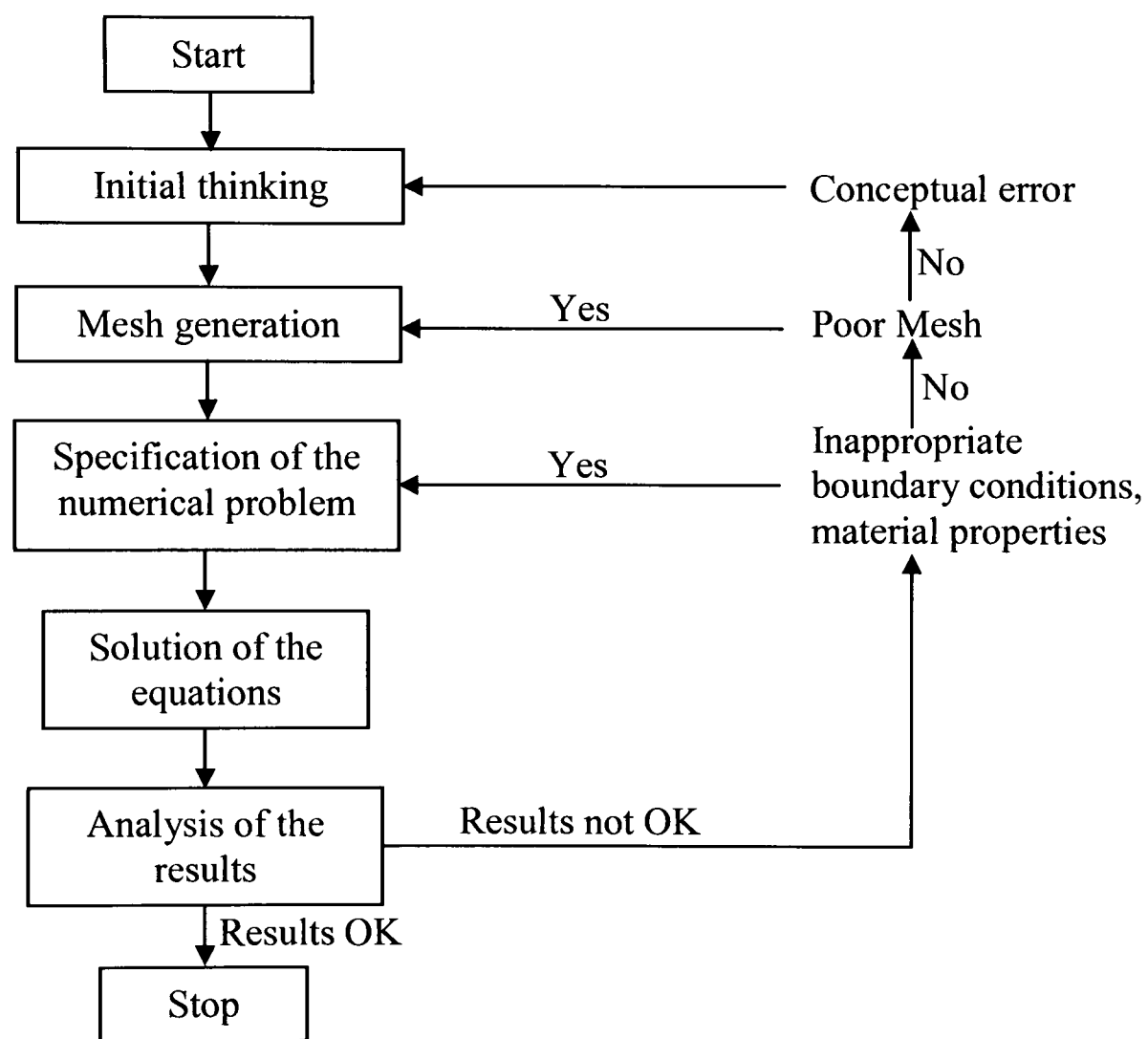


Figure 3-1: The process flow chart for computer modelling [57].

Figure 3-1 shows a flow chart that describes the general process of computer modelling. According to Mottram et al [57], the first step of the computer modelling is the *initial thinking*. In this step the modeller must carry out a detailed study of the problem to be

solved. The physical geometry, the expected structural behaviour of the geometry with loads, the loading conditions, and the material properties etc. should all be studied carefully. The second step is the *mesh generation*. In this step a computer model must be created prior to the mesh generation. Mesh generation means the break down of the geometry into small sub-regions on which the numerical equations can be developed. The next step is the *specification of the numerical problem* where boundary conditions are assigned to the nodes and elements that are created in the mesh generation step. In *solution of the equations* step, computer uses programming software to obtain a numerical solution for the meshed geometry. The last step of the computer modelling is the *analysis of the results*. The modeller must verify the results prior to the generation of any solution data.

The computer modelling procedure described above can be carried out with the help of a commercial software package that includes a pre-processor, a solver and a postprocessor. A pre-processor requires geometry in the numerical form, the mesh, the initial and boundary conditions, the material properties etc. The solver uses the information provided by the pre-processor and carries out the numerical calculation to predict results and finally the post-processor unit of the software displays the predicted results.

3.3 Tools of Computer Modelling

There is a number of commercial modelling software such as ANSYS [59], ABAQUS [60], ALGOR [61], MARC [62], NASTRAN [63], and COMSOL [64] that can be used to perform thermal, mechanical and thermo-mechanical analysis of electronic packaging assemblies. Other software products such as FLOTHERM [65] or FLUENT [66] can be used to model the fluid flow phenomena around the electronic package. Public domain software such as SURFACE EVOLVER [67] can be used to predict the shape of the solder joint for an electronic packaging interconnection. In this PhD work ABAQUS [60], SURFACE EVOLVER [67] and multi-physics modelling software PHYSICA [68] have been used to predict the behaviours of electronic packaging interconnections.

3.4 Computer Modelling for Electronic Packaging Interconnections

One of the main advantages of the computer modelling is that it can predict the possible behaviours of a device before it has been physically built in real space. Therefore, by using computer modelling it is possible to design an electronic product with high quality and reliability prior to the manufacturing of that product. The use of computer modelling to investigate the effects of a range of parameters not only reduces the experimental costs but also cuts the total production time i.e. the lead time of a product. Apart from these advantages, computer modelling also helps to understand the physics of failure of an electronic product under different loading conditions and predicts the life-cycle of that product. In the following section, computer modelling studies regarding solder and adhesives electronic packaging interconnections that have been carried out by a number of researchers will be reviewed.

3.4.1 Computer Modelling of Solder-based Interconnections

Solder joint life cycle can be divided into two stages. In the solder joint formation stage, the main concern during this stage is how good quality solder joints can be formed. The second stage is when the solder joints are subject to thermal-mechanical loading and the failure mode analysis and lifetime predictions are the major issues. Computer modelling method can be used to analyze the issues encountered in both stages.

In the surface mount technology, solder paste (a mixture of alloy powder, liquid flux, flux activators and solvents) is used to mount the components on the printed circuit board. Stencil printing technique is used to deposit the solder pastes precisely on the positions where components to be placed. The blade of the stencil printing machine spreads the solder paste over the soldering areas. Ekere et al [69] and Mannan et al [70] have pointed out that the settings of blade speed, blade angle, blade pressure along with the rheological behaviour of the solder paste composition affect the soldering process. Therefore, Bailey et al [71] have carried out a computer modelling to investigate the effects of these

parameters. The modelling has been carried out as seen in Figure 3-2 where the blade squeezes the solder paste to flow through the aperture of the stencil. It has been found that the pressure on the stencil surface exerted by the blade increases almost linearly with the increase of the blade velocity. It has also been noticed that the smaller the blade angles the higher the pressure on the stencil surface is.

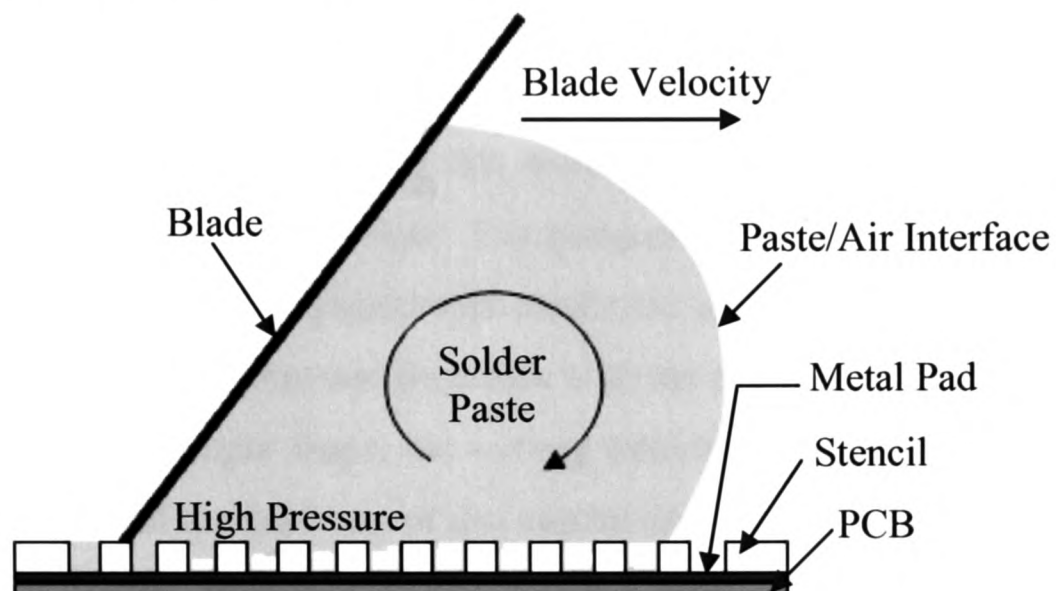


Figure 3-2: Schematic of the stencil printing used for computer analysis in [71].

He and Ekere et al [72] has performed the computer simulation of solder paste packing inside the apertures of ultra fine pitch stencil printing technique. They have found that mean solid volume fraction of the paste packed inside the apertures is less if the particle diameter is very large. As a result, a weak solder joint may form after the reflow treatment. They have also pointed out that the shape of the aperture has a great influence on the packing of solder pastes inside the apertures. The use of circular apertures instead of square apertures offers better results in the solder paste printing. The solder paste consists of solder particles and vehicle that acts as a flux to remove the oxide layers of the metal surfaces. The computer modelling performed by Mannan et al [73] has revealed that the solder paste flux can not eliminate oxides completely at the early stage of reflow process. During the reflow of a small volume of solder paste, a reduced oxygen concentration atmosphere is essential for the coalescence of the solder paste particles.

After the stencil printing of the solder paste, components are placed on the circuit board. The whole assembly is then ready for the reflow for the formation of permanent solder

joints. During the reflow, the solder alloy melts at a temperature that is higher than the melting point of that solder. Before solidifying, the molten solder wets the required soldering area. Yasuda et al [74] have used a computer model to investigate a range of parameters that affect the wetting behaviour of a solder alloy during the reflow. The computer model used for the study is shown in Figure 3-3. It is seen that a copper conductor is being immersed into a liquid solder pot. The modelling has been performed with the assumption that the contact angle is always zero degree (which is practically quite impossible). The main purpose of this modelling is to investigate the parameters that can influence the wetting behaviour. The computer analysis has identified that the wetting force per perimeter of a cylinder type conductor increases with the increase in the diameter of the liquid solder print and decreases with the increase in the solder thickness. If the conductor is in rectangle shape, the wetting force per perimeter increases with the increase of the width and the thickness of that conductor.

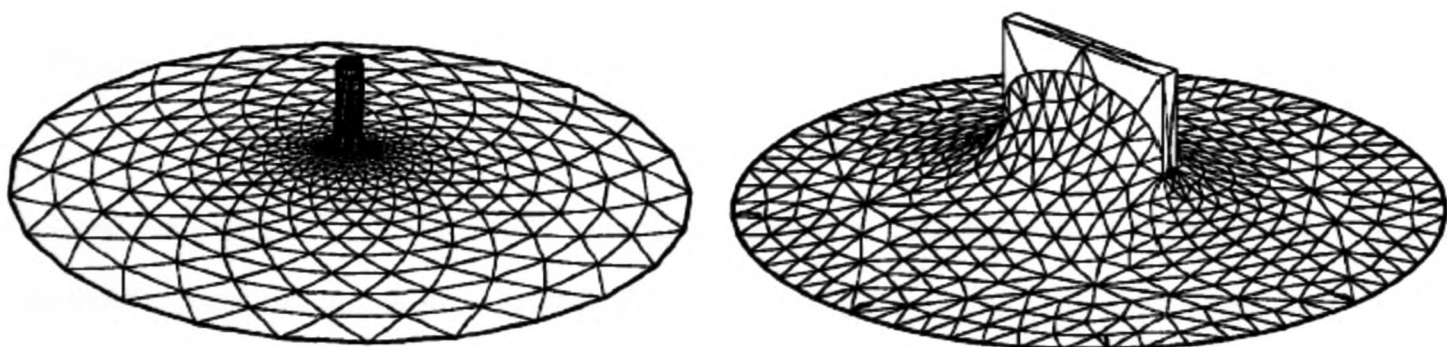


Figure 3-3: Wetting behaviour of a solder alloy [74].

Warren et al [75] has carried out a numerical and computer modelling for the reactive wetting of liquid Sn-Bi solder on solid Bi substrate. It has been shown that the spreading of a liquid alloy droplet is very fast at the initial stage of wetting, slows down over time and eventually reaches equilibrium state. Both the wetting and the dissolution of solid substrate in the liquid solder occur simultaneously. The dissolution of the solid substrate at the solder droplet-substrate interface is higher at the centre compared to the edges.

Immediately after the wetting, solder alloy starts to solidify as the reflow temperature falls down to the room temperature. During solidification, both the mechanical restraint

and the localized thermal shrinkage develop a thermal stress at the joint location. Kim et al [76] have studied the accumulated stress in their solidification modelling for chip scale package. The schematic of the model used for computer analysis is shown in Figure 3-4. They found that the stress is different in each solder ball and the maximum stress develops at the corner solder ball. It has also been found that the stress causes the deformation of the package and influences the formation of solidification defects.

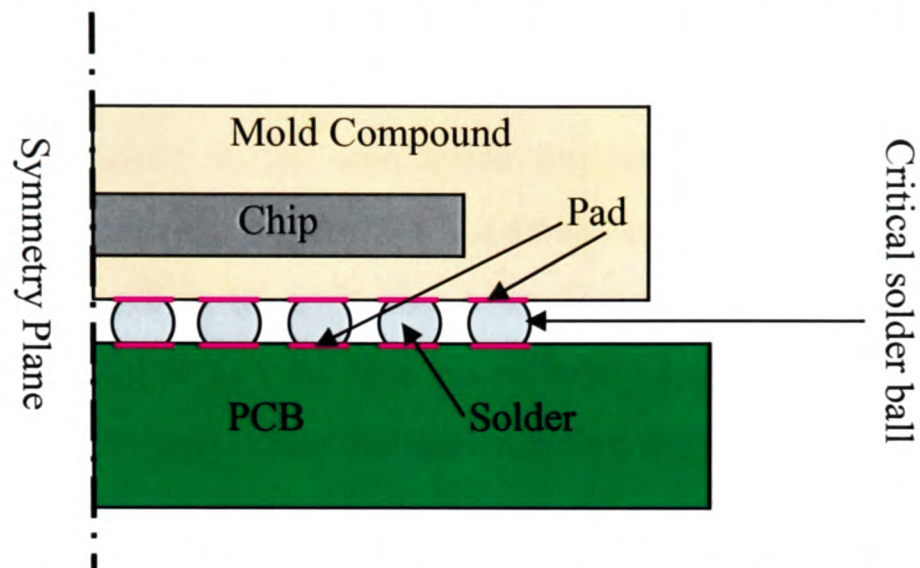


Figure 3-4: Schematic of the chip scale package assembly used in [76] to analyze the solidification process of solder.

Fatigue damage of solder joint during temperature cycling is a serious issue for an electronic package assembly as reported by Zhang et al [77]. In this study a computer model of a multi chip module (MCM) package has been analyzed to identify the effects of the package dimensions on the fatigue life of solder joints during a thermal cycling from $-40\text{ }^{\circ}\text{C}$ to $+125\text{ }^{\circ}\text{C}$. It has been found that an increase in the heat spreader thickness by 50% reduces the solder fatigue life by 12% whereas an increase in the substrate thickness by 50% reduces the solder life time by 39%. A number of researchers [78][79][80] have predicted the fatigue life of electronic packaging interconnections without considering the glass transition temperature, T_g of the materials. Tsai et al [81] has performed a computer modelling of MAP-BGA (matrix array package-ball grid array) assembly to investigate the deformation of the package under thermal loads. It has been pointed out that T_g of the die attach adhesive has a great impact on the package deformations. At high temperature loading condition, the package deformation on account of the T_g is about 25% less compared to the deformation without considering the

T_g of the die attach material. Therefore, the reliability prediction of BGA package can be overestimated if the T_g of the assembly materials are not considered.

3.4.2 Computer Modelling for Adhesive-based Interconnections

It has been discussed in chapter 2 that the curing of an adhesive used for electronic packaging interconnections is very important. Sufficient degree of curing can only be achieved when the adhesive receives sufficient heat. Wu et al [82] used a computer model to investigate the heat transfer in the anisotropic conductive adhesive (ACF) during bonding of chip-on-flex assembly. Figure 3-5 shows the temperature distribution in the assembly after 1 s of bonding time. It has been found that the required bonding temperature reaches the ACF within the first 1 s of bonding time. Therefore, ACF gets enough time to be cured properly since the total bonding time is 30 s. It has also been found that the thicker the bumps of the chip the higher the stresses generated in the ACF.



Figure 3-5: Temperature distribution ($^{\circ}\text{C}$) in the adhesive-based flip chip assembly [82].

For ACF-based interconnections, apart from the bonding temperature, the bonding pressure also plays an important role in the electrical performance of an ACF-joint. Yim et al [83] has derived an analytical model to predict the effect of particle deformation on the contact resistance of an ACF-joint. A computer model has been used to predict the bump-particle-pad interfacial contact areas against the bonding forces. Figure 3-6 represents a typical example of the particle deformation under a bonding force. Modelling results predicted that the higher the bonding force the greater the contact area and the

lower the contact resistance. An experimental investigation apparently agreed with the modelling results but it has also been pointed out that although high pressure increases the contact area, a separation among the metal coatings eventually increases the contact resistance.

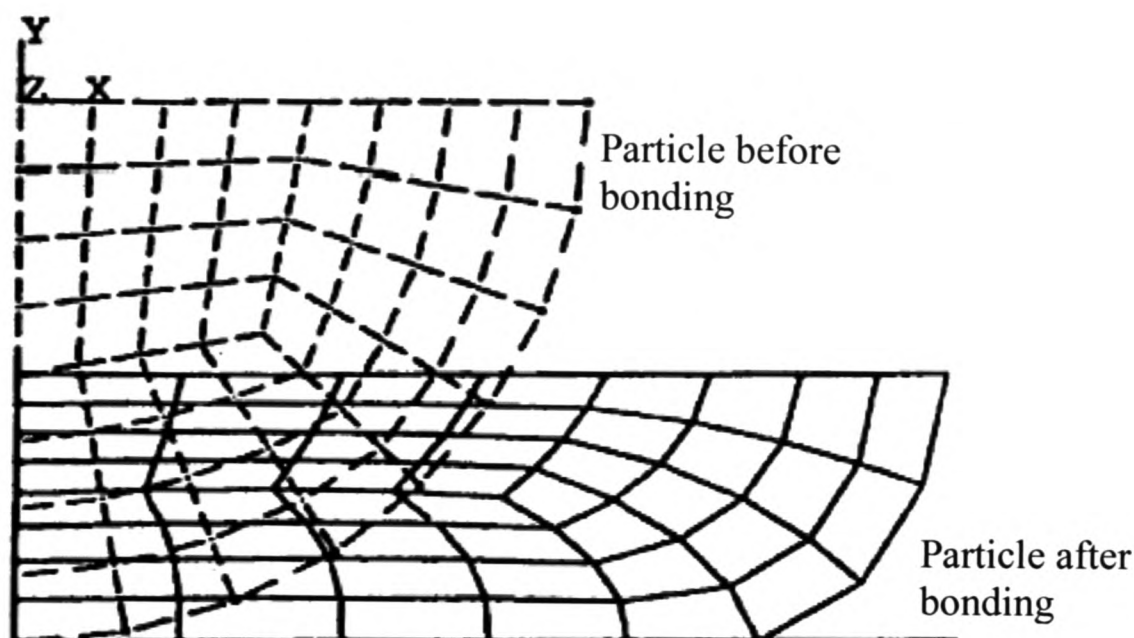


Figure 3-6: Computer grids show the one-quarter of the conductive particle before and after bonding [83].

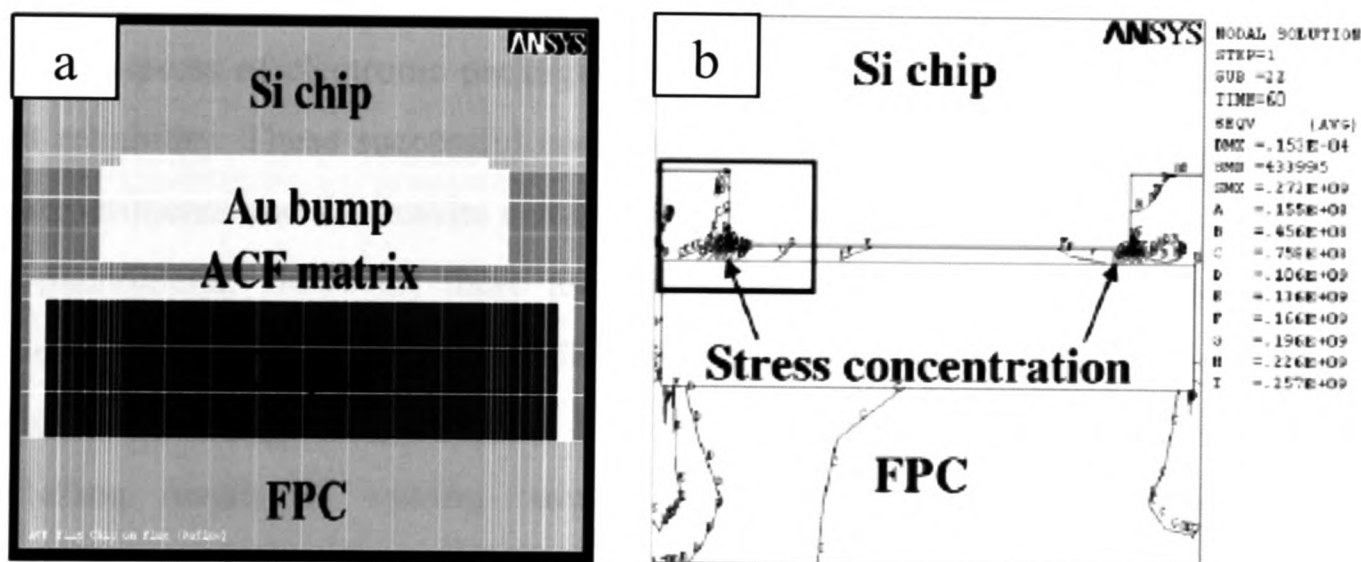


Figure 3-7: Thermo-mechanical analysis of ACF-based flip chip assembly; (a) computer model of the package and (b) stress distribution in the package [84].

Mechanical reliability of an ACF-based electronic packaging interconnection is as important as the electrical reliability. Kim et al [84] has performed a computer modelling analysis to investigate the thermo-mechanical reliability of an ACF-based chip-on-flex

assembly. The computer model of the assembly is shown in Figure 3-7(a). The stress concentration in the package has been documented when the whole assembly is subjected to an elevated temperature and the results are shown in Figure 3-7(b). It is found that the two edges of the bump-ACF interfaces experience high stress values. Therefore, these two regions are most vulnerable to the threat of delamination.

Computer modelling of the moisture induced failures in an adhesively bonded flip chip assembly has been carried out by Teh et al [85]. It has been found that in-plane hygroscopic swelling of the substrate and the adhesive causes the deformation of the package generates considerable amount of tensile stresses along the bond-line. The maximum tensile stresses are found at the centre of the package. Therefore, the failure of the adhesive joint initiates at the middle of the package and propagates outwards to the edge. The modelling results have been validated with the experimental observations.

3.5 Closure

This chapter gives some ideas about the capability of computer modelling to analyze various aspects of electronic packaging interconnections from the joint formation to the joint reliability. These successful computer modelling analyses have helped to augment the experiments and the results can be used to understand the physical processes behind the phenomena. However, there are still many questions that need to be answered regarding the reliability of solder/adhesives interconnect. For example, to the best of the author's knowledge, no work has been done before this PhD work to compare the modelling results of wetting balance tests with the experiments to predict the concentration of the solid metal in the liquid solder during wetting balance test. There is also a lack of research on the temperature changes in the adhesives during flip chip bonding process, and this has not helped the understanding of the root causes of the delamination along the anisotropic conductive film joint of the flip chip assembly under thermal-mechanical loads. In light of this, some new computer modelling work has been carried out in this study in order to address some of the issues related to the experimental work described in Chapter 4 and 5.

Chapter 4

Study of Interconnections formed with Lead-free Solder Alloys

4.1 The Background and the Objectives of this Work

In the electronic packaging industries, the binary eutectic Sn-Pb solder has been used extensively for many decades to attach the electronic components to the printed circuit boards, which are made of organic laminate substrate, copper traces and dielectric layers [86]. The low liquidus temperature and a narrow solidus-liquidus temperature range that satisfy everyday soldering requirements are the main reasons of the popularity of the Sn-Pb solder [87]. This solder alloy is popular also because its properties are relative well known and the reliability of the products using it are satisfactory [88][89]. Moreover, the low price and good availability of this solder is also a factor in its widespread use in the electronic packaging industries. Recently, the use of Sn-Pb solder has become very limited because of environmental concerns and the coming into effect of new regulations

[18]. Hence, the development of solders without Pb (lead), i.e. Pb-free solders, has been conducted on a worldwide basis [90][91]. Since Sn fulfils the metallurgical, the environmental, the economic and the supply criteria, the productions of Pb-free solders have been directed towards the Sn-based binary or ternary alloys as reported by Wu et al [92]. A number of eutectic or near eutectic Pb-free solders such as Sn-In, Sn-Bi, Sn-Ag, Sn-Ag-Cu, Sn-Cu are being used as the replacements of Sn-Pb solders. The limited solubility of Ag in Sn at liquid state makes more stable and uniform microstructure of the Sn-Ag solder system. The addition of a small amount of Cu in the Sn-Ag solder can prevent the dissolution of Cu from the base metal [93]. Previous studies [94][95] have focused on the consumption of base metals such as Cu and Ni –P and it has been found that the Sn-Ag solder consumes more base metal than the Sn-Cu solder whereas moderate amount of base metal consumption has been observed for the Sn-Ag-Cu solder. Although the above mentioned lead-free solders are now being extensively used as interconnect materials, the melting temperatures of all those solders are higher than the eutectic Sn-Pb solder. The addition of a small amount of Bi (1 wt%, for example) into the Sn-Ag-Cu solder reduces the melting temperature by about 4 °C [96]. Several researchers [92][97][98] have already investigated the joint strength and the fatigue properties of Sn-Ag-Cu and Sn-Ag-Cu-Bi solder alloys and found that an addition of a certain amount of Bi into the Sn-Ag-Cu solder increases the tensile strength and the hardness of that solder. Ashram et al [99] has found that an addition of 0.5wt% Zn to the Sn-0.7Cu solder increases the hardness and the yield stress but this lowers the creep resistance whereas an addition of Bi into this solder deteriorates the creep resistance. Wu et al [100] has found that an addition of 0.5wt% rare earth (RE) elements into the Sn-0.7Cu alloy refines the β -Sn grains and the intermetallic particles in the β -Sn matrix. It has also been found that the mechanical properties, the hardness and the creep resistance can also be improved with the addition of RE elements. Young et al [101] has studied microstructural evolution of Sn-2.7Cu-0.2Ni solder with Cu and Pt-Ag metallised Al₂O₃ substrate. However, to the author's knowledge, the information regarding the effect of adding small amount of Bi into Sn-Ag-Cu solder and Ni into Sn-Cu solder alloys on the wetting behaviour was not available before this work was carried out. It is well known that Sn in the Sn-Pb or the Sn-based lead-free solders reacts with Cu very rapidly to form Cu-Sn intermetallic

compounds (later this term will be referred as IMCs) at the solder-Cu interface. Therefore, Ni is often used as a diffusion barrier layer on the Cu bond pad for BGA and flip chip bumps to prevent the excessive growth of Cu-Sn IMCs.

Since Cu and Ni are often used in the under bump metallization, clear understanding of the wetting behaviours of a newly developed solder alloy on these two metals are very important. Besides, the wettability and the solder joint integrity are linked to each other and they define the quality of any solder. The lifetime of a solder joint largely depends on the physical and the mechanical properties of that solder and the substrate. The thickness of the IMC layer that forms at the solder-substrate interface has a significant effect on the solder joint strength as well as on the reliability [102]. Thus, the design of a good solder joint requires the wettability information about the joint materials.

During the wetting reaction, the dissolution behaviour of the substrate material into the molten solder dominates the growth of the IMC. Previous studies [94][103][104][105] have focused on the dissolution behaviour and the IMC formation in solder on the Cu and the Ni substrates. It has been found that the entire volume of the solder can be saturated very quickly with the dissolved substrate materials. The faster the diffusion rate of the substrate material the quicker the consumption of the substrate and the thicker the IMC layer is. The diffusion rate depends to a large extent on the elemental compositions of the solder and the substrate.

Because of their low melting points, solders normally work at high homologous temperatures even at the room temperature condition [97]. When solders have to be used in an isothermal aging condition, the formation of a thick IMC layer degrades the solder joint lifetime [106]. Although the National Electronics Manufacturing Initiative (NEMI) has recommended Sn-Ag-Cu solder alloy for reflow soldering and Sn-Cu solder alloy for wave soldering as the replacements of eutectic Sn-Pb solder [107], their IMC growth rates are higher than that of the Sn-Pb solder alloy and this may influence the joint strength and the long-term reliability. Due to the high concentration of Sn, Sn-Ag-Cu lead-free solder possesses a high rate of interfacial reaction with Cu and forms Cu-Sn

IMC. As a result, the Cu (supplied from the substrate) is consumed rapidly by the molten Sn-Ag-Cu solder. If all the Cu substrate is consumed, the Cu-Sn compound tends to transform from a scallop-like morphology to spheroid-type morphology [108] and this degrades the joint strength. Therefore, when a fourth-element is added to the Sn-Ag-Cu solder alloy to reduce the melting temperature or to improve the wettability, the new alloy must have a suitable rate of the consumption of the substrate materials and an acceptable growth rate of the IMC layers.

Although previous studies [95] have shown that Sn-Cu solder consumes less amount of base metal than the Sn-Ag and the Sn-Ag-Cu solders and the IMC thickness is acceptable, its wetting capability is inferior to other solder alloys. Because of this, the Sn-Cu solder can only be used for through holes and it's only suitable for single sided wave soldering on printed circuit boards [109]. One possible way of improving the wettability is to alloy this solder with other elements. Recently it has been discovered that the concentration of alloying elements can also control the reaction properties of Sn-Cu solder [110] and hence the microstructural evolution and the IMC formation [111]. Usually, the interfacial reaction takes place during wetting (the initial condition of soldering at liquid state) and thereafter in aging condition (throughout the operational life in solid state). Tu et al [112] has reported that the wetting reaction is four orders of magnitude faster than the solid state reaction during aging and the morphologies of the reaction species are completely different. Therefore, when an additional element is added to the Sn-Cu solder to improve its wettability, it must be ensured that the new alloy composition does not encourage a higher IMC layer growth rate.

In this work 1wt% Bi has been added to the Sn-2.8Ag-0.5Cu solder and 0.3wt% Ni has been added to the Sn-0.7Cu solder because small amount (<3wt%) of Bi lowers alloy melting point and increases hardness and tensile strength; on the other Ni is available, environmentally friendly, reduces the chance to form tin whiskers and doesn't alter the original properties of the parent alloy. According to the above discussions, in order to make the newly developed Sn-2.8Ag-0.5Cu-1.0Bi and Sn-0.7Cu-0.3Ni solders successful lead-free joining materials, the following conditions must be met.

1. Bi improves the wettability of Sn-2.8Ag-0.5Cu solder and Ni improves the wettability of Sn-0.7Cu solder.
2. The addition of Bi into Sn-2.8Ag-0.5Cu solder and Ni into Sn-0.7Cu solder helps to reduce the consumption of substrate material and inhibits the excessive growth of the IMC layer during soldering.
3. Addition of Bi into Sn-2.8Ag-0.5Cu solder and Ni into Sn-0.7Cu solder helps to reduce the growth rate of the IMC layers during isothermal ageing.

To facilitate the investigations of the above mentioned fundamental issues, the entire work has been structured as follows:

1. The wettability of Sn-2.8Ag-0.5Cu-1.0Bi solder on Cu and Ni substrates will be compared with that of the Sn-Pb solder. That will help to understand how close or how far the wettability of the lead-free solder to that of the leaded solder is.
2. A comparison between the wetting behaviours of Sn-2.8Ag-0.5Cu and Sn-2.8Ag-0.5Cu-1.0Bi solders on Cu and Ni substrates will be made. This will help to understand how the addition of Bi influences the wettability of Sn-2.8Ag-0.5Cu solder.
3. The wetting behaviours of Sn-0.7Cu and Sn-0.7Cu-0.3Ni solders on Cu and Ni substrates will be compared. This will also help to identify the effect of the addition of Ni on the wettability of Sn-0.7Cu solder.
4. Computer modelling of the wetting behaviours of the solders will be carried out to investigate the effect of several parameters such as substrate perimeter, immersion depth, contact angle, and solder bath radius on the wettability.
5. The dissolution of the substrates into the solders during wetting reaction and the growth of the IMC layer at the solder-substrate interfaces will be investigated. The results will be compared between Sn-2.8Ag-0.5Cu and Sn-2.8Ag-0.5Cu-1.0Bi solders, and between Sn-0.7Cu and Sn-0.7Cu-0.3Ni solders respectively. Computer modelling of the dissolution of Cu into the molten solders will also be performed to understand the diffusion process.

6. The growth behaviour of the IMC layers during isothermal ageing will be investigated and the results will be presented as the comparisons between Sn-2.8Ag-0.5Cu and Sn-2.8Ag-0.5Cu-1.0Bi solders and Sn-0.7Cu and Sn-0.7Cu-0.3Ni solders respectively.

The wettability of the solders can be evaluated using a number of methods such as the area of spread test, the edge dip and capillary rise test, the globule wetting test method, rotary dip test, wetting balance test, and microwetting balance test. In this work, the widely used wetting balance test will be carried out as this is the most versatile method [113] and is suitable for the quantitative information about the wettability of specimens in any shape and a wide range of geometric dimensions.

4.2 Experimental Procedures

4.2.1 The Measurement of Contact Angle and Wetting Force

The wettability test was performed using the solderability tester MENISCO ST 50 with computer control and data acquisition functions. The tests were performed with the solder bath temperature set at 255 °C, 275 °C and 295 °C and the dwell time set at 10 s. The immersion depth and the immersion speed were set at 3 mm and 21 mm/sec respectively.

During the soldering process the wetting interaction was dominated by three surface energies namely the surface energy of the substrate/flux γ_{SF} , surface energy of the substrate/liquid solder interfacial area γ_{SL} and the surface energy of the liquid solder/flux γ_{LF} . The equilibrium contact angle was measured with the help of these three surface energies through the Young-Dupré equation

$$\gamma_{SF} = \gamma_{SL} + \gamma_{LF} \cos\theta_c \quad (4.1)$$

where θ_c is the contact angle. The lower the contact angle the higher the wettability is. The notations and the shape of the solder surface during the wetting balance test are shown in the Figure 4-1.

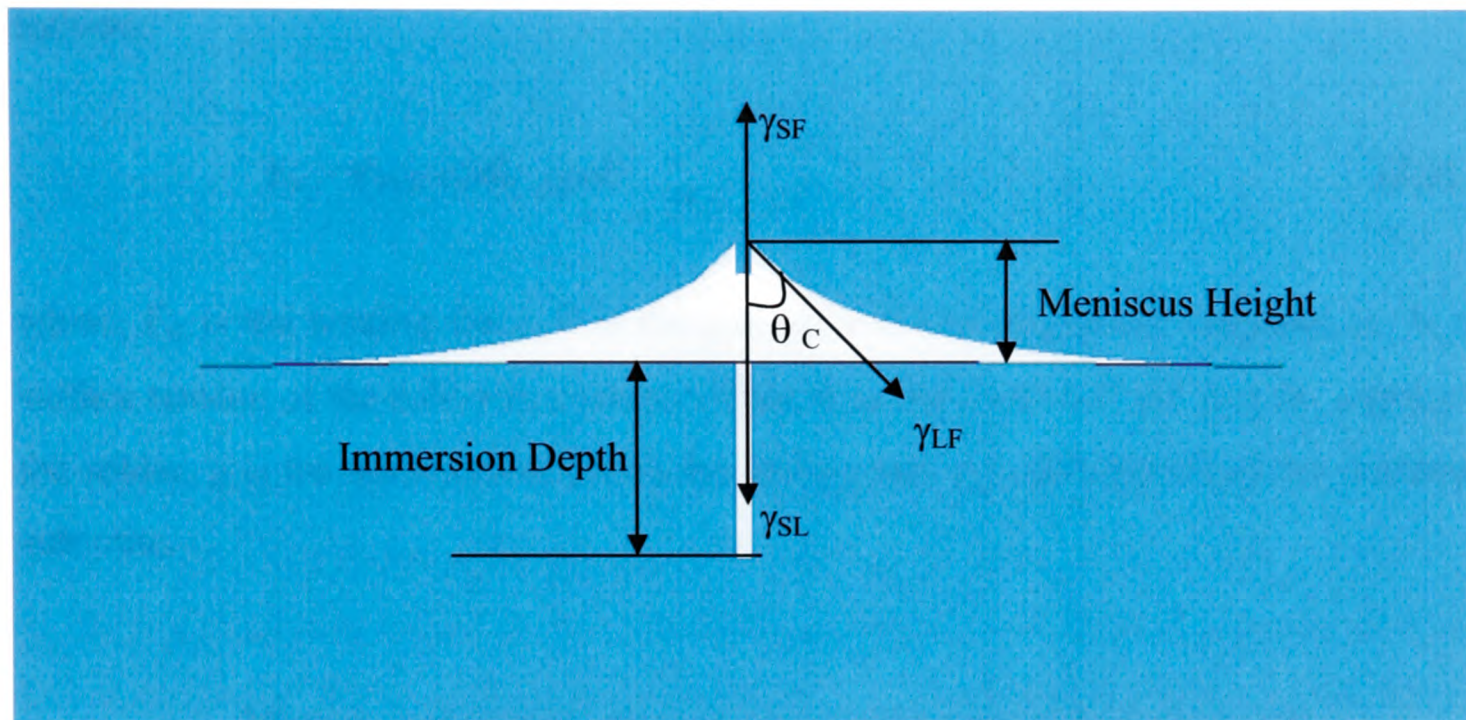


Figure 4-1: The test configuration for the wetting balance technique and modelling.

At the initial stage of the wetting balance test, an upward force is exerted on the partially immersed substrate. This force is caused by the temporary non-wetting at this stage [114]. After certain period of time, wetting takes place around the substrate and the solder bath surface becomes flat. Then, as wetting proceeds, the molten solder rises along the substrate. It will eventually reach a maximum height. The difference between this maximum height and the solder bath surface level is known as the meniscus height (see Figure 4-1). The wetting force exerted by the molten solder on the test substrate is directly proportional to this meniscus height [115] and therefore it also changes with time and reaches a maximum value. The time it takes to reach a preset wetting force is called the wetting time. The wetting force and the wetting time are often used as the criteria for the wettability of the solder. Good wettability means higher wetting force and shorter wetting time. In this work, the wetting force is used as the wettability parameter in the

experiments. A typical wetting force vs. time curve in the wetting balance test is shown in the Figure 4-2.

The total wetting force was calculated by subtracting the buoyancy force (exerted by the displaced solder by the immersed substrate volume) from the surface tension force as follows:

$$F_w = P\gamma_{LF} \cos\theta_c - \rho gV \quad (4.2)$$

where, F_w is the wetting force, P is the perimeter of the submerged substrate, γ_{LF} is the surface tension of the solder in contact of flux, θ_c is the contact angle, ρ is the density of the solder, g is the acceleration due to the gravity and V is the volume of the immersed substrate.

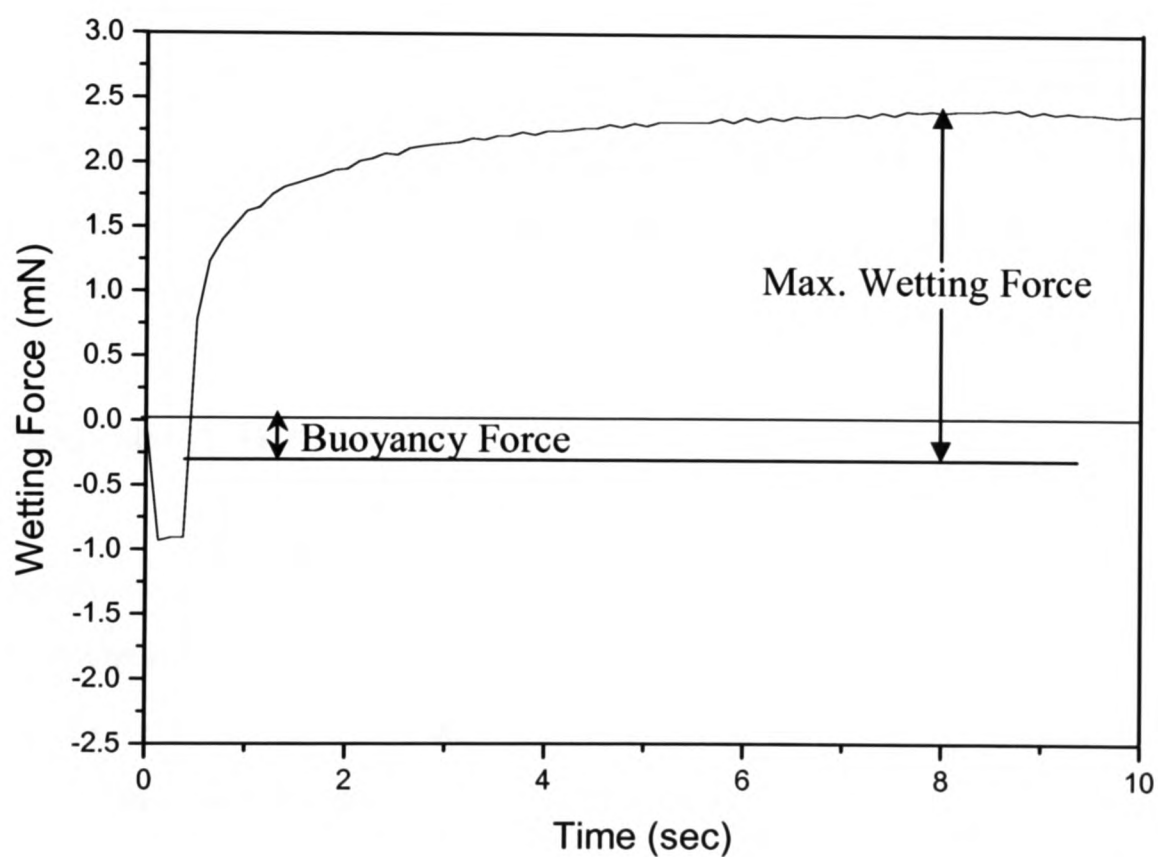


Figure 4-2: A typical force-time curve for the wetting balance test.

4.2.2 Substrate Preparation

Pure (99.99%) Cu and Ni were cut from rolled plain sheet materials into rectangular specimens. They were then flattened. Before conducting the wetting balance tests, the substrates were degreased with a 1:1 solution of HCL and deionised water for 1-3 minutes. Finally, they were cleaned using ethanol and dried to remove any contamination. These substrates were then coated with flux and used for the tests.

4.2.3 Solders and Fluxes

The Sn-2.8Ag-0.5Cu, Sn-2.8Ag-0.5Cu-1.0Bi, Sn-0.7Cu and Sn-0.7Cu-0.3Ni lead-free solders with melting temperatures of 218, 214, 227 and 227 °C respectively were assessed for their wettabilities. The Sn-37Pb solder which has the eutectic temperature of 183 °C was also studied for comparison. For simplicity, these solders will be called the Sn-Ag-Cu, Sn-Ag-Cu-Bi, Sn-Cu, Sn-Cu-Ni and Sn-Pb solders. Three fluxes were used to evaluate the wettability for different solder/flux systems; they are the NC (no-clean), R (non-activated) and the WS (Water Soluble) type. The surface tensions of these fluxes are 370 mN/m, 445 mN/m and 415 mN/m.

4.2.4 Analysis of Microstructures

The microstructures at the interface between solder and substrate were investigated through a Philips XL 40 FEG scanning electron microscope (SEM) equipped with an energy dispersive X-ray spectrometer (EDX). The samples were prepared by dipping the test coupons into molten solders and then they were taken out to cool to room temperature. They were then mounted using resin and hardener and cured at room temperature. They were then mechanically ground and polished in order to obtain fine cross sections of the solder/substrate interfaces. Finally, the cross-sectioned samples were gold-coated and ready for the SEM/EDX analysis.

4.2.5 Dissolution of Substrates into Solder during Wetting

In order to study the dissolution of substrates in molten solders, solder/Cu and solder/Ni reaction couples were prepared through the wetting balance tests as described above. Pure (99.99%) Cu and Ni of thickness 0.22 mm were used as substrate. Sn-2.8Ag-0.5Cu, Sn-2.8Ag-0.5Cu-1.0Bi, Sn-0.7Cu and Sn-0.7Cu-0.3Ni lead-free solders were used for soldering. Sn-37Pb solder was also used as a reference soldering material. A commercial NC flux was used in this experiment. The tests were performed with the soldering temperatures of 255, 275 and 295 °C and the total reaction time was 10 s. The microstructures of solder/substrate interfaces were investigated as described in section 4.2.4.

4.2.6 The Growth of IMC Layer during Isothermal Aging

A number of Cu-substrates with NC-flux were dipped in molten Sn-2.8Ag-0.5Cu, Sn-2.8Ag-0.5Cu-1.0Bi, Sn-0.7Cu and Sn-0.7Cu-0.3Ni lead-free solder baths at 255 °C. The samples were then aged isothermally in a high-temperature oven for 2, 6, 10 and 14 days respectively. The temperature inside the oven was maintained at 150 °C with a maximum variation of ± 1 °C. The growth of the IMC layer was investigated through the microstructural analysis as described in section 4.2.4.

4.3 Computer Modelling Procedures

4.3.1 Wetting Balance Tests

Computer modelling of the wetting balance test was carried out using the software SURFACE EVOLVER [67]. The dimensions of the test specimens used in the modelling work were the same as that of the experiment. The contact angles measured from the wetting balance tests were used in the modelling to estimate the corresponding maximum wetting forces and the meniscus heights. The solution of the computer model in Figure 4-

3 shows the meniscus at the solder-substrate interface due to the surface tension. The effects of several parameters such as the substrate perimeters and the immersion depths on the wettability of Sn-Ag-Cu-Bi solder alloy were investigated. The effects of contact angles, solder bath depths and bath radius on the wettability have also been investigated for this lead-free solder.

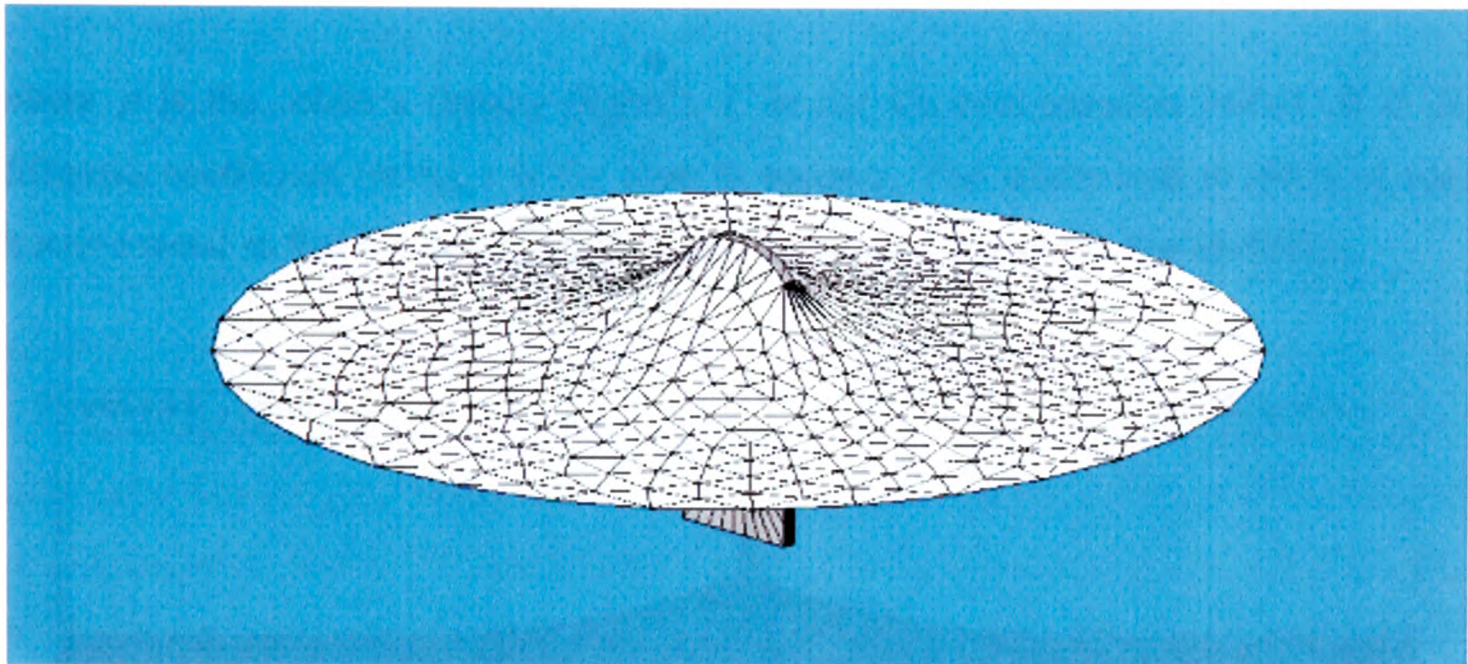


Figure 4-3: The solution of the computer model showing the meniscus height at the solder-substrate interface due to the surface tension.

4.3.2 Dissolution of Substrates into Molten Solders during Wetting Balance Tests

The dissolution of substrate into the molten solder bath during the wetting balance test was modelled and analyzed by using the modelling software PHYSICA [68]. The shape of the solder around the substrate was modelled using the software tool SURFACE EVOLVER and then exported to the software PHYSICA in the dissolution studies. In this section, the Pb-free Sn-0.7Cu solder and the lead containing Sn-37Pb solder are studied to find out the amount (wt%) of the dissolved Cu into these solders in the wetting process. The estimated dissolved amount is then compared with the experimental measurements to verify the modelling results. The dissolved amount (wt%) is measured

experimentally with the help of EDX analysis of scanning electron microscopy (SEM). The computer grid used in the analysis is shown in Figure 4-4.

The governing equation for the diffusion problem is

$$\frac{\partial \rho C}{\partial t} + \nabla \cdot (D \nabla C) = 0.0 \quad (4.3)$$

where ρ is the solder's density (kg/m^3), C is the Cu concentration (wt%), D is the diffusion coefficient (m^2/s), t is the time in seconds. The solder bath is made of non-reactive metal so that the only Cu diffusion is taking into account in the modelling.

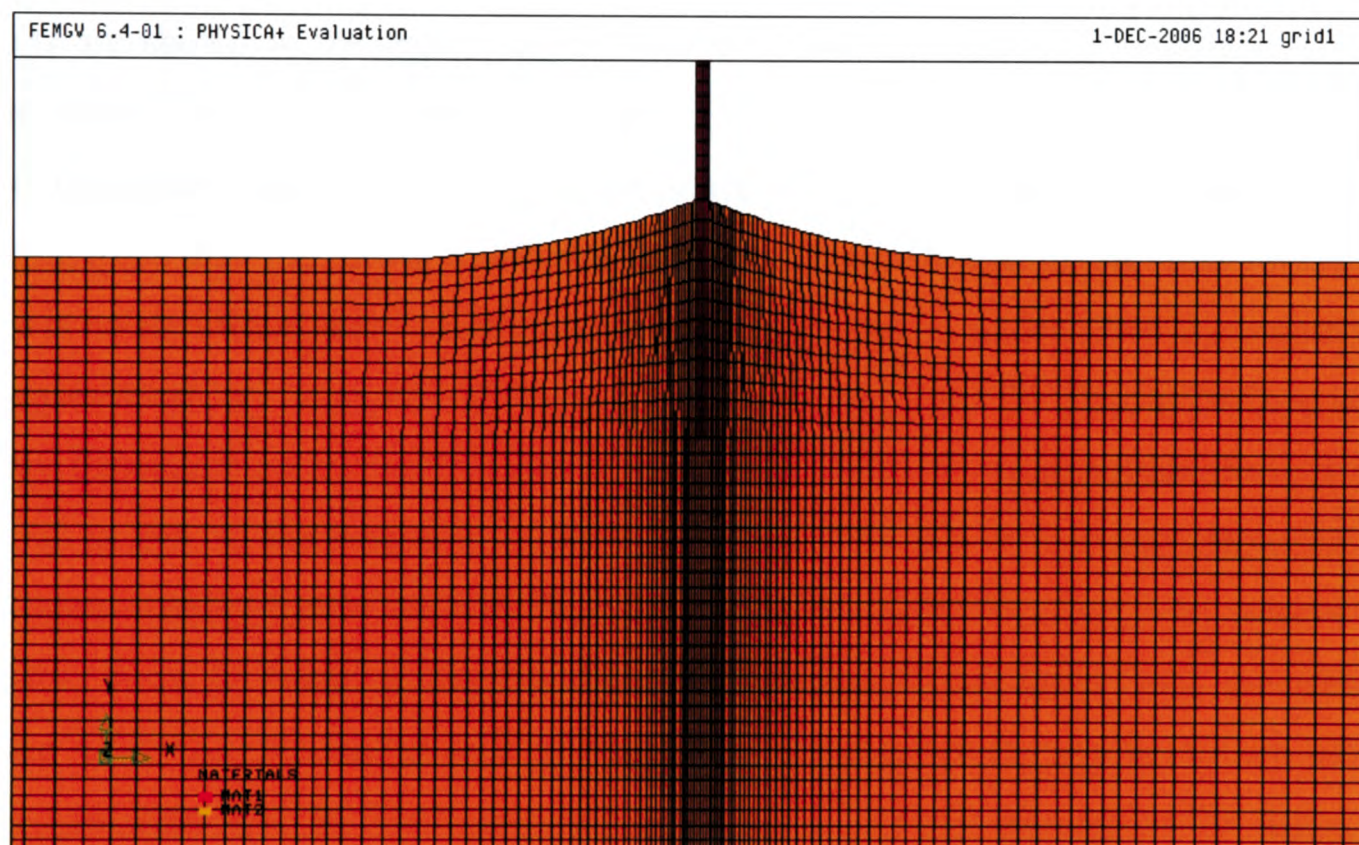


Figure 4-4: Computer mesh used in the analysis of dissolution of Cu into solder during wetting balance tests.

4.4 Results and Discussions

4.4.1 Wetting Behaviours of Pb and Pb-free Solders on Cu and Ni Substrates

4.4.1.1 Wetting Behaviours of Sn-2.8Ag-0.5Cu-1.0Bi Lead-free Solder and Sn-37Pb Solder on Cu and Ni Substrates

The maximum wetting forces as a function of solder bath temperatures for Cu-substrate are shown for three fluxes in the Figures 4-5 (a), (b) and (c). Experimental and modelling results are shown in the figures as the measured and the estimated respectively. From these three figures, it is evident that the experimental and the modelling results show very good agreement. For all the three-fluxes, the eutectic Sn-Pb solder system has the higher wetting force than the Sn-Ag-Cu-Bi solder system. Figure 4-5(a) for NC-flux reveals that there is no significant increase in the wetting force for Sn-Pb solder when the temperature increases from 255 °C to 295 °C. The maximum wetting force for Sn-Ag-Cu-Bi solder is highly dependent on the solder bath temperatures. When the temperature changes from 255 °C to 295 °C the wetting force increases from 1.84 mN to 2.38 mN. However, the maximum wetting forces for both the eutectic Sn-Pb and the Sn-Ag-Cu-Bi solders with WS-flux have increased noticeably with the increase of the solder bath temperature. Figure 4-5(c) reveals that at 255, 275 and 295 °C temperatures, the maximum wetting forces are 2.62 mN, 2.77 mN and 3.15 mN respectively for eutectic Sn-Pb solder and 1.84 mN, 1.95 mN and 2.45 mN respectively for Sn-Ag-Cu-Bi solder. Therefore, the increase in the reflow temperature results in better wettability with NC and WS fluxes. When R-type flux is used as shown in Figure 4-5(b), the maximum wetting force increases with the increase in the solder bath temperature for eutectic Sn-Pb solder whereas Sn-Ag-Cu-Bi solder exhibits similar wetting force for 275 °C and 295 °C temperatures. Hence, R-type flux may not be suitable for efficient soldering with the lead free Sn-Ag-Cu-Bi solder.

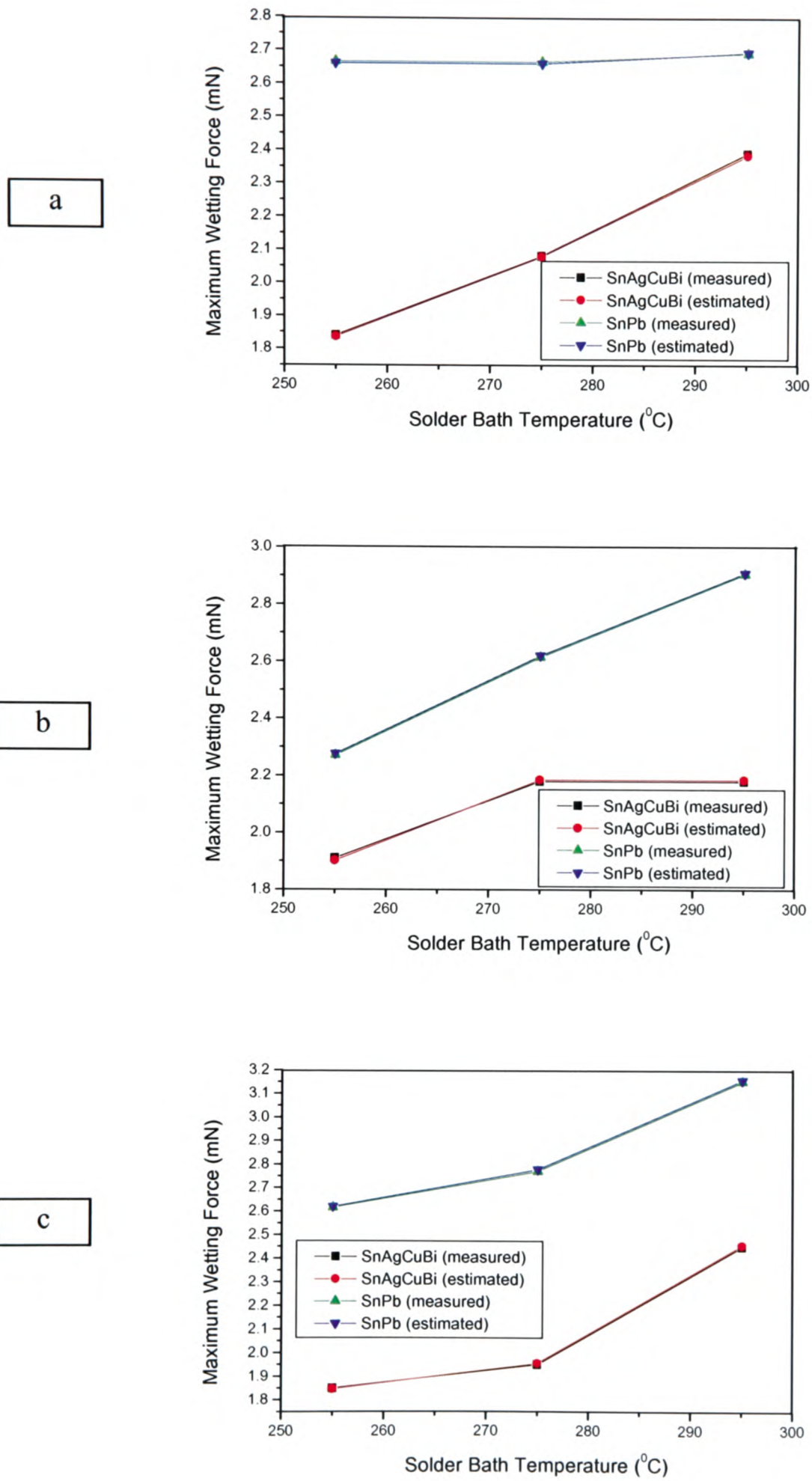


Figure 4-5: Wetting forces as a function of solder bath temperatures for Cu-substrate with (a) NC- flux (b) R-type flux and (c) WS-flux.

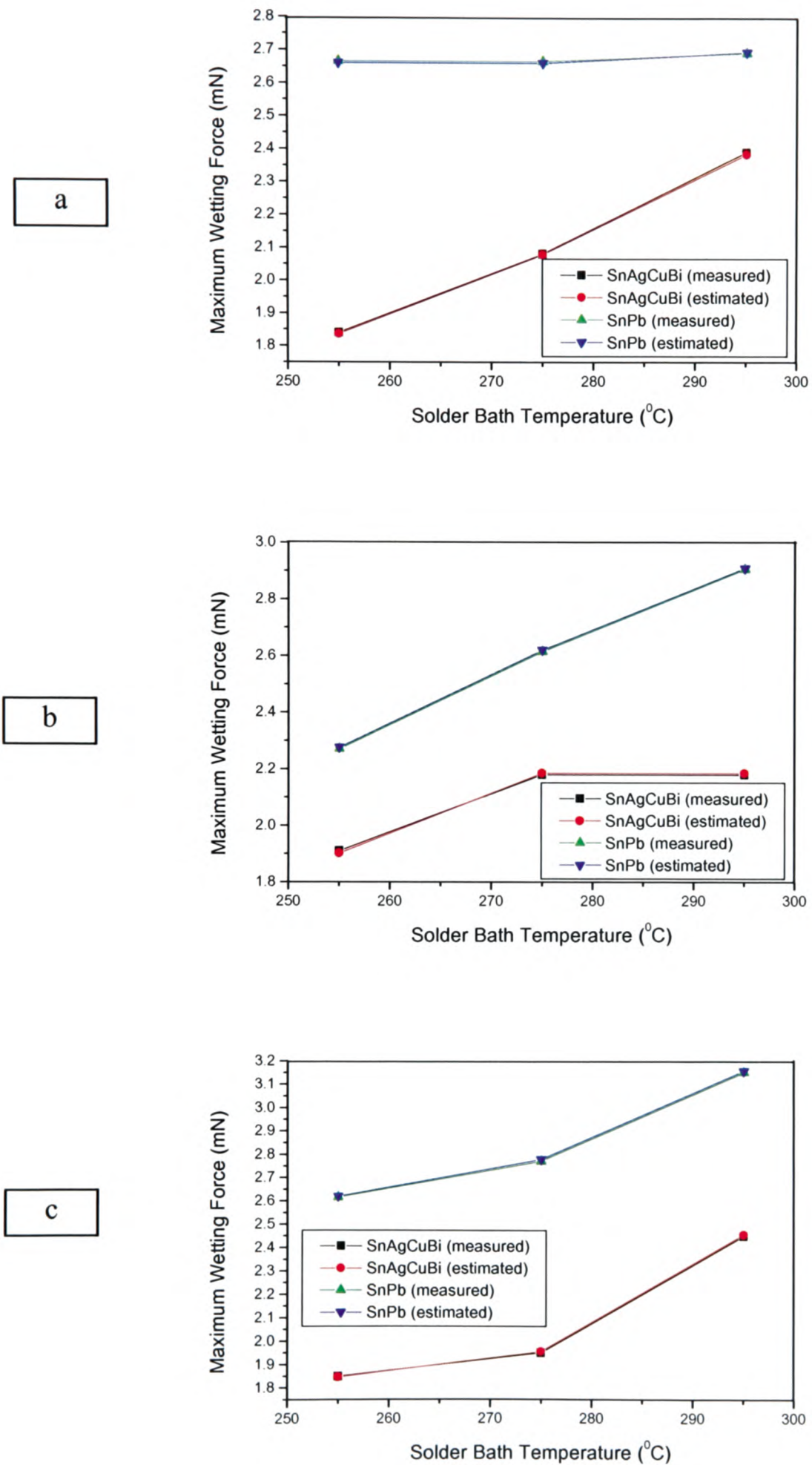


Figure 4-6: Wetting forces as a function of solder bath temperatures for Ni-substrate with (a) NC- flux (b) R-type flux and (c) WS-flux.

The maximum wetting forces for Sn-Ag-Cu-Bi solder in comparison with Sn-Pb solder are shown in Figures 4-6 (a), (b) and (c) for Ni substrate. In the case of NC-flux as shown in Figure 4-6(a), there is no difference in maximum wetting forces for Sn-Pb solder at 255 and 275 °C temperature, whereas Sn-Ag-Cu-Bi solder notices the increase in the maximum wetting force values from 0.137 mN to 0.270 mN for these two temperatures. In the case of 295 °C temperature both Sn-Ag-Cu-Bi and Sn-Pb solders exhibit better wettability by showing the maximum wetting forces as 0.455 mN and 0.778 mN respectively.

Negative wetting force i.e. non-wetting regardless the solder-types and solder bath temperatures occurred when the R-type flux is used as shown in Figure 4-6 (b). Here, the wetting force curves for both Sn-Ag-Cu-Bi and Sn-Pb solders move from negative to zero/positive wetting force with the increase in the solder bath temperature.

Figure 4-6 (c) shows that the WS-flux results in the best wettability among the three-fluxes on Ni-Substrate. For the Sn-Pb solder, the maximum wetting force increases when the solder bath temperature increases from 255 to 275 °C but it decreases when the temperature increases from 275 °C to 295 °C. The wettability of the Sn-Ag-Cu-Bi solder increases with the bath temperature it has slightly better wettability than the eutectic Sn-Pb solder at 295 °C solder bath temperature.

The maximum wetting forces and corresponding meniscus heights are estimated through the computer modelling by varying the parameters such as substrate perimeters, immersion depths. The results are shown in Figures 4-7 and 4-8. Equation (4.2) implies that when the contact angle θ_c increases, the surface tension force decreases. If the wettability is very poor, θ_c will be large and wetting force may become negative. According to equation (4.2), it is evident that the surface tension force is the product of substrate perimeter P , and the solder/flux surface tension γ_{LF} and the cosine value of contact angle θ_c . Figure 4-7 exhibits the dependency of the wetting force and the meniscus height on the perimeter (P) of the substrate.

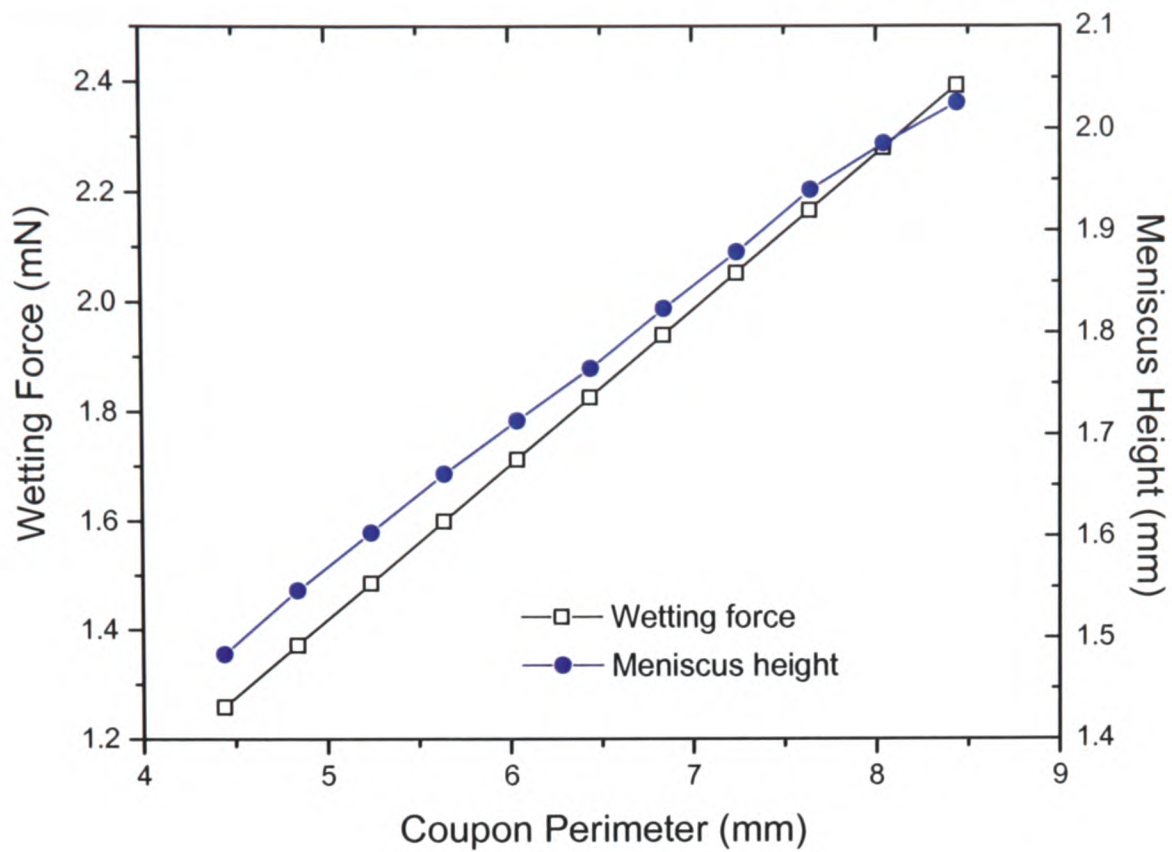


Figure 4-7: Dependency of estimated wetting force and meniscus height on the substrate perimeter with SnAgCuBi-solder.

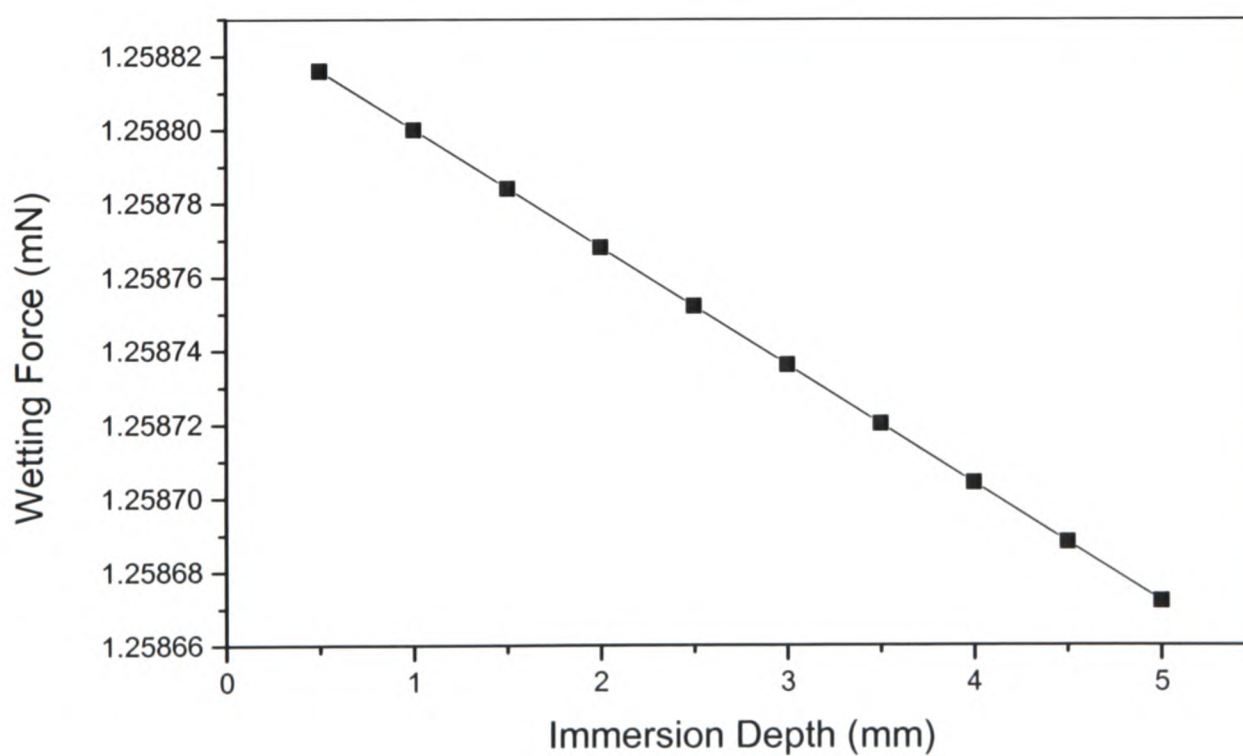


Figure 4-8: Effect of immersion depth on the estimated wetting force for SnAgCuBi solder.

In this simulation, the perimeter value is controlled by changing the width of the substrate. The result shows that for wider substrate both the wetting force and the meniscus height increase. Potentially meniscus height measurement can be used to estimate the wettability but according to this modelling result the shape of the specimen can affect the results. The effect of the immersion depth has also been modelled. Figure 4-8 shows that increasing the immersion depth results in decreased wetting force. This is caused by the increase of the buoyancy force as the immersion depth increases.

4.4.1.2 Wetting Behaviours of Sn-2.8Ag-0.5Cu and Sn-2.8Ag-0.5Cu-1.0Bi Solders on Cu and Ni Substrates

Figure 4-9 shows the typical force-time curves for the NC-flux with Cu and Ni substrates where the solder bath temperature was 255 °C. Based on the wetting force data, the contact angles can be calculated and used as another measure of the solders' wettability for the particular flux/substrate used. Figure 4-10 represents the typical contact angle-time curves for NC-flux with Cu and Ni substrates respectively for a solder bath temperature of 255 °C. These curves are the results of Equation (4.2) and they clearly show that when the wetting force increases the contact angle decreases.

In Figure 4-11, two solder surface profiles are shown. One is for an ad hoc wettable system with a wetting angle of 10° and the other is for a nonwetable system with a wetting angle of 120°. For the wettable system (Figure 4-11a), the molten solder climbs up the substrate. For the non-wetting system (Figure 4-11b), meniscus height is negative and the wetting force is also negative. Lopez et al [114] has given a wettability guide using the contact angle values (see Table 4-1). According to this guide, the wetting is perfect when the contact angle is less than 10° and it's poor when the contact angle is greater than 55°.

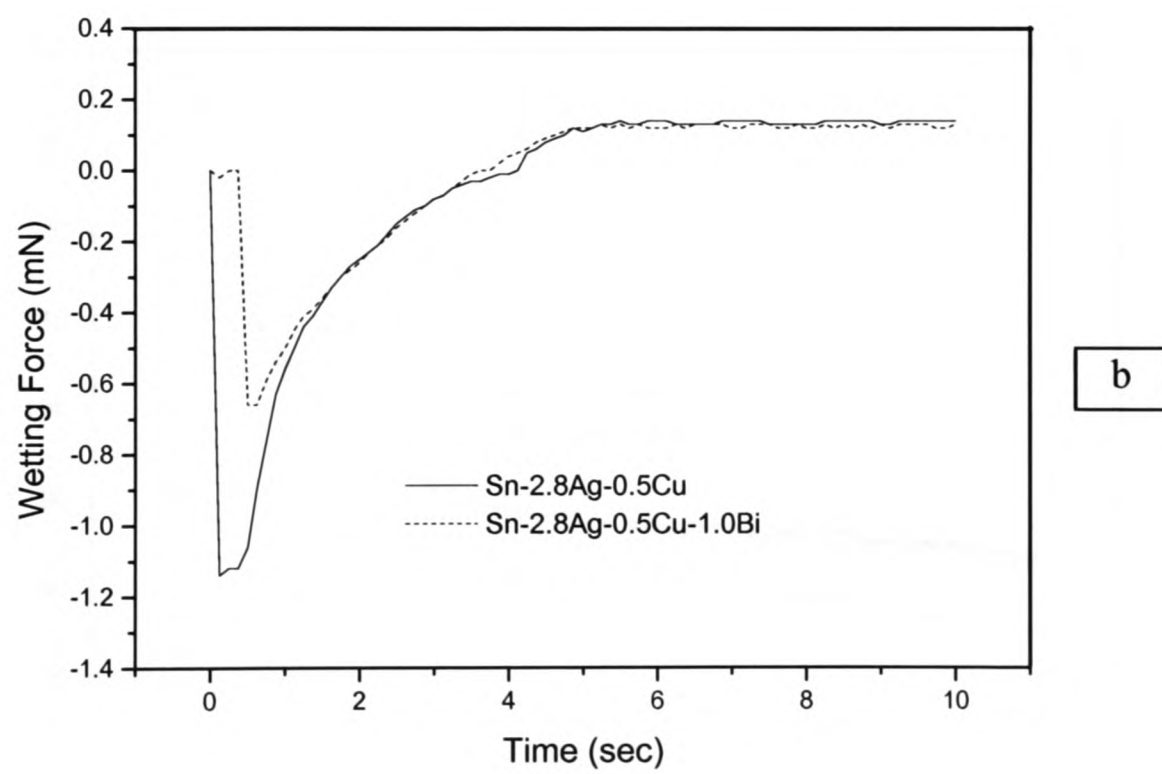
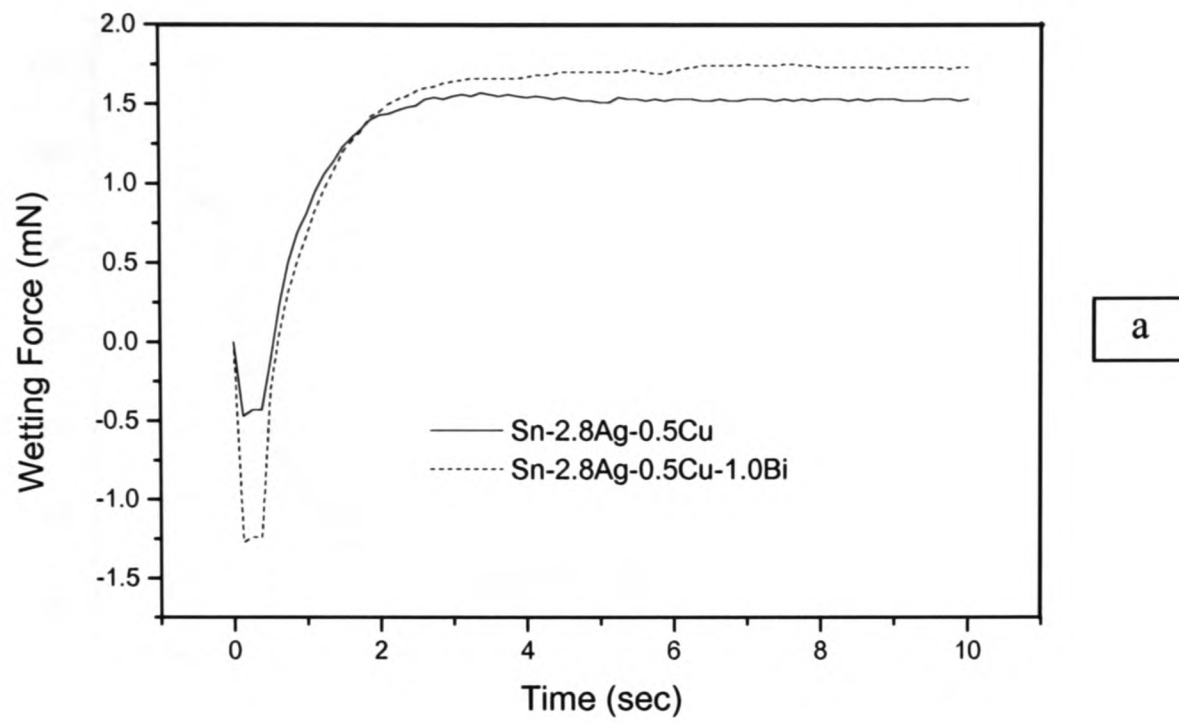
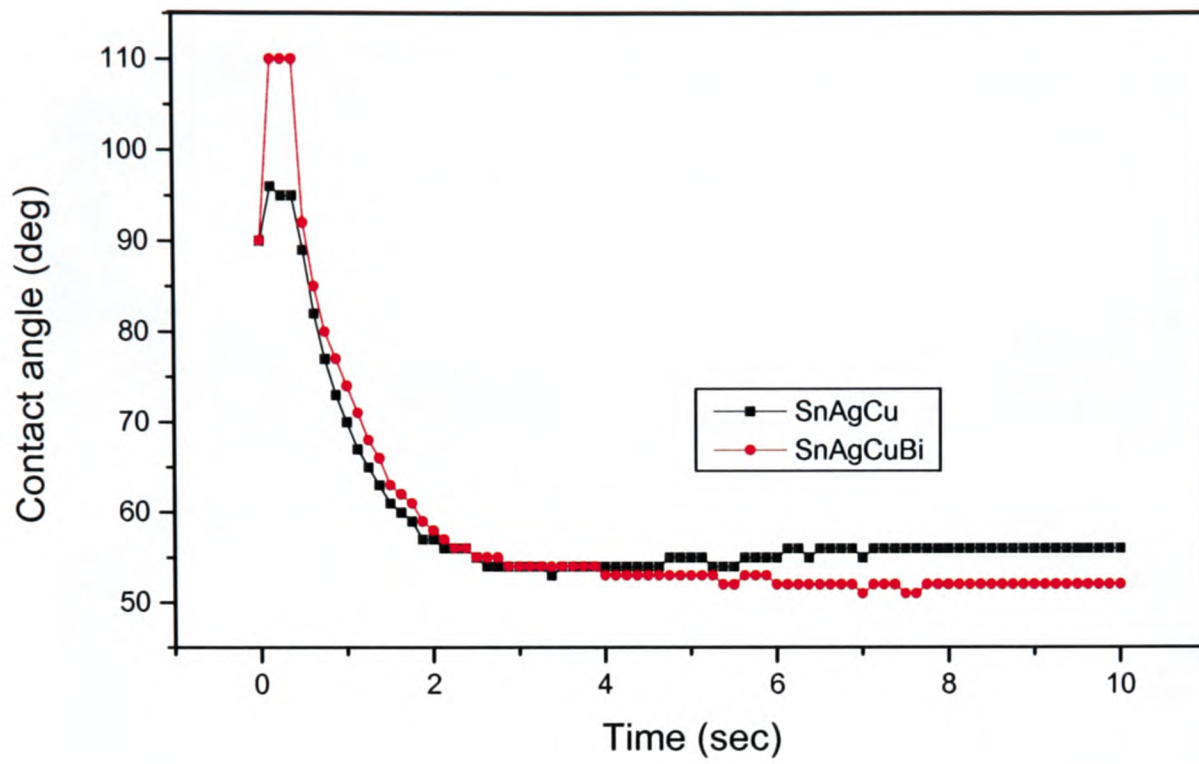
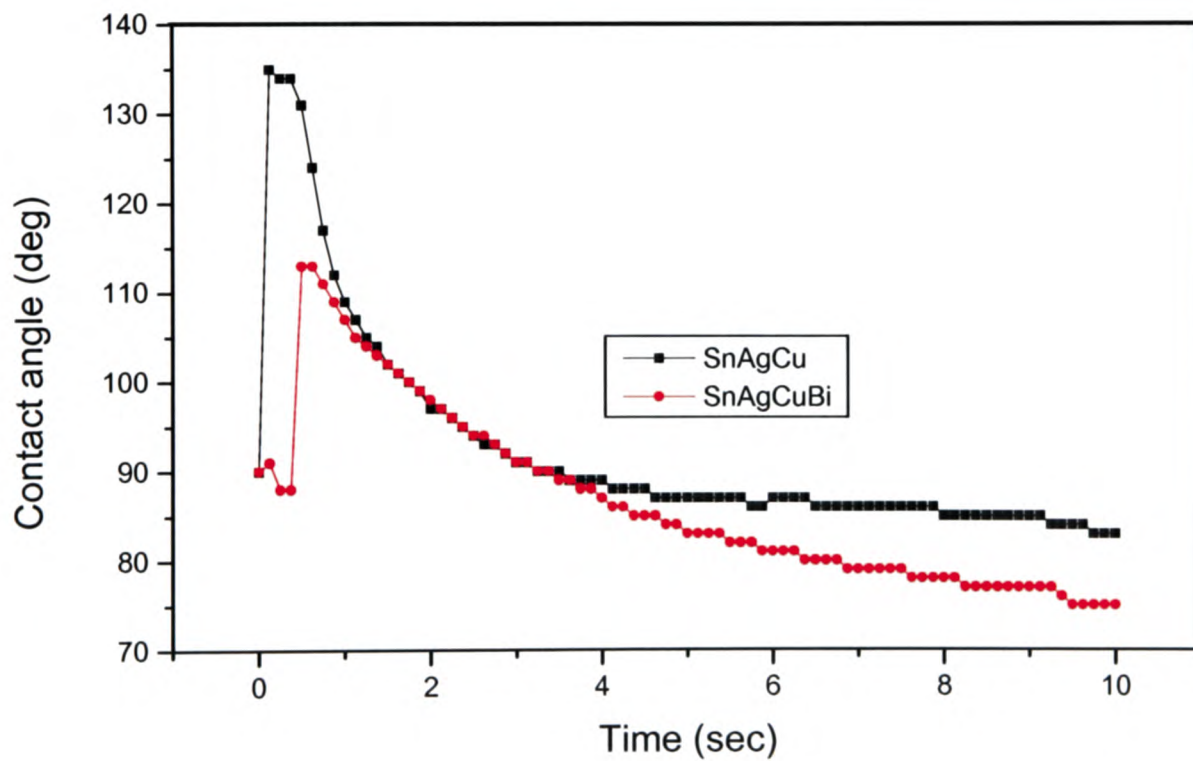


Figure 4-9: Force-time curve for (a) Cu and (b) Ni substrates with NC-flux. Immersion depth = 3 mm, immersion speed = 21mm/sec, immersion time = 10 s and solder bath temperature = 255 °C.



(a)



(b)

Figure 4-10: Contact angle-time curve for (a) Cu and (b) Ni substrates with NC-flux. Immersion depth = 3 mm, immersion speed = 21mm/sec, immersion time = 10 s and solder bath temperature = 255 °C.

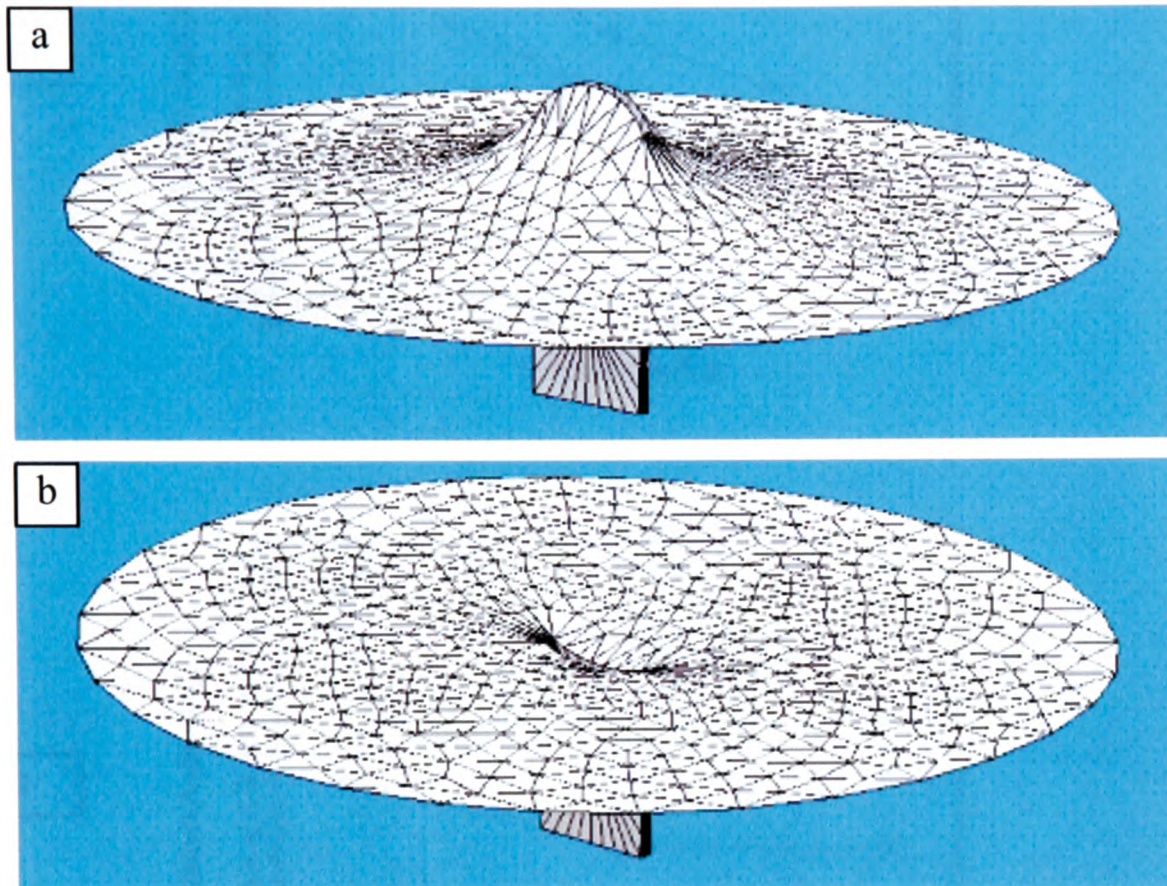


Figure 4-11: Modeling results showing the conditions of (a) wetting (contact angle = 10°) and (b) non-wetting (contact angle = 120°).

Table 4-1: Wettability evaluation based on the contact angles (θ_c)

Range of Contact Angle (θ_c)	Relative wettability
$0^\circ < \theta < 10^\circ$	Perfect
$10^\circ < \theta < 20^\circ$	Excellent
$20^\circ < \theta < 30^\circ$	Very good
$30^\circ < \theta < 40^\circ$	Good
$40^\circ < \theta < 50^\circ$	Adequate
$55^\circ < \theta < 70^\circ$	Poor

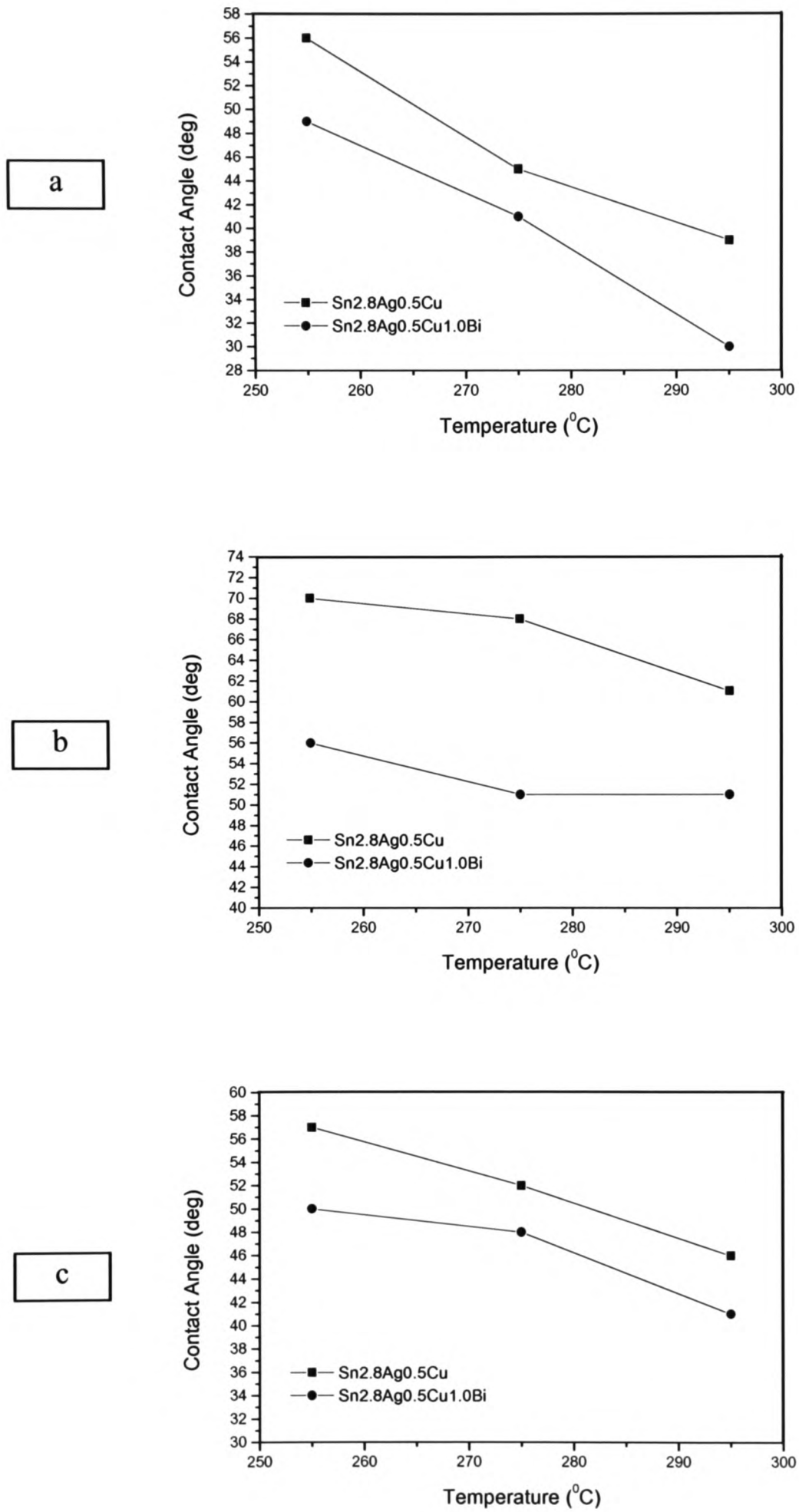


Figure 4-12: Contact angles as a function of solder bath temperatures for Cu-substrate with (a) NC-flux, (b) R-flux and (c) WS-flux.

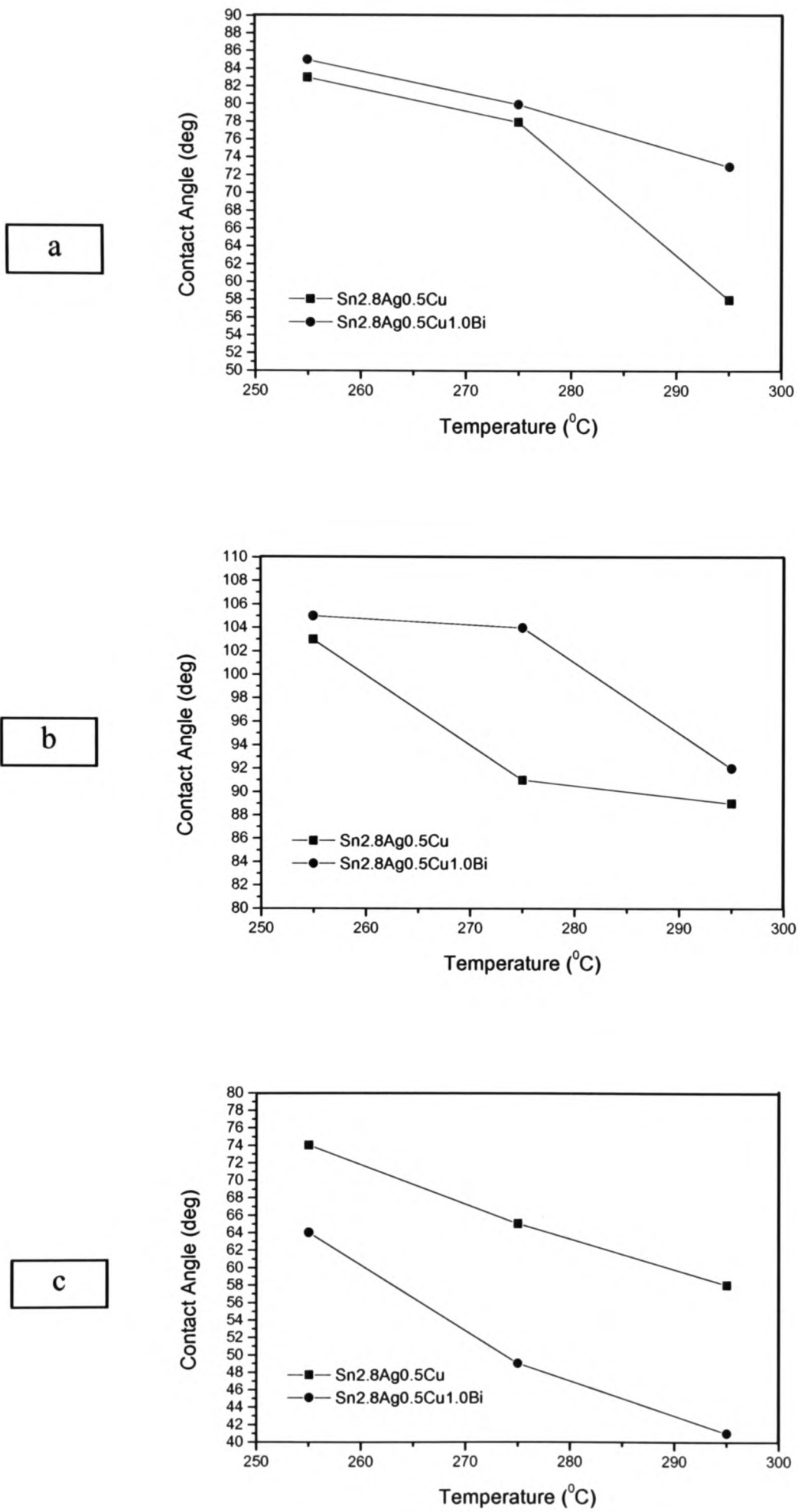


Figure 4-13: Contact angles as a function of solder bath temperatures for Ni-substrate with (a) NC-flux, (b) R-flux and (c) WS-flux.

Figure 4-12(a) shows the contact angles for the NC-flux/Cu substrate system. It is found that the contact angles for Sn-2.8Ag-0.5Cu-1.0Bi and Sn-2.8Ag-0.5Cu solders at 255 °C are 49° and 56° respectively whereas these values become as 41° and 45° respectively when the solder bath temperature increases to 275 °C. When the solder bath temperature increases to 295 °C, the contact angle is 30° for the Sn-2.8Ag-0.5Cu-1.0Bi solder and 39° for the Sn-2.8Ag-0.5Cu solder. For all solder bath conditions, Bi-containing solder gives lower contact angles. According to the guideline in Table 4-1, very good wetting can be achieved with the Bi-containing solder if the soldering can be performed at temperatures higher than 295 °C.

Figure 4-12(b) shows the contact angles for the R-type flux. The contact angles for the Sn-2.8Ag-0.5Cu solder are surprisingly high in comparison with the Sn-2.8Ag-0.5Cu-1.0Bi solder. The contact angles of Sn-2.8Ag-0.5Cu solder for 255, 275 and 295 °C solder bath temperatures are 70, 68 and 61 degrees respectively whereas these values for Sn-2.8Ag-0.5Cu-1.0Bi solder are 56, 51 and 51 degrees respectively. According to Table 4-1 it can be said that the wettability of Sn-2.8Ag-0.5Cu solder with the R-type flux is poor. Therefore, an addition of 1wt% Bi into the Sn-2.8Ag-0.5Cu solder may help to achieve adequate wetting with R-type flux. Figure 4-12(c) represents the wetting behaviour of these two lead-free solders with WS-flux where similar trend in the contact angles with the increase of solder bath temperature has been presented. In this case, the Sn-2.8Ag-0.5Cu-1.0Bi solder exhibits better wettability than the Sn-2.8Ag-0.5Cu solder.

Contact angles for the Sn-2.8Ag-0.5Cu and Sn-2.8Ag-0.5Cu-1.0Bi solders on Ni substrate with three different solder bath temperatures with NC-flux are shown in Figure 4-13(a). Contact angles of Sn-2.8Ag-0.5Cu and Sn-2.8Ag-0.5Cu-1.0Bi solders at 255 °C are 83 and 85 degrees respectively whereas these values are 78 and 80 degrees respectively for 275 °C bath temperature. For the Sn-2.8Ag-0.5Cu solder, the contact angle decreases rapidly as the bath temperature is increased to 295 °C and the contact angle decreases from 78 to 58°. At this temperature, the Sn-2.8Ag-0.5Cu-1.0Bi solder has a very large contact angle of 73 degree, which is a sign of relatively poor wetting.

When the R-type flux is used, both solders exhibit very large contact angle with the indication of non-wetting. Though the contact angles for both solders decrease with the increase of solder bath temperature as shown in Figure 4-13(b), the improvement in the wetting behaviour is not very significant. Therefore, it can be said that the R-type flux may not be suitable for soldering purposes with the Sn-2.8Ag-0.5Cu and the Sn-2.8Ag-0.5Cu-1.0Bi solders.

It is believed that the addition of Bi into the Sn-2.8Ag-0.5Cu solder could enhance its wettability on the Ni-substrate and this expectation does not come true for either NC or R-type fluxes. However, the expected results have been documented for WS-fluxes as shown in Figure 4-13(c). The contact angles at 255 °C are 74 and 64 degrees for the Sn-2.8Ag-0.5Cu and the Sn-2.8Ag-0.5Cu-1.0Bi solders respectively. When the solder bath temperature is increased to 275 °C the contact angle is 65° for the Sn-2.8Ag-0.5Cu solder and 49° for the Sn-2.8Ag-0.5Cu-1.0Bi solder. At a bath temperature of 295 °C, the contact angles are 58 and 41 degrees for the two solders.

The modelling results for the wetting balance test shown in Figure 4-14 reveal that increase in the contact angle results in the decrease in the wetting force and the meniscus height. This happens because the cosine value of large contact angle produces negative surface tension force, which in turn lowers the total wetting force. The dependency of the meniscus height on the contact angle is clearly shown in Figure 4-15. The effects of solder bath depth have also been investigated and as expected wetting forces are not dependent on this parameter.

When solder bath radius changes the wetting force still remains unchanged but shown in Figure 4-16 the meniscus height decreases. This means that wetting force is not sensitive to bath size but the bath radius needs to be sufficiently large to achieve constant meniscus height.

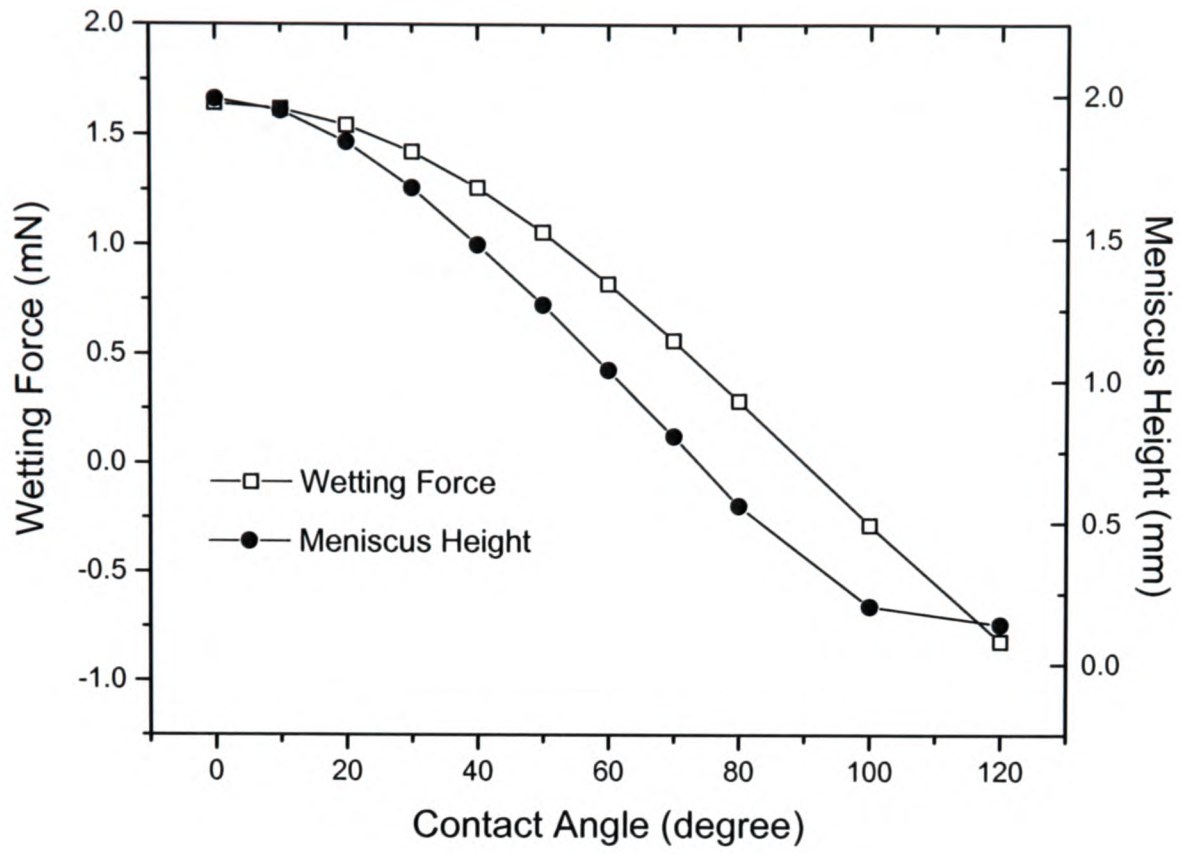


Figure 4-14: Wetting force and meniscus height versus contact angle.

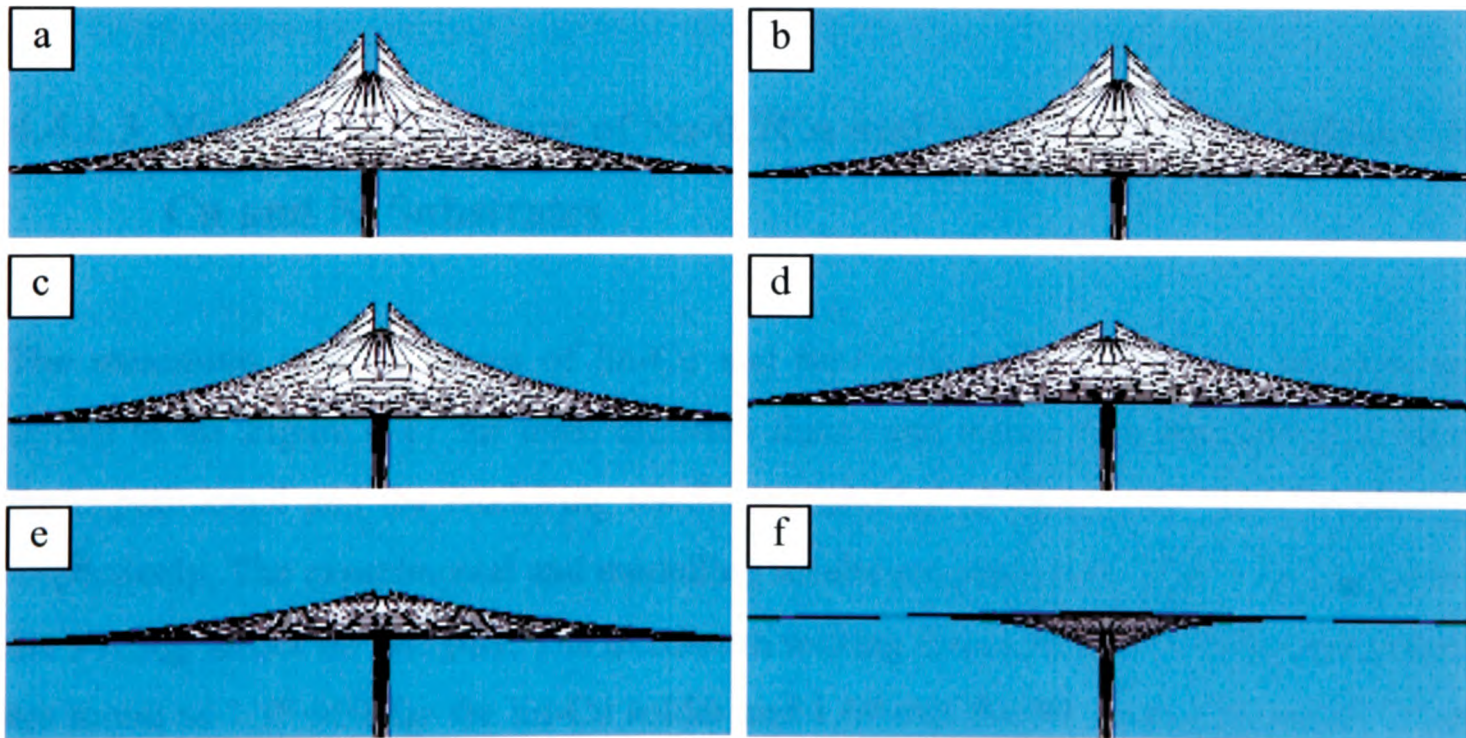


Figure 4-15: Modelling results showing meniscus heights with contact angles (a) 0°, (b) 20°, (c) 40°, (d) 60°, (e) 80° and (f) 120°.

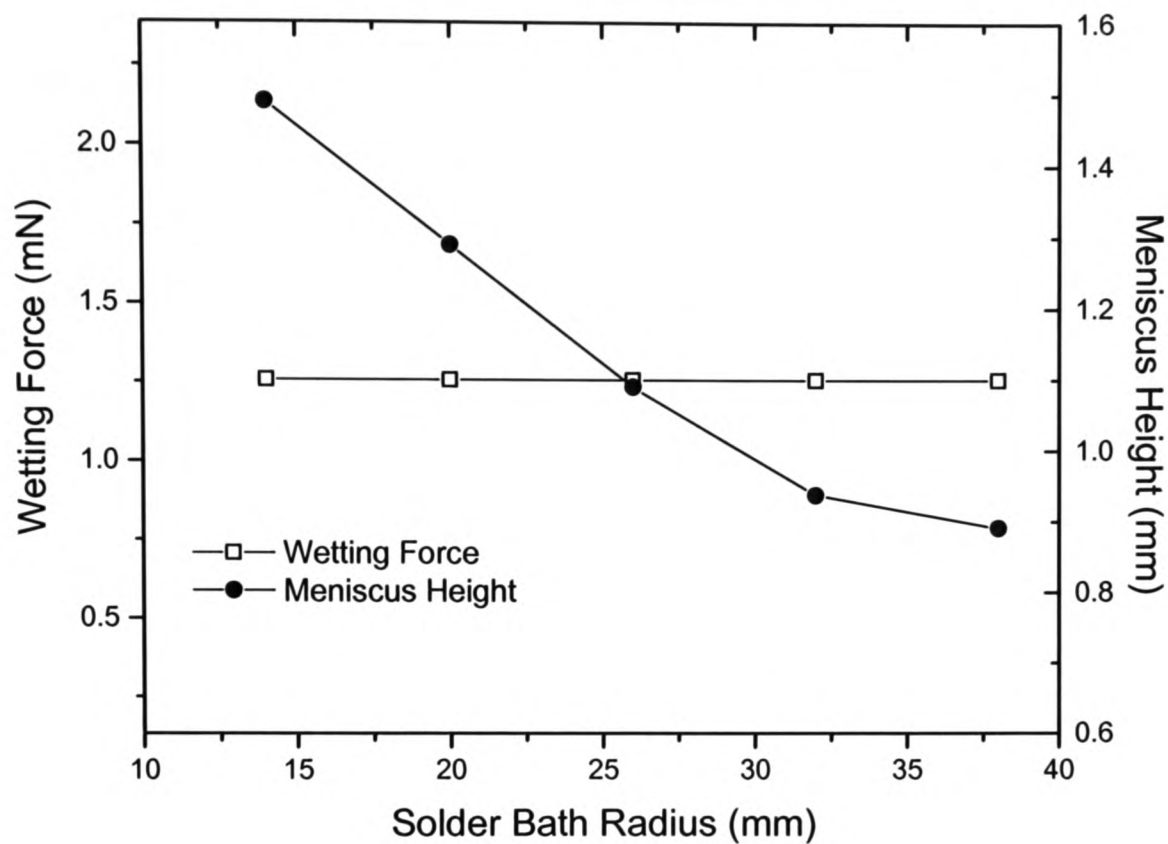


Figure 4-16: Wetting force and meniscus height versus solder bath radius.

4.4.1.3 Wetting Behaviours of Sn-0.7Cu and Sn-0.7Cu-0.3Ni Solders on Cu and Ni Substrates

The maximum wetting forces of Sn-Cu and Sn-Cu-Ni solders with Cu substrate are shown in the Figure 4-17 for three different fluxes and solder bath temperatures. Here, the experimental and the modelling results are labelled as “measured” and “estimated” respectively. The experimental and modelling results are consistent. Figure 4-17(a) shows the wetting forces for NC flux. The maximum wetting forces for 255 °C bath temperature are found as 1.39 mN for the Sn-Cu solder and 1.69 mN for the Sn-Cu-Ni solder. When the bath temperature increases to 275 °C, these values become 1.54 mN and 1.94 mN respectively. Moreover, better wettability has been seen when the solder bath temperature

is raised to 295 °C. For this temperature, the maximum wetting forces are recorded as 1.65 mN for Sn-Cu solder and 2.05 mN for Sn-Cu-Ni solder. Therefore, higher soldering temperature increases the wetting forces and enhances the wetting properties. Similar trend has been observed for solders when WS flux is used as shown in Figure 4-17(c). For the 255 °C bath temperature, the maximum wetting forces for Sn-Cu and Sn-Cu-Ni solders are 1.33 mN and 1.48 mN respectively. The maximum wetting force increases from 1.58 mN to 1.71 mN for Sn-Cu solder when the solder bath temperature is increased from 275 °C to 295 °C. For a similar increase in the solder bath temperature, the maximum wetting force for Sn-Cu-Ni solder increases from 1.75 mN to 1.96 mN.

It is evident from Figure 4-17(a) and (c) that the wettability of Sn-Cu-Ni solder is higher than that of the Sn-Cu solder, but as shown in Figure 4-17(b) for the R-type flux the opposite is true. This figure reveals that wettability of Sn-Cu-Ni solder is less than that of Sn-Cu solder for all the temperatures.

Figure 4-18 shows the maximum wetting forces of Sn-Cu and Sn-Cu-Ni solders with Ni substrate. Figure 4-18(a) represents the wetting forces for NC flux with three different solder bath temperatures. It has been found that when the solder bath temperature is 255°C the maximum wetting force is 0.19 mN for the Sn-Cu solder and 0.29 mN for the Sn-Cu-Ni solder. As solder bath temperature increases the wettability of both solders increases. However, negative wetting forces are recorded i.e. non-wetting has occurred when R-type flux is used as shown in Figure 4-18(b). Although both solders are non-wettable on Ni substrate with R-type flux, the Sn-Cu solder is much worse than the Sn-Cu-Ni solder. Higher solder bath temperature helps the wetting forces to rise towards positive values. Figure 4-18(c) represents the maximum wetting forces with WS-flux. At above 275 °C, a further increase in solder bath temperature doesn't improve the wettability of the Sn-Cu solder but it improves the wettability of the Sn-Cu-Ni solder.

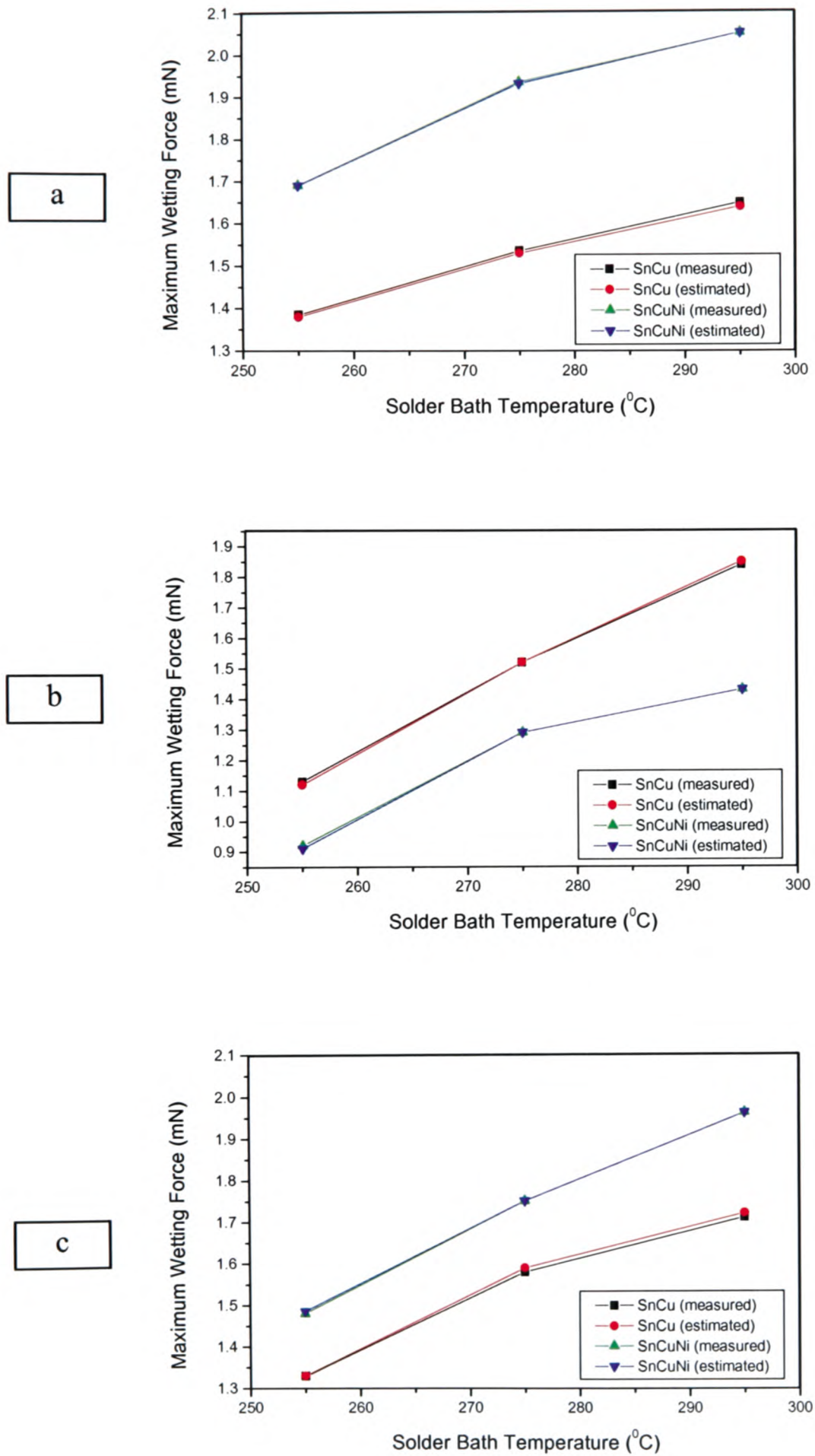


Figure 4-17: Wetting forces as a function of solder bath temperatures for Cu-substrate with (a) NC-flux, (b) R-flux and (c) WS-flux.

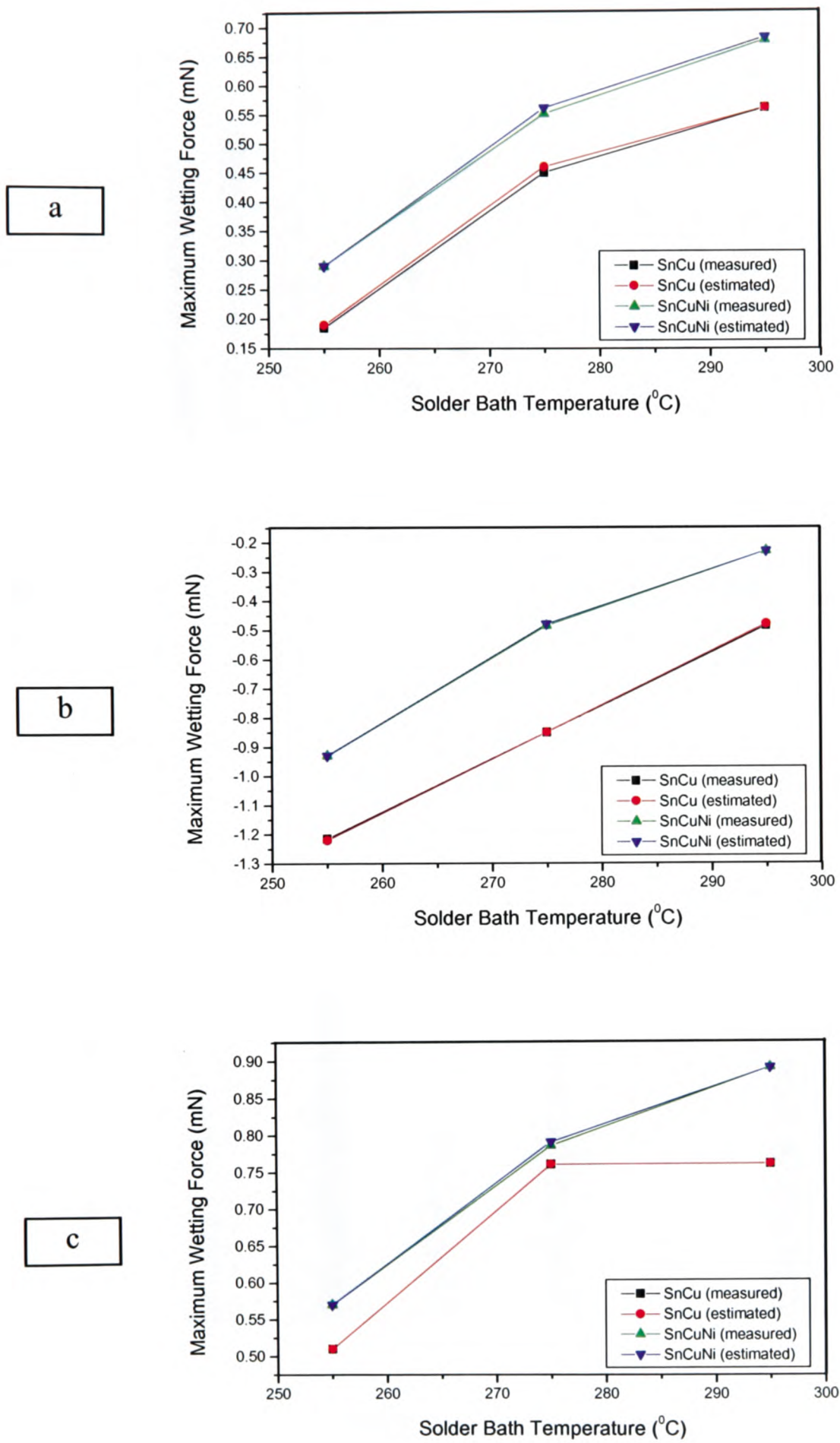


Figure 4-18: Wetting forces as a function of solder bath temperatures for Ni-substrate with (a) NC-flux, (b) R-flux and (c) WS-flux.

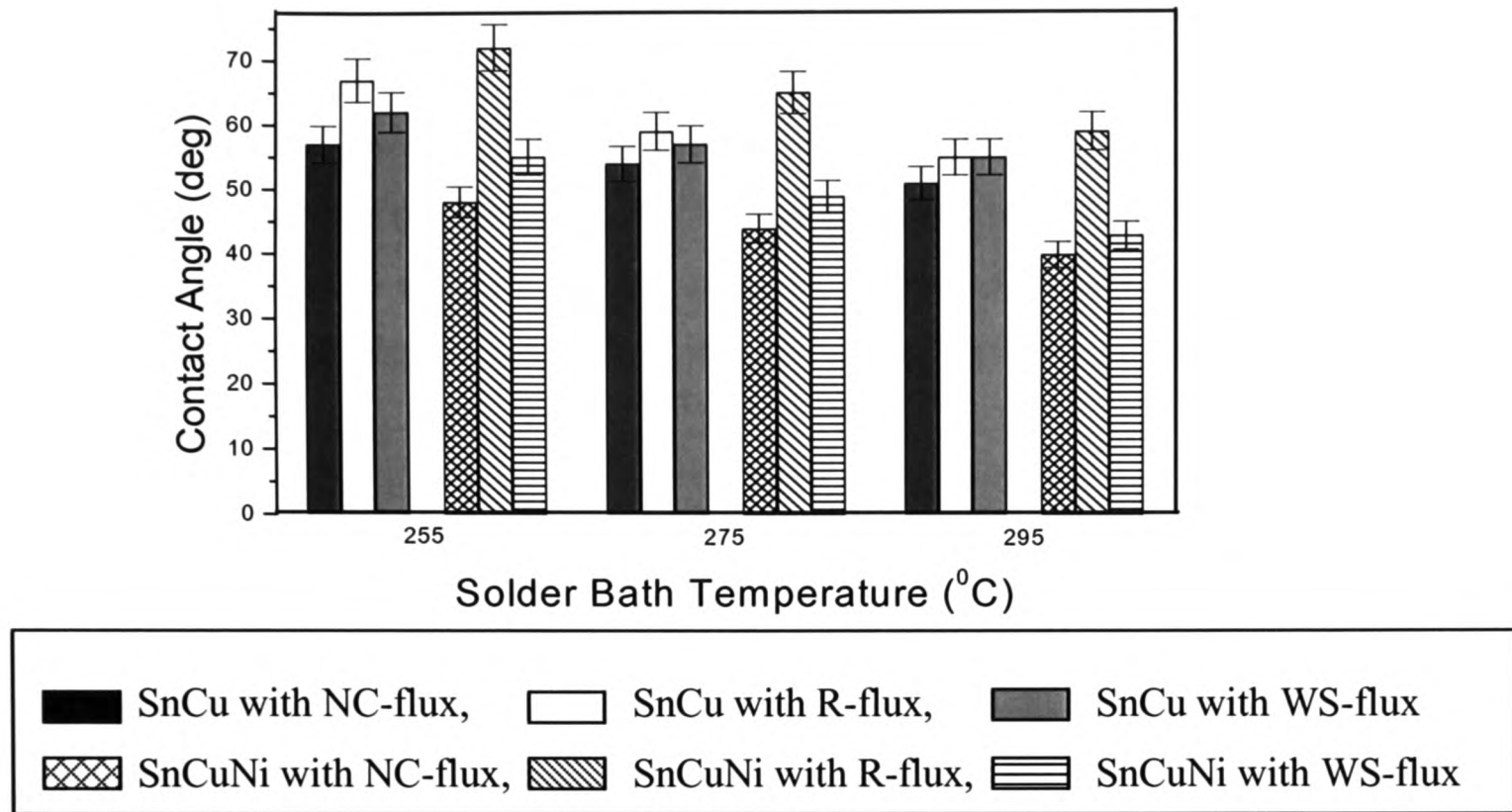


Figure 4-19: Comparative contact angle formations on Cu-substrate.

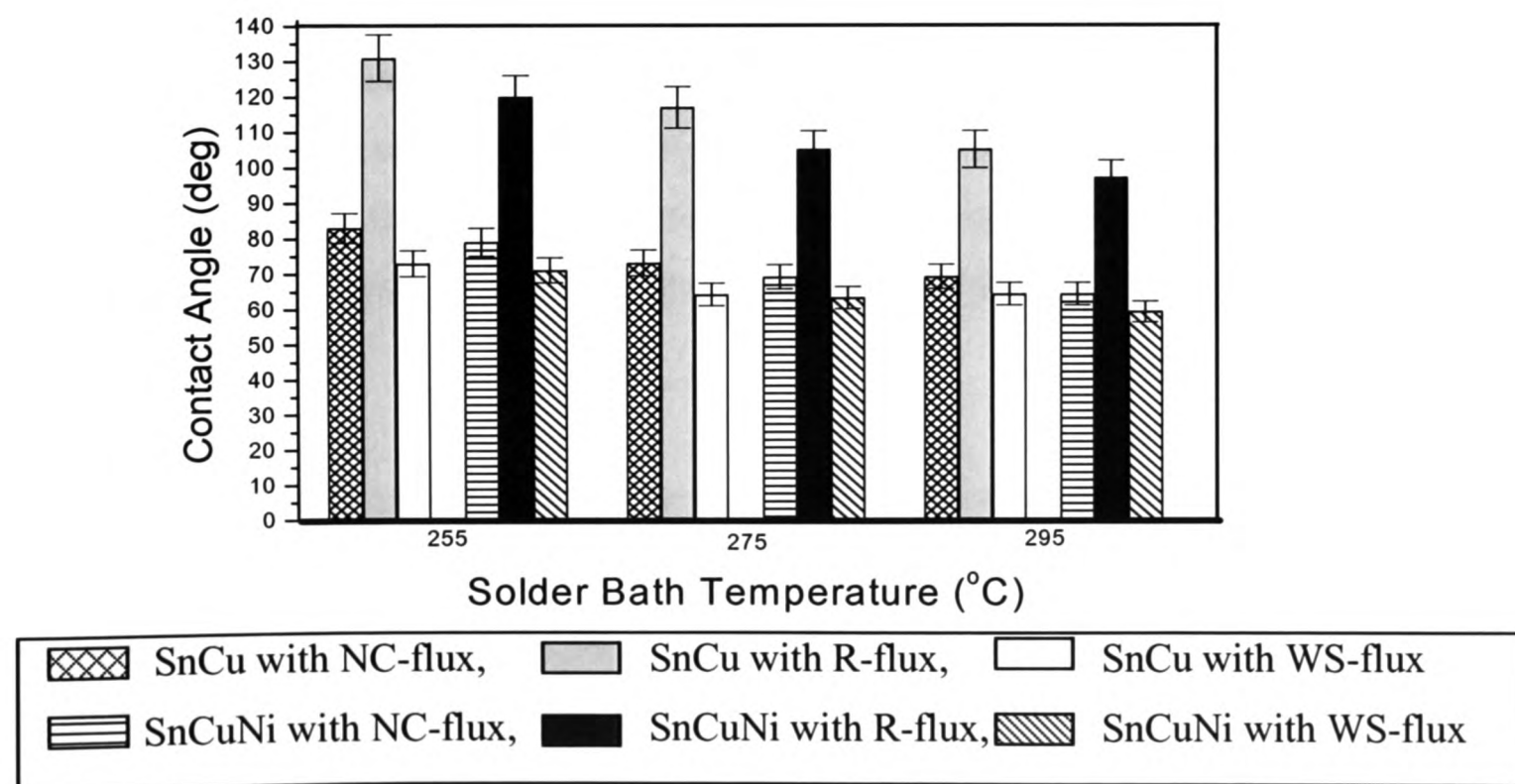


Figure 4-20: Comparative contact angle formations on Ni-substrate.

The contact angles of Sn-Cu and Sn-Cu-Ni solders with three different fluxes and three bath temperatures are shown in Figure 4-19 for Cu substrate and in Figure 4-20 for Ni substrate. In general, the NC flux gives the lowest contact angles with Cu substrate and WS flux gives the lowest contact angles with Ni substrate for both solders at all three solder bath temperatures. Therefore, it can be concluded that NC flux is suitable for Cu substrate, WS flux is suitable for Ni substrate, and the R-flux is not suitable for Ni substrate. Moreover, the addition of 0.3wt% Ni into the Sn-0.7Cu solder can improve the wettability.

4.4.1.4 Discussions

The wetting force is one of the most important parameters that determine the quality of the wetting reaction and the bond quality. The Ad-Hoc IPC/EIA Steam Aging Task Group suggests that adequate soldering can be achieved with parts showing a wetting force of 150 $\mu\text{N}/\text{mm}$ whereas others have suggested that a wetting force need only be positive for good soldering [38]. Therefore, based on the results presented in Figures 4-5, 4-6, 4-17 and 4-18 it can be concluded that the newly developed Sn-2.8Ag-0.5Cu-1.0Bi and Sn-0.7Cu-0.3Ni solders are wettable on the Cu and the Ni substrates when the NC and WS fluxes are used but they are not wettable when the R-type flux is used. In most cases, the wettability can be improved by increasing the solder bath temperature. In order to understand these findings, it is useful to discuss about the role of flux, solder bath temperature and surface tensions on the wettability of Sn-2.8Ag-0.5Cu-1.0Bi and Sn-0.7Cu-0.3Ni solders.

The purpose of the flux is to remove the tarnish film from the substrate surface to provide a clean and non-oxidized surface so that the substrate can be properly wetted by the molten solder. This is achieved by a component in the flux that, after the solvent has evaporated and the solids of the flux are molten, forms a continuous film over the surfaces that inhibits access of oxygen to the hot metal surfaces of the substrates. This property is only related to the chemical nature of the flux and the additives and

independent of the solid contents of the flux [116]. The R-type flux is a non-activated rosin flux with only pure colophony in a solvent [36]. For example, the R-type flux consists of 40% pure water-white rosin in alcohol [38]. The pure colophony of R-type flux exhibits a weak cleaning action due to its one $-\text{COOH}$ group in its large molecule [36]. Therefore, only very thin tarnish layers can be removed from the substrate surfaces and results in poor wetting. In electronics packaging, the R-type flux tends to be left as residues at the solder-substrate interface after the soldering and these flux residues degrade the electrical performance of the solder joint. According to Equation (4.1) ($\theta_c = \cos^{-1}[\{\gamma_{\text{SF}} - \gamma_{\text{SL}}\} / \gamma_{\text{LF}}]$) the contact angle decreases if the substrate-flux interfacial tension γ_{SF} increases and/or the solder-flux interfacial tension γ_{LF} decreases. Since γ_{SL} is determined by the solder-substrate interface metallurgy only and it is insensitive to the flux [117], the contact angle is dominated by the type of flux. In this work the R-type flux results in a solder-flux interfacial tension of 445mN/m that is higher than other two fluxes and this is why the contact angles are high and the wetting forces become negative (Figures 4-6b & 4-18b) regardless the solder bath temperatures.

Figures 4-12, 4-13, 4-19 and 4-20 reveal that comparatively NC-flux result in lower contact angle values than R-flux or WS-flux regardless the solder types and the temperatures for Cu-substrate. For Ni substrate, the WS flux performs the best for both the solders. For both the Cu and the Ni substrates the R-flux shows the worst performance. The NC flux possesses the lowest solder-flux interfacial tension value (370mN/m) among the three fluxes and this is thought to be responsible for the best wetting performance on the Cu substrates. The WS-flux provides high fluxing activity because it contains: (i) a chemically reactive compound that cleans the substrate surface, (ii) a wetting agent that helps to spread the flux components over the substrate surface. It also contains a solvent such as alcohol or water that provides an even distribution of flux components over the substrate surfaces. The glycols or water-soluble polymer materials of the WS flux provide close contact between the activator and the substrate surface for heat conduction [36]. Because of these characteristics, the WS flux has resulted in the best wettability for Ni substrate despite it having a higher solder-flux interfacial tension (415mN/m) than NC-flux. As for the R-type flux, its poor cleaning capability and the

higher solder-flux interfacial tension (445mN/m) is responsible for its worst performances. From figures 4-12, 4-13, 4-19 and 4-20, it is also evident that higher solder temperature improves the wettability as the contact angles decrease for all fluxes. This is because of the thermally induced changes to the molecular structure of flux that lowers the γ_{LF} value and improves its oxide removal capacity. Moreover, the surface tensions of tin, lead and solder alloys generally decreases as the temperature increases and shows a continuous smooth exponential function from the high surface tension component (for example Sn) to the low (for example Pb) [38].

4.4.2 Reactions of Cu and Ni Substrates with Solders during the Wetting Balance Tests

4.4.2.1 Dissolution of Substrates into Molten Solders

During the wetting balance tests, chemical and metallurgical reactions take place when substrates come into contact with molten solder. The reactions cause continuous atomic diffusion from the substrate into solder. As a result, the substrate materials dissolve into solder and the thicknesses of the substrates decrease. The substrate dissolution rate depends on a few factors such as the solder volume, the solder bath temperature, the duration of the soldering, the chemical activities of the flux used, and the solid solubility of the substrate material in the molten solder, etc.

The Nernst-Shchukarev equation describes the dissolution process of any solid (for example, Cu or Ni) in a liquid (for example, liquid solder) [118]. The differential form of this equation is

$$\frac{dc}{dt} = k \frac{S}{V} (c_s - c) \quad (4.4)$$

where, c is the instantaneous concentration of the dissolved Cu or Ni, t is the time, c_s is the saturation concentration or the solubility limit of Cu or Ni at a given temperature, k is

the dissolution rate constant, s is the surface area of Cu or Ni substrates in contact with the liquid solder, v is the volume of the entire liquid solder.

Mannan et al [119] has pointed out that equation (4.4) is applicable only for the stable solubility condition where ' c ' doesn't exceed ' c_s '. But in reality, c exceeds c_s at metastable solubility condition. Therefore, the stable solubility limit c_s (obtained from equilibrium phase diagram) should be replaced by metastable solubility limit c_2 (where $c_2 > c > c_s$). However, at the beginning of the reactions, i.e. $t = 0$, the instantaneous concentration, c of Cu or Ni should be equal to 0. Therefore, replacing c_s by c_2 the integral form of the equation (4.4) gives

$$c = c_2 [1 - \exp(-k st/v)] \quad (4.5)$$

The logarithmic form of this equation is

$$\ln \left[\frac{c_2}{c_2 - c} \right] = kst/v \quad (4.6)$$

Therefore, the dissolution rate constant, k can be expressed as

$$k = \frac{\ln [c_2 / (c_2 - c)]}{st/v} \quad (4.7)$$

The above equations indicate that the whole dissolution process depends on c_2 , the super saturation concentration or the metastable solubility limit of Cu or Ni at a given temperature, and k , the dissolution rate constant. Since at constant pressure, the saturation concentration only depends upon the temperature [118], the dissolution rate of Cu or Ni is expected to increase as the soldering temperature increases. From equation (4.7) it is clear that for constant values of s , t and v , the dissolution rate depends on the value of $(c_2 - c)$. The dissolution rate k decreases with time as c increases with the continuous diffusion of Cu or Ni atoms. Therefore, for any constant reaction temperature, initially the consumption/dissolution of Cu or Ni substrate by the molten solder is higher and then decreases gradually over time and eventually follows the parabolic path [103]. In this work, the dissolution of the solid substrates into molten solder has been measured for three different temperatures and a fixed period time. The main aim of this dissolution

study is to figure out how the addition of Bi or Ni influences the consumption behaviour of the corresponding lead-free solders. For comparison purpose, the dissolution of substrates into the Sn-Pb solder has also been studied. The results of this study will be used to calculate the diffusion coefficient in Section 4.4.2.3.2. Since the dissolution measurement has been carried out at a fixed time, a detail history of the dissolution of the substrate over the reaction time can not be obtained from this investigation.

4.4.2.1.1 Dissolution of Cu and Ni Substrates into Sn-37Pb Solder

Figure 4-21 shows the consumptions of Cu and Ni substrates into liquid Sn-Pb solder during the wetting balance tests. After the wetting balance tests, the samples were cross-sectioned to measure the remaining thickness of Cu or Ni using Scanning Electron Microscope (SEM). The dissolved Cu and/or Ni are determined by deducting this remaining thickness of Cu and/or Ni from their original thickness. Because of the symmetry, half of the measured dissolved thickness is used defined as the dissolved thickness of the substrate.

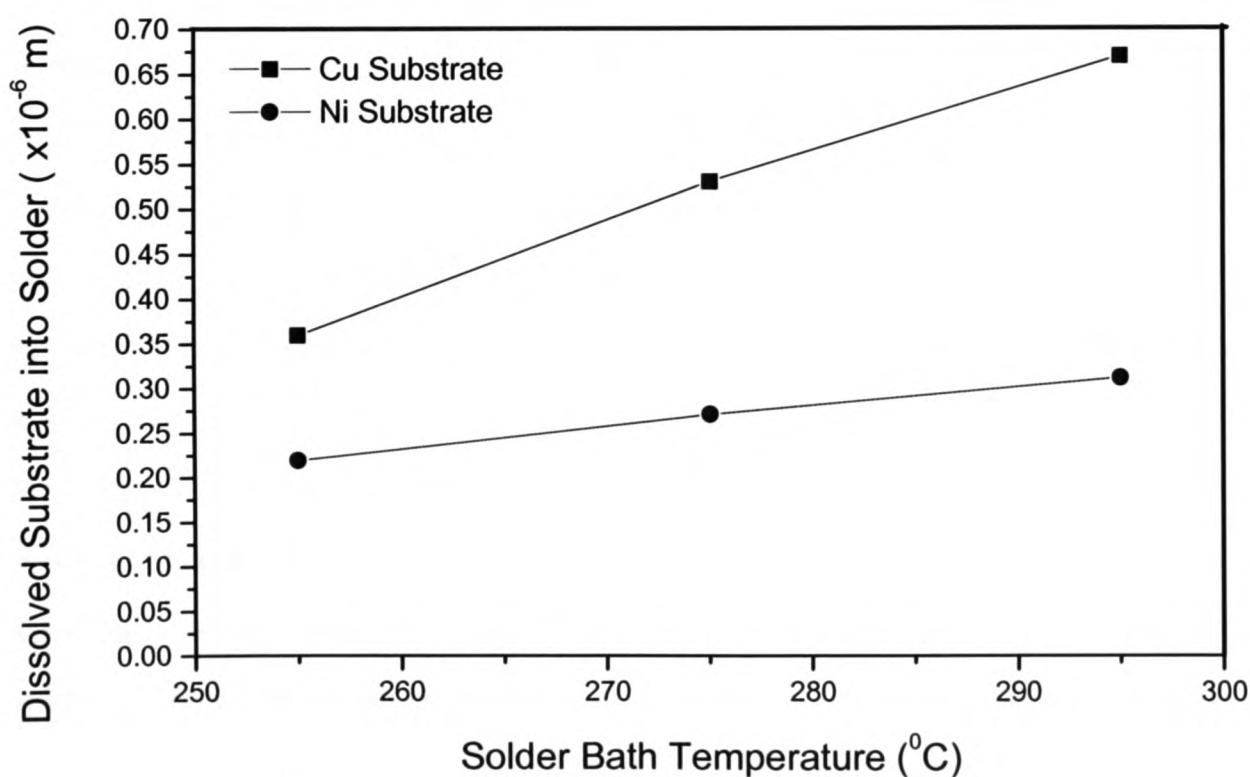
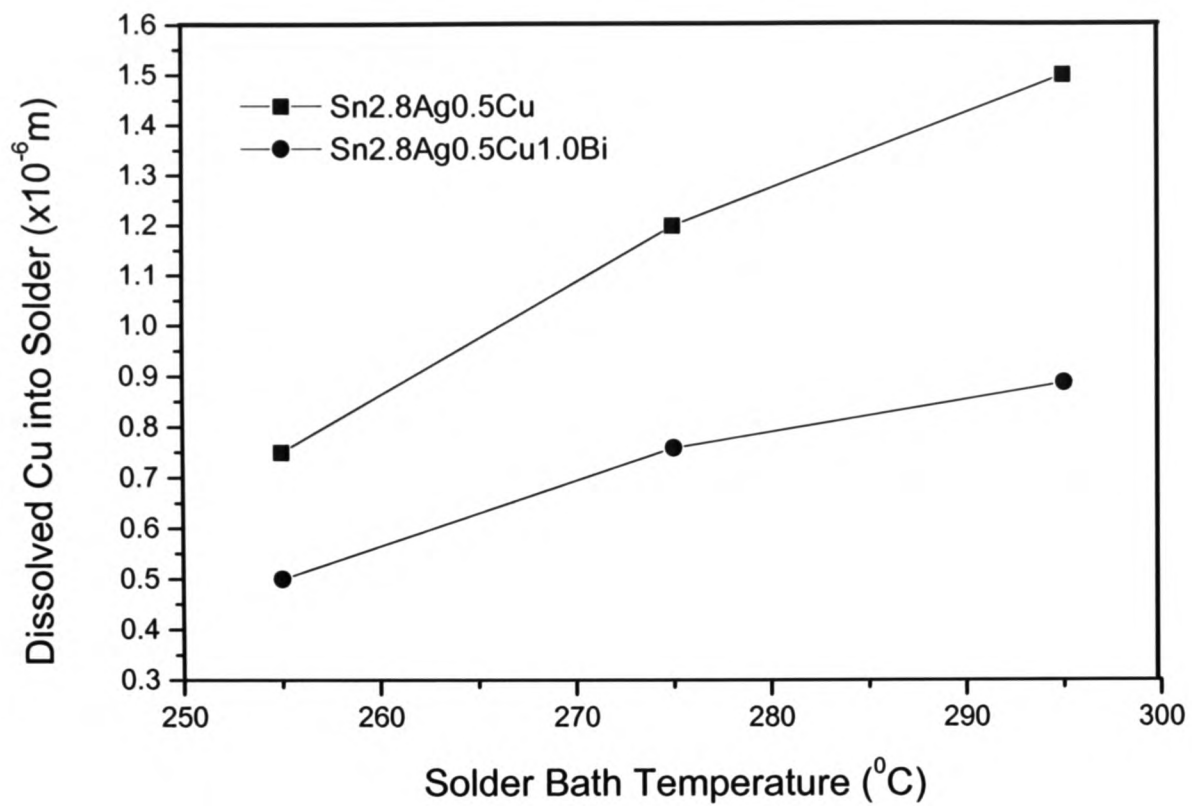


Figure 4-21: Single side dissolutions of Cu and Ni substrates into molten Sn-Pb solder during the wetting balance test with NC-flux.

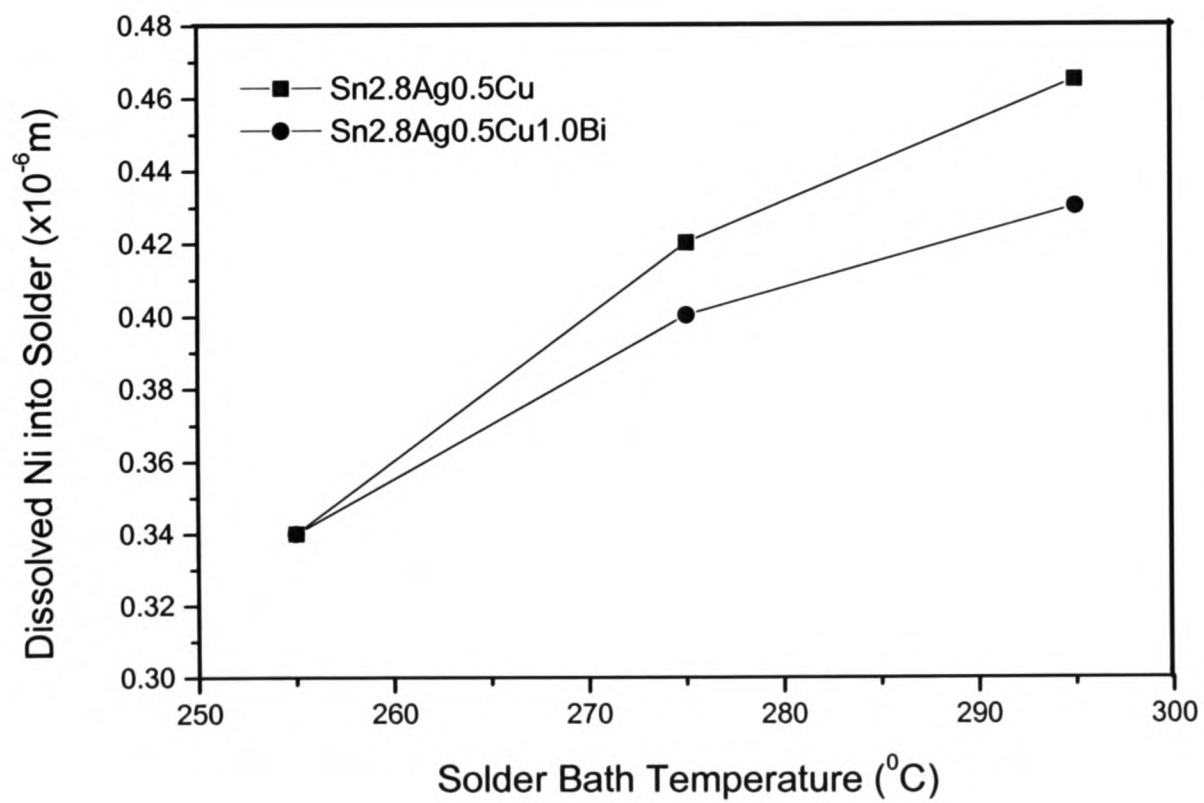
It has been found that the dissolution, which is much higher for Cu than that for Ni, increases with the increase in the soldering temperature. At 255, 275 and 295 °C soldering temperatures, the dissolved Cu thicknesses are 0.36, 0.63 and 0.87 μm respectively whereas the dissolved Ni thicknesses are 0.22, 0.27 and 0.31 μm respectively. Kim et al [103] found that the dissolution of Cu into Sn-Pb solder at 240 °C for 10 s reactions is 0.32 μm which is very close to what has been found here for the temperature of 255 °C.

4.4.2.1.2 Dissolution of Cu and Ni Substrates into Sn-2.8Ag-0.5Cu and Sn-2.8Ag-0.5Cu-1.0Bi Solders

The dissolved Cu and Ni thicknesses into the molten Sn-2.8Ag-0.5Cu and Sn-2.8Ag-0.5Cu-1.0Bi solders during wetting reactions are shown in Figure 4-22(a) and (b). As shown in Figure 4-22, dissolutions of both the Cu and the Ni are higher for these two lead-free solders than that of the conventional Sn-Pb solder. Since the dissolution of the substrates for these two lead-free solders are higher, the formation of IMCs should be higher compared to the Sn-Pb solder. This will be discussed in the following sections. Figure 4-22(a) reveals that Sn-2.8Ag-0.5Cu-1.0Bi solder dissolves less Cu than that of the Sn-2.8Ag-0.5Cu solder. The dissolution of Cu in the Sn-2.8Ag-0.5Cu solder is almost two times higher than that in the Sn-2.8Ag-0.5Cu-1.0Bi solder. The dissolution rate increases with the increase in the soldering temperature. Kim et al [103] reported that since the amount of Cu is limited and some Cu must remain after all the reflows and subsequent reworks to avoid dewetting, the understanding of the consumption of Cu is very important. Based on our investigation, it can be said that the addition of Bi into the Sn-2.8Ag-0.5Cu solder can help reduce the consumption of Cu. Similar conclusion can be made about Ni-substrate as well since the results shown in Figure 4-22(b) reveals that the dissolution of Ni into the Sn-2.8Ag-0.5Cu-1.0Bi solder is less than that in the Sn-2.8Ag-0.5Cu solder. The results also show that the dissolution of the Ni is much lower than that of the Cu for both lead-free solders. Other researchers [120][121] have found the similar results for Sn-Pb and Sn-Ag-Cu solders.



(a)



(b)

Figure 4-22: Single side dissolution of (a) Cu and (b) Ni substrates into molten SnAgCu and SnAgCuBi solders during the wetting balance test with NC-flux.

4.4.2.1.3 Dissolution of Cu and Ni Substrates into Sn-0.7Cu and Sn-0.7Cu-0.3Ni Solders

Figure 4-23(a) shows the dissolution of Cu substrates in the Sn-0.7Cu and Sn-0.7Cu-0.3Ni molten solders. At 255 °C solder bath temperature, Sn-0.7Cu solder can dissolve around 0.70 μm Cu whereas Sn-0.7Cu-0.3Ni solder dissolves around 0.67 μm Cu. With the increase in the solder bath temperature, more Cu can be dissolved into the molten solder. At 275 and 295 °C, the dissolved Cu thickness can be as high as 0.75 and 0.81 μm respectively for Sn-0.7Cu solder and 0.72 and 0.76 μm respectively for Sn-0.7Cu-0.3Ni solder. Figure 4-23(b) shows the dissolution of Ni into these two solders at three different solder bath temperatures. From this figure it is evident that the dissolution of Ni also increases with soldering temperature. The dissolved Ni into the Sn-0.7Cu solder has been found to be 0.31, 0.38 and 0.44 μm respectively at 255, 275 and 295 °C whereas the dissolved Ni in the Sn-0.7Cu-0.3Ni solder has been found to be 0.27, 0.36 and 0.40 μm respectively at the three soldering temperatures. Therefore, it is clear that the dissolutions of the substrates increase with the increase in the soldering temperature and the rate of increase is higher for the Sn-0.7Cu solder than for the Sn-0.7Cu-0.3Ni solder. It is also evident from Figure 4-23(a) and (b) that the dissolution is higher for the Cu substrate than that for the Ni substrate. Kim et al [103] has reported that dissolution mainly occurs through the channels between the grains at the solder-substrate interface and the dissolution rate is very important to determining the processing parameters and their limits of solder joints on thin-film metallization in electronic packaging. Therefore, the understanding of the effects of adding Bi or Ni on the dissolution behaviour of lead-free solders is very important. In previous section, it has been seen that higher soldering temperature enhances the wettability but it is now clear that soldering temperature increase also speeds up dissolution of the substrate materials, possibly caused by the enhanced chemical reaction and/or an increase in the number of diffusion channels in the IMC layer. Since the dissolution is less for Sn-2.8Ag-0.5Cu-1.0Bi solder in comparison with Sn-2.8Ag-0.5Cu solder and for Sn-0.7Cu-0.3Ni solder compared to the Sn-0.7Cu

Chapter-4: Study of Interconnections formed with Lead-free Solder Alloys

solder, it is thus assumed that the addition of 1.0wt% Bi into Sn-2.8Ag-0.5Cu solder or 0.3wt% Ni into Sn-0.7Cu solder helps to reduce the formation of channels between the grains and hence controls the whole dissolution process during wetting and soldering.

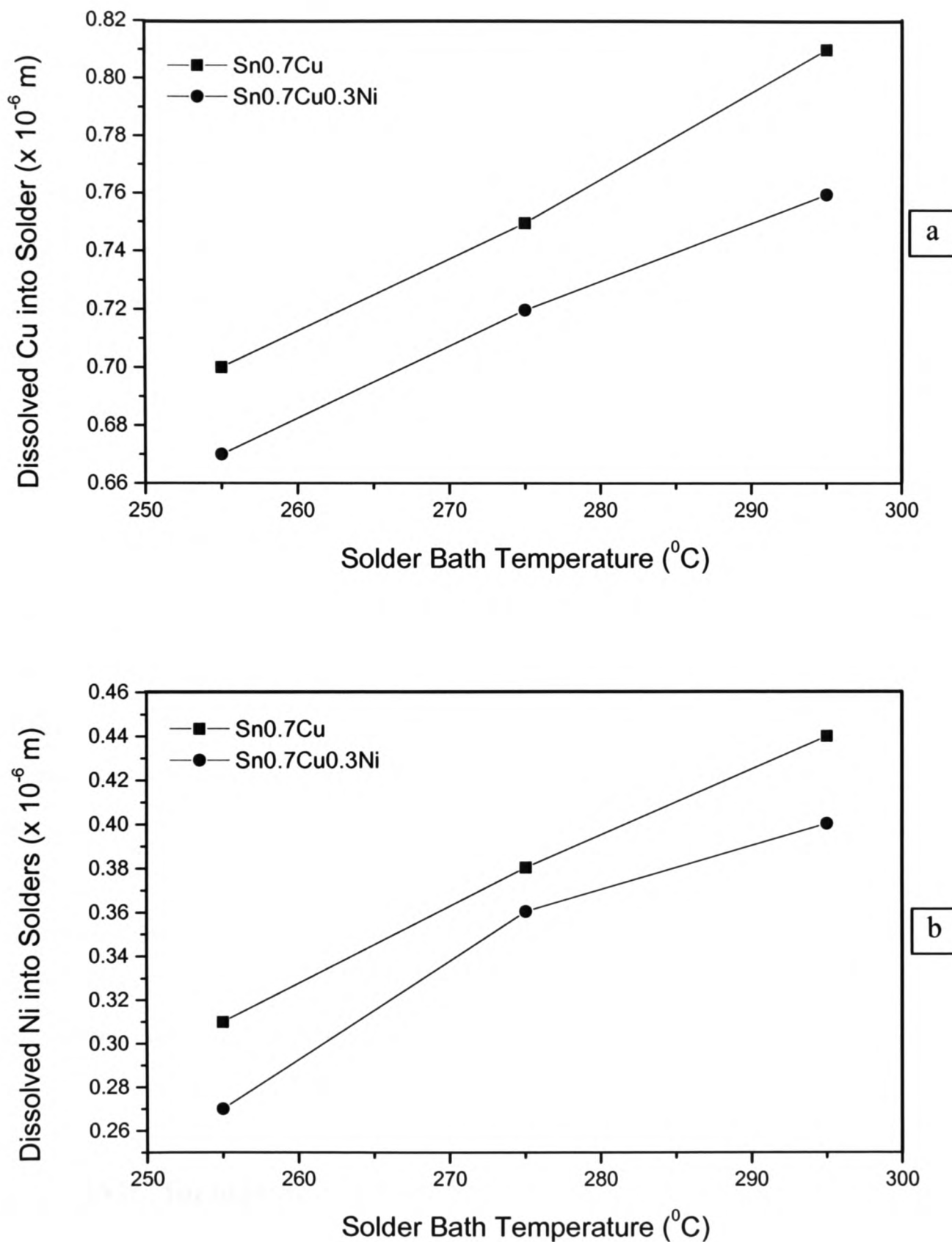


Figure 4-23: Single side dissolution of (a) Cu and (b) Ni substrates into molten SnCu and SnCuNi solders during the wetting balance test with NC-flux.

4.4.2.2 IMC formations of Sn-Pb and Pb-free Solders on Cu and Ni Substrates during Wetting

When molten solders wet the surface of solid Cu or Ni substrate, the dissolution of Cu or Ni into the liquid solders causes the formation of IMC layer at the solder-substrate interface. The presence of IMC is a sign of good wetting and metallurgical bonding; but excessive IMC deteriorates the solder joint quality and reduces the life span. Lee et al [122] has found that the joint strength of SnPb/Cu and Sn/Cu systems decreases due to an increase in IMC thickness. Chen et al [123] has also found that the fracture site during a tensile test shifts from the solder matrix to the IMC layer that is formed with a long reaction time and a significant degradation of the tensile properties occurred for the Sn/Ni and Sn-0.7Cu/Ni joints.

Reactive properties and IMC formations of lead-free solders such as Sn-Ag and Sn-Cu solders are extremely sensitive to the concentrations of the alloying elements [111]. Moreover, as it has been reported by Wu et al [100], alloying strongly affects the melting temperature and the creep behaviour. Therefore, the addition of the third or fourth element into the well known Sn-Cu and Sn-Ag-Cu solders may result in the criterion described in section 4.1 not being met. It has already been seen in earlier sections that an addition of 1 wt% Bi into Sn-2.8Ag-0.5Cu solder or 0.3wt% Ni into Sn-0.7Cu solder enhances the wettability and reduces the substrate consumptions. In the following sections, the effect of adding 1wt% Bi into Sn-2.8Ag-0.5Cu solder and 0.3wt% Ni into Sn-0.7Cu solder on the IMC formations during the wetting balance tests will be discussed.

4.4.2.2.1 IMC formations of Sn-37Pb Solder on Cu and Ni Substrates

In this section the characteristics of IMC layers in the Sn-Pb/Cu and Sn-Pb/Ni soldering systems are analyzed. Figure 4-24 shows the microstructures of Sn-Pb solders with Cu and Ni substrates. An EDX analysis has indicated that Pb is not present along the

solder/Cu and/or solder/Ni interfaces. Therefore, Pb does not contribute to the formation of IMCs. In fact, only Cu-Sn IMCs have been found for the Sn-Pb solders with Cu substrates as shown in the Figure 4-24(a). The Cu-Sn reaction is selective [103] and therefore a very rough scallop like Cu_6Sn_5 IMC layer has been detected.

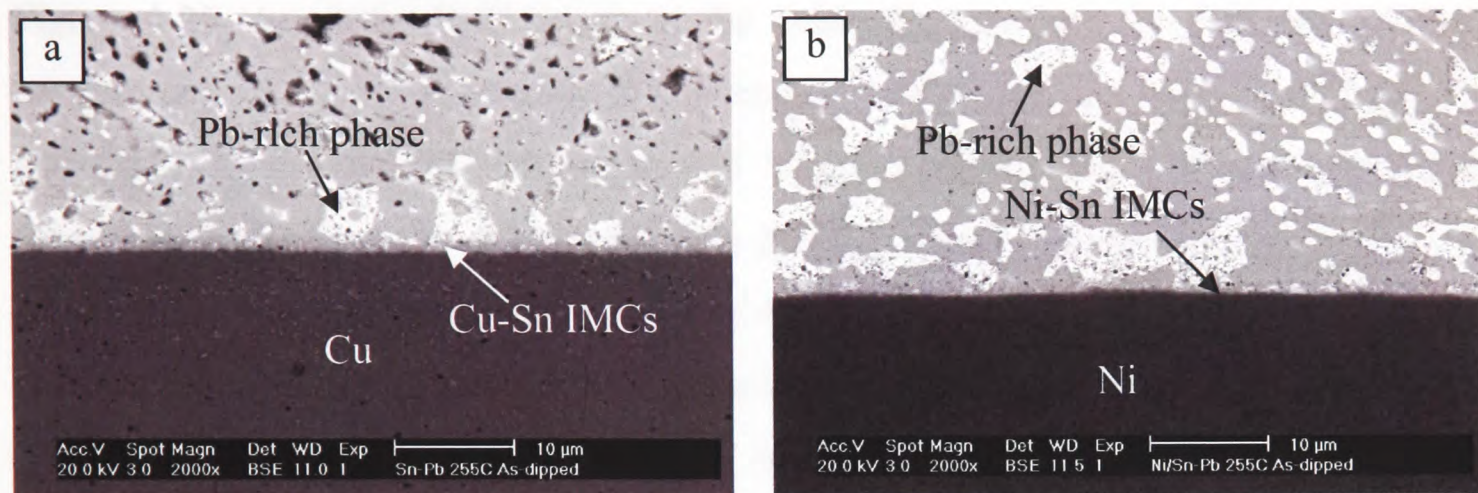


Figure 4-24: SEM images showing the wetting reactions at 255 °C between: (a) Sn-Pb and Cu, (b) Sn-Pb and Ni.

During the wetting balance tests, Cu atoms diffuse from the substrate into the solder while the Cu substrate is immersed in the molten solder bath. This diffusion process takes place through the channels in the IMC and it results in an increase in the IMC layer thickness. These channels remain open for the Pb-free solders whereas they are closed for the Sn-Pb solder after a certain period. For this reason, the IMC layers for lead-free solders are expected to be thicker than that of the Sn-Pb solder. Cu_6Sn_5 IMCs also appear in the solders other than the solder/Cu interfaces when the concentrations of Cu in the bulk of the molten solder reach the threshold limit for the formation of Cu_6Sn_5 . As a result, a significant number of Cu_6Sn_5 compounds have been found in the bulk of Sn-Pb/Cu soldering system.

In the case of Ni-substrate, a binary Ni-Sn IMC layer has been detected for Sn-Pb solder as shown in Figures 4-24(b). The IMC layer thickness for Ni-substrate is very thin ($0.586 \mu\text{m}$) compared to that for the Cu-substrate ($0.860 \mu\text{m}$). Therefore, it can be concluded that Ni-atoms do not diffuse into the solder as much as Cu atoms do.

4.4.2.2.2 IMC formations of Sn-2.8Ag-0.5Cu and Sn-2.8Ag-0.5Cu-1.0Bi Solders on Cu and Ni Substrates

Figure 4-25 shows the IMC layers at the solder/Cu interface for different soldering temperatures. Table 4-2 shows that the thicknesses of the IMC layers for Sn-2.8Ag-0.5Cu and Sn-2.8Ag-0.5Cu-1.0Bi solders at 255 °C are 1.52 μm and 1.01 μm respectively (Figure 4-25a(i) & a(ii)). Figure 4-25b(i) & b(ii) reveal that an increase in the bath temperature from 255 to 275 °C results in an increase in the IMC layer thicknesses to 2.23 μm and 1.57 μm respectively for these two solders. If the solder bath temperature is 295 °C, the IMC layer thickness increases dramatically to 3.26 μm for Sn-2.8Ag-0.5Cu solder (Figure 4-25c(i)). However, at this temperature, the IMC thickness for Sn-2.8Ag-0.5Cu-1.0Bi solder is 1.64 μm. Therefore, an increase in the solder bath temperature results in an increase of the IMC layer thickness and the rate of increase is greater for the Sn-2.8Ag-0.5Cu solder than for the Sn-2.8Ag-0.5Cu-1.0Bi solder. As shown in Figure 4-26, similar trend has been found with the Ni substrate. Table 4-2 shows that the IMC layer thicknesses for Sn-2.8Ag-0.5Cu solder are 0.668 μm, 0.860 μm and 0.908 μm respectively at 255, 275 and 295 °C solder bath temperatures, and at these three temperatures the IMC thicknesses for Sn-2.8Ag-0.5Cu-1.0Bi solder are 0.669 μm, 0.810 μm and 0.890 μm respectively. Since the dissolution rate of Ni in molten solder is smaller compared to that of Cu (Figure 4-21, 22, 23), the thickness of IMC layer on Ni is also smaller compared to that on Cu.

Table 4-2: Growth of IMC layer during soldering of SnAgCu and SnAgCuBi solders

Soldering Temperature (°C)	IMC Thickness (μm)			
	Cu Substrate		Ni Substrate	
	SnAgCu	SnAgCuBi	SnAgCu	SnAgCuBi
255	1.52	1.01	0.668	0.669
275	2.23	1.57	0.860	0.810
295	3.26	1.64	0.908	0.890

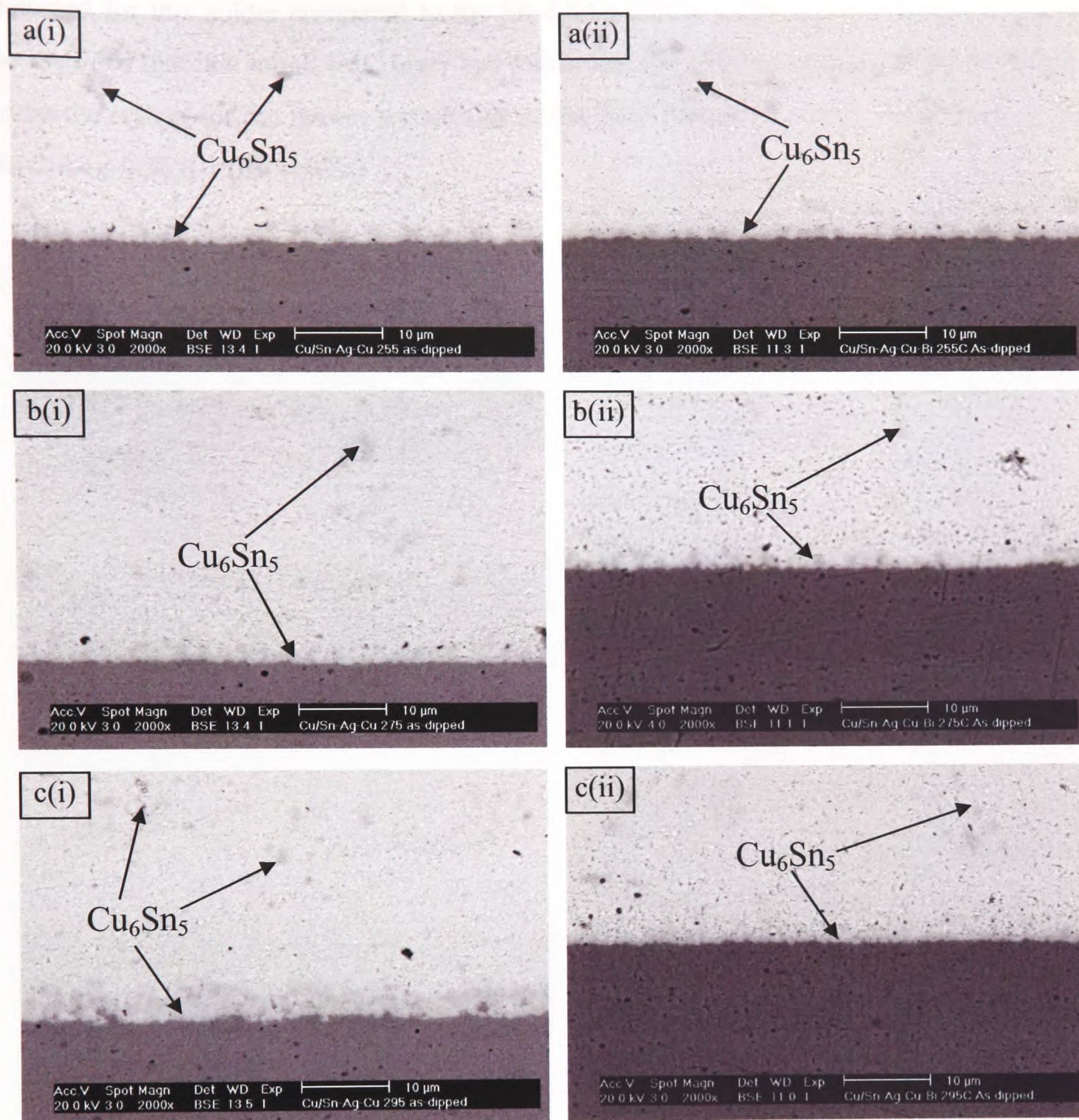


Figure 4-25: Solder-Cu interfaces after dipping into (i) SnAgCu, (ii) SnAgCuBi solders at a) 255 °C, b) 275 °C and c) 295 °C.

Figure 4-25 and 4-26 show that the addition of Bi into the Sn-2.8Ag-0.5Cu solder lowers the growth of the IMC layer. EDX analyses for these two solders confirm that the detected IMC layers for the solder/Cu and the solder/Ni systems are Cu_6Sn_5 and $(\text{Cu}_{1-x}\text{Ni}_x)_6\text{Sn}_5$ respectively. During the wetting reaction, these scallop-type IMCs have formed due to the continuous diffusion of Cu and Ni into the molten solder. As the dissolution of substrate is higher for the Sn-2.8Ag-0.5Cu solder (Figure 4-22), rougher scallops are

Chapter-4: Study of Interconnections formed with Lead-free Solder Alloys

detected for this solder compared to the Sn-2.8Ag-0.5Cu-1.0Bi solder. Therefore, it can be assumed that this rough IMC layer has influenced the wetting behaviour and is thought to be the reason for the poorer wettability of the Sn-2.8Ag-0.5Cu solder compared to the Sn-2.8Ag-0.5Cu-1.0Bi solder.

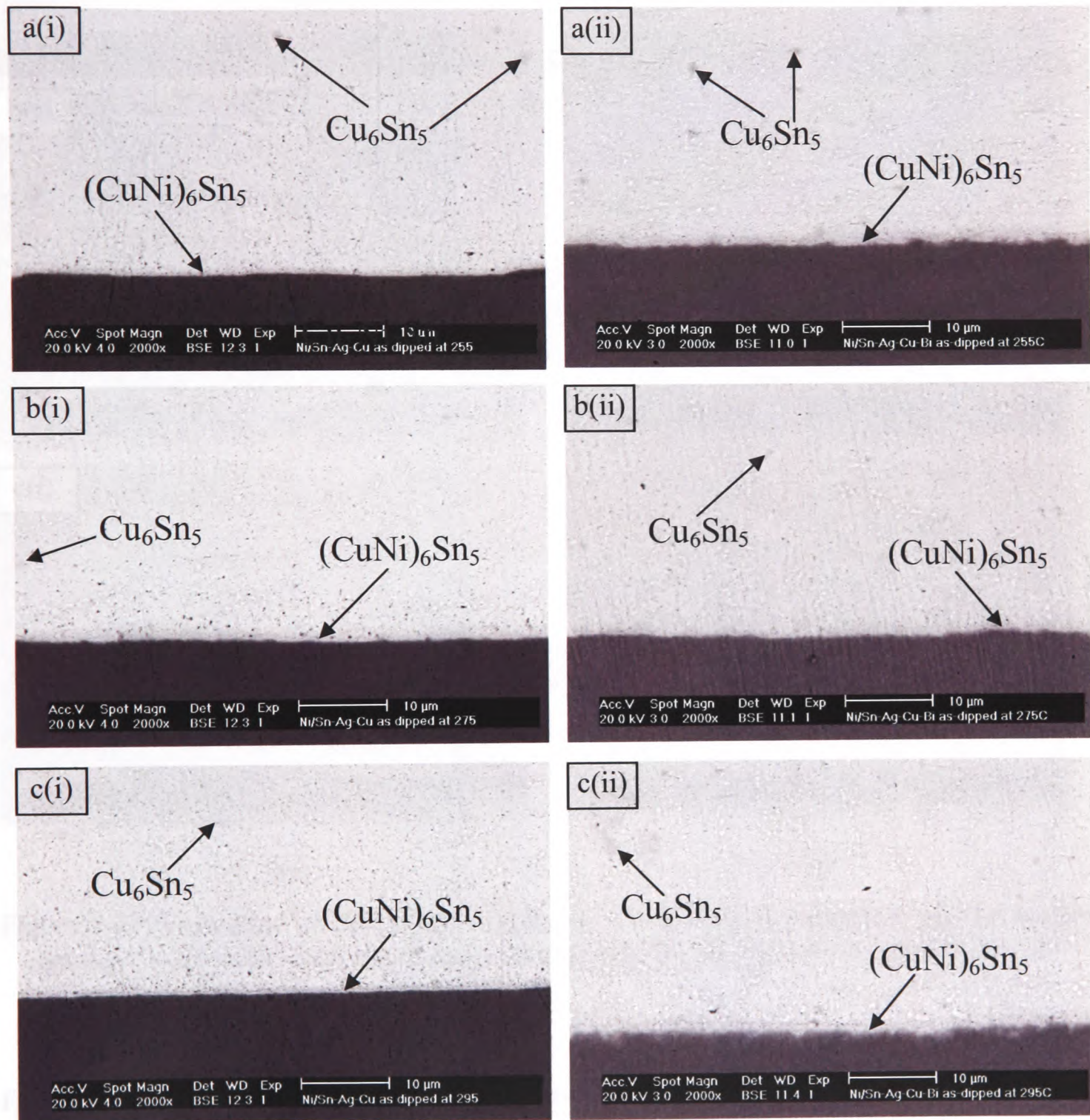


Figure 4-26: Solder-Ni interfaces after dipping into (i) SnAgCu, (ii) SnAgCuBi solders at a) 255 °C, b) 275 °C and c) 295 °C.

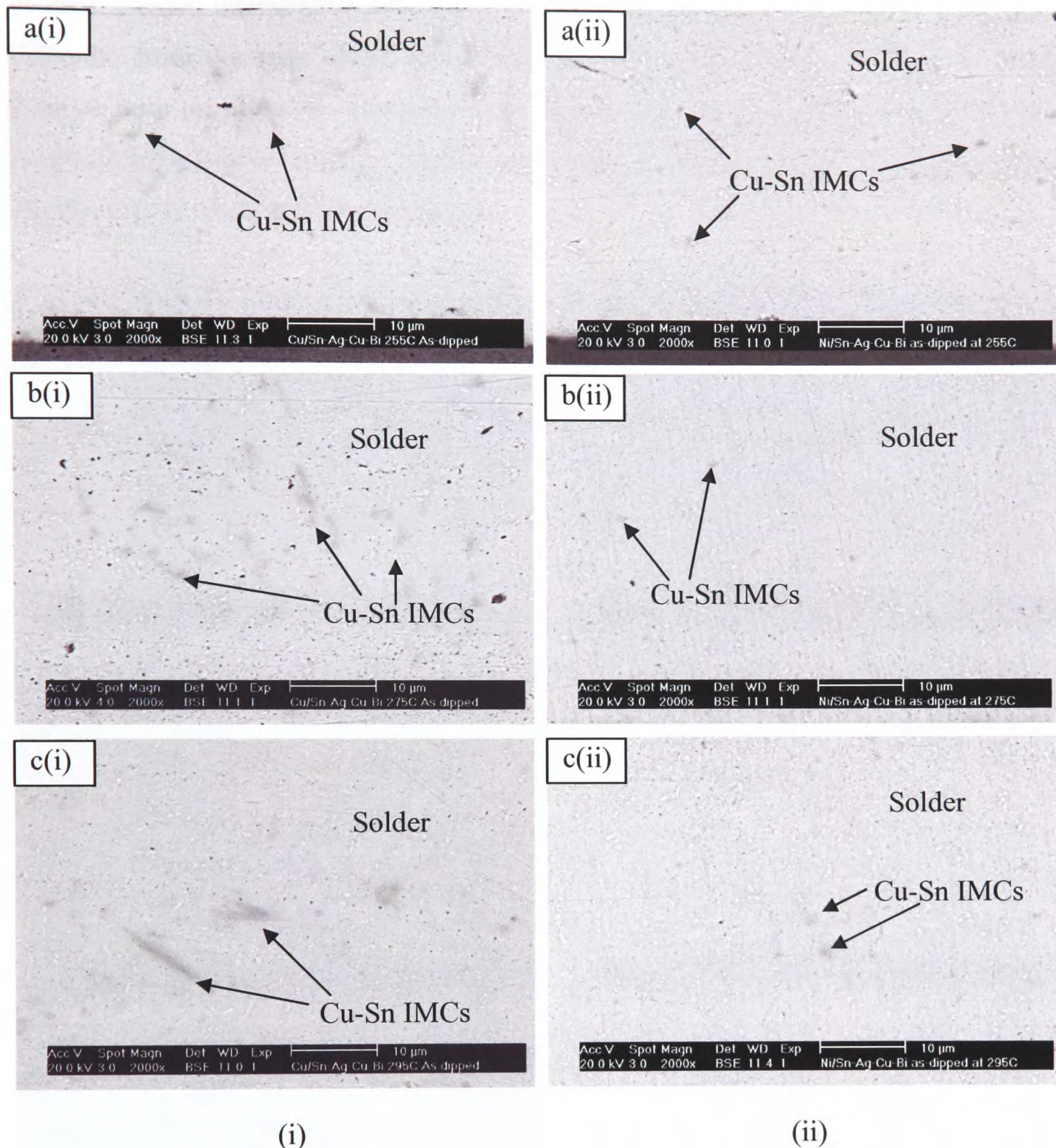


Figure 4-27: Formation of IMCs after dipping (i) Cu and (ii) Ni-substrates into the molten Sn-Ag-Cu-Bi solder bath. Bath temperatures: (a) 255 °C, (b) 275 °C and (c) 295 °C.

Figure 4-27 represents the morphology of Sn-Ag-Cu-Bi solder after dipping the Cu and Ni substrate into it. It is evident that a larger number of IMC grains can be found in the bulk of the solder at 275 °C (Figure 4-27b(i) & b(ii)) than at 255 °C (Figure 4-27a(i) & a(ii)) whereas an increase in the solder bath temperature to 295 °C results in a decrease in the number and an increase in the size of the IMCs (Figure 4-27c(i) and c(ii)). This is due

Chapter-4: Study of Interconnections formed with Lead-free Solder Alloys

to the increased interfacial reaction at elevated temperature that has enhanced the atomic diffusion from the base metal into the bulk of the solder. By correlating the wetting balance tests results with the morphological analysis of the solidified solder, it can be concluded that higher soldering temperature enhances the wettability due to the increased reactions at the solder/substrate interface.

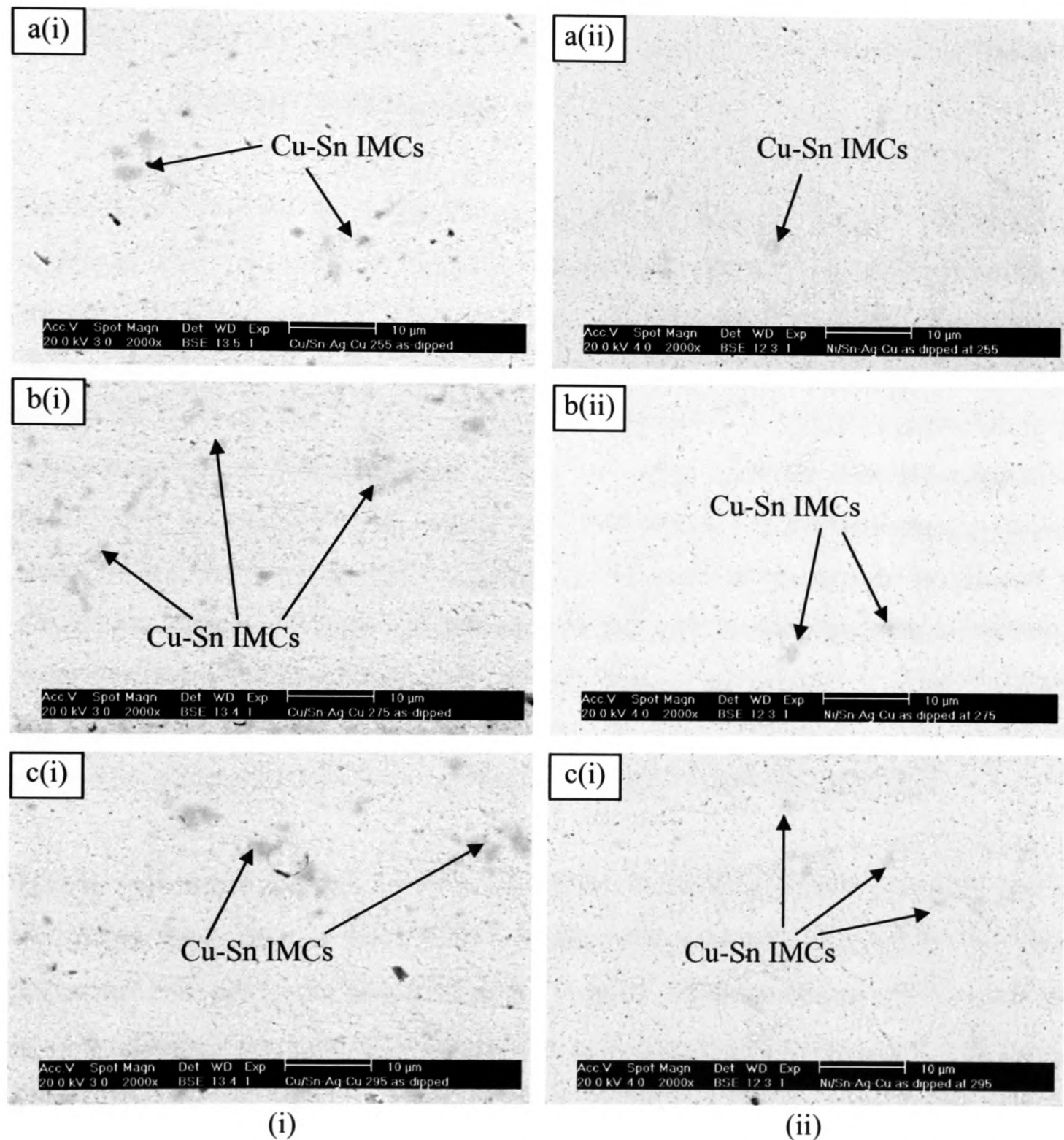


Figure 4-28: Formation of IMCs after dipping (i) Cu and (ii) Ni-substrates into the molten Sn-Ag-Cu solder bath. Bath temperatures: (a) 255 °C, (b) 275 °C and (c) 295 °C.

Figure 4-28 represents the morphology of Sn-Ag-Cu solder after dipping the Cu and Ni substrate into it. Similar to the Sn-Ag-Cu-Bi solder, the sizes of IMC in the bulk of this solder increases with the increase of the soldering temperature. However, the rates of IMC growth with both the Cu and the Ni substrates during soldering are higher for the Sn-Ag-Cu solder than for the Sn-Ag-Cu-Bi solder.

4.4.2.2.3 IMC formations of Sn-0.7Cu and Sn-0.7Cu-0.3Ni Solders on Cu and Ni Substrates

Figure 4-29 represents the solder-Cu interfaces after dipping into Sn-Cu and Sn-Cu-Ni solders at 255, 275 and 295 °C soldering temperatures. An EDX analysis has confirmed that the IMC formed at the SnCu/Cu interface is Cu_6Sn_5 whereas $(\text{CuNi})_6\text{Sn}_5$ is found at the SnCuNi/Cu interface. The atomic percentage of Ni in the $(\text{CuNi})_6\text{Sn}_5$ compound is around 3.23 - 3.66. Since Sn has a higher affinity of Cu [124], Sn supplied from the solder matrix reacts with Cu (supplied from the solder itself and from the substrate) to form Cu_6Sn_5 compounds. In the case of Sn-Cu-Ni solder, it is believed that Ni from the solder matrix has diffused into the solder-Cu interfaces which in turn has formed the $(\text{CuNi})_6\text{Sn}_5$ compounds. Similar compounds for SnCuNi/Cu soldering systems have been found by other researchers [110][125]. As it has been reported by J. Y. Park et al [126], the deposition of Ni into the Cu_6Sn_5 compounds doesn't cause any distortion or new phase formation as the atomic size difference between Cu and Ni is only 2%.

Figures 4-29 shows the IMC layers at the solder-Cu interfaces. Table 4-3 shows that the IMC layer thicknesses at the 255 °C soldering temperature is 1.46 μm for the Sn-Cu solder and 1.42 μm for the Sn-Cu-Ni solder. Table 4-3 also shows that at 275 °C the IMC layer thicknesses are 1.49 and 1.45 μm for Sn-Cu and Sn-Cu-Ni solders respectively. This implies that the higher soldering temperature has resulted in a faster atomic diffusion of Cu and this helps to speed up nucleation of Cu_6Sn_5 compounds at the interface. At 295 °C, the IMC layer thicknesses are 1.52 and 1.51 μm for the Sn-Cu and Sn-Cu-Ni solders respectively. From Figure 4-30 it is also evident that higher soldering temperatures not only increase the IMC layer thickness (Figure 4-29) but also cause larger nucleation of

Chapter-4: Study of Interconnections formed with Lead-free Solder Alloys

Cu_6Sn_5 and/or $(\text{CuNi})_6\text{Sn}_5$ compounds in the bulk of the solder. As a result, the number of IMCs has been increased in the bulk of the solder with the increase in the soldering temperature. It is also evident that larger numbers and sizes of IMCs are found in the bulk of the solder for Sn-Cu solder than for the Sn-Cu-Ni solder. However, in the Sn-Cu-Ni solder matrix, $(\text{CuNi})_6\text{Sn}_5$ forms in the bulk of the solder due to the presence of Ni in the solder matrix.

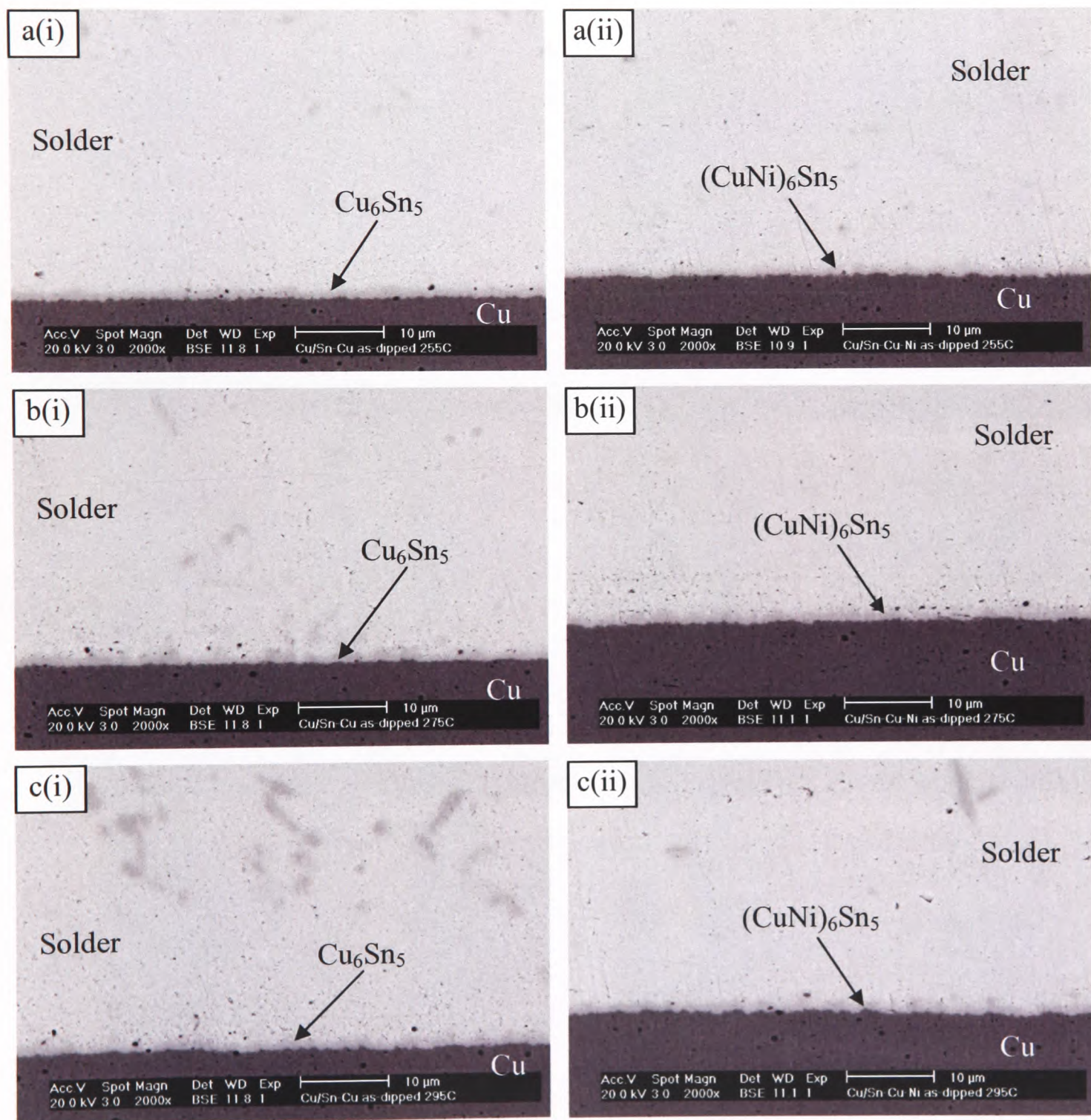


Figure 4-29: Solder-Cu interfaces after dipping into (i) Sn-Cu, (ii) Sn-Cu-Ni solders at a) 255 °C, b) 275 °C and c) 295 °C.

Chapter-4: Study of Interconnections formed with Lead-free Solder Alloys

Table 4-3: Growth of IMC layer during soldering of SnCu and SnCuNi solders

Soldering Temperature (°C)	IMC Thickness (μm)			
	Cu Substrate		Ni Substrate	
	SnCu	SnCuNi	SnCu	SnCuNi
255	1.46	1.42	0.70	0.68
275	1.49	1.45	0.88	0.87
295	1.52	1.51	0.92	0.90

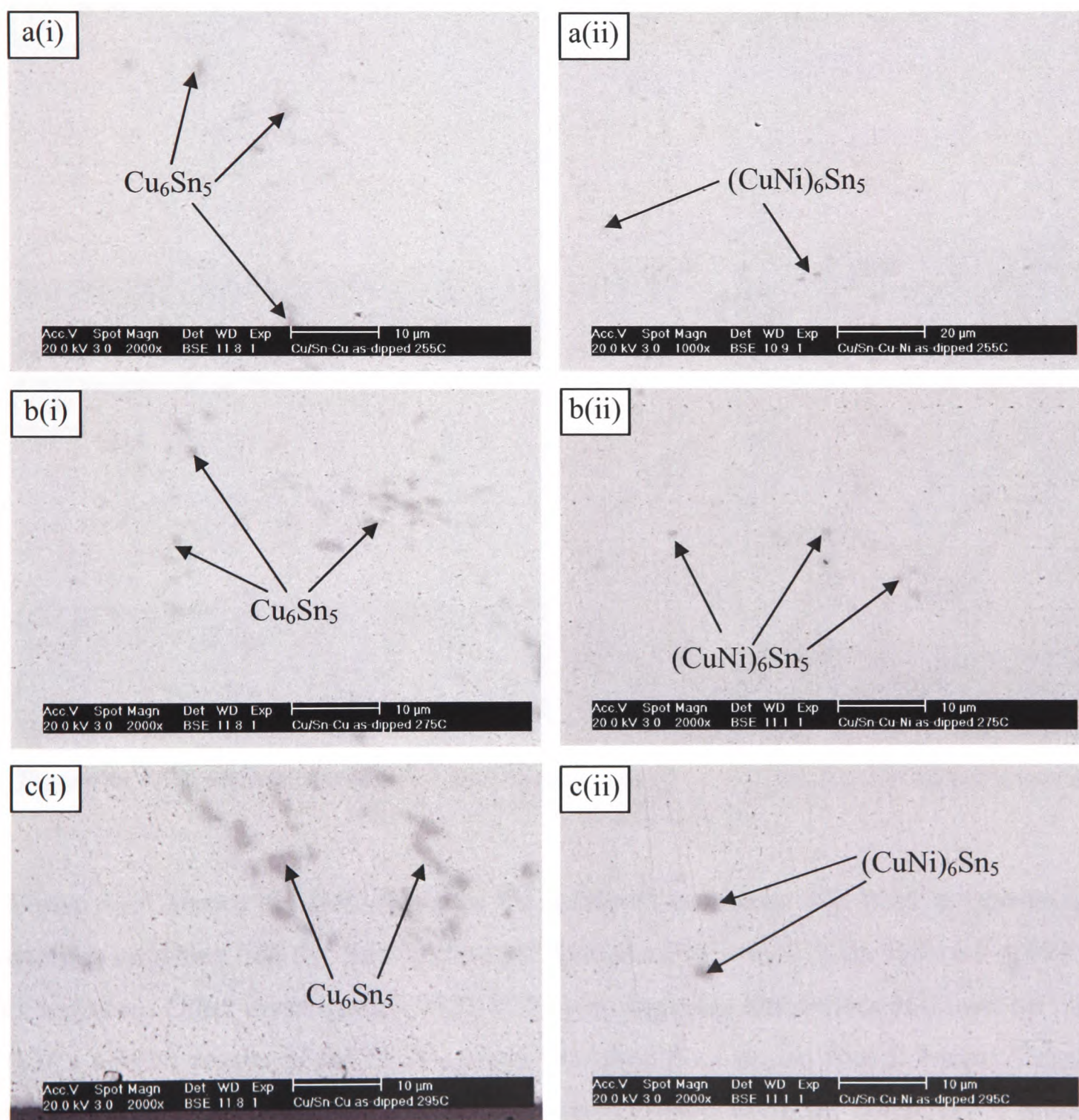


Figure 4-30: Formation of IMCs after dipping Cu-substrate into the molten (i) Sn-Cu, (ii) Sn-Cu-Ni solders bath. Bath temperatures: (a) 255 °C, (b) 275 °C and (c) 295 °C.

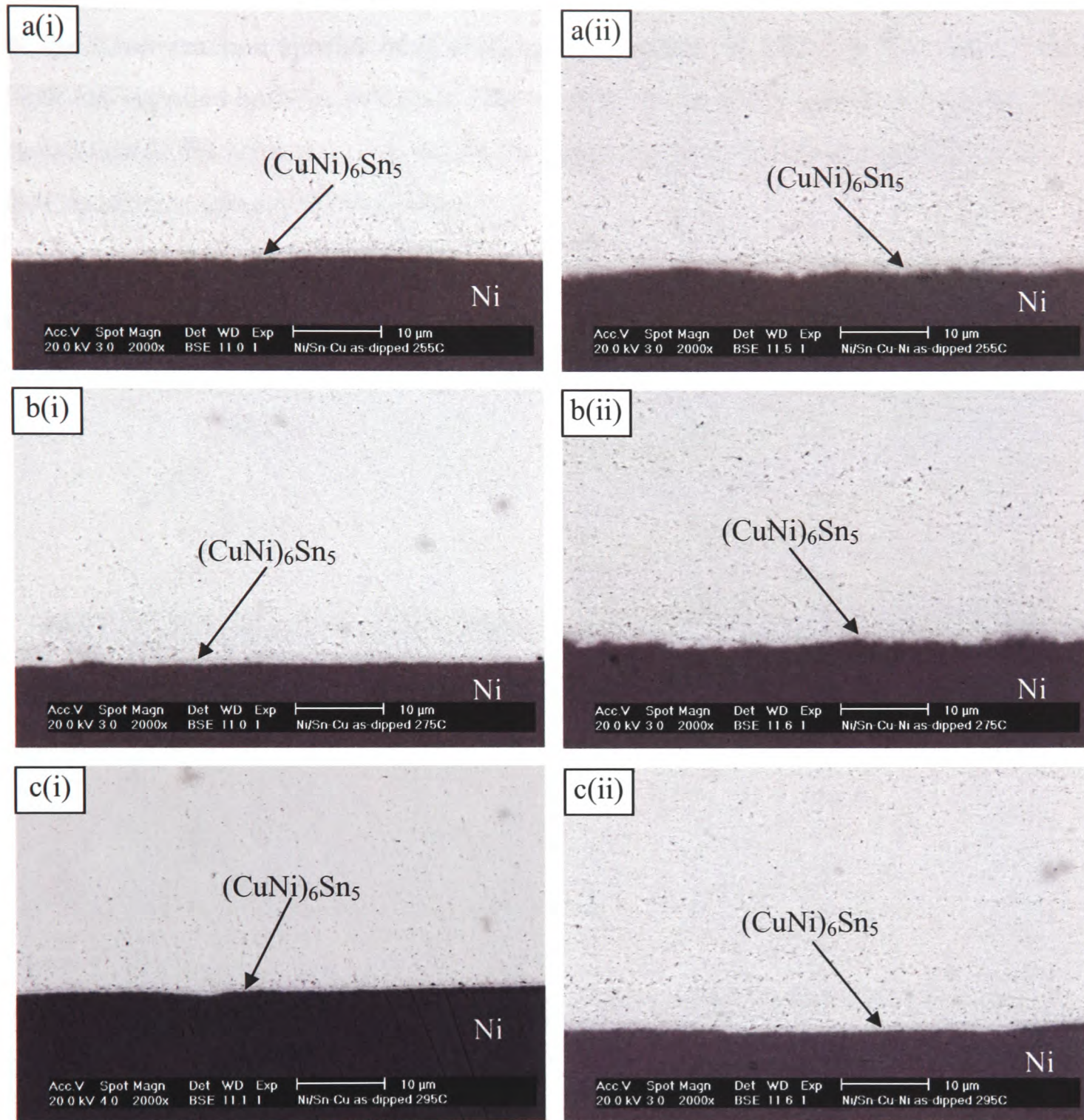


Figure 4-31: Solder-Ni interfaces after dipping into (i) Sn-Cu, (ii) Sn-Cu-Ni solders at a) 255 °C, b) 275 °C and c) 295 °C.

Figure 4-31 shows the IMC layers at the solder/Ni interfaces. An EDX compositional analysis confirms that the IMC compound formed at the interface for both the solder is $(\text{CuNi})_6\text{Sn}_5$. Other investigators [123][127] have suggested that the reaction between Sn-0.7Cu and Ni results in the Ni_3Sn_4 phase but when the reaction time is longer, Cu_6Sn_5 phase would form. In this work, it has been noticed that $(\text{CuNi})_6\text{Sn}_5$ compound is present at the interface. The formation of this compound may be due to the limited availability of

Chapter-4: Study of Interconnections formed with Lead-free Solder Alloys

Ni in solder which has prevented the formation of Ni_3Sn_4 and encouraged the production of the faster reaction species of $(\text{CuNi})_6\text{Sn}_5$ compounds. In this case, the solder matrix itself has supplied both Sn and Cu to react with Ni to form this ternary compound. Other researchers [128] have also noticed the formation of same type of compounds in the Sn-0.7Cu solder reacting with Ni substrate.

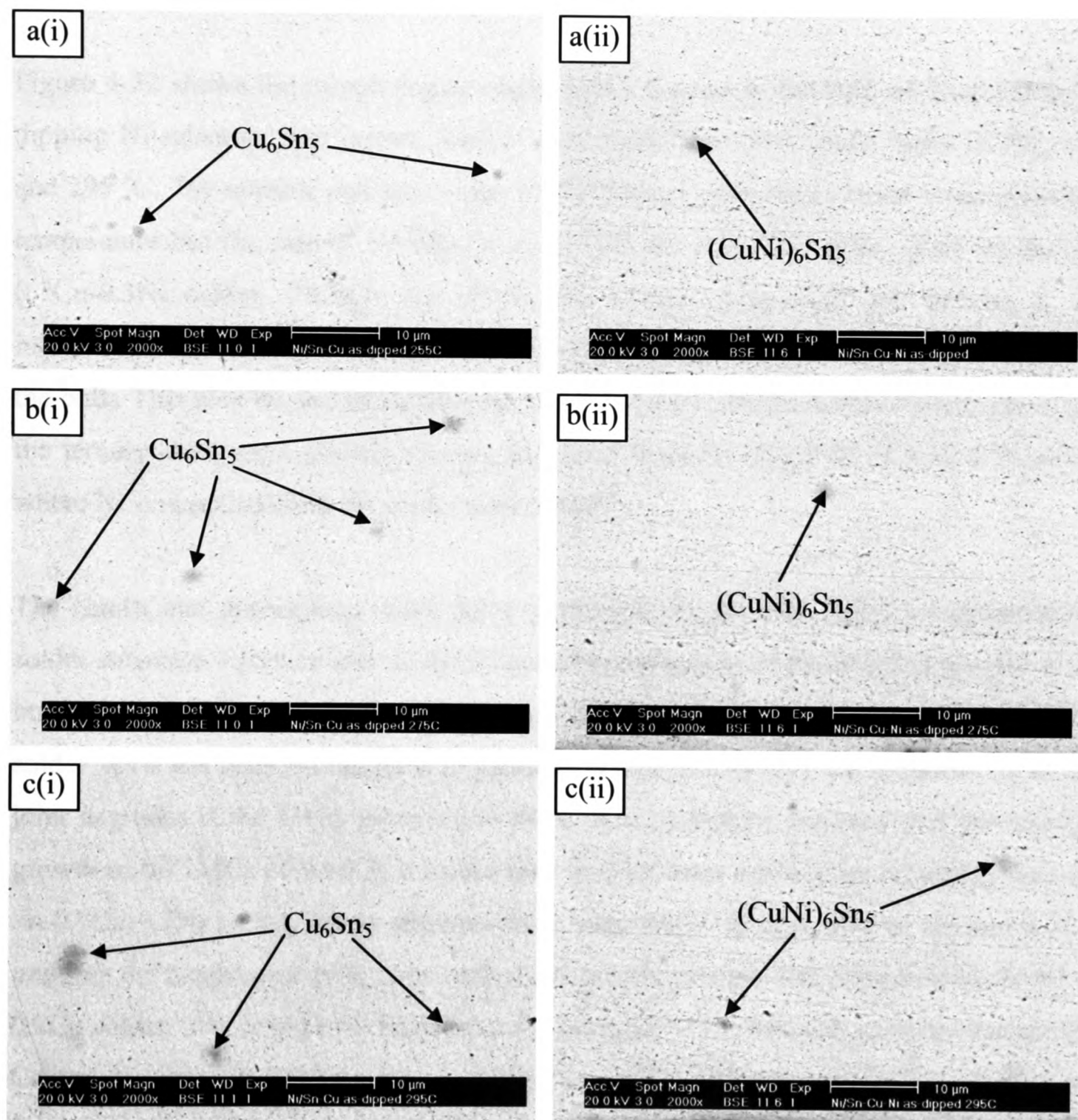


Figure 4-32: Formation of IMCs after dipping Ni-substrate into the molten (i) Sn-Cu, (ii) Sn-Cu-Ni solder baths. Bath temperatures: (a) 255 °C, (b) 275 °C and (c) 295 °C.

From Figure 4-31 it is also found that the IMC layer has increased for both the solders with the increase in the soldering temperature. At 255, 275 and 295 °C, the IMC layer thicknesses have been measured as 0.70, 0.88 and 0.92 μm respectively for the Sn-0.7Cu solder and 0.68, 0.87 and 0.90 μm respectively for Sn-0.7Cu-0.3Ni solder (Table 4-3). In this case a slightly thinner IMC layer has formed at the Sn-0.7Cu-0.3Ni/Ni interface than at the Sn-0.7Cu/Ni interface.

Figure 4-32 shows the morphologies of the IMCs formed in the bulk of the solder after dipping Ni-substrate into molten Sn-0.7Cu or Sn-0.7Cu-0.3Ni solder baths at 255, 275 and 295 °C. The number and size of the IMCs increase with the increase in the soldering temperature but the rate of increase is higher for the Sn-0.7Cu solder than for the Sn-0.7Cu-0.3Ni solder. Though the $(\text{CuNi})_6\text{Sn}_5$ ternary compound has formed at the interface for the SnCu/Ni soldering system, the binary compound Cu_6Sn_5 has formed in the bulk. This may be due to the limited diffusion of Ni into the solder matrix. However, the ternary compound $(\text{CuNi})_6\text{Sn}_5$ has also been found in the bulk of Sn-Cu-Ni solder where Ni is supplied from the solder matrix itself.

The results and discussions above have confirmed that the IMC layer formation at the solder-substrate interface and the heterogeneous nucleation of the reaction species in the bulk of the solder is higher for the Sn-0.7Cu solder than that for the Sn-0.7Cu-0.3Ni solder. As it has been investigated in previous studies [123][129], the reliability of solder joint degrades if the IMCs layer is too thick. It is, therefore, believed that the stronger growth of the IMCs of Sn-0.7Cu solder may lead to lower solder joint reliability than the Sn-0.7Cu-0.3Ni solder. Many attempts have been made (as described in Section 4.1) to improve the mechanical properties such as the tensile strength and creep behaviour of Sn-0.7Cu solder. Wu et al [100] found that the addition of 0.5wt% RE elements (especially Ce and La) into Sn-0.7Cu solder can increase creep resistance. Young et al [101] has found that the addition of 0.2wt% Ni into Sn-2.7Cu solder can reduce the growth rate of Cu_6Sn_5 and Ag_3Sn compounds when PtAg/ Al_2O_3 and Cu/PtAg/ Al_2O_3 substrates are used. However, in this study it has been found that an addition of 0.3 wt% Ni into Sn-0.7Cu solder enhances the wettability, reduces the consumption of substrate material during

soldering and decreases the growth of IMCs at the interfaces as well as in the bulk of the solder.

4.4.2.3 Modelling the Dissolution of Cu Substrate into Sn-37Pb and Sn-0.7Cu Solders during the Wetting Balance Tests

4.4.2.3.1 Mathematics of Diffusion

In earlier sections, it has been mentioned that the dissolution or consumption of Cu and Ni substrates into the liquid solders is the consequence of the continuous atomic diffusion through the solder/metals interfaces. The mathematical theory of such kind of diffusion is based on the hypothesis that the rate of transfer of diffusing substance through unit area of an interfacial section is proportional to the concentration gradient measured normal to the section area [130], i.e.

$$F = -D \left(\frac{\partial C}{\partial x} \right) \quad (4.8)$$

where, F is the rate of transfer per unit area of the interfacial section, C is the concentration of diffusing substance, x is the space coordinate measured normal to the interfacial section and D is the diffusion coefficient. The negative sign represents the diffusion towards lower concentration or “downhill” diffusion [131]. If the diffusion is one-dimensional or if there is a gradient of concentration only along the x-axis, the fundamental differential equation of diffusion for time t is as

$$\frac{\partial C}{\partial t} = D \frac{\partial^2 C}{\partial x^2} \quad (4.9)$$

Equations (4.8) and (4.9) are usually referred to as the Fick’s first and second laws of diffusion. When the initial concentration of the diffusing substance (Cu or Ni) in the

solder is C_o and the interface is maintained at a constant concentration C_1 as shown in the Figure 4-33, the solution of the diffusion equation is

$$\frac{C(x) - C_1}{C_o - C_1} = \text{erf} \frac{x}{2\sqrt{Dt}} \quad (4.10)$$

where, $C(x)$ is the concentration distribution of the diffusing substance in the solder, t is the time. The error function, erf and its complement erfc are defined as [132]:

$$\text{erf}(x) = 1 - \text{erfc}(x) = 1 - \frac{2}{\pi} \int_0^x e^{-\eta^2} d\eta \quad (4.11)$$

$$\text{where, } \eta = \frac{x}{2} \sqrt{Dt} \quad (4.12)$$

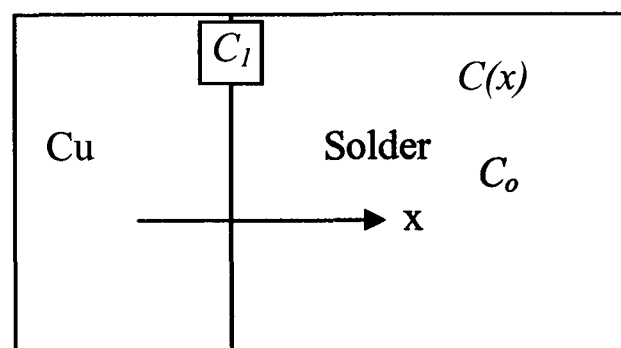


Figure 4-33: Diffusion path of the Cu atoms into liquid solder. C_o is the initial concentration of the diffusing substance in the solder; C_1 is the constant concentration at the solder-Cu interface and $C(x)$ is the concentration distribution of Cu in the solder.

The rate at which the total amount of mass, M_t of diffusing substance per unit interfacial area changes is given by

$$\frac{dM_t}{dt} = - \left(D \frac{\partial C(x)}{\partial x} \right)_{x=0} = (C_1 - C_o) \frac{D}{\sqrt{\pi Dt}} \quad (4.13)$$

Integration with respect to t of equation (4.13) gives the total mass loss of diffusing substance per unit area at time t as

$$M_t = 2(C_1 - C_0) \left(\frac{Dt}{\pi} \right)^{\frac{1}{2}} \quad (4.14)$$

From equation (4.14), the mathematical expression of diffusion coefficient can be expressed as

$$D = \left[\frac{M_t}{2(C_1 - C_0)} \right]^2 \left(\frac{\pi}{t} \right) \quad (4.15)$$

It can be assumed that total mass loss of the diffusing substance (Cu or Ni) is equal to the amount of dissolved diffusing substance in the solder. Therefore, from the mass balance of the diffusing substance, the dissolved thickness can be expressed as [103]

$$\Delta h = \left(\frac{C}{100} \right) \left(\frac{V}{A} \right) \left(\frac{\rho_{solder}}{\rho_{substrate}} \right) \quad (4.16)$$

where, C is the wt% of diffusing substrate in the liquid solder, V is the volume of the liquid solder, A is the interfacial area between liquid solder and diffusing substance, ρ_{solder} and $\rho_{substrate}$ are the density of liquid solder and the density of the diffusing substrate respectively.

If the unit of C is in wt%, dissolved thickness Δh can be expressed in terms of the total mass loss per unit area of the diffusing substrate as

$$\Delta h = M_t \left(\frac{\rho_{solder}}{\rho_{substrate}} \right) \quad (4.17)$$

Substituting equation (4.17) into equation (4.15), the diffusion coefficient D can be expressed as

$$D = \left[\frac{\Delta h}{2(C_1 - C_o)} \frac{\rho_{substrate}}{\rho_{solder}} \right]^2 \frac{\pi}{t} \quad (4.18)$$

The above equation is applicable only for the flat copper surface with fixed Cu-solder boundary where convection doesn't take place.

4.4.2.3.2 Calculation of Diffusion Coefficients from the Data obtained from the Wetting Balance Tests

The diffusion coefficients of Cu for Sn-37Pb and Sn-0.7Cu solders can be estimated using equation (4.18). The density of the diffusing substance i.e. the density of Cu is denoted by ρ_{Cu} and the densities of Sn-37Pb and Sn-0.7Cu solders are 8.96, 8.40 and 7.30 gm/cc respectively. The densities of solders have been calculated from the density of the pure Sn (7.29 gm/cc), pure Cu (8.96 gm/cc) and Pb (11.34 gm/cc) by using the equation $1/\rho_{solder} = (f_{Sn}/\rho_{Sn}) + (f_{Pb \text{ or } Cu} / \rho_{Pb \text{ or } Cu})$ [36], where, f_{Sn} is the mass fraction of tin and $f_{Pb \text{ or } Cu}$ is the mass fraction of Pb or Cu in the solder. Densities of Sn, Cu and Pb have taken from [133]. The total consumed thickness from both sides of the Cu substrate by the Sn-Pb and the Sn-Cu solders are the 2 times of the values shown in the Figures 4-21 and 4-23(a). The initial concentration of Cu in the Sn-37Pb and Sn-0.7Cu solders are 0.0 and 0.7wt% respectively, i.e. $C_o = 0.0$ for Sn-37Pb solder and 0.007 for Sn-0.7Cu solder. The constant concentration at the fixed boundary of Cu-solder interface can be calculated for different temperatures from the Cu-Sn phase-diagram shown in the Figure 4-34. From this figure, C_1 at 255 °C is estimated as 1.30 wt%. The calculated diffusion coefficient D for Sn-37Pb and Sn-0.7Cu solders are $2.74 \times 10^{-10} \text{ m}^2/\text{s}$ and $6.44 \times 10^{-9} \text{ m}^2/\text{s}$ respectively. In the EDX analysis described earlier, it has been seen that the concentration of Cu in the

Sn-Ag-Cu-Bi solder is 2.6wt% at 255 °C soldering temperature [26]. In this case the same value has been used for both solders as the saturation limit by assuming that the maximum concentration of Cu is 2.6 wt% in the molten solders.

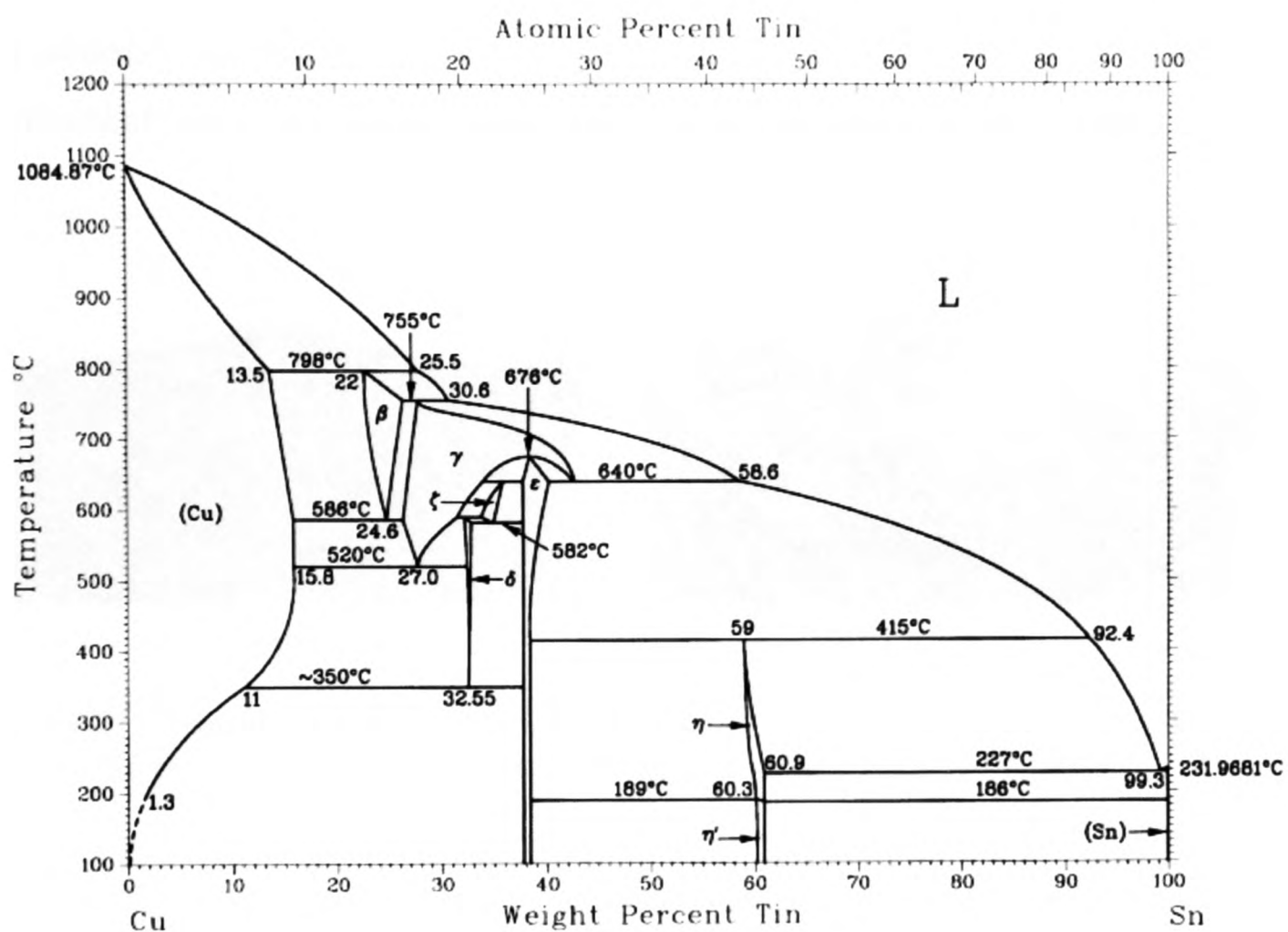


Figure 4-34: Cu-Sn phase diagram [134].

4.4.2.3.3 Modelling Results and Discussions

Figure 4-35 shows snapshots of the concentration of Cu atoms in the molten solder bath of Sn-37Pb and Sn-0.7Cu after 10 s of reaction time. The colour variations represent different Cu concentration values around the Cu/solder interfaces. Higher Cu concentration is observed at the interfaces where Cu comes into contact with the molten solders. This concentration of Cu is the source of the IMCs layer shown in Figure 4-29. It

Chapter-4: Study of Interconnections formed with Lead-free Solder Alloys

is clear that higher amount of Cu can be diffused into the Sn-0.7Cu solder compared to the Sn-37Pb solder. The diffusion coefficient is one of the major factors that govern the rate at which solid Cu dissolve in the molten solder. The coefficient value is lower for the Sn-37Pb than for Sn-0.7Cu solder because the rate of consumption of Cu also depends on the speed of the Sn-Cu reaction. The higher amount (99.3wt%) of Sn in the Sn-0.7Cu solder requires more and more Cu atoms for the reaction whereas the Sn-37Pb solder that contains only 63wt% Sn needs less amount of Cu atoms.

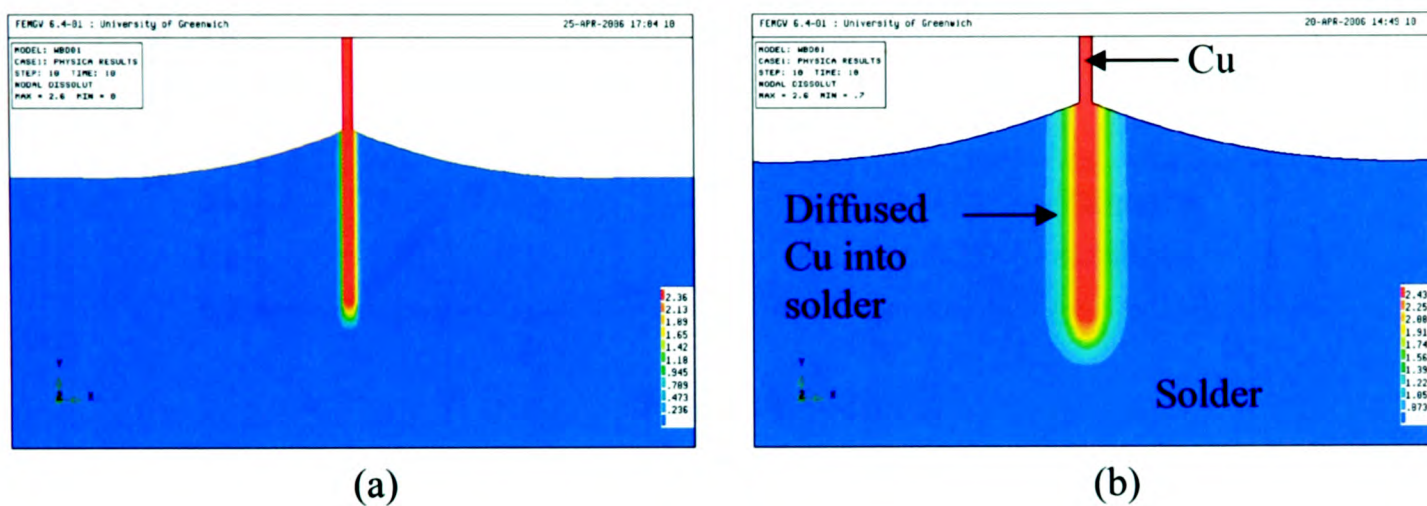


Figure 4-35: Dissolution of Cu substrate after 10 s of reaction with (a) Sn-37Pb and (b) Sn-0.7Cu solders (colour bars represent Cu concentrations in wt%).

Figure 4-36 and 4-37 show the estimated dissolved amount (wt%) of Cu at the solder/Cu interfaces and that in the bulk of the solders over reaction time. The concentration of Cu at the interface (Figure 4-36) for both solders is very high compared to the concentration into the bulk of the solder (Figure 4-37). Figure 4-36 reveals that the concentration of Cu near the interfaces of Sn-37Pb/Cu soldering system increases relatively slowly whereas the concentration increases much faster in the early stage of the reaction in the Sn-0.7Cu/Cu soldering system and slows down. The Cu concentration in the Sn-0.7Cu solder reaches saturation over a shorter period of time than that in the Sn-37Pb solder. Therefore, during the assembly of electronic component to the substrate with lead-free Sn-0.7Cu solder, the total amount of Cu on the interconnection pad may be consumed within a very short period of time. The absence of Cu on the substrate then may cause dewetting during reworking of the package.

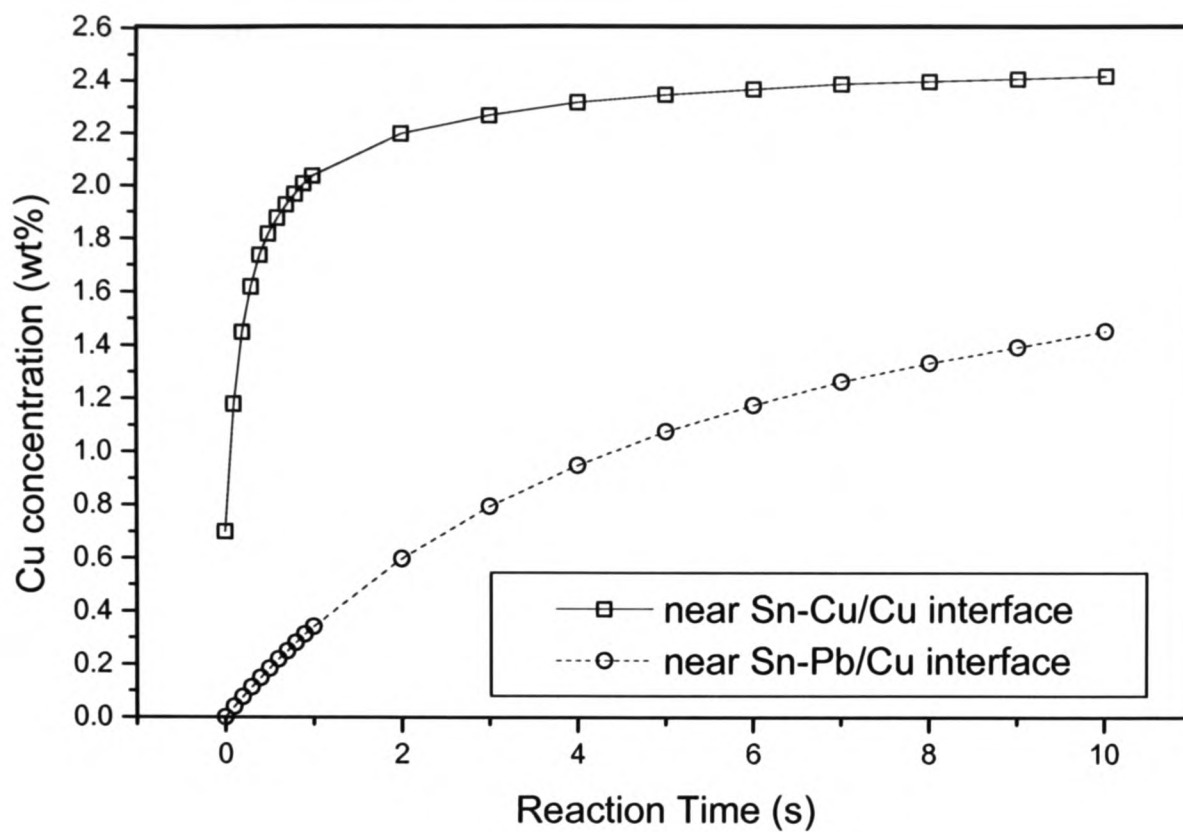


Figure 4-36: Concentration of Cu over reaction time (near interface).

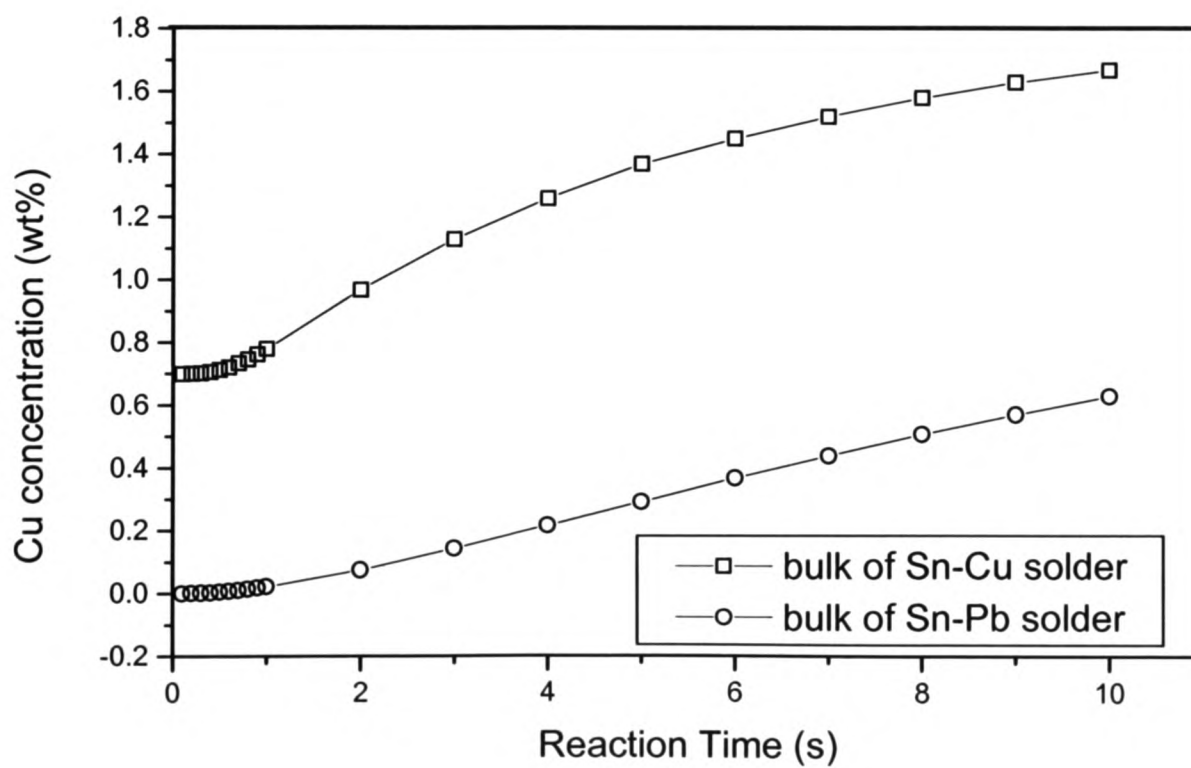


Figure 4-37: Concentration of Cu over reaction time (in the bulk of solders).

Figure 4-37 shows that Cu concentration in the bulk of Sn-37Pb increases almost linearly whereas the concentration increase in the Sn-0.7Cu solder is close to the parabolic form. This indicates that in all parts of the Sn-0.7Cu solder, Cu saturation can be reached over a relatively short period of time. Therefore, it can be expected that the higher concentration of Cu in the lead-free solder may result in the higher rate of IMC formation compared to the lead-bearing solder. In section 4.4.2.2, it has been seen that the IMC layer thickness at 255 °C soldering temperature is 0.86 μm for Sn-37Pb solder and 1.46 μm for Sn-0.7Cu solder.

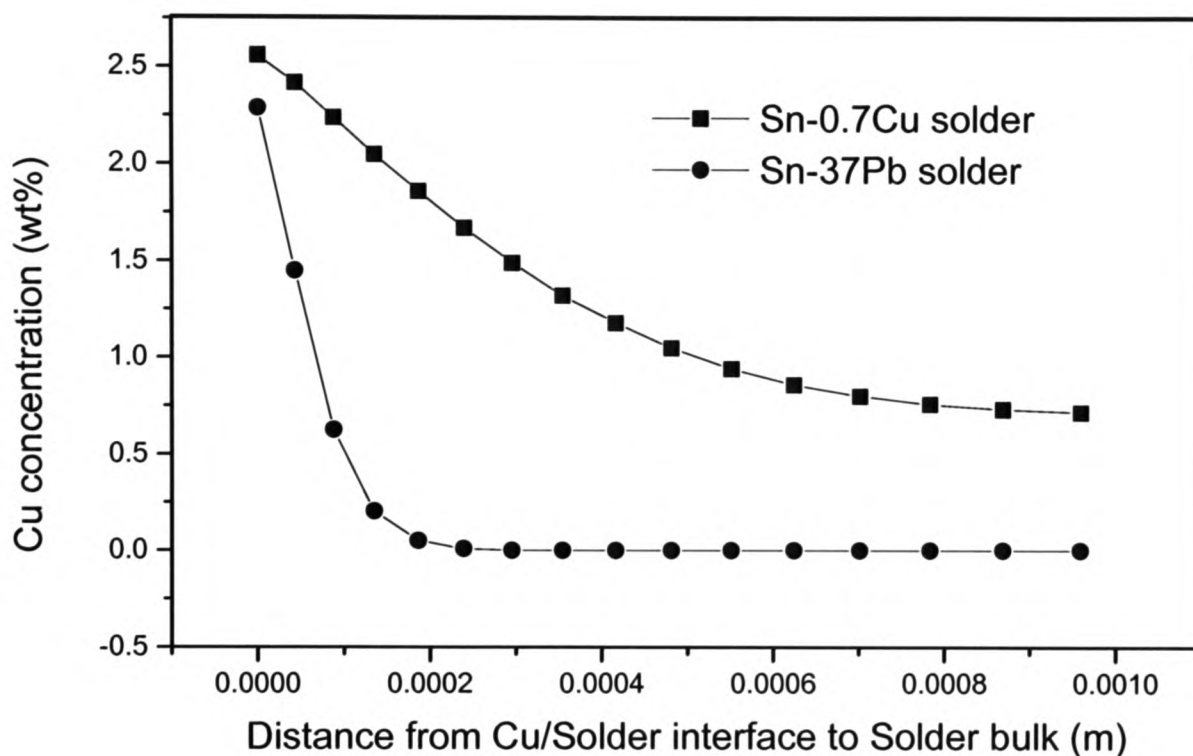


Figure 4-38: Cu concentration at various distances from the solder-Cu interface towards the bulk of the solder.

Figure 4-38 shows the concentration of Cu in the Sn-37Pb and Sn-0.7Cu solders after 10 sec of wetting reaction. It is clearly seen that the concentration decreases from the interfaces to the bulk of the solders and the decrease is gradual in the Sn-0.7Cu solder and rapid in the Sn-37Pb solder. The maximum Cu concentrations are found at the solder/Cu interfaces and the maximum values are 2.56wt% and 2.29wt% for the Sn-0.7Cu/Cu and Sn-37Pb/Cu solders respectively. Experimental results have shown a continuous Cu-Sn compound layer along the interfaces where 55at% Cu and 45at% Sn were detected.

Modelling results show that the Cu atoms from the substrate and the existing Cu atoms in solder accumulate at the interfaces to form such kind of IMC compounds. An EDX analysis of experimented samples has confirmed that the average Cu-concentration at different locations in the bulk of the Sn-37Pb and Sn-0.7Cu solders ranges between 0.68 - 1.05 wt% and 1.07 - 1.30 wt% respectively. Modelling results shown in Figure 4-38 are consistent with the experimental results. Since Cu atoms can diffuse further into the Sn-0.7Cu solder from the interface, it is expected that Cu atoms can accumulate in the solder bulk far away from the solder/substrate interfaces. Therefore Cu can react with Sn in the bulk of solder to form Cu-Sn IMCs compounds and this may explain the experimental results shown in Figures 4-29 and 4-30. Kim et al [103] has found that 0.15-0.5wt% Cu can concentrate in the bulk of the Sn-Pb solder during solder reflow at 200 °C. However, the concentration values found in this study is higher than this value. This may due to the higher soldering temperature, larger solder volume and bigger solder/Cu interfacial areas that have been used in this work.

4.4.3 Growth Behaviours of IMC Layers on Cu-Substrate during Isothermal Aging of Pb-free Solders

4.4.3.1 IMC Layer formations in Sn-2.8Ag-0.5Cu and Sn-2.8Ag-0.5Cu-1.0Bi Solders

Backscattered electron microscopy images of Figure 4-25a(i) & a(ii) have showed the IMC layers that have formed between the solder and the Cu substrate just after the wetting reaction at 255 °C. An EDX analysis has confirmed that Ag and Bi doesn't contribute to the formation of the IMCs at the solder-Cu interface and therefore, this IMC layer consists of only Cu_6Sn_5 in which the concentration of Cu and Sn are 55 at% and 45 at% respectively. When the Cu substrate is dipped in the molten solder, the growth of the scallop-like Cu_6Sn_5 IMCs depends on the coarsening of the Cu_6Sn_5 scallops and on the interfacial reaction [135]. In the soldering process, Cu atoms of the substrate diffuse into the solder matrix through the Cu_6Sn_5 layer. When the concentration of Cu in the solder

exceeds the threshold limit, the Cu_6Sn_5 compounds also form in the bulk of the solder as shown in the Figures 4-27a(i) & 4-28a(ii). The thicknesses of the Cu_6Sn_5 IMC layers for the interfacial reaction of Sn2.8Ag0.5Cu/Cu and Sn2.8Ag0.5Cu1.0Bi/Cu soldering systems are 1.52 μm and 1.01 μm respectively. Also, the Cu_6Sn_5 IMC formation in the bulk of the solder is higher for Sn2.8Ag0.5Cu/Cu soldering system than that in the Sn2.8Ag0.5Cu1.0Bi/Cu soldering system (Figures 4-27(a) & 4-28(a)). After the soldering process, the IMCs layers continue to grow with thermal treatments. After 2 days of solid-state aging, the thicknesses of Cu_6Sn_5 IMC layer for Sn2.8Ag0.5Cu/Cu (Figure 4-39(a)) and Sn2.8Ag0.5Cu1.0Bi/Cu (Figure 4-39(b)) soldering systems have increased to 3.47 μm and 3.17 μm respectively. In the solid-state aging, the IMC growth at the valleys between two adjacent scallops is faster than at the peaks of the scallops as reported by Lee et al [135]. As a result, the Cu_6Sn_5 IMC layer is transformed from the scallop-like shape (Figure 4-25(a)) to the layer-type shape (Figure 4-39). The heterogeneous nucleation of Ag_3Sn compound is also noticed for both solders after 2 days of aging (Figure 4-39). It has been stated earlier that the formation of Cu_6Sn_5 is mainly due to the reaction of Sn in solder and Cu atoms diffused from the substrate. The diffusion of Cu atoms is much faster during the soldering reaction than during the solid-state aging process. Moreover, the diffusivity of Cu in the Sn is also faster than the diffusivity of Ag in the Sn [135]. Therefore, only Cu_6Sn_5 IMC was detected for as-dipped soldered condition. Furthermore, Ag_3Sn compounds have formed after 2 days of aging due to the selective formation of Cu_6Sn_5 compounds in the solder matrix.

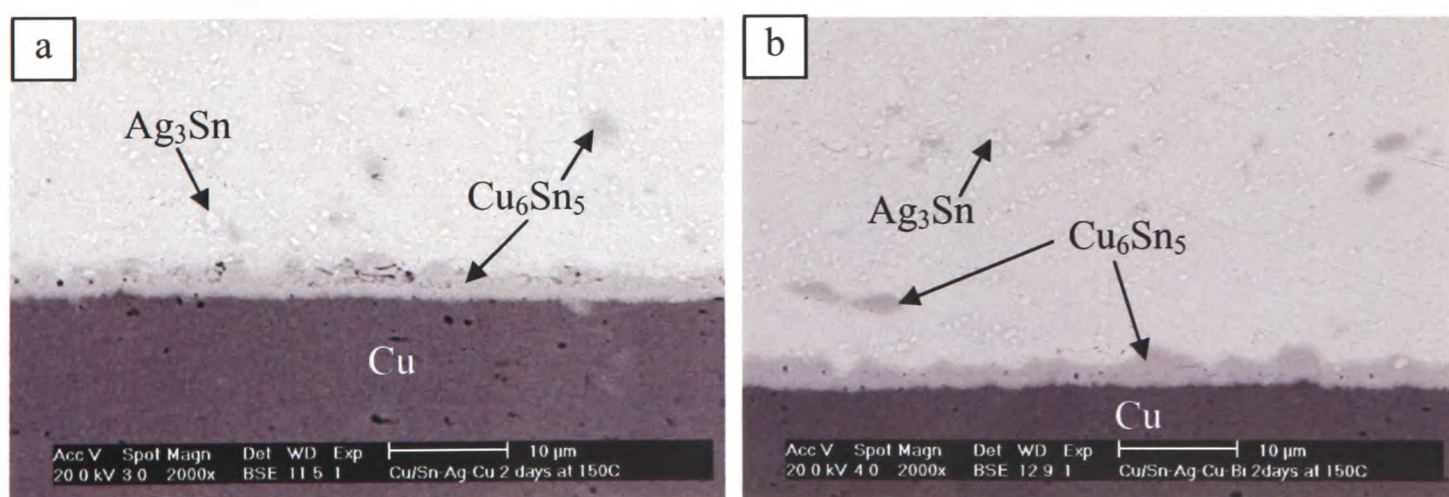


Figure 4-39: SEM images showing the solder-Cu interfaces after 2 days of aging for a) Sn-2.8Ag-0.5Cu and b) Sn-2.8Ag-0.5Cu-1.0Bi solders.

Chapter-4: Study of Interconnections formed with Lead-free Solder Alloys

After 6 days of aging, a slightly more planar IMC layer has been found for the Sn-2.8Ag-0.5Cu-1.0Bi solder (Figure 4-40(b)) than the Sn-2.8Ag-0.5Cu solder (Figure 4-40(a)). At this stage, the Cu_6Sn_5 IMC layer thicknesses for Sn-2.8Ag-0.5Cu/Cu and Sn-2.8Ag-0.5Cu-1.0Bi/Cu soldering systems have been measured as 5.65 μm and 4.50 μm respectively. In this case, the sizes of the Cu_6Sn_5 and the Ag_3Sn IMCs are larger in Sn-2.8Ag-0.5Cu solder matrix than in the Sn-2.8Ag-0.5Cu-1.0Bi solder. Therefore, an addition of 1wt% Bi into the Sn-2.8Ag-0.5Cu solder reduces the nucleation of Cu_6Sn_5 and Ag_3Sn IMCs in the solder matrix. A similar trend of IMC formation has also been found for both solders after 10 days of aging.

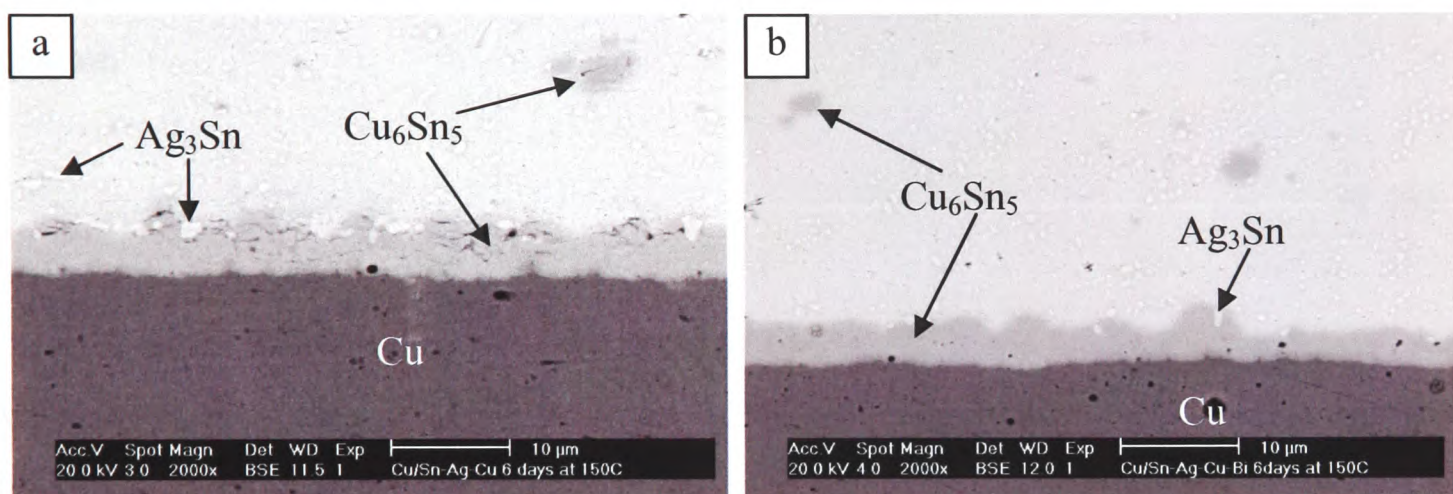


Figure 4-40: SEM images showing the solder-Cu interfaces after 6 days of aging for a) Sn-2.8Ag-0.5Cu and b) Sn-2.8Ag-0.5Cu-1.0Bi solders.

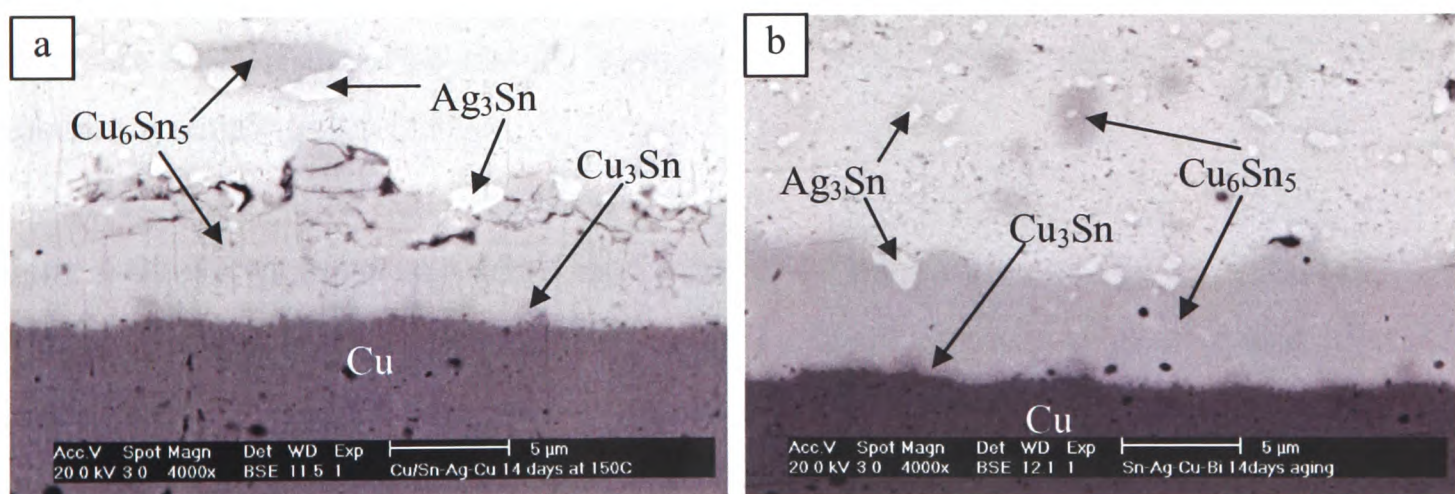


Figure 4-41: SEM images showing the solder-Cu interfaces after 14 days of aging for a) Sn-2.8Ag-0.5Cu and b) Sn-2.8Ag-0.5Cu-1.0Bi solders.

The thicknesses of IMC layers after 14 days of aging for the Sn-2.8Ag-0.5Cu/Cu and the Sn-2.8Ag-0.5Cu-1.0Bi/Cu soldering systems have been measured as 7.50 μm and 6.20 μm respectively. An additional thin layer beneath the Cu_6Sn_5 layer for both solders has been detected (Figure 4-41(a) & (b)). An EDX analysis has confirmed that this layer is Cu_3Sn with a composition of 76at% Cu and 24at% Sn. When the supply of Sn through the IMC layer is limited, the diffused-Cu from substrate reacts with the existing Cu_6Sn_5 compounds and forms Cu_3Sn compounds underneath the thick Cu_6Sn_5 compound layer [90].

The thickness of the IMC layer formed during the aging can be expressed by a simple equation

$$Y - Y_0 = kt^n \quad (4.19)$$

where, Y is the thickness of the IMC layer at time t , Y_0 is the initial thickness, k is the IMC growth rate constant and n is the time exponent. It has been reported that during a solid-state aging process, the growth of IMCs generally follows either the linear law or the parabolic law [136]. The growth rate is controlled by the reaction rate at the growth site if the IMC growth follows the linear kinetics. If the growth follows the parabolic law the growth is controlled by the volume diffusion. For the diffusion-controlled growth of the IMC, the layer thickness after aging should be proportional to the square root of the time power law relationship that can be expressed as $Y - Y_0 = kt^{1/2}$ where the value of time exponent n equals to 0.5 [137].

Figure 4-42 shows the thickness of the Cu_6Sn_5 IMC layer as a function of the square root of the aging time. It shows that the IMC layer thickness increases almost linearly over the square root of the aging time and the growth is faster for Sn2.8Ag0.5Cu/Cu soldering system than the Sn2.8Ag0.5Cu1.0Bi/Cu soldering system. From this figure it is evident that the growth of Cu_6Sn_5 IMC layer for both soldering systems follows the parabolic growth kinetics and therefore the Cu-Sn IMCs growth is diffusion-controlled. Other researchers [138][139] have also confirmed this.

In order to identify the IMCs growth mechanism for the Sn2.8Ag0.5Cu/Cu and the Sn2.8Ag0.5Cu1.0Bi/Cu soldering systems, the growth rate constant, k has been determined using the multivariable linear regression analysis of Y versus $t^{0.5}$ data. The slopes of the curves shown in the Figure 4-42 result in k values of $2.21 \times 10^{-17} \text{ m}^2/\text{s}$ and $1.91 \times 10^{-17} \text{ m}^2/\text{s}$ for the Sn2.8Ag0.5Cu/Cu and the Sn2.8Ag0.5Cu1.0Bi/Cu soldering systems respectively. Therefore, the growth rate of the IMCs layer during the isothermal aging is higher for Sn2.8Ag0.5Cu/Cu soldering system than the Sn2.8Ag0.5Cu1.0Bi/Cu soldering system. This difference in growth rate is clearly visible in the SEM images shown in Figures 4-39 – 4-41. The correlation coefficient R^2 for the two linear regression analysis is 0.9942 for Sn2.8Ag0.5Cu/Cu soldering system and 0.9913 for the Sn2.8Ag0.5Cu1.0Bi/Cu soldering system. This implies that the IMC formations for both soldering systems closely follow the diffusion controlled mechanism.

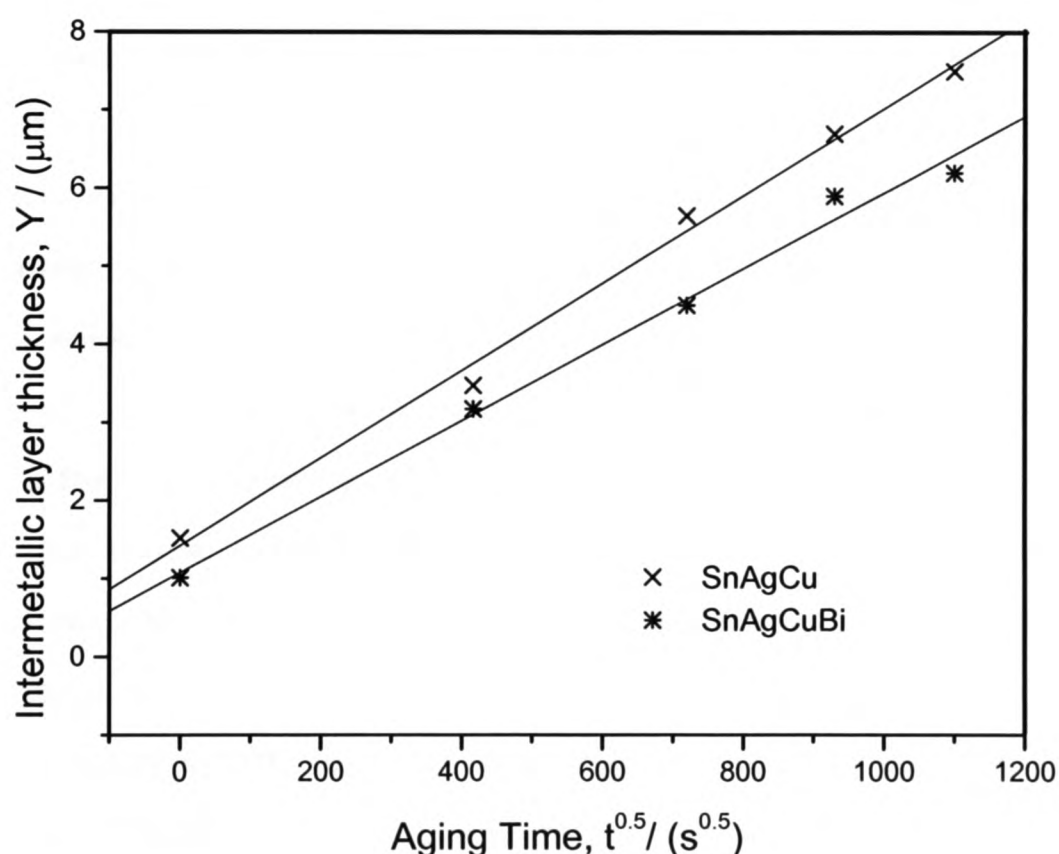


Figure 4-42: Thickness of IMC layer as a function of square root of the aging time.

The actual value of the time exponent n for the growth of IMCs layer during isothermal aging can also be calculated in the linear regression analysis of the following logarithmic form of equation (4.19) [140].

$$\ln(Y - Y_0) = n \ln(t) + \ln(k) \quad (4.20)$$

The n values for Sn2.8Ag0.5Cu/Cu and Sn2.8Ag0.5Cu1.0Bi/Cu soldering systems are found to be 0.57 and 0.45 respectively and these n values define the behaviours of the diffusion process as well as the IMC layer formation in the Sn2.8Ag0.5Cu/Cu and the Sn2.8Ag0.5Cu1.0Bi/Cu soldering systems.

The above discussions demonstrate that the IMC layer thickness increases due to the Cu diffusion process and Cu diffusion rate is higher in the Sn-2.8Ag-0.5Cu solder than in the Sn-2.8Ag-0.5Cu-1.0Bi solder. During the soldering reaction, Cu atoms diffuse from the substrate and react with Sn atoms to form IMCs at the solder-substrate interface and within the bulk of the solder. This Cu diffusion takes place through the channels of the IMC layer. However, the interfacial reaction is not fast enough to consume all the diffused Cu atoms. Therefore, the unreacted and free Cu atoms can diffuse further into the bulk of the solder and react with Sn to form Cu_6Sn_5 compounds there. As a result, the concentration of Cu in the bulk of the solders decreases which encourages further diffusion of Cu from the substrate. When the Cu concentration is close to saturation in the bulk of the solder, Cu_6Sn_5 compounds begin to deposit usually on the existing IMC layer. As a consequence, the thickness of IMC layer increases. Similarly, the IMC layer thickness increases during the solid-state aging with the gradual diffusion of Cu into the solder. Relative rougher IMC layer has been found in the Sn2.8Ag0.5Cu/Cu soldering system than in Sn2.8Ag0.5Cu1.0Bi/Cu soldering system after 14 days of aging (Figure 4-41), and this is because of the higher consumption rate of Cu in the Sn-2.8Ag-0.5Cu solder than in the Bi-containing solder (Figure 4-43).

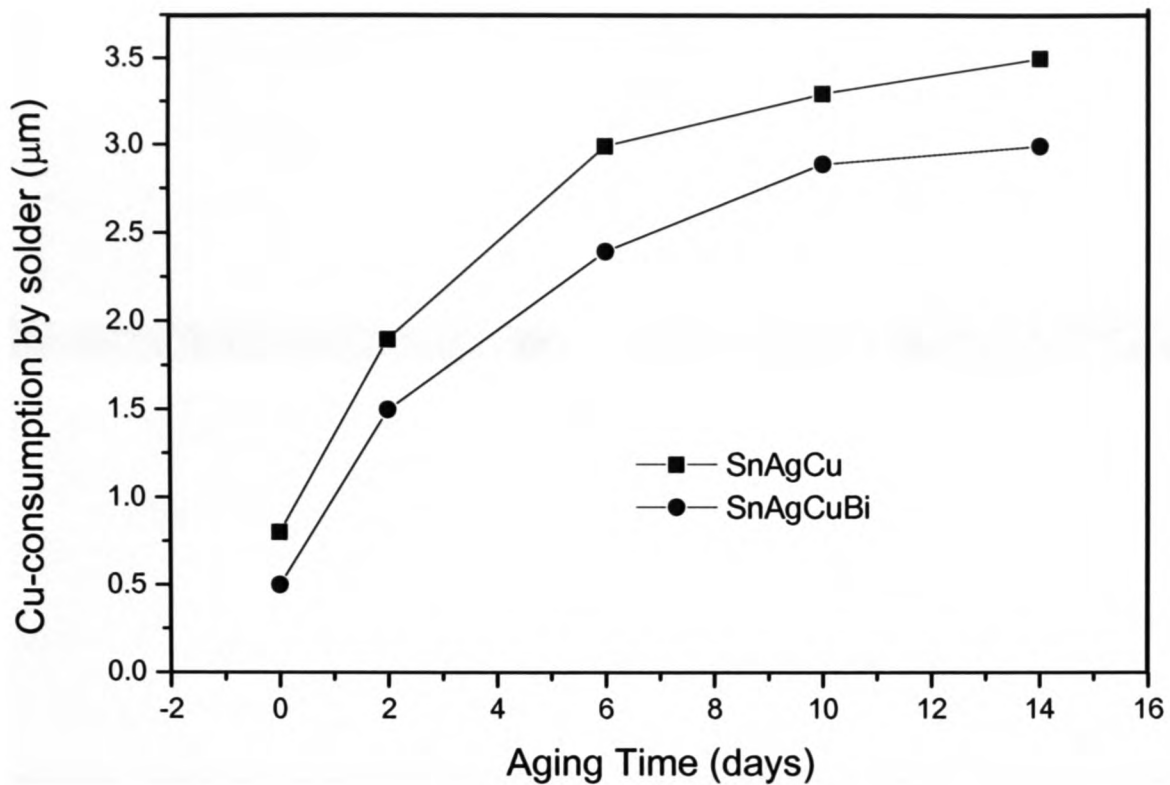


Figure 4-43: Cu-consumptions in solders as functions of the aging time.

The images in Figure 4-44 show the IMCs in the bulk of the Sn-2.8Ag-0.5Cu and Sn-2.8Ag-0.5Cu-1.0Bi solders. In Figures 4-44a(i) and b(i), it can be seen that small amount of Cu_6Sn_5 and Ag_3Sn have formed after 2 days of aging. The sizes of these IMCs increase slowly with the aging time (Figure 4-44a(i-iv) and b(i-iv)). Moreover, the sizes of intermetallic phases are bigger in the Sn-2.8Ag-0.5Cu solder than in the Sn-2.8Ag-0.5Cu-1.0Bi solder. Therefore, Bi plays a strong role in the Cu diffusion process as well as in the formation and the growth of IMCs. According to the Sn-Bi binary phase diagram, the solid solubility of Bi in Sn at room temperature is about 1 wt%. At high temperature this solubility limit increases to 11wt% at 120 °C and 21wt% at 139 °C [97]. Vianco et al [141] has found Bi-precipitations on the Cu_6Sn_5 IMC layer and this is thought to be caused by the Bi-rejection from the Sn-matrix. However, in this study no such precipitation of Bi has been found possibly because the amount of 1wt% of Bi that has been added into the solder is small.

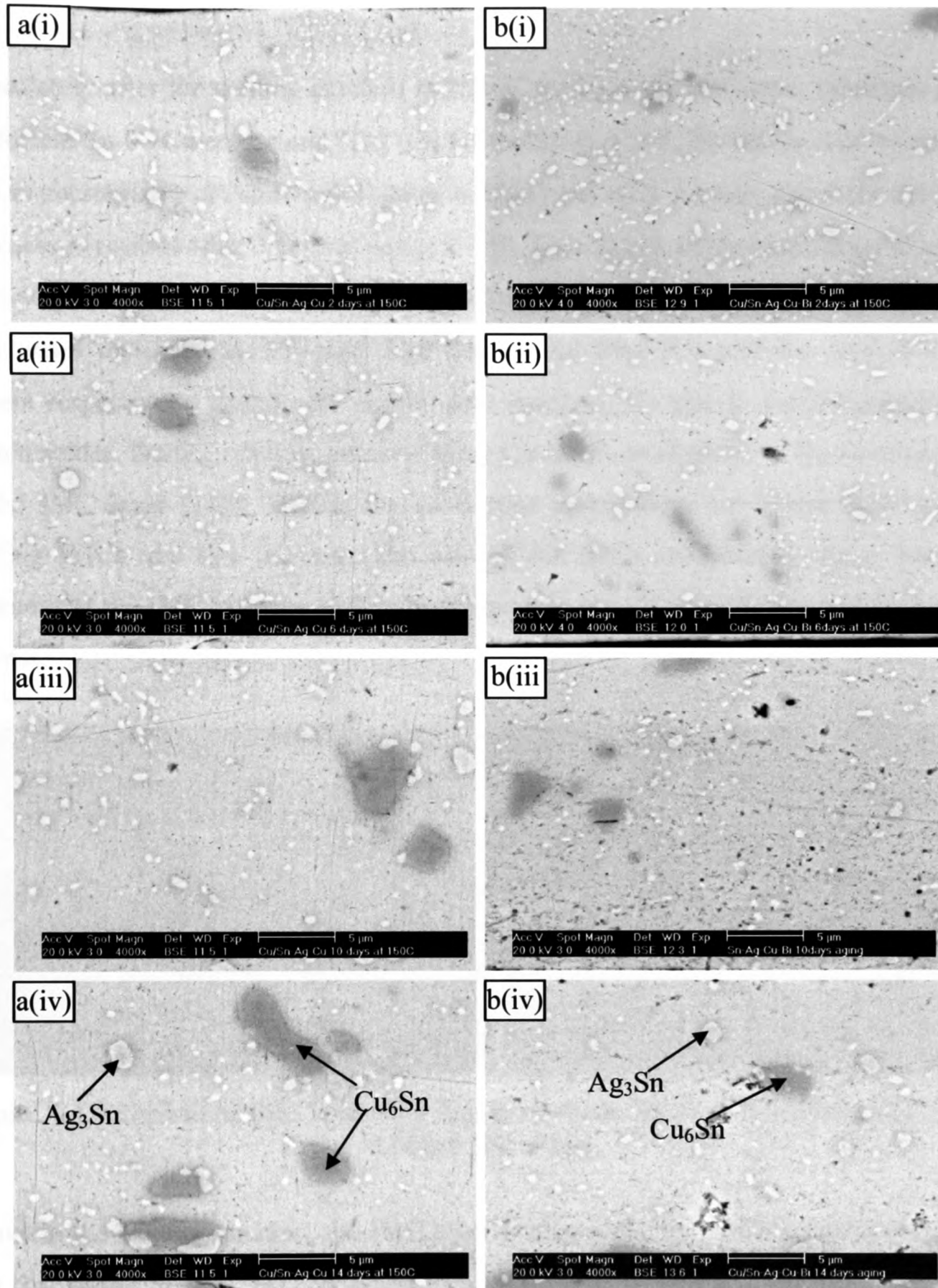


Figure 4-44: Formation of IMCs in the bulk of a) Sn-2.8Ag-0.5Cu and b) Sn-2.8Ag-0.5Cu-1.0Bi solders after aging at 150 °C for i) 2 days, ii) 6 days, iii) 10 days and iv) 14 days.

4.4.3.2 IMC Layer formations in Sn-0.7Cu and Sn-0.7Cu-0.3Ni Solders

Immediately after the wetting reaction at 255 °C for 10 s, the IMC layer thickness is 1.46 μm for the Sn-0.7Cu solder and 1.42 μm for the Sn-0.7Cu-0.3Ni solder. The solder cross section micrographs are shown in Figures 4-29a(i) and a(ii). An increase in the IMC layer thickness is noticed after 2 days of aging at 150 °C as shown in the backscattered electron microscopic images in Figure 4-45. The Cu_6Sn_5 and the $(\text{CuNi})_6\text{Sn}_5$ IMC layer thicknesses increased to 2.74 and 2.30 μm for the Sn-0.7Cu and the Sn-0.7Cu-0.3Ni solders respectively. During the liquid state reaction, Cu atoms dissolve quickly into molten solder. During cooling, some of these Cu atoms precipitate on the existing grains of the IMC layer [142]. During the solid state aging some Cu atoms react with the existing IMCs and this increases the size of the IMCs compounds. As a result, the thickness of the IMC layer as well as their nuclei in the solder bulk increase in the aging process.

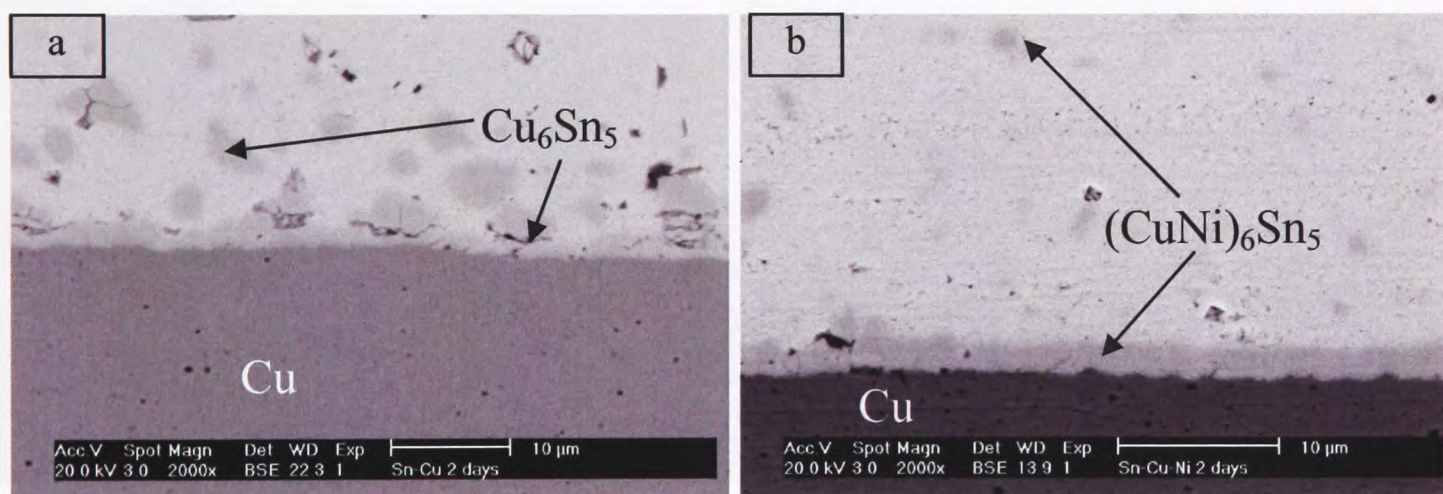


Figure 4-45: Growth of IMC layer after 2 days of aging. (a) Sn-0.7Cu solder and (b) Sn-0.7Cu-0.3Ni solder.

Unlike in the wetting reaction, the IMC layer thickness for Sn-0.7Cu solder is still higher than that of the Sn-0.7Cu-0.3Ni solder. The nucleation of IMCs at the interfaces is also higher for the Sn-0.7Cu solder. According to the results obtained from the experiment, the Sn-0.7Cu solder has consumed more Cu than Sn-0.7Cu-0.3Ni solder during the wetting reaction and, therefore, the abundant supply of Cu enhances the higher growth rate of IMCs during the solid state aging. Surprisingly the trend reversed after 6 days of

aging. As shown in the Figure 4-46, the IMC layer thicknesses of Sn-0.7Cu and Sn-0.7Cu-0.3Ni solders increased to 4.04 and 4.89 μm after 6 days of aging. After 2 days of aging, Sn-0.7Cu has the rougher IMC layer, but after 6 days of aging the Sn-0.7Cu-0.3Ni solder has the rougher IMC layer. It has been mentioned earlier that atomic diffusion from the substrate continues in the solid state reaction. Generally diffusion occurs in the direction normal to the solder-substrate interfaces through the less dense parts of the IMC layer where valleys are located. Therefore, the growth in these valleys is faster and eventually these valleys will be filled. This may explain why the morphology of IMC layer becomes planar and stable during the solid state aging. Laurila et al [143] has found that the addition of more than 5wt% Ni results in thicker growth of IMC layer and the rate of IMC formation depends on the concentration of Ni. In this study, the amount of Ni added into the solder is very small (0.3wt%) and it has been noted that after 6 days of aging higher IMC layer thickness has been found in the Ni containing solder. This result may be due to an increase in the concentration of Ni in the IMC as the aging time is very long, e.g. 6 days.

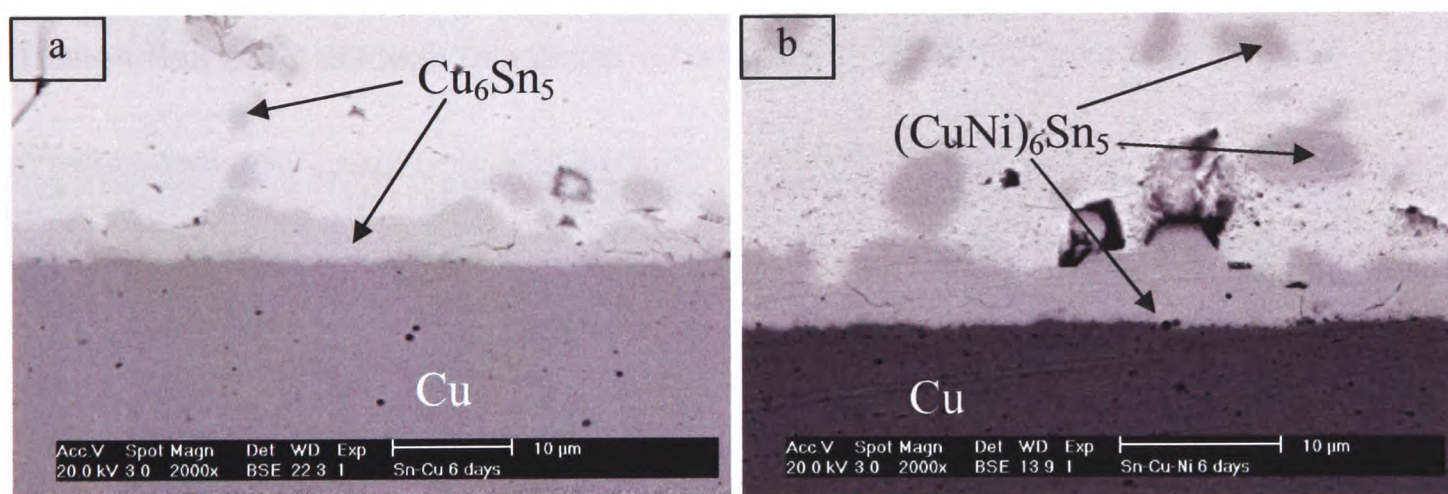


Figure 4-46: Growth of IMC layer after 6 days of aging. (a) Sn-0.7Cu solder and (b) Sn-0.7Cu-0.3Ni solder.

The microstructures of IMC layer at the solder/Cu interfaces after 10 days of aging are shown in Figure 4-47. The thickness of IMC layer has increased to 5.31 μm for the Sn-0.7Cu solder and 5.80 μm for the Sn-0.7Cu-0.3Ni solder. In the case of Sn-0.7Cu solder, a thin layer of IMCs has been found adjacent to the Cu substrate. An EDX analysis has confirmed that this layer is the Cu_3Sn compound which is composed of 75 at% of Cu and

25 at% of Sn. Thermodynamically it is proved that the driving force for Cu_6Sn_5 phase formation is higher than that for the Cu_3Sn phase formation and Cu_3Sn forms only if there is a short supply of Sn atoms [142][144]. Therefore, in the aging process, the limited supply of Sn at the Cu/IMC interface results in the formation of the Cu_3Sn layer. However, this Cu_3Sn layer was not observed after dipping and wetting. The experimental results of Laurila et al [143] imply that a very thin layer of Cu_3Sn forms after reflow or wave soldering and this layer can only be detected using a scanning electron microscope (SEM) after 64 minutes of contact time at 250 °C. Since the contact time in this experiment is only 10 seconds, the probability of forming a detectable Cu_3Sn layer is very small. It is interesting to note that Cu_3Sn layer could not be detected in the case of Sn-0.7Cu-0.3Ni solder after 10 days of aging and $(\text{CuNi})_6\text{Sn}_5$ is the only IMC that has been observed. Therefore, adding 0.3 wt% Ni can suppress the growth of Cu_3Sn layer. Similar results have been found by Ohriner [145] and he suggested that the Ni containing solder cannot form Cu_3Sn layer due to Ni's effects on the thermodynamic or the kinetics of the reactions in solder. Laurila et al [143] claims that the growth of Cu_3Sn layer is suppressed for the kinetic reasons as the growth rate of $(\text{CuNi})_6\text{Sn}_5$ IMC layer is faster and thus the diffusion flux of Sn through this phase is too small to allow the growth of Cu_3Sn .

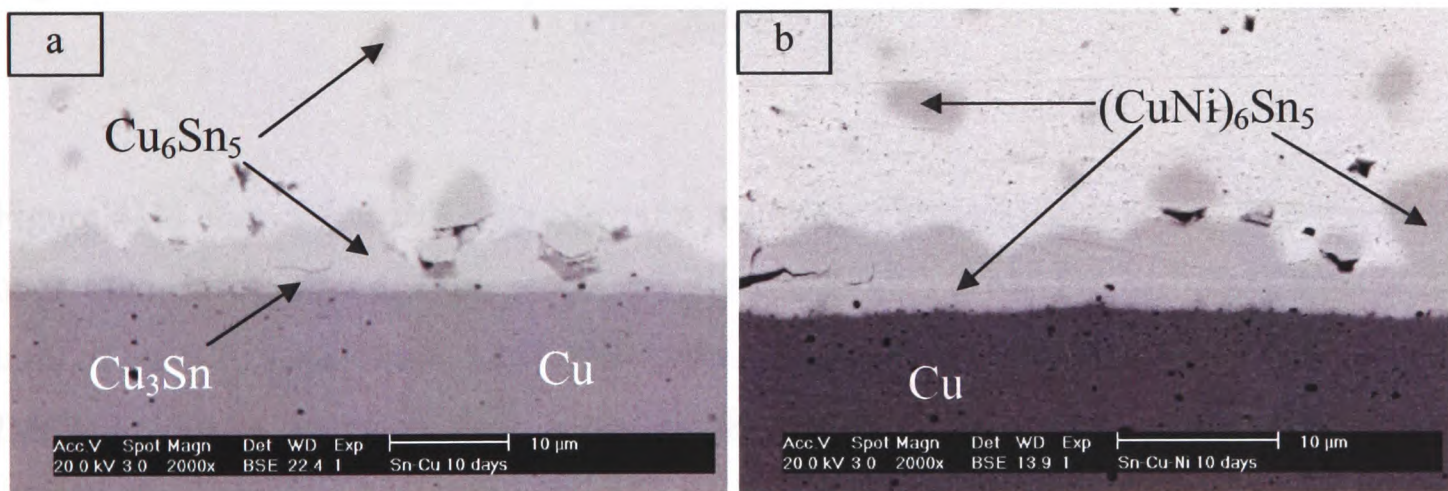


Figure 4-47: Growth of IMC layer after 10 days of aging. (a) Sn-0.7Cu solder and (b) Sn-0.7Cu-0.3Ni solder.

A dramatic increase in the thickness of $(\text{CuNi})_6\text{Sn}_5$ IMC layer is observed for the case of Sn-0.7Cu-0.3Ni solder after 14 days of aging as shown in the Figure 4-48. The thickness of IMC layer for this solder is 7.90 μm and for Sn-0.7Cu solder it is just 5.95 μm. The

reaction time of 14 days seems long enough for Ni to accumulate in the existing IMC layer. This is the possible reason of the dramatic increase in the IMC layer thickness in the Sn-0.7Cu-0.3Ni solder. The Cu_3Sn layer in the Sn-0.7Cu solder also increased after 14 days of aging and this indicates that the interface reaction suffers from a short supply of Sn when the aging time is long. Figure 4-48 also shows that IMC layers in both solders are broken and this situation is more severe for the Sn-0.7Cu-0.3Ni solder than the Sn-0.7Cu solder. This might have been caused by the polishing process during the preparation of the samples. As Mattila et al [146] have also reported that the IMC layer becomes more brittle when Ni is added making it susceptible to mechanical fracture.

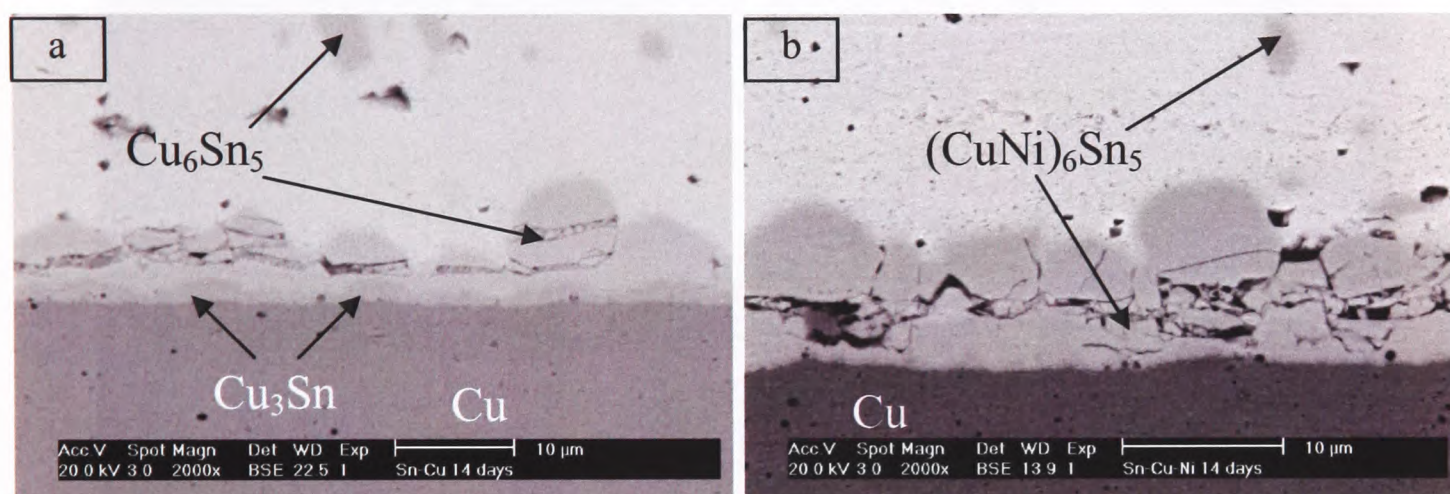


Figure 4-48: Growth of IMC layer after 14 days of aging. (a) Sn-0.7Cu solder and (b) Sn-0.7Cu-0.3Ni solder.

Figure 4-49 shows that IMCs also form in the bulk of the solders and they become larger over time during aging. Figures 4-49a(i-iv) and b(i-iv) show the microstructure in the bulk of Sn-0.7Cu and Sn-0.7Cu-0.3Ni solders. It is clearly visible in these figures that the IMCs gradually increase their sizes as the aging time increases. The size of the $(\text{CuNi})_6\text{Sn}_5$ compound in the bulk of Sn-0.7Cu-0.3Ni solder increases more rapidly compared to the Cu_6Sn_5 compound in the bulk of Sn-0.7Cu solder. Therefore, the addition of Ni into the Sn-0.7Cu solder influences the growth of IMCs.

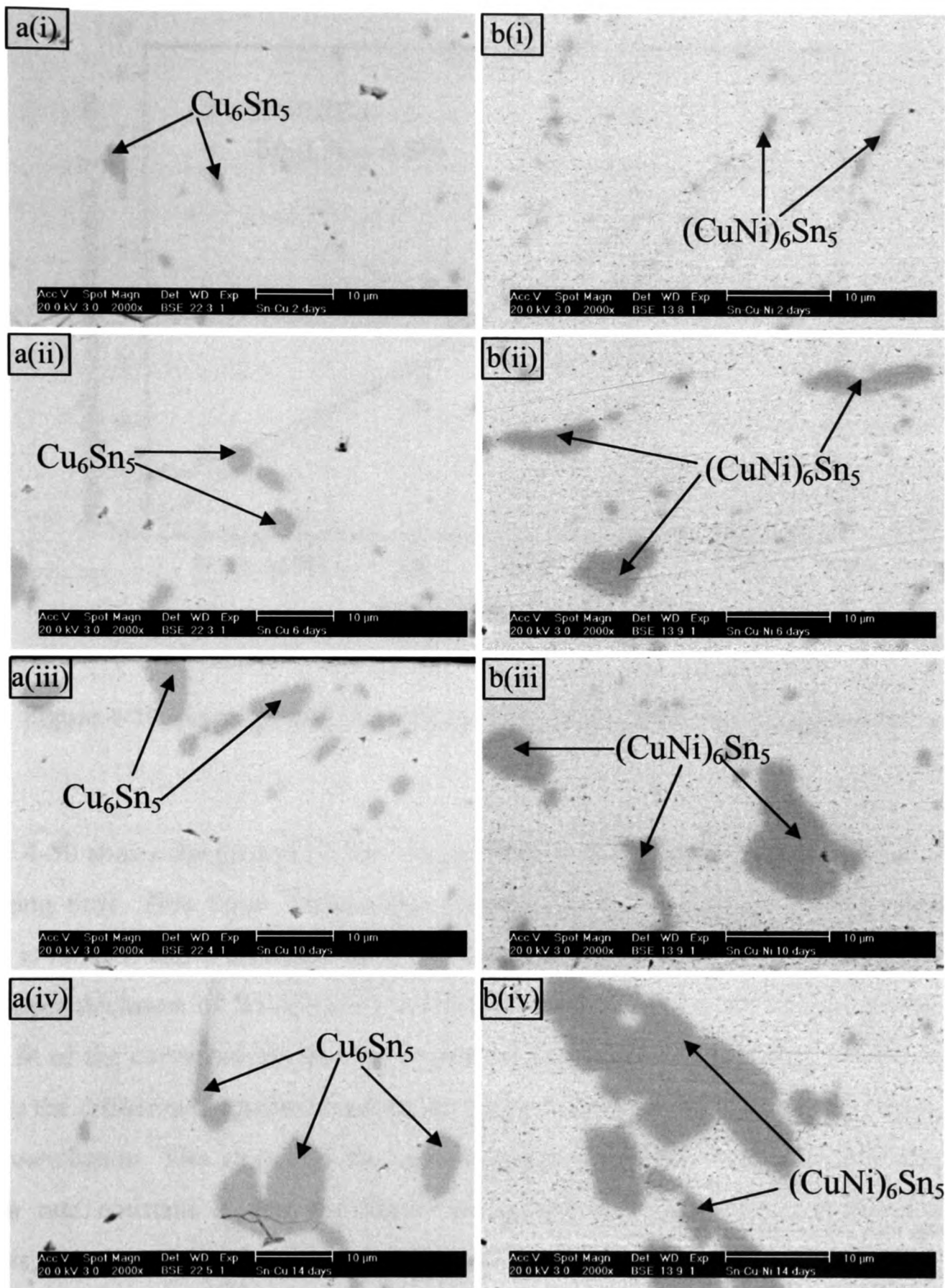


Figure 4-49: IMC formations in the bulk of (a) Sn-0.7Cu and (b) Sn-0.7Cu-0.3Ni solders with Cu substrate during aging for (i) 2 days, (ii) 6 days, (iii) 10 days and (iv) 14 days.

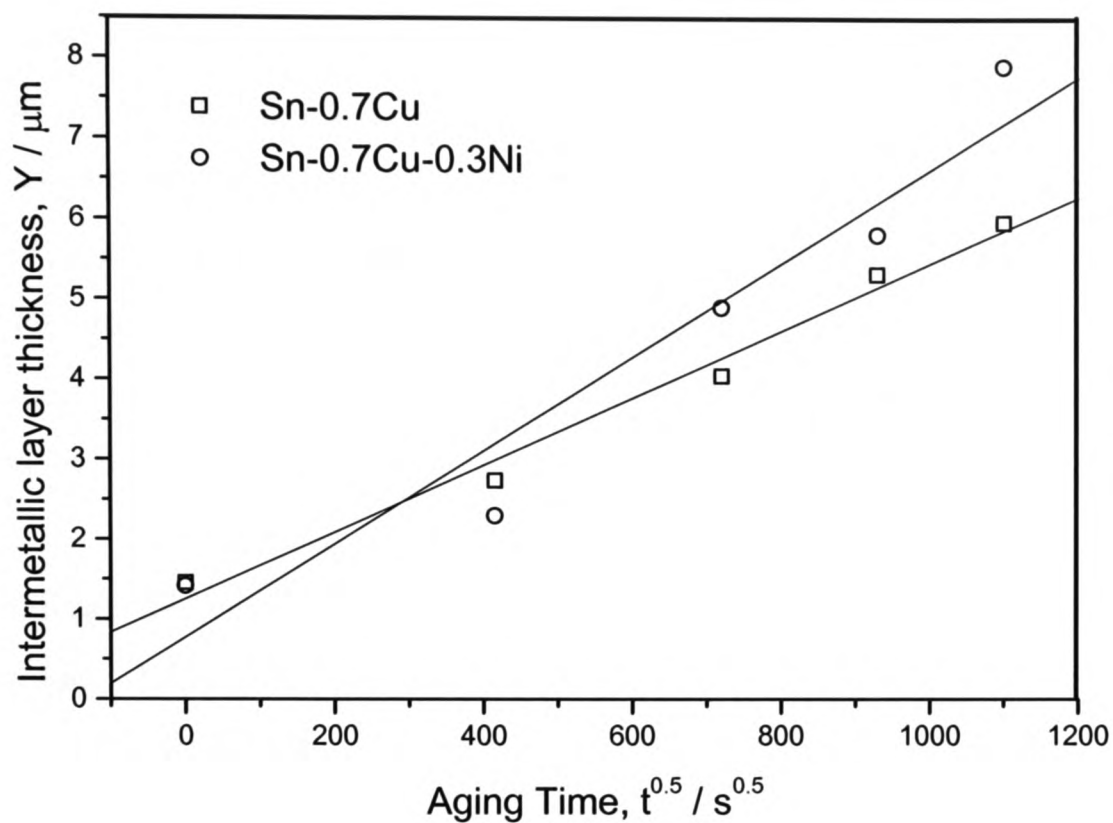


Figure 4-50: Average IMC layer thickness versus square root of aging time.

Figure 4-50 shows the growth of IMC layer thickness as a function of the square root of the aging time. This figure reveals that initially the IMCs layer in the Ni-containing solder is thinner, and it then increases non-linearly over time and eventually exceeds the IMC layer thickness of Sn-0.7Cu/Cu soldering system after 6 days of aging time. The linear fit of the curve reveals that the growth of IMC layer during aging of both solders follows the diffusion-controlled mechanism. Other researchers [138][139] have drawn the same conclusion. The slopes of the curves shown in Figure 4-50 give the values of growth rate constant k . For the Sn-0.7Cu/Cu and the Sn-0.7Cu-0.3Ni/Cu soldering systems, they have been found to be $1.41 \times 10^{-17} \text{ m}^2/\text{s}$ and $1.89 \times 10^{-17} \text{ m}^2/\text{s}$ respectively. This means that the growth rate of IMC layer during the solid-state aging is higher for the Sn-0.7Cu-0.3Ni/Cu soldering system than the Sn-0.7Cu/Cu soldering system.

4.5 Closure

In this chapter extensive work has been carried out to investigate the effects of adding 1wt% Bi into the Sn-2.8Ag-0.5Cu solder and 0.3wt% Ni into the Sn-0.7Cu solder on the wetting behaviour, the consumption of the substrate materials, and the growth behaviour of the IMCs. Computer modelling has also been carried out to study the solders' wettability and to understand the diffusion behaviours of substrate materials in liquid solders. Based on the experimental and modelling investigations the following conclusions can be drawn:

1. In general, the wettability of the lead-free solders is not as good as that of the Sn-Pb solder. Adding Bi into the Sn-Ag-Cu solder and Ni into the Sn-Cu solder can improve the wettability. Wettability is strongly dependent on the type of the flux. It has been found that in general, NC-flux is suitable for Cu-substrate whereas WS-flux is suitable for Ni substrate, but for the Sn-2.8Ag-0.5Cu solder on Ni substrate, good wettability has been observed with both the NC and the R-type fluxes. The wettability is also temperature dependent, the higher the soldering temperature the better the wettability is.
2. Computer modelling of the wetting balance tests confirmed that contact angles have significant effects on the wetting force and the corresponding meniscus heights. The increase in the depth and the radius of the solder bath has little effect on the wetting force, but the meniscus height decreases when the bath radius exceeds 14 mm.
3. Higher temperature increases the dissolution of Cu and Ni into the molten solders and increases the IMC layer thickness at the solder-substrate interface. Rapid consumption of the substrates and a high rate of growth of the IMCs during the soldering are found for the Sn-2.8Ag-0.5Cu solder compared to those of the Sn-2.8Ag-0.5Cu-1.0Bi solder. Similar comparison can be made between the Sn-0.7Cu solder and the Sn-0.7Cu-0.3Ni solder.

4. Computer modelling has shown that the diffusion rate of Cu from the substrate during the wetting is higher in the Pb-free solder than in the Sn-Pb solder. An EDX analysis has been used to measure the Cu concentration in the solder. There is a good agreement between the predicted value and the measured value.
5. It has been found that immediately after the soldering reaction, the IMC layer thickness is comparatively higher in the Sn-2.8Ag-0.5Cu solder than that in the Sn-2.8Ag-0.5Cu-1.0Bi solder. Since the dissolution rate of Ni into the solders is slower compared to that of Cu, the growth of the IMC layer on Ni is also slower compared to that on Cu. It has been found that an addition of 1wt% Bi into the Sn-2.8Ag-0.5Cu solder reduces the nucleation rate of Cu_6Sn_5 and Ag_3Sn IMCs in the solder matrix as well as at the solder-substrate interface during isothermal aging.
6. It has been found that the addition of Ni into the Sn-0.7Cu solder changes the composition of the IMCs that are formed at the solder-Cu interfaces and also in the bulk of the solder matrix during the wetting reaction. A thin layer of Cu_3Sn has been found between the Cu_6Sn_5 layer and the Cu substrate after 10 days of aging of the Sn-0.7Cu/Cu soldering system. However, this Cu_3Sn layer is totally absent in the case of Ni containing Sn-0.7Cu solder. Compared to the Sn-0.7Cu solder, the Ni-containing solder exhibits lower rate of growth of the IMC layer during the wetting and during the first two days of aging. However, the thickness of IMC layer increases dramatically after 6 days of aging and eventually exceeds the IMC layer thickness of the Sn-0.7Cu/Cu soldering system. It can be concluded for the solid-state reaction of longer time (for examples 6 or more days) that an addition of 0.3wt% Ni into the Sn-0.7Cu solder encourages the acceleration of the growth of the IMCs over time at the solder-substrate interface and also in the bulk of the solder matrix.

Chapter 5

Study of Interconnections formed with Anisotropic Conductive Films

5.1 The Background and the Objectives of this Work

The manufacturing of miniaturized and environmentally friendly product has become the most important trend in recent years for the electronic packaging industries. The use of anisotropic conductive films (ACFs) as an alternative to solders and underfill encapsulations for the direct mounting of chips to circuit boards helps to fulfil this trend. The flip chip technology that uses ACFs is not only environmentally benign, it also offers extremely fine pitch capability, a simple structure and manufacturing process with low processing temperature, light weight and small product size. [147][148][149][150][151]. There are a number of flip chip technologies such as Chip-on-Glass (COG), Chip-on-Flex (COF) and Chip-on-Board (COB) where ACFs are used extensively for the manufacturing of mobile and portable electronic devices such as cellular phones and personal digital assistances.

ACFs are composite materials that consist of an adhesive matrix and conductive particles. The adhesive matrix is a thermosetting epoxy that holds randomly dispersed conductive particles and protects the metallic contacts from mechanical damage and provides mechanical strength to the joints. The conductive particles are made of solid metal or metal-coated polymers that provide electrical connection between the conductors of the chip and the substrate. The number density of the conductive particles in an ACF varies from one product to another, but the particle volume fraction is usually between 0.5 and 5.0 per cent. However, due to the small particle size of 3.5 μm in diameter, in a typical ACF, the concentration of the conductive particles can be as high as 3.5 millions/ mm^3 [152][153]. Under high heat and pressure, conductive particles of ACF make contact with both the bump of the chip and the pad of the substrate but not with each other [154][155][156]. Therefore, unlike joints formed with isotropic conductive adhesives (ICAs), in ACF joints do not have direct metallic contact in all the direction. Conducting path is formed only after the pressure is applied to the chip and substrate so that conductive particles can make contact with both the chip and the substrate. Due to the lack of direct contact among conductive particles, ACF technology is very suitable for fine pitch assembly and so this is why it is used in more and more applications in flip chip technology [157]. However, in spite of the various advantages of using ACFs, it is still difficult to use ACFs for volume production because ACF materials are very temperature sensitive and this makes it difficult to integrate the ACF technique in manufacturing processes that involve a range of temperature [158].

The successful formation of the flip chip interconnection using ACFs depends on, among factors, how the physical properties of that adhesive changes during the bonding process. The temperature rises in the ACF joint when the bonding machine delivers heat from the heater to the backside of the Si-chip. The heat comes through a number of metallic contacts where the thermal conductivities of each of those materials are the key parameters in determining the temperature change in the ACF joint. In the bonding process, it is necessary to ensure that the ACF really gets the preset bonding temperature so that the adhesive matrix can cure properly. Once the temperature in ACF has reached the bonding temperature, the adhesive matrix melts to become a viscous fluid and some

of the conductive particles are distributed between bumps and pads. Then, cross-linkage of the polymer molecules takes place and it is more and more difficult for the particles to move as the adhesive becomes more and more viscous [159]. Since the physical, electrical and mechanical properties of ACFs largely depend on the degree of curing of the epoxy composition in the adhesive [160], there has been a great deal of interests in investigating the effect of the ACF curing on the electrical and mechanical performance of ACF-based flip chip assemblies. Substantial work has been carried out on ACF-based flip chip assemblies using thermal cycling [149] and environmental tests [151]. However, there is still a lack of knowledge about how ACF joints age at raised temperatures. Since thermosetting epoxy based ACFs are very temperature sensitive and difficult to rework after curing, it is important that the curing of the ACF is optimized to ensure good reliability.

Unlike the solder joints where metallurgical reactions take place at the solder-metalization interfaces, ACF joints form through mechanical contacts among the bump of the flip chip, pad of the substrate and the conductive particles. Because of the pressure that is applied on the back of the mounting chip, the contact spots at the bump-particle and particle-pad interfaces spread out and make an effective contact area through which electrical conduction occurs. Here, the clamping force that holds the deformed conductive particle is applied through the bump and the pad. Figure 5-1 shows a typical flip chip joint with anisotropic conductive film.

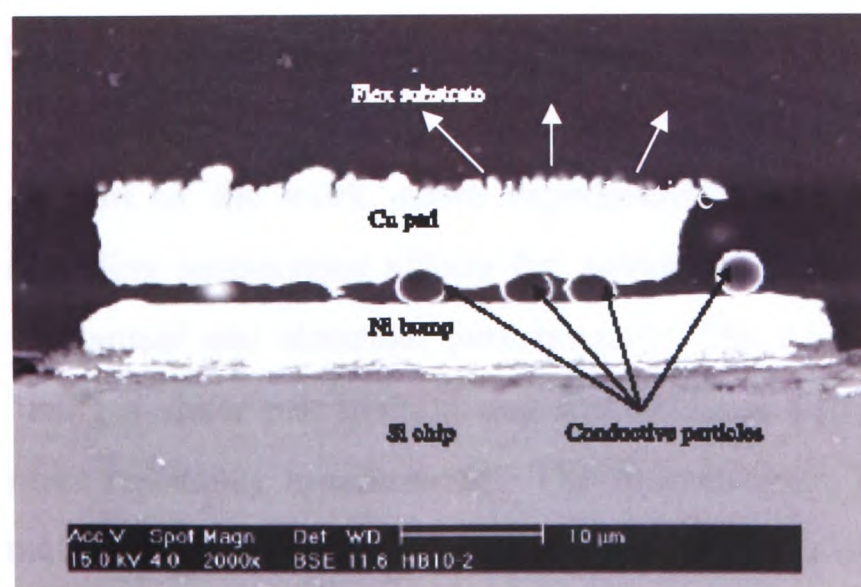


Figure 5-1: A typical flip chip joint with anisotropic conductive film [159].

Since there is no firm metallurgical connections in ACF joints, the relaxation of clamping force may induce a small gap at the particle-metallization interfaces and this may dislodge the deformed particle. As a result, a discontinuity of electrical conduction among the bump, the particle and the pad may occur. Therefore, it is very important to investigate the factors that can degrade the ACF joints and can influence the mechanical and electrical reliability. The mechanical reliability for Chip-on-Flex assembly is just as important, and this is tested under bending, twisting, vibrating, key push and impact. Bending in particular is the main form of mechanical stress that is tested for an assembled PCB [161]. Although over the last few years many investigators have successfully studied the residual bending stresses generated due to the differences in the coefficients of thermal expansion (CTE) of the various materials in the assembly in the curing process [162], very little work has been done on the effect of external bending load on the electrical reliability of ACF joints.

The objective of this chapter is to describe the work that aims at understanding the factors that play important roles in the performance and the reliability of the ACF interconnections.

The work described in this chapter can be divided into four parts. In the first part of the work, experiments have been carried out to understand how the temperature changes in the ACF during the bonding process and how the temperature affects the physical properties of that ACF, especially the glass transition temperature. Computer modelling has also been carried out to augment the experimental observations.

In the second part of the work, more experiments have been carried out to understand how the bonding temperature affects the curing of the adhesive and how the curing affects the mechanical and electrical performances. The ACF joint strength has been characterized using a shear test method and the electrical performance has been examined using contact resistance measurement. The samples have been tested before and after an isothermal ageing process so that the sensitivity of the post-cured ACF to the environmental temperature can be evaluated. The results of this study may help the

development of ACFs with higher heat resistance, so that ACFs can be used as an alternative to lead-free solders for high temperature applications.

In the third part of the work, computer modelling technique has been used to analyze ACF-based flip chip assemblies in order to observe the stress variation along the bond line under different isothermal aging conditions. By analyzing the stress concentration in the assembly, the most critical position of the flip chip assembly has been identified.

In the fourth part of the work, a computer model of an ACF based flip chip assembly under the three-point bending test condition has been studied so that the effect of bending stress on the electrical reliability of ACF joints can be investigated. Experimental work has also been carried out to measure the real-time contact resistance during the three-point bending test.

5.2 Experimental Procedures

5.2.1 Materials Selection

5.2.1.1 The chip

The dimensions of the silicon chip used for the experiments are $11 \times 3 \times 1 \text{ mm}^3$ with $50 \mu\text{m}$ square bumps. On the chip there are a total of 368 Au-Ni bumps ($18 \mu\text{m}$ in height) and they are located at the periphery of the chip. There are 60 daisy-chained bump groups along the length of the chip and each group contains 5 bumps as shown in Figure 5-2. Of these 5 bumps, one pair of adjacent ones is for the insulation resistance measurement and the remaining three bumps are for the contact resistance measurement.

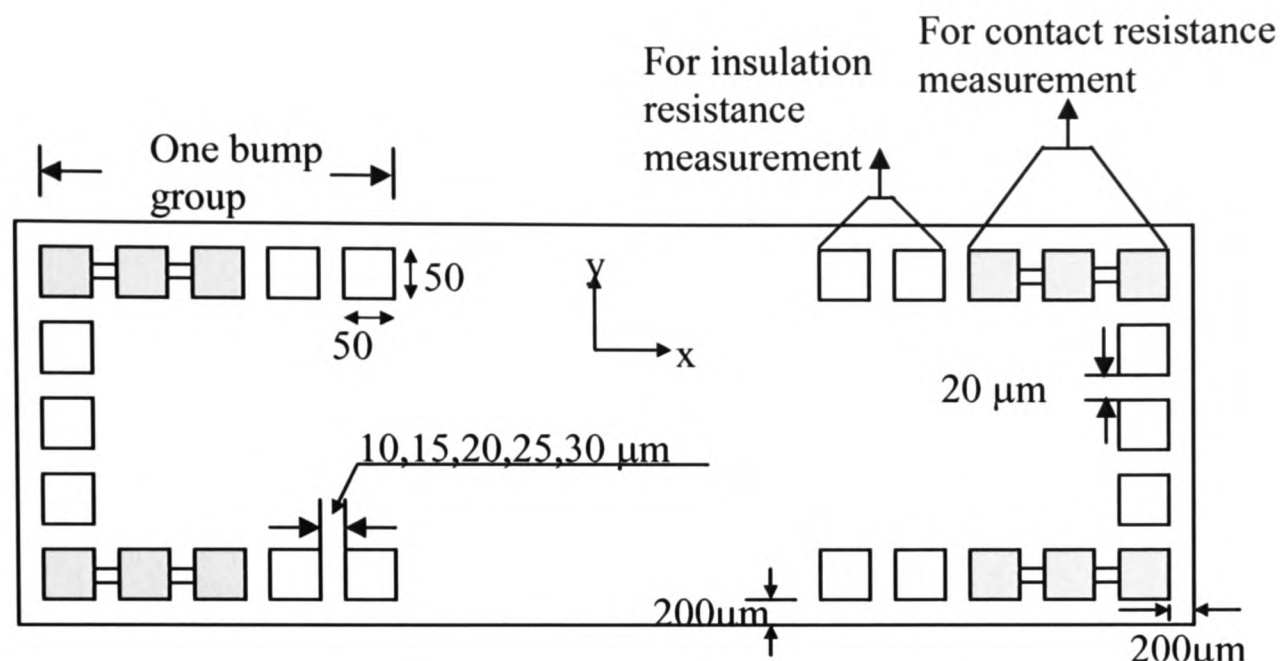


Figure 5-2: Schematic of a flip chip with daisy-chained bump groups.

5.2.1.2 Flexible Substrate

The dimensions of the flexible printed circuit board (FPCB) that were used in the experiments as substrate are $48 \times 40 \times 0.0414 \text{ mm}^3$. The substrate is constructed by electroplating a layer of $12 \text{ }\mu\text{m}$ -thick copper (Cu) as the circuit traces on a $25 \text{ }\mu\text{m}$ thick polyimide (PI) film. The surface of the copper traces was then plated with $4 \text{ }\mu\text{m}$ thick nickel (Ni) using electroless plating technique. Finally, a $0.4 \text{ }\mu\text{m}$ thick gold (Au) is formed on the Ni layer using sputtering method for oxidation prevention. Thus a pad of the substrate is made of Au, Ni and Cu and the total thickness is $16.4 \text{ }\mu\text{m}$.

5.2.1.3 Glass Substrate

The dimensions of the glass substrate used in the experiment are $40 \times 40 \times 1 \text{ mm}^3$. On the surface of the glass substrate a layer of 500-700 nm thick Indium-Tin-Oxide (ITO) trace patterns is formed and it functions as the electrodes/conductors. The patterns of the traces are specially designed to match the flip chip bumps layout in order to establish the electrical circuitry. Another plane glass substrate that has the same dimensions as the

above mentioned substrate but without the trace patterns was also used to carry out the microscopic investigations of the ACF samples that were cured at different temperatures.

5.2.1.4 FR-4 Substrate

FR4 printed circuit boards were also used in the experiment as substrates which had the same geometry as the flexible substrate. The thickness of this type of substrates is 1.6 mm.

5.2.1.5 Anisotropic Conductive Films (ACFs)

Two types of ACFs are used in this part of the work: type A and type B.

Type A: A commercially available ACF with a thickness of 35 μm was used for mounting the chip on the substrate. The conductive particles are polymer spheres with a diameter of 3.5 μm and they are covered with a 0.15 μm thick Ni-layer and a 0.05 μm thick Au-layer. The polymer's glass transition temperature T_g is 130 $^{\circ}\text{C}$. This type of ACF is shown schematically in Figure 5-3.

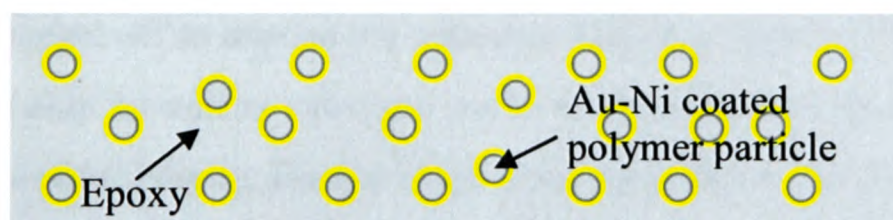


Figure 5-3: Cross-sectional view of ACF of the type A.

Type B: This is another commercially available ACF with a thickness of 24 μm . It was used for mounting the chip on the substrate. The conductive particles are Ni-Au coated polymer spheres of 4 μm in diameter. On the metal coating of the particles, there is an insulation layer and the purpose of this layer is to prevent electrical bridging. During the bonding process, as the particles are pressed, particles deform and the insulation layer

breaks so that electrical contacts can be established. This type of adhesive consists of two layers. One layer is a 12 μm anisotropic conductive film (ACF) and the other is a 12 μm nonconductive adhesive film (NCF). The number density of the conductive particles in the adhesive is $1.8 \times 10^6/\text{mm}^3$. A schematic representation of this type of ACF is shown in Figure 5-4.

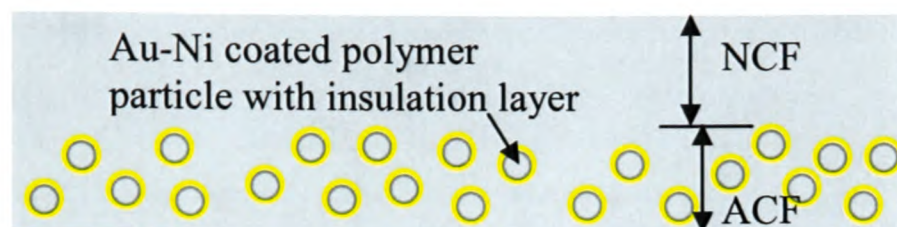


Figure 5-4: Cross-sectional view of ACF of the type B.

5.2.2 Bonding Process

Prior to the pre-bonding stage of the bonding process, the ACF was removed from the refrigerator and allowed to warm up to the room temperature. A protective transparent thin polymer layer was peeled off before the ACF could be mounted on the flexible substrates. Then, the ACF was pre-bonded to the flexible substrates using the Karl Suss manual bonder and the process parameters are listed in Table 5-1. After that, the white paper film was peeled off to expose the adhesive film. An organic solvent (acetone) was used to clean the chip as well as substrate marks to eliminate any foreign particles and to ensure good alignment. Finally, the test chips were mounted on the pre-bonded substrates using a Toray FC2000 Flip Chip Bonder. The final bonding conditions are also shown in Table 5-1.

Table 5-1: Bonding parameters

Parameters	Pre-bonding	Final-bonding
Temperature ($^{\circ}\text{C}$)	90	160 - 240
Force (N)	10	60 -100
Time (s)	7	3 -10

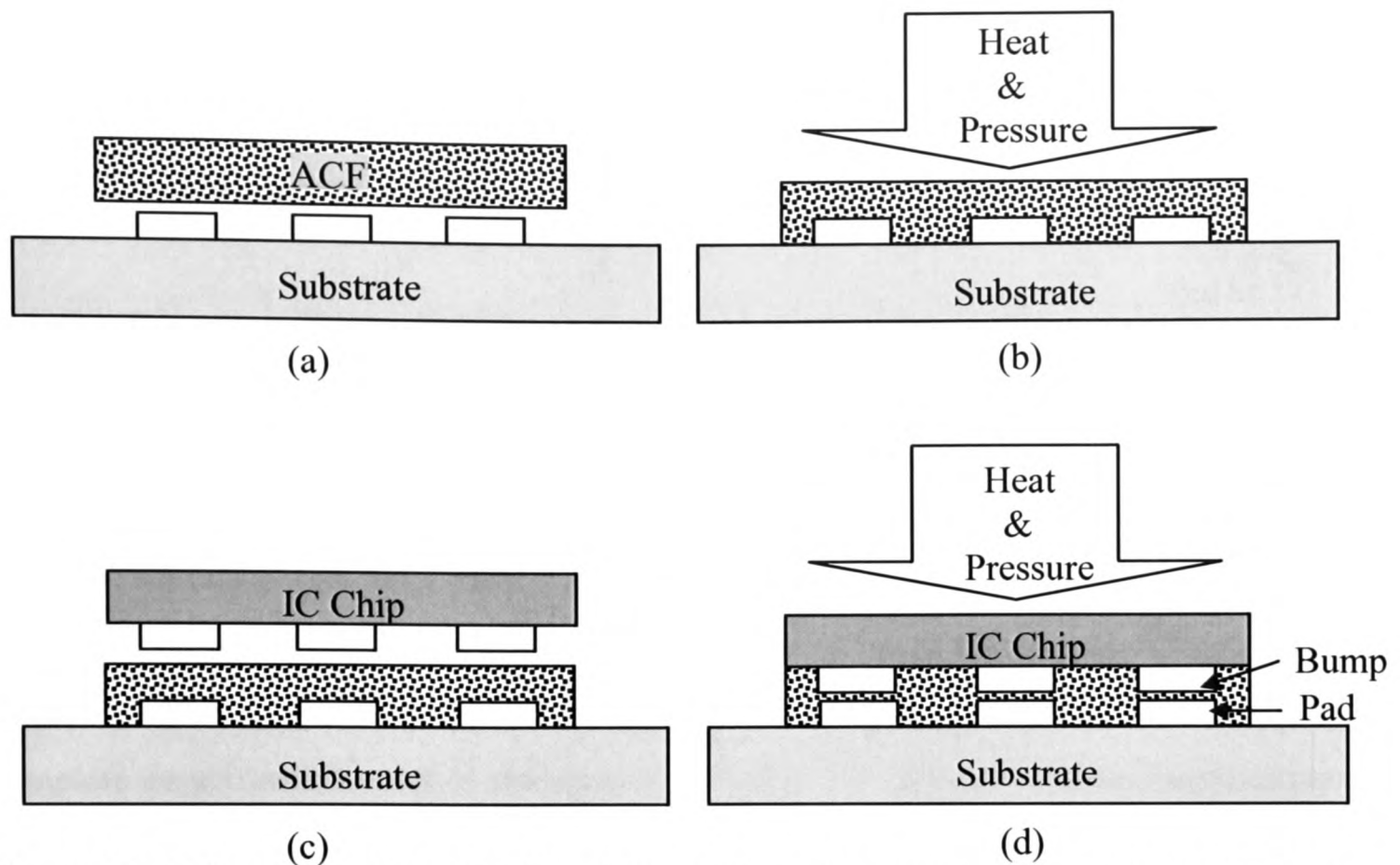


Figure 5-5: Schematic of the ACF flip chip bonding process; (a) placement of ACF on the substrate, (b) pre-bonding, (c) alignment between chip and substrate, (d) final bonding.

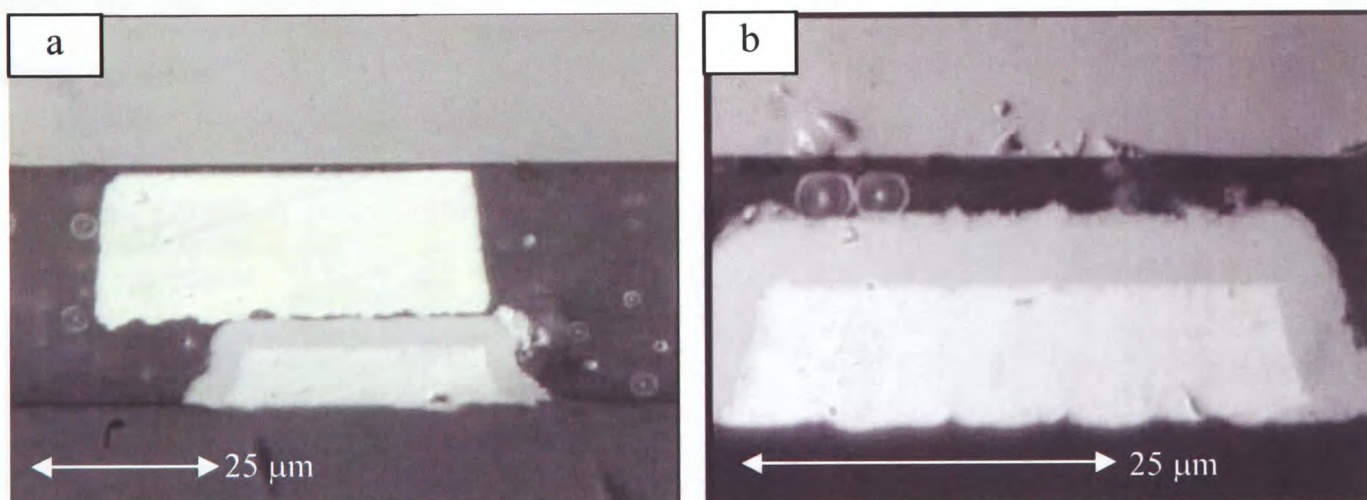


Figure 5-6: Typical flip chip joints through anisotropic conductive films with (a) Au-bump flip chip, (b) bumpless flip chip.

During the ACF bonding process, heat and pressure are applied to the component and the conductive particles between bumps and pads change their shape from sphere to ovoid and the conduction paths between the bump of the chip and the pad of the substrate in the z-direction are formed [158]. The bonding process is illustrated schematically in Figure

5-5. The cross sections of ACF joints using an Au-bump flip chip and a bumpless flip chip are shown in Figure 5-6 (a) and (b). These pictures show that the appearance of an ACF joint depends on the type of the mounting chip.

5.2.3 Experimental Setup

5.2.3.1 Bonding Temperature Measurement in the ACF

A thermocouple data logger (Agilent 34970A) with computer-controlled data acquisition system was used to measure the real-time temperature in the ACF. One end of the tape-type thermocouple was placed at the centre of the stage of the flip-chip bonding machine (Toray 2000) to measure the temperature in ACF for the flip chip on glass assembly. The other end of the thermocouple was connected to the data logger. The complete experimental setup is shown in the Figure 5-7. A total of three thermocouples were used to measure the temperatures at two corners and at the middle of the ACF. However, it was decided that the temperature measured at the centre should be used as the ACF temperature because the temperatures at the corners were found to have been affected by the ambient. The ACF temperature was recorded throughout the whole bonding process.

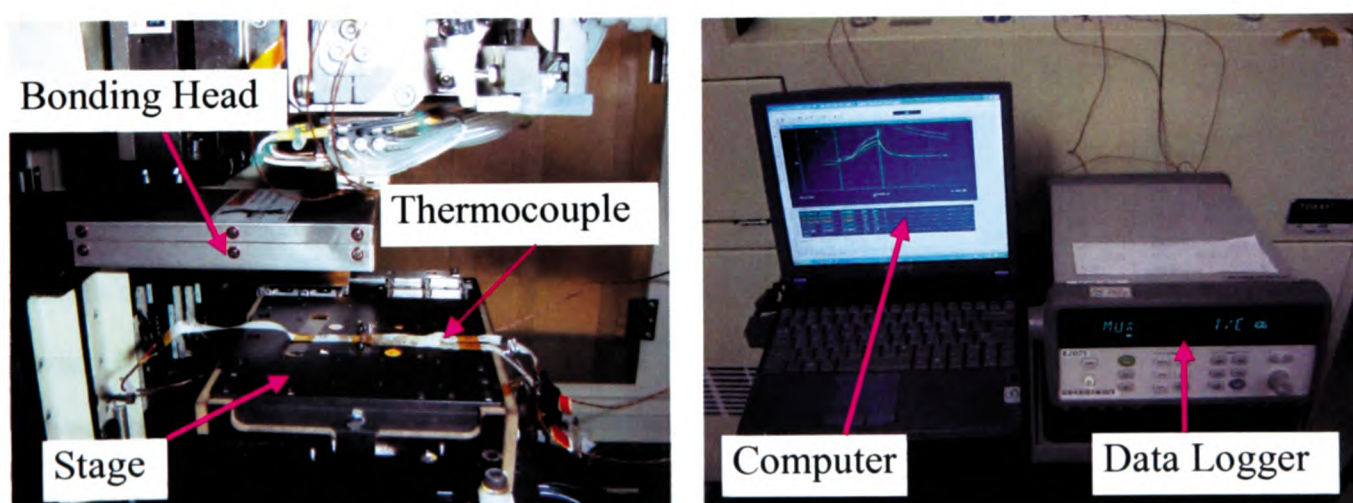


Figure 5-7: Experimental setup to measure the real-time temperature in ACF; (a) Position of thermocouple on the stage; (b) Computer-controlled data logger setup to grab the temperature in fractions of seconds.

5.2.3.2 Dynamic Mechanical Analysis (DMA) of ACF

The physical properties of the Type-B ACF were characterized through the TA instruments' Dynamic-Mechanical Analyzer (DMA Q800). The DMA multi-frequency stress mode was used to test the samples (11 mm x 1.5 mm x 0.024 mm). The temperature range that was scanned was from 30 °C to 220 °C with a ramp rate of 5 °C/min. Before the experiment was carried out, the ACF was taken out from the refrigerator and allowed to warm up to the room temperature. It was then cut into small pieces and cured at 170, 190 or 210 °C for 3, 5 or 10 s. The samples were then ready for the DMA test. The instrument was calibrated prior to the experiment.

5.2.3.3 Differential Scanning Calorimeter (DSC) tests of ACF

Differential scanning calorimeter (DSC) is widely used to study phenomena such as melting, crystallization, glass transition and chemical reactions. It measures the rate of heat flow as a function of temperature and time during both endothermic and exothermic transitions within the sample, and provides quantitative information regarding the enthalpy changes in each material [163][164]. The thermosetting-epoxy based ACF was tested using a modulated differential scanning calorimeter (MDSC 2910) with a computerized data acquisition system. Before conducting the experiment, some ACF was removed from the refrigerator and allowed to warm up to the room temperature. This ACF sample was considered to be uncured. The cured samples were obtained by peeling the ACF off the flip chip assemblies bonded at 160, 180, 200, 220 and 240 °C. Small quantities of ACF (~ 10 mg) were weighed and put in an aluminium hermetic pan and the pan was then sealed ready for the DSC test. In this study, a baseline test for each experimental condition was carried out by using two empty sample pans. The curing reaction was considered complete when the rate curves levelled off to the corresponding baseline test results. In the tests, the temperature was increased from 30 °C to 250 °C at a ramp rate of 10 °C/min. The same baseline and ramping rate were used for all six samples. The degree of curing was calculated from the following relationship [147]

$$\alpha = \frac{Q_r - Q_R}{Q_r} \quad (5.1)$$

where, α is the degree of curing, Q_r is the total exothermic heat of the uncured ACF sample and Q_R is the residual heat of the cured ACF sample.

5.2.3.4 Adhesion Strength Measurement

The adhesion strength of the ACF joints before and after the thermal ageing was measured using an INSTRON Mini 44 Tensile tester. The chip-on-flex assembly was attached firmly on to a FR4 board with a rigid supporting back to hold the entire assembly as depicted in the Figure 5-8.

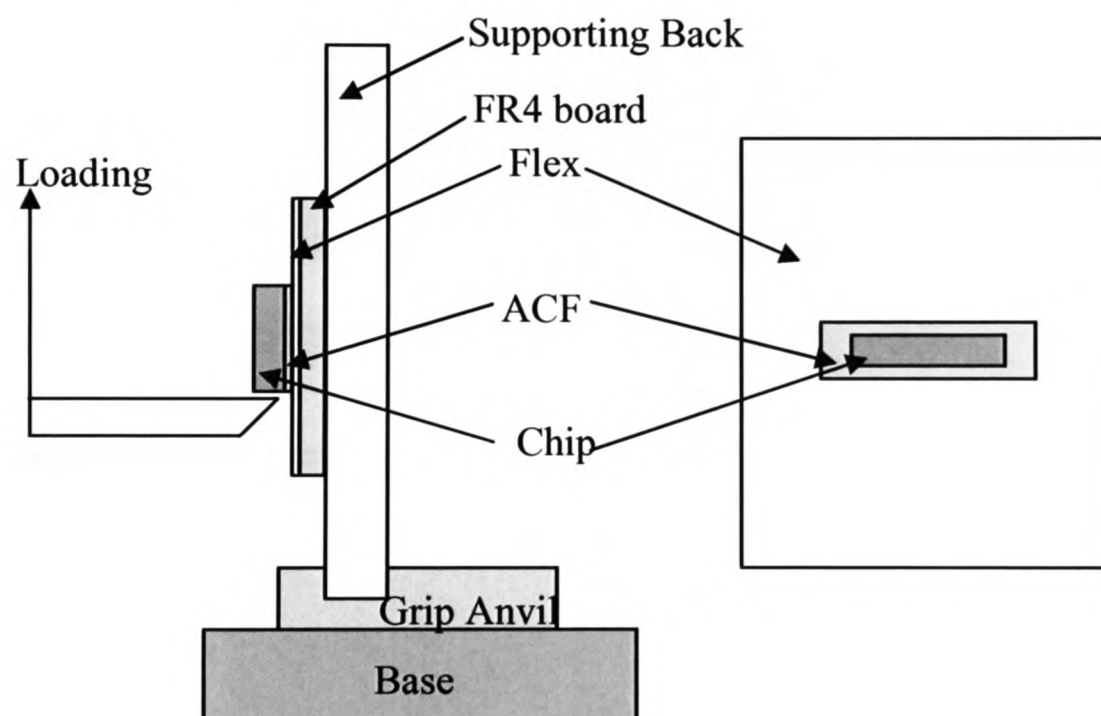


Figure 5-8: A schematic diagram of the shear test.

Five as-bonded samples for each bonding condition were tested. Another five samples for the same bonding conditions were studied after they had gone through the thermal ageing process. The upward crosshead speed was set as 10 mm/min for all the samples. The load needed to shear-off the chip from the flexible substrate was measured five times for each bonding condition and the mean value was taken as the shear load.

5.2.3.5 Thermal Ageing Tests of ACF Joints

The ACF assemblies shown in Figure 5-9 were bonded at different temperatures. They were then aged for 600 minutes at a constant temperature of 150 °C. The samples were also aged at 60, 100 and 140 °C for 600 minutes to investigate the ageing temperature effect.

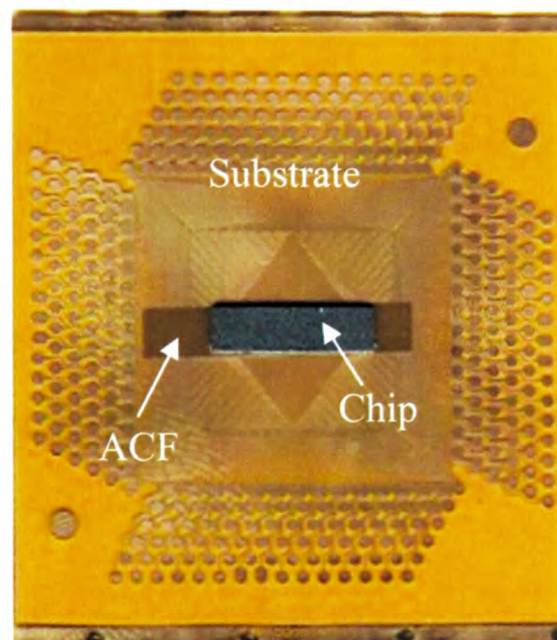


Figure 5-9: Typical flip chip assembly with ACF.

5.2.3.6 Contact Resistance Measurement

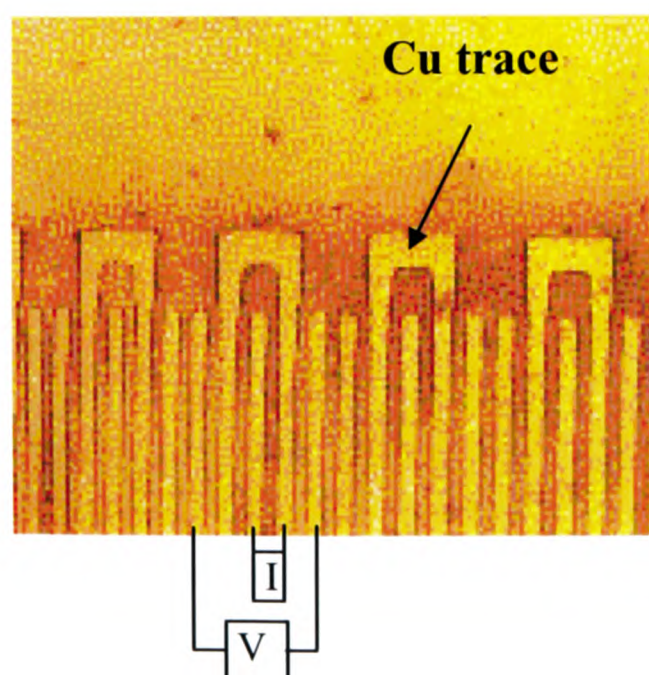


Figure 5-10: Circuitry of contact resistance measurement using four-point probe method.

Contact resistance was measured by using the four-point probe method as depicted in Figure 5-10. During the measurement, a 1 mA current (I) was applied to the circuit and the voltage (V) was measured using a Hewlett Packard 3478A Multimeter for each bump group, and the contact resistance (R) was calculated using the Ohm's law.

5.2.3.7 3-point Bending Tests of ACF Joints

The daisy-chained chip shown in Figure 5-2 was bonded as described above on the FR4 substrate with 60 N of applied force and 10 s of bonding time. A special set up was developed to measure real-time contact resistance using the four-point probe method during the bending test (the schematic circuitry of four-point probe method is shown in Figure 5-10). Bending test was conducted by an INSTRON MINI-44 universal tensile tester with a crosshead speed of 50mm/min as depicted in Figure 5-11.

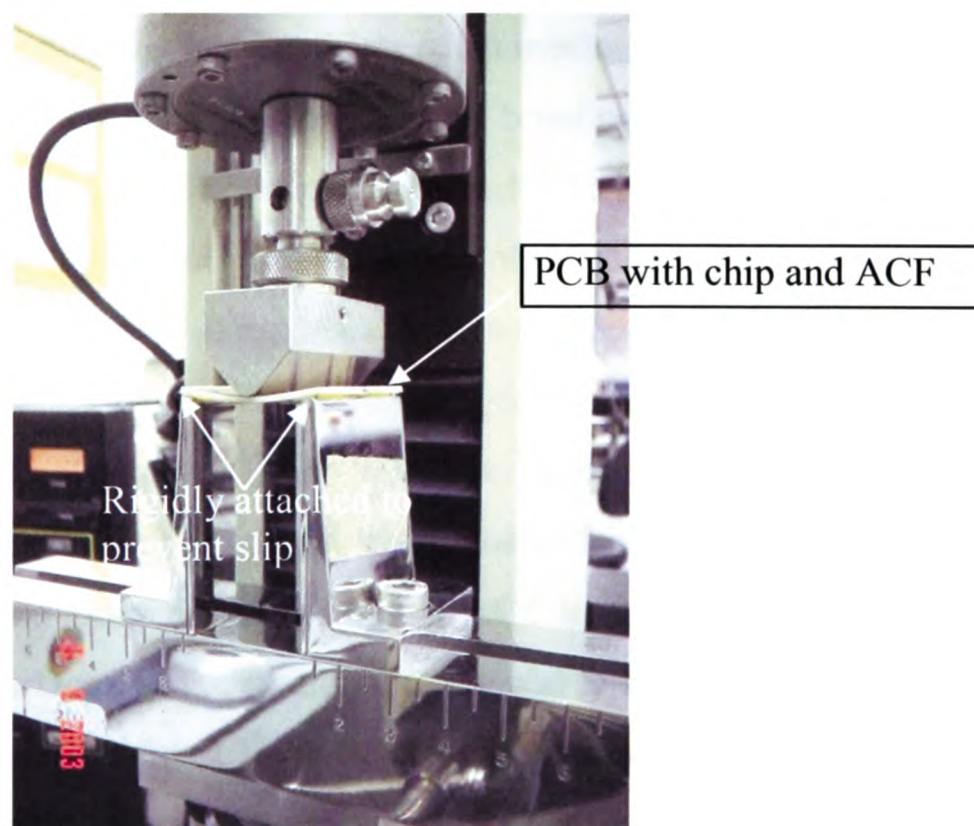


Figure 5-11: Experimental setup of 3-point bending tests.

5.2.3.8 Failure Analysis

The ACF interconnections were investigated using a Philips XL40 FEG scanning electron microscope (SEM). The ACF assemblies were sectioned, molded and polished before they could be used for this analysis. A total of 30 bump-groups along the length of the chip were examined to identify the failure mechanisms at the bump-particle and/or particle-pad interfaces.

5.3 Computer Modelling Procedures

5.3.1 Bonding Temperature Measurement in the ACF

A 2-dimensional computer model of the flip chip on glass assembly was built in order to predict the ACF temperature during bonding. The structure of the model is shown in Figure 5-12. A multi physics modelling software PHYSICA [68] was used for the analysis. In this model the bonding head consists of an insulator, a ceramic heater with a heating trace and a bonding tool. It is assumed that the bonding head is already in contact with the back of the chip. The ACF sample is placed between the chip and the glass substrate. The whole assembly is placed at the centre of the stage. Inside the stage, there is a block of quartz glass which is also modelled as it is an important part of the stage and it acts as a heat spreader. The dimensions of the geometry are similar to the actual bonding machine and are shown in Table 5-2. The material properties used in this simulation are shown in the Table 5-2 and are taken from references [165] and [133]. It is assumed that heat transfers from the heater to the ACF by conduction only. It is also assumed that the outer surfaces of the model are exposed to an ambient temperature of 30 °C and a heat transfer coefficient of 10 W/m²K for the natural convection is applied on these boundary surfaces. The observation point is located at the centre of the ACF so that the results can be compared with the experiment. The temperature load is applied at the heating trace.

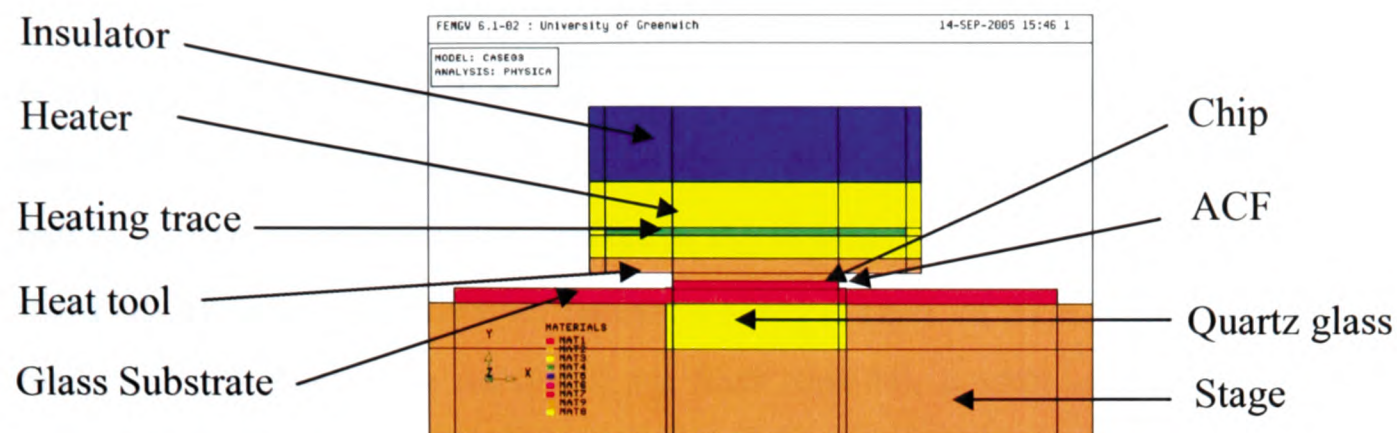


Figure 5-12: Computer model to simulate the heat transfer during bonding of chip-on-glass assembly.

Table 5-2: Dimensions and thermal properties used in the modelling

Geometry & Material	Dimensions		Material Properties		
	Length (X) (mm)	Height (Z) (mm)	Density (kg/m ³)	Thermal Conductivity (W/mK)	Specific Heat Capacity (J/kg-K)
Chip	11	0.5	2329	124.00	702
Heat Tool- Top Part	22	1.0	3960	30.00	850
Heat Tool- Bottom Part	11	0.5			
Ceramic Heater	22	5.0	3260	120.0	734
Heating Trace	20	0.5	11520	138.0	251
Insulator	22	5.0	2500	1.50	700
ACF	12	0.035	4000	150.0	800
Glass Substrate	40	1.0	2500	0.75	730
Quartz glass	12	3.0	2200	1.38	741
Stage	130	40	7900	16.30	500

5.3.2 Thermal Ageing Tests of ACF Joints

A slice model of the ACF-based chip on flex assembly was built to find out the root causes of the electrical failures during the isothermal ageing. Due to the symmetry, only half of a slice is considered as shown in the Figure 5-13. The model consists of a silicon (Si) chip mounted on a flexible substrate using a layer of ACF. The bump of the chip is made of 9 μm thick pure Au and 9 μm thick pure Ni. A total height of 16.4 μm (0.4 μm Au + 4 μm Ni + 12 μm Cu) is modelled as the pad of the substrate. The substrate itself is made of a 25 μm thick polyimide film. In the model, the gap between the bump and the pad is 2 μm and this is actually the height of the deformed conductive particle and the adhesive matrix. Constant temperatures of 150, 140, 100 or 60 $^{\circ}\text{C}$ are applied on the boundaries to find out the effect of the ageing temperature on the failure of ACF joints. The material properties used in this simulation are obtained from the references [82] and [166] they are listed in Table 5-3.

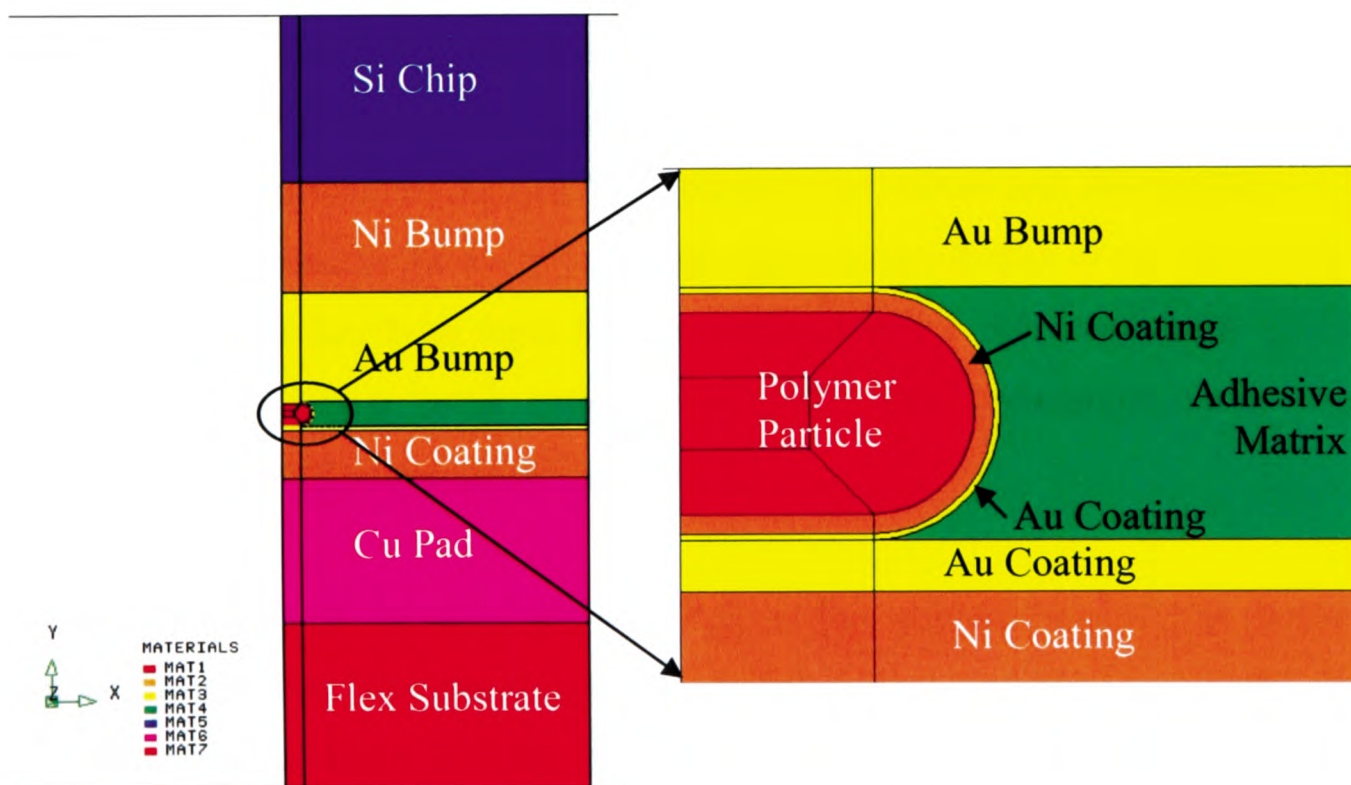


Figure 5-13: (a) A slice model of chip-on-flex assembly with ACF; (b) close view of ACF joint.

Table 5-3: Material properties used in the simulation

Properties	Polymer Particle	Nickel	Gold	ACF (adhesive matrix)	Chip	Copper	Flex
Young's Modulus, E (MPa)	25	204000	77200	1450	131,700	110000	4000
Poisson's ratio ν	0.4	0.31	0.42	0.4	0.3	0.343	0.3
Thermal Expansion, α (10^{-6} /K)	70.00	13.1	14.40	133	2.7	16.4	20

5.3.3 3-point Bending Tests of ACF Joints

The deformation of a material under mechanical loading depends on the magnitude and the direction of the load applied as well as the geometry of the object. In this case only the elastic deformation of materials was considered because the aim is to study the overall deformation and stress distribution in the structure as external loads are applied. The particular point interest is the stress and deformation at the edges of the ACF-chip and ACF-substrate interfaces. As it will be shown later, stress and deformation in ACF may have strong effects on the electrical conduction characteristics of an ACF joint. The computer model that has been used for this analysis has a fine mesh with 12,238 3-dimensional 8-node linear brick elements (C3D8I). The commercial finite element software ABAQUS [60] was used for the analysis.

Due to the symmetry of the assembly only half of the whole assembly was considered throughout the analysis. The structure of the model is shown in the Figure 5-14. In this model, the dimensions of the chip are 10 mm x 3 mm x 1 mm and the chip is mounted on a FR-4 printed circuit board using ACF. It is known that ACF is visco-elastic [167] but for simplicity all the materials in this model are considered as elastic, isotropic and homogeneous. In reality FR-4 is anisotropic but in the xy-plane it is nearly isotropic and

as it has pointed out in [168] that the properties in z-direction do not affect the results significantly in this particular structure. The metal-coated polymer particles in the ACF are not included in the computer model because this would create a formidably large multiscale model with numerous tiny particles. The ACF properties used in the modelling are the average properties of the matrix and the particles.

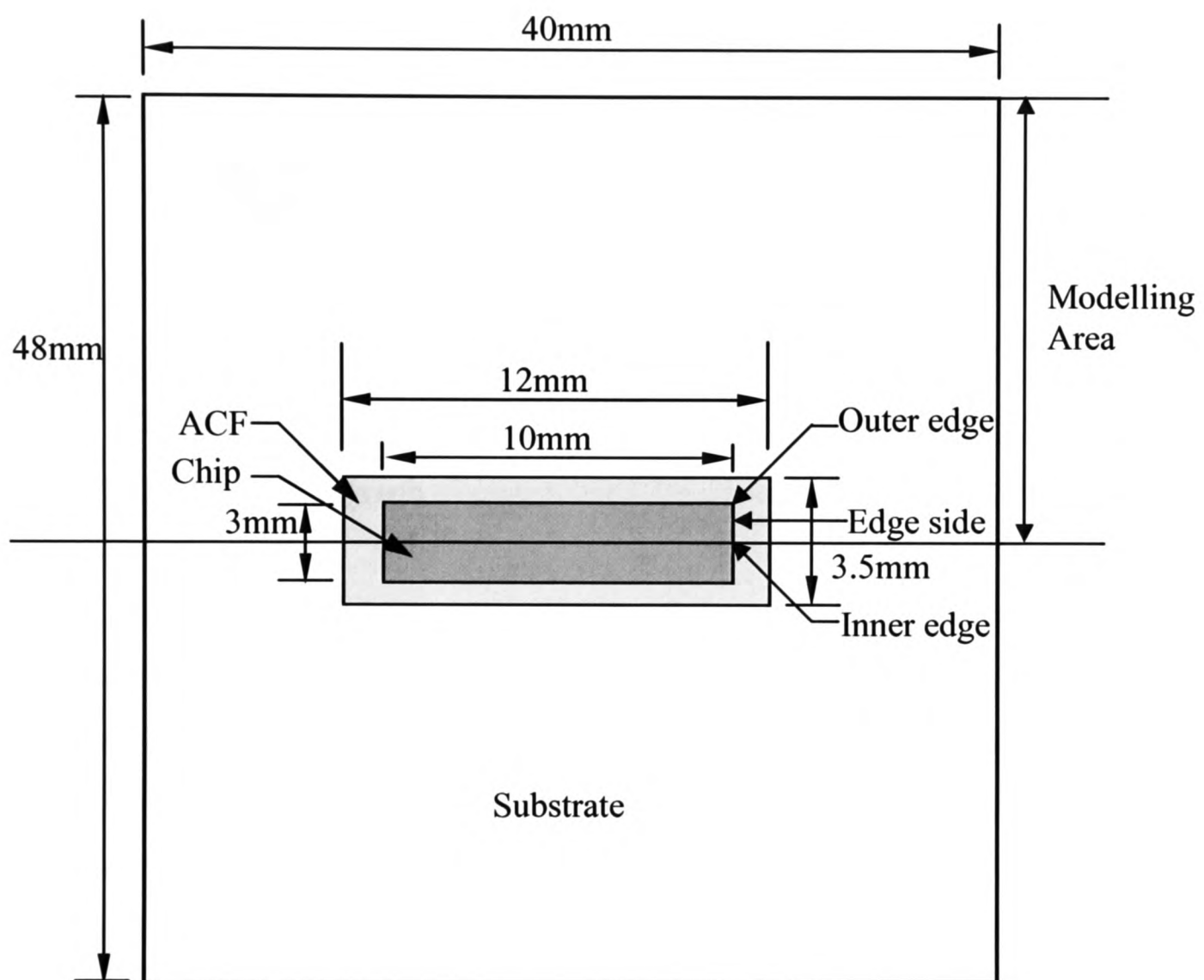


Figure 5-14: General configuration of the chip on board assembly (top view-chip side).

The Au/Ni bumps of the chip and the Cu-pads of the substrate used for the experimental verification of computer modelling were not included in the model because they don't affect significantly the overall deformation and stress levels in the bending test. However, the thickness of ACF layer between chip and substrate actually depends on the height of the bump and the height of the pad. During the bonding process, ACF becomes visco-elastic fluid under the bonding temperature. The applied bonding pressure on the top of

the chip suppresses ACF between the chip and the substrate. When the bonding pressure is applied, the reduction in the ACF thickness is limited by the maximum deformation of the conductive particles. For this study, the height of the deformed conductive particle was measured from the SEM photograph as shown in the Figure 5-15.

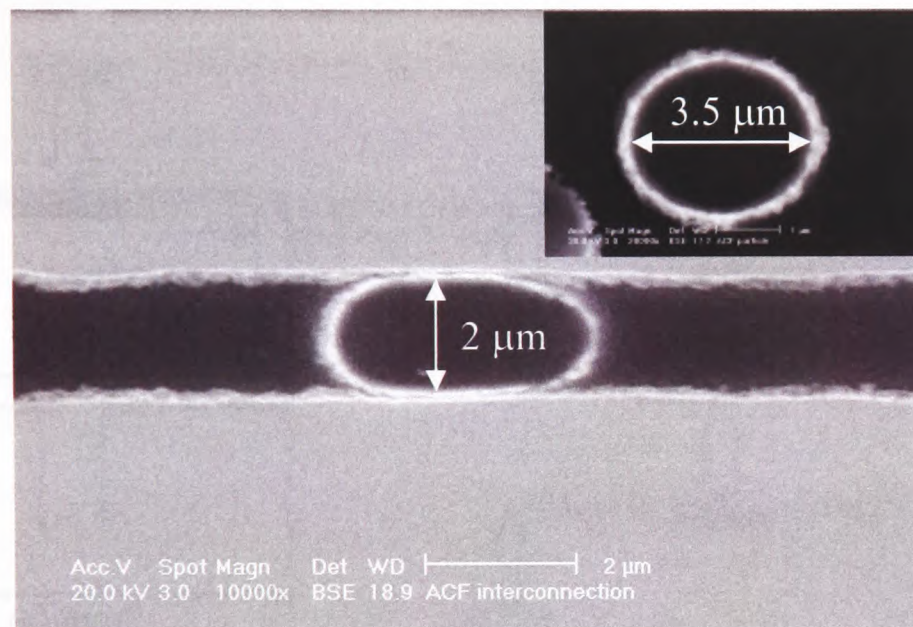


Figure 5-15: SEM photograph of undeformed (inset) and deformed ACF particle.

The total ACF thickness is the sum of the heights of the copper pad, the Au/Ni bump and the deformed particles. For example, if the height of the bump and the pad are 16 μm and 12 μm respectively, and the deformed particle's height in the z-direction is 2 μm after bonding, then the ACF thickness is 30 micron. From the SEM picture of the free particle shown in the inset of Figure 5-15, it is clear that the particle is spherical in shape before bonding but after the bonding process it become oval and the average height decreases from 3.5 to 2 μm . The dimensions of the model geometry are shown in Table 5-4.

Table 5-4: Dimensions of the model geometry in mm

Dimensions (mm)	Length	Width	Thickness
Substrate (FR-4)	40	24	1.6
ACF	12	1.75	0.03
Chip	10	1.5	1

In the analysis, it is assumed that the force load is applied on the top of the PCB (FR-4) over an area of $24 \times 5 \text{ mm}^2$ at the middle of the assembly. The values of the applied force range from 2 to 20 N. The PCB is supported at both ends. The loading conditions corresponding to the modelling setup is shown in the Figure 5-16.

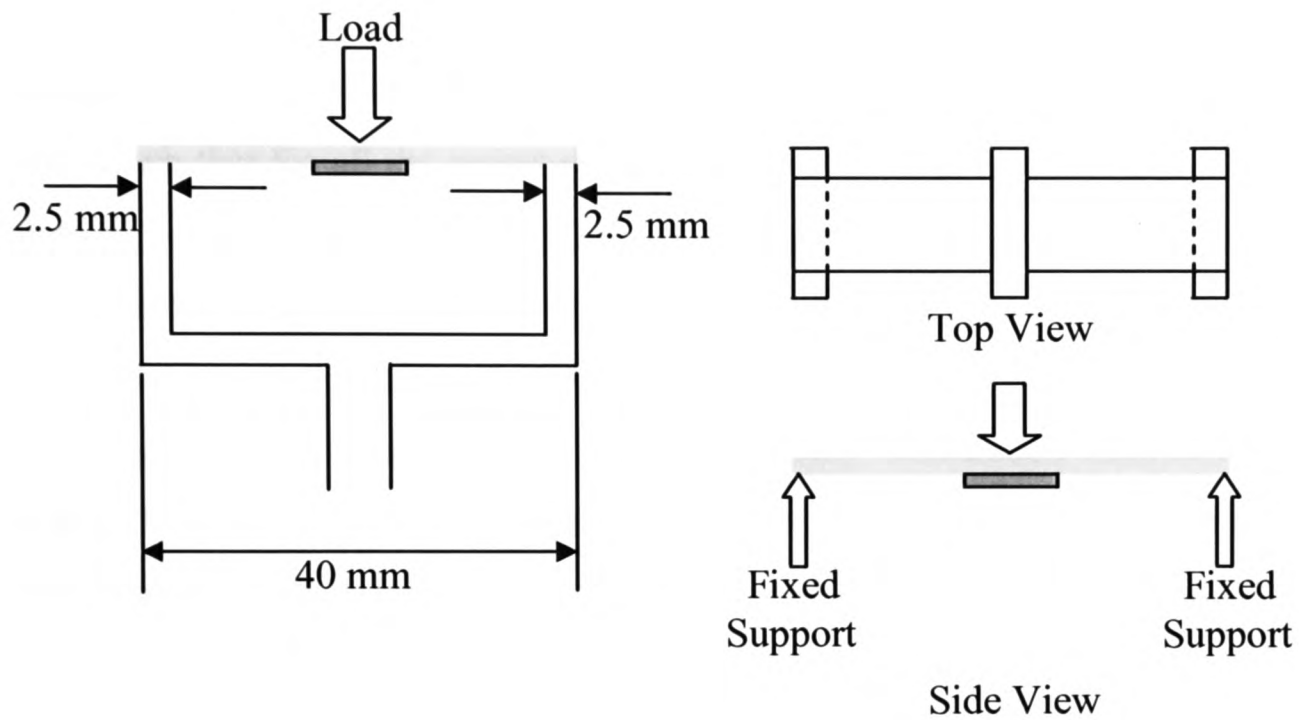


Figure 5-16: A schematic model of 3-point bending.

The maximum principal stress at the corner positions of the ACF-chip joint was investigated in this work. It was expected that because of the difference in the stiffness of the substrate and the chip, uneven deformation of these two parts at the corners of the ACF-chip would occur. This uneven deformation would cause large deformation in the region of the ACF close to the corners. In this modelling work, this deformation in the ACF and the possible interconnection failure at the corner positions has been investigated. The mechanical properties of the materials used in this study are shown in the Table 5-5. All the properties were obtained from references [82] and [166].

Table 5-5: Mechanical properties of materials used in modelling

Properties	ACF	Chip	FR4
Young's Modulus, E (Mpa)	1450	131700	16270
Poisson's Ratio, ν	0.3	0.3	0.12

5.4 Results and Discussions

5.4.1 Measurement of Temperature in the ACF during Bonding

The measured temperature values in the ACF during bonding of chip on glass assemblies are shown in Figure 5-17, 5-18 and 5-19. Generally, the experimental results are consistent with the modelling results. Both the modelling and the experimental results have shown that for all the preset maximum bonding temperatures, the ACF temperature ramps up very quickly during the first couple of seconds and then changes slowly in the rest of the bonding process. Experimental results show that the temperature becomes very close to the required maximum bonding temperatures of 170, 190 and 210 °C respectively within the first 1 second. As the maximum bonding temperature rises in the ACF within the first 1 second of the bonding time, there should be enough time for the ACF to be cured properly if the total bonding time is long enough. Therefore, the total bonding time must have a great impact on the curing of the adhesive matrix.

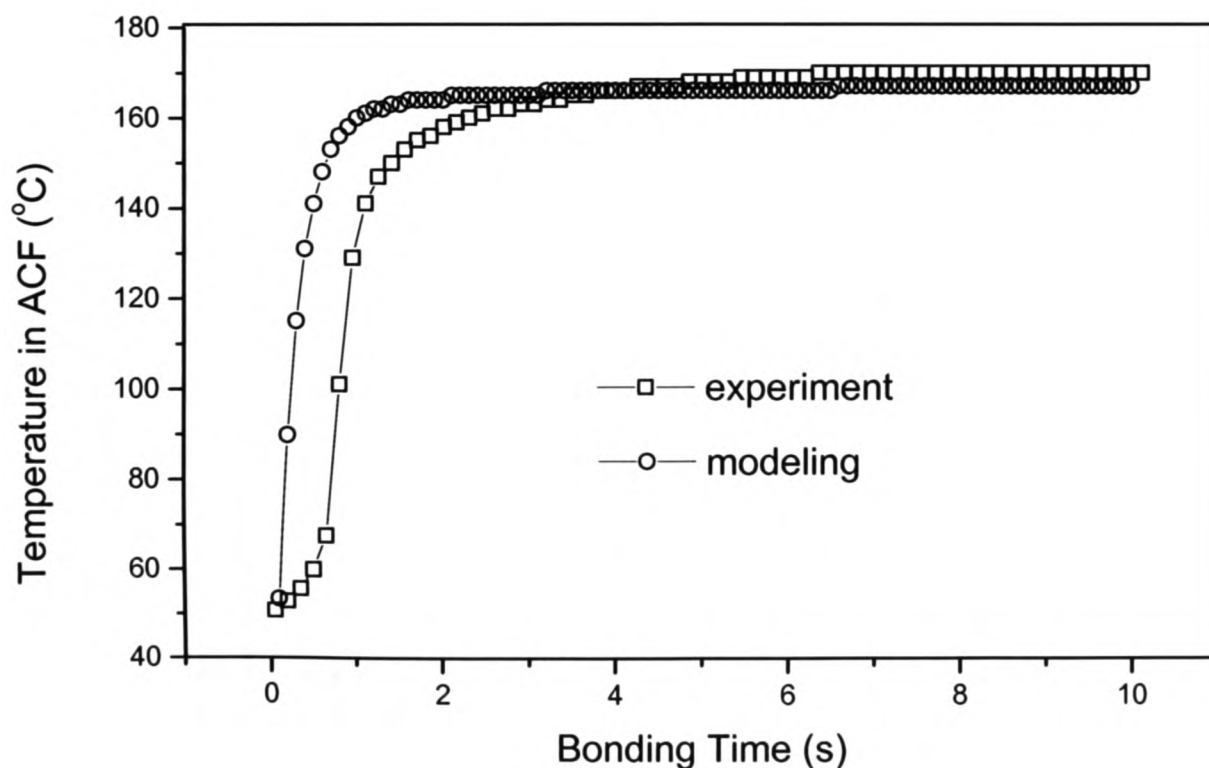


Figure 5-17: The temperature in the ACF. The bonding time is 10 s, the bonding temperature is 170 °C and the bonding pressure is 80 N.

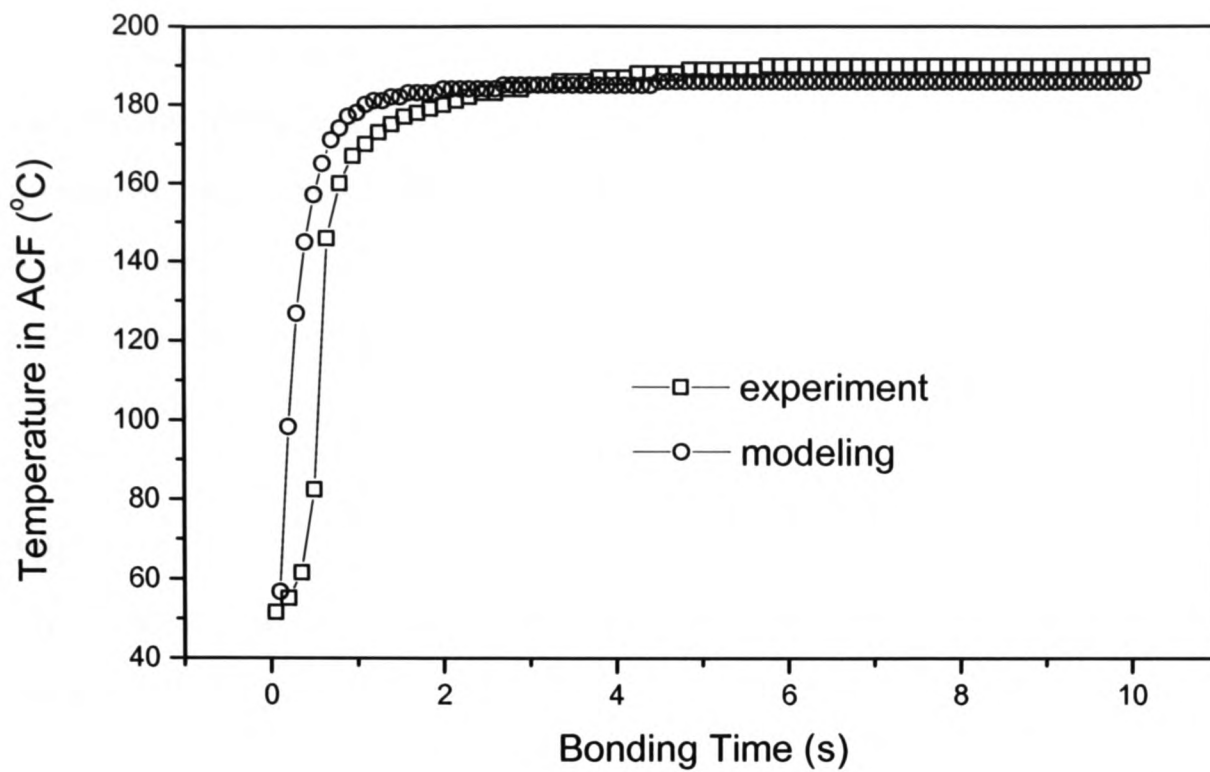


Figure 5-18: The temperature in the ACF. The bonding time is 10 s, the bonding temperature is 190 °C and the bonding pressure is 80 N.

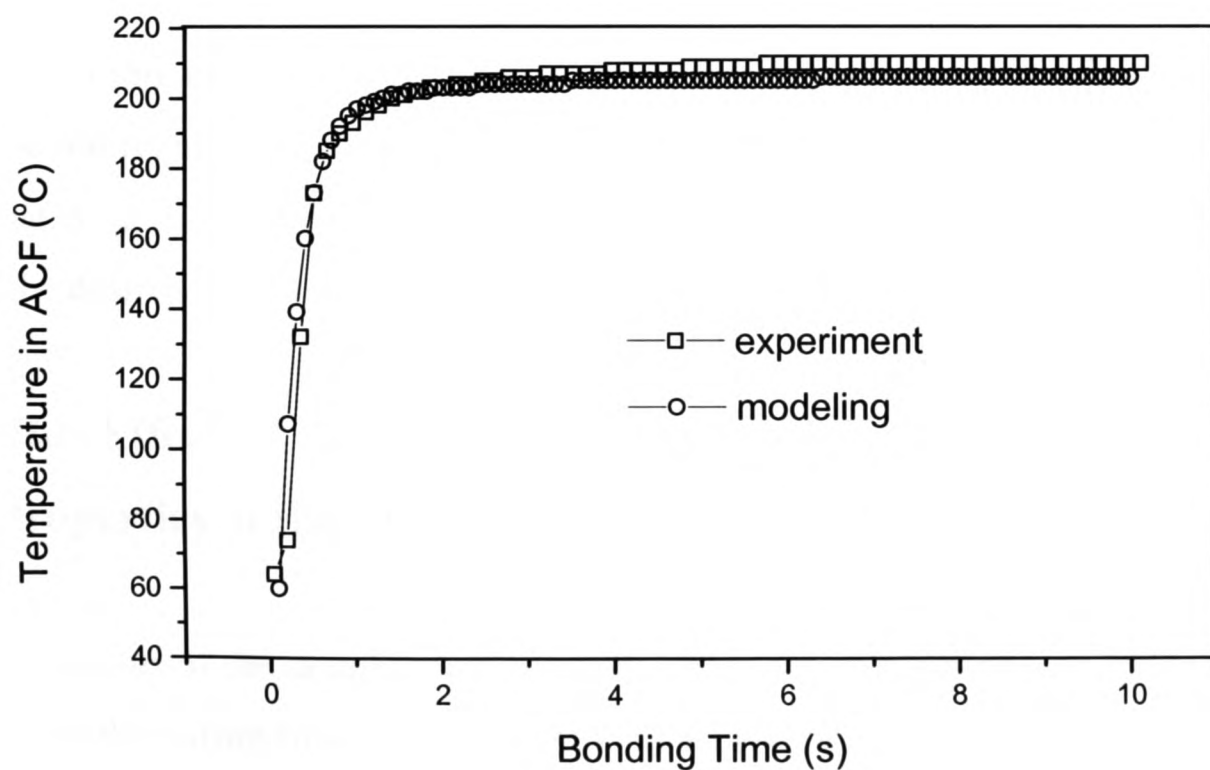


Figure 5-19: The temperature in the ACF. The bonding time is 10 s, the bonding temperature is 210 °C and the bonding pressure is 80 N.

It is interesting to note that according to the experimental results the preset maximum bonding temperature is reached in the ACF after 6 s but in general, the target temperature is expected to reach the adhesive within 2 s of the bonding time. Besides, according to the modelling results, the temperature becomes steady after only 1 s of the bonding time. This difference between the measured and predicted results may be due to the sluggish performance of the heater. A number of metallic contacts between the heater and the ACF may also be responsible for the slow heat delivery.

The modelling results have also revealed that the temperature in the ACF could be as high as 167, 186 or 206 °C at the end of bonding when the preset maximum bonding temperatures are 170, 190 or 210 °C respectively. The difference between a preset and the predicted temperature in the ACF, ΔT_b , is about 3 or 4 °C. (In the following discussion, this temperature difference will be referred as ΔT_{be} for the experiment.) This means that in order to achieve the correct bonding temperature in ACF, ΔT_b must be taken into account. The preset temperatures in the bonding machine should be the sum of the required bonding temperature in the ACF and ΔT_b . The value of ΔT_b depends on the heater and heat tool material. The thermal conductivity of the heat tool can significantly affect ΔT_b . In this experiment, ΔT_{be} values are 130, 150 and 170 °C respectively in order to achieve the required bonding temperatures of 170, 190 and 210 °C respectively. This shows that ΔT_{be} can't be fixed for all bonding temperatures and need to be optimized to achieve the desired bonding temperatures in the ACF.

5.4.2 The Effect of Bonding Temperature and Time on the Physical Properties of the ACF

The loss modulus of the samples cured at 170, 190 and 210 °C are shown in Figures 5-20 and 5-21 for the curing times of 3 and 10 s. In all the cases, the loss modulus increases first as the scanning temperature increases and then decreases after reaching a peak value. The temperature which corresponds to the peak is the glass transition temperature of the sample. For the bonding temperature of 170 °C, the glass transition temperatures of the

Chapter-5: Study of Interconnections formed with Anisotropic Conductive Films

samples that have been cured for 3, 5 and 10 s are 54.31, 56.02 and 92.29 °C respectively. For the samples that are cured at 190 °C the glass transition temperatures are 69.19, 84.05 and 108.21 °C for curing times of 3, 5 and 10 s respectively. For the bonding temperature of 210 °C, the glass transition temperatures for the samples cured at 3, 5 and 10 s are 75.23, 87.02 and 106.05 °C respectively.

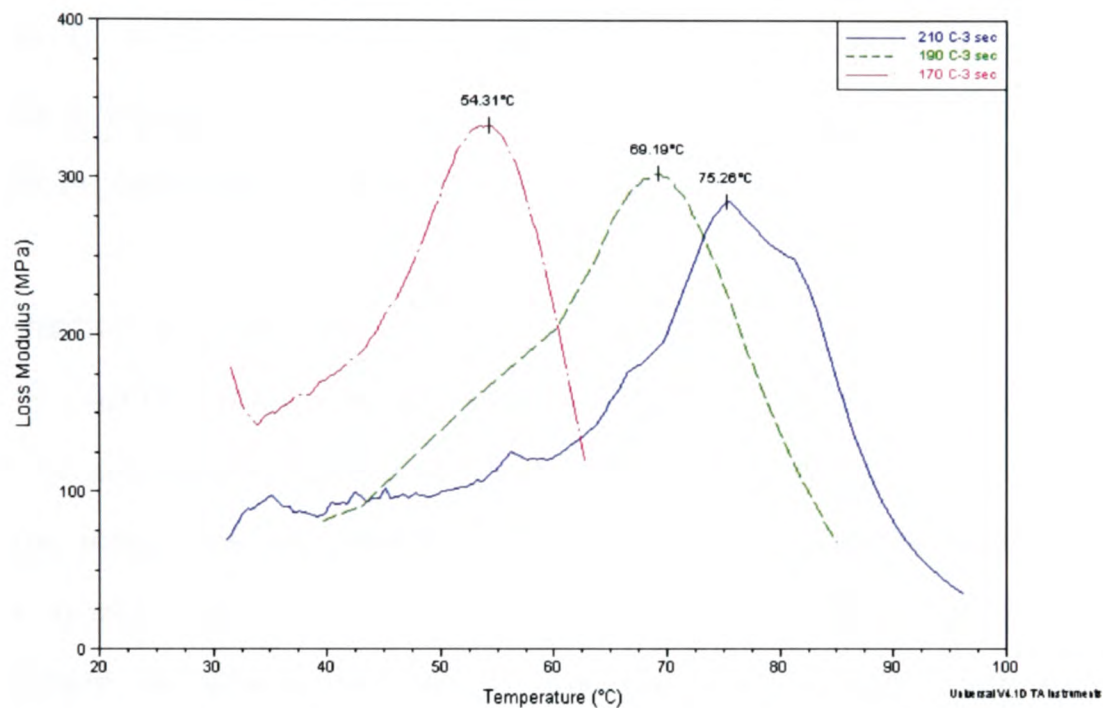


Figure 5-20: The loss modulus of the ACF samples cured at 170, 190 and 210 °C for 3 s.

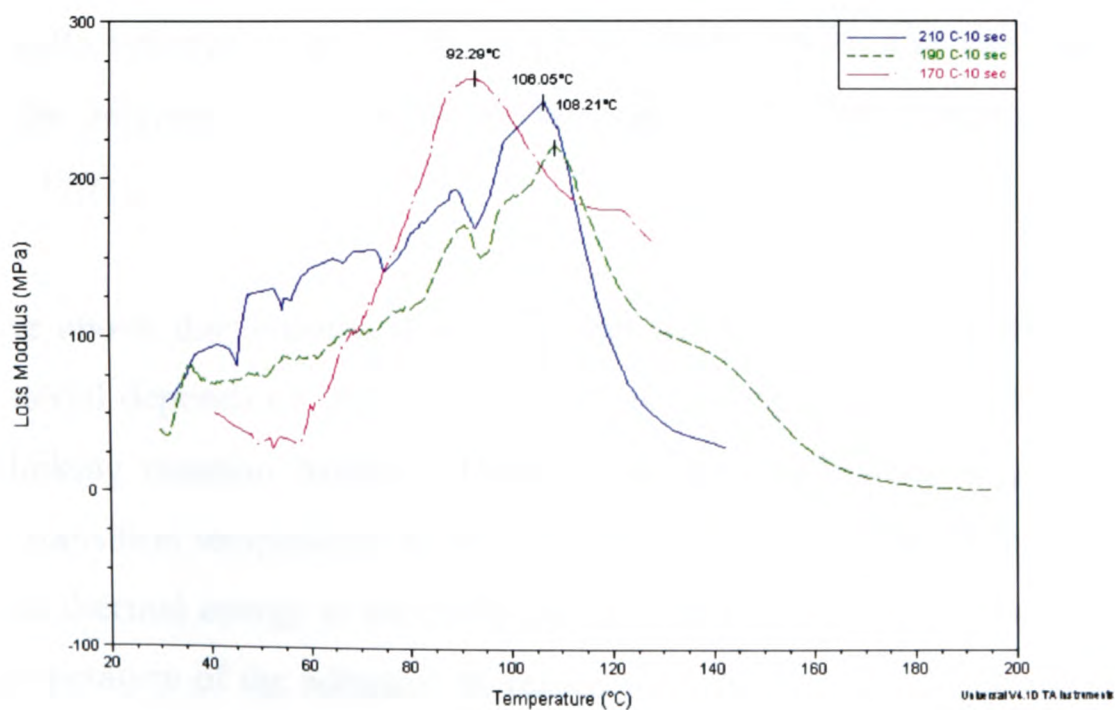


Figure 5-21: The loss modulus of the ACF samples cured at 170, 190 and 210 °C for 10 s.

Therefore, it can be concluded that the glass transition temperature increases with the increase of curing time for all the three bonding temperatures that have been used in this work. For the curing times of 3 and 5 s, the samples that are cured at 210 °C have the maximum glass transition temperatures whereas for the curing time of 10 s the maximum glass transition temperature is in the sample that is cured at 190 °C. The sample that is cured at 210 °C has a lower glass transition and higher loss modulus than the sample that is cured at 190 °C. As the loss modulus is a damping term that describes the dissipation of energy into heat when a material is deformed [169], it can be said that the adhesive property might be deteriorated when the samples are cured at 210 °C for 10 s.

The glass transition is a property of the amorphous portion of a semi-crystalline solid. The crystalline portion remains in the crystalline state during the glass transition. At low temperature, the amorphous regions of a polymer material remain in the glassy state and in this state the molecules are in such a form that this state can be regarded as a frozen state. In this frozen state, the molecules may vibrate slightly but do not have any segmental motion in which portions of the molecule wriggles around. When the amorphous regions of a polymer are in the glassy state, the material is generally hard, rigid, and brittle. When an amorphous polymer is heated, the temperature at which it changes from a glassy to the rubbery form is called the glass transition temperature, which is usually referred to as T_g . At this temperature, molecules can start to wriggle around and the polymer now is in its rubbery state that lends softness and flexibility to the polymer [170].

Based on the above discussions, it is clear that the glass transition temperature of an adhesive material depends on its curing condition. During the curing process, polymeric chain crosslinking reaction happens. Higher degree cross-linking of polymer leads to higher glass transition temperature as the polymeric chains become more constrained and require higher thermal energy to have segmental motion. This is the reason why the glass transition temperature of the adhesive increased with the increase of curing/bonding time and temperature. However, the glass transition temperature for the sample cured at 210

°C for 10 s decreased rather than increased. The possible reason behind this may be that this particular curing condition helped the formation a homogeneous mixture of adhesive with the diluents, which are made of small molecules, and this had led to the decrease of the glass transition temperature because smaller molecules have higher free volume than polymer segments [171]. The difference in the appearance of the adhesive cured at 210 °C for 10 s can be seen in Figure 5-22.

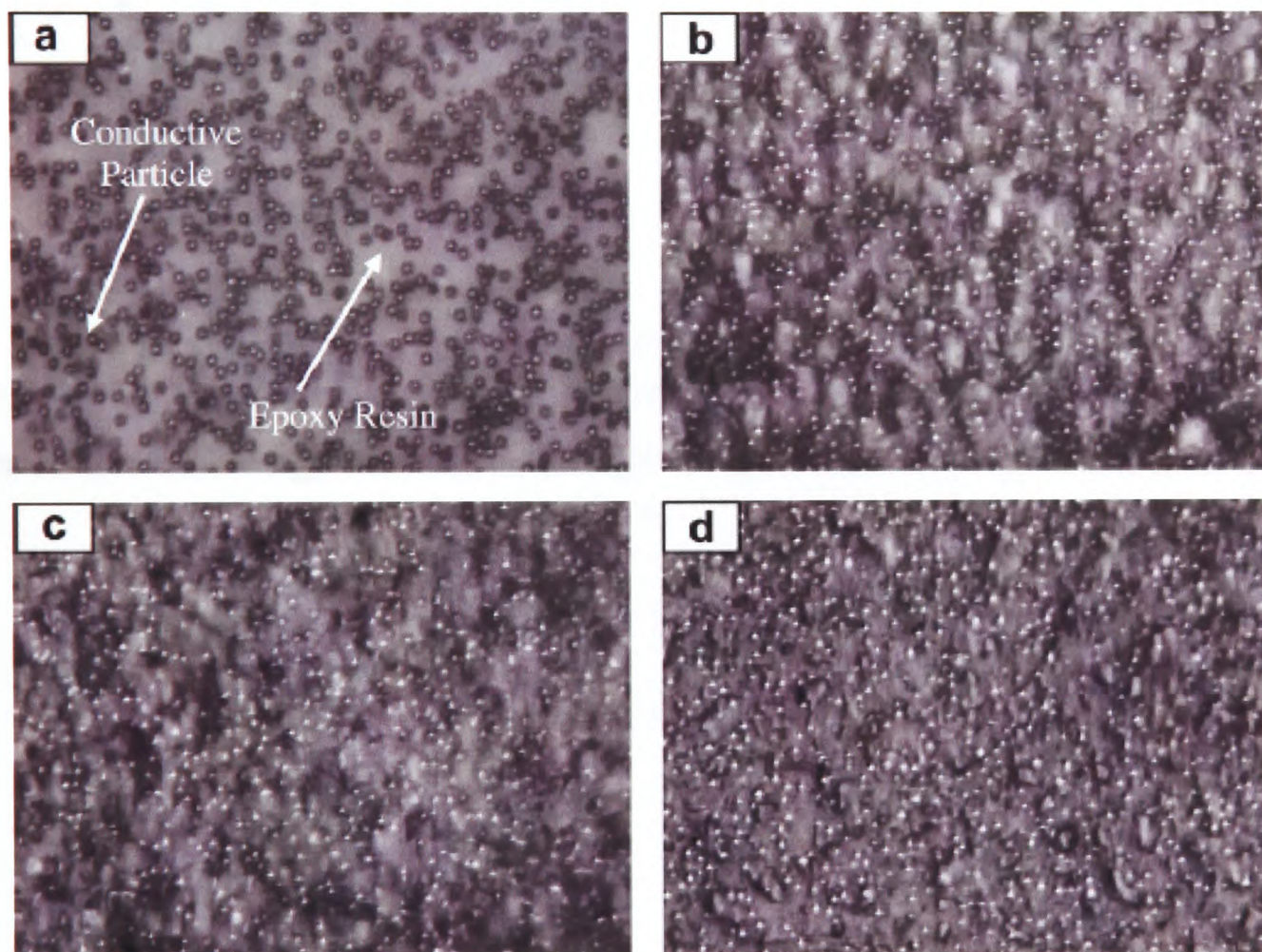


Figure 5-22: The appearance of (a) the uncured (raw) ACF and cured (b) at 170 °C, (c) at 190 °C and (d) at 210 °C. (Optical pictures, magnification = 20 X)

Figure 5-23 and 5-24 show the changes of the storage modulus over temperature changes. It can be seen that the storage modulus dropped as the temperature rose from the room temperature. The sudden drops in the modulus values occur at or near the glass transition temperatures because at this temperature the adhesives become rubbery and the adhesive matrix deforms more easily. It has been noticed that in general the temperature at which

Chapter-5: Study of Interconnections formed with Anisotropic Conductive Films

this sudden change of the modulus happens has shifted for the samples which are cured at high temperatures and longer times except for the sample cured at 210 °C for 10 s.

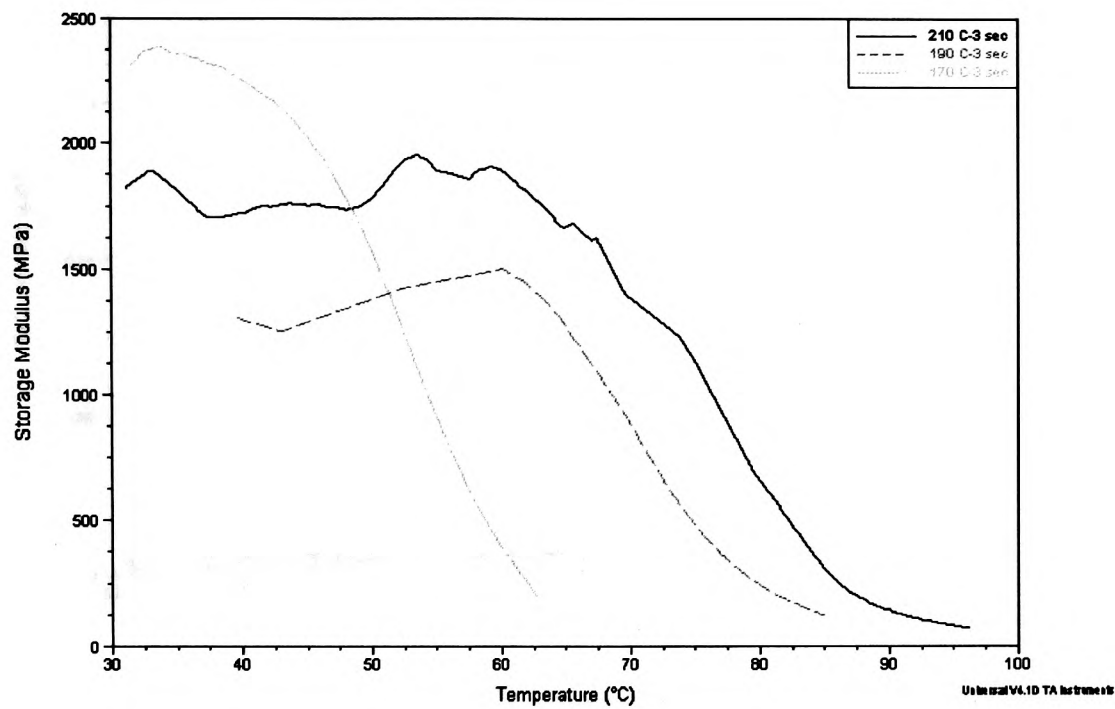


Figure 5-23: The storage modulus of the ACF samples cured at 170, 190 and 210 °C for 3 s.

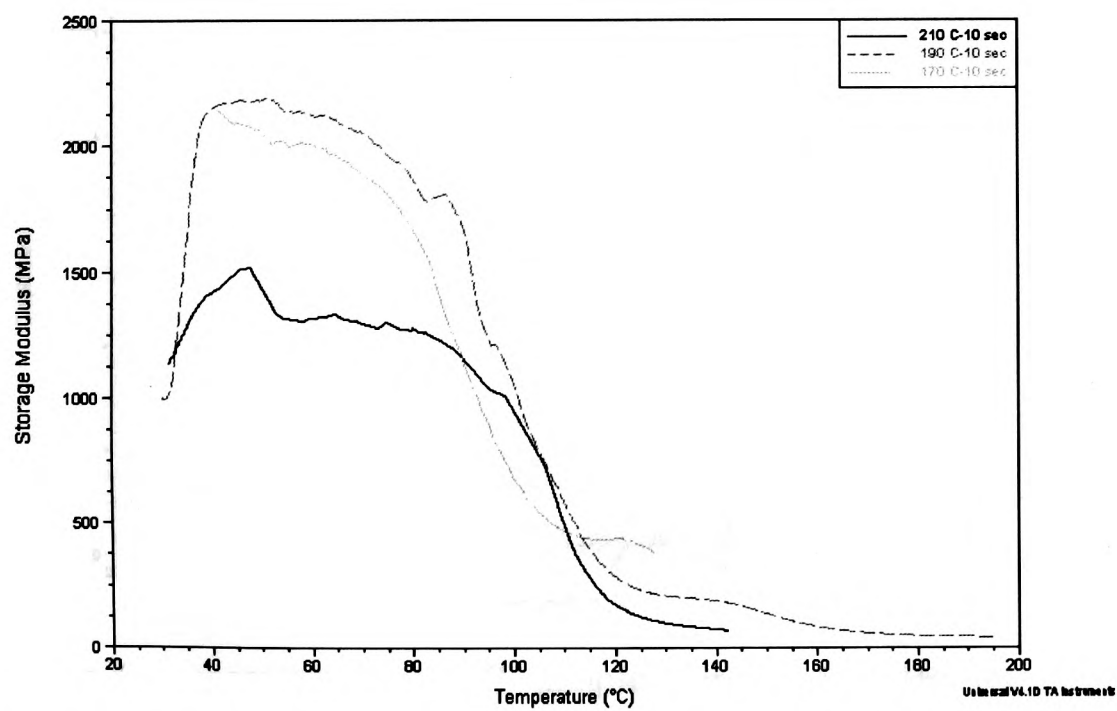


Figure 5-24: The storage modulus of the ACF samples cured at 170, 190 and 210 °C for 10 s.

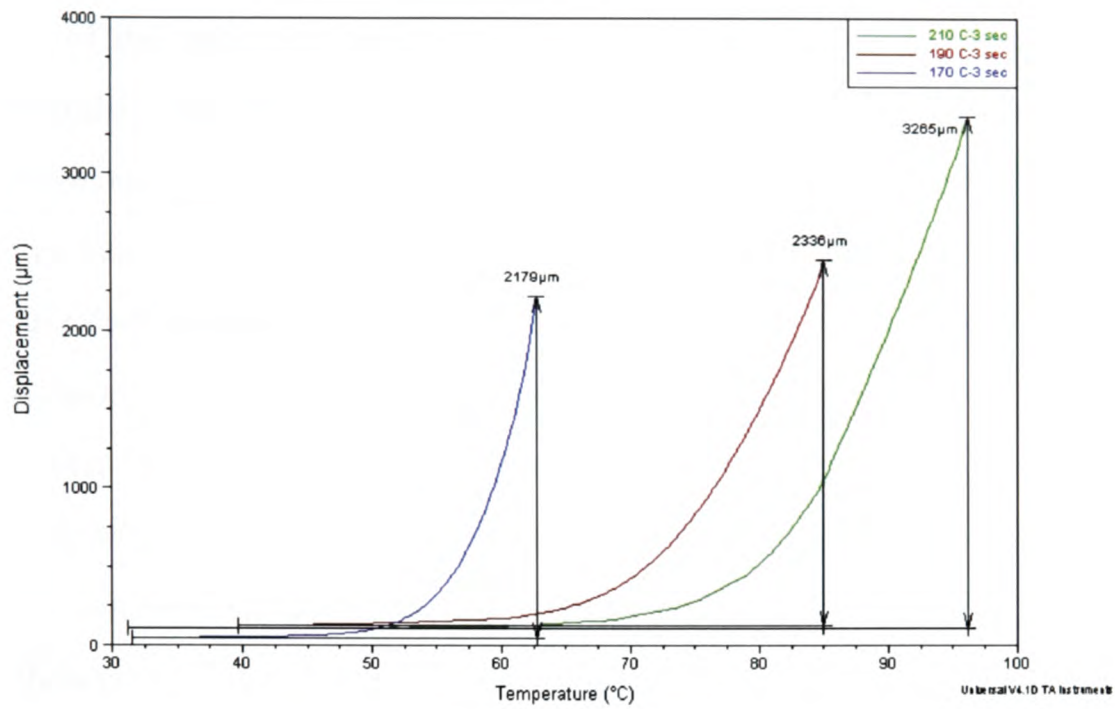


Figure 5-25: The displacement of the ACF samples cured at 170, 190 and 210 °C for 3 s.

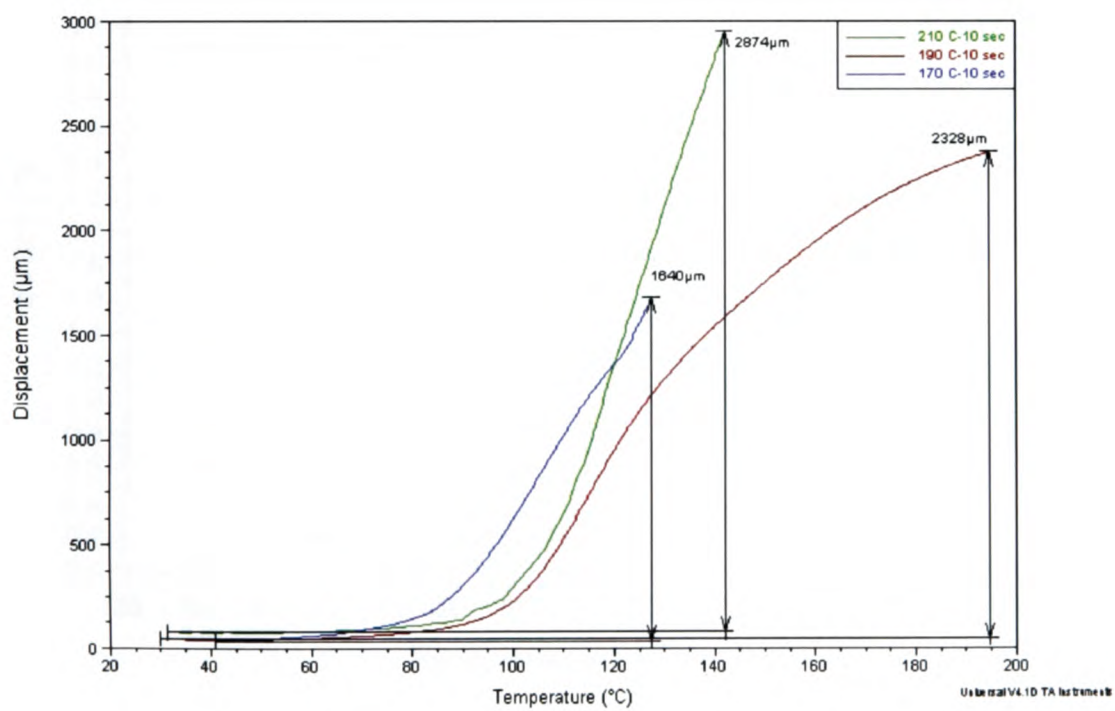


Figure 5-26: The displacement of the ACF samples cured at 170, 190 and 210 °C for 10 s.

The adhesive samples deform under the tensile condition of the DMA test environment. This deformation changes with time and temperature. Figure 5-25 shows the displacements of the adhesive samples cured at 170, 190 and 210 °C for 3 s. It is found that the temperature affects the displacement. The adhesive deformation increases with the temperature more rapidly after crossing the glass transition point. As the curing temperature increases, the transition temperature also shifts to the higher value. Figure 5-26 shows the displacements for the adhesives cured at 170, 190 and 210 °C for 10 s. In this case, the rapid change of the displacement for the sample cured at 190 °C occurs at a higher temperature compared to those cured at 170 and 210 °C. Similar results have been obtained for the measured strains in the samples as shown in Figures 5-27 and 5-28. From these results it can be concluded that the optimum bonding temperature and time for this particular adhesive are 190 °C and 10 s respectively.

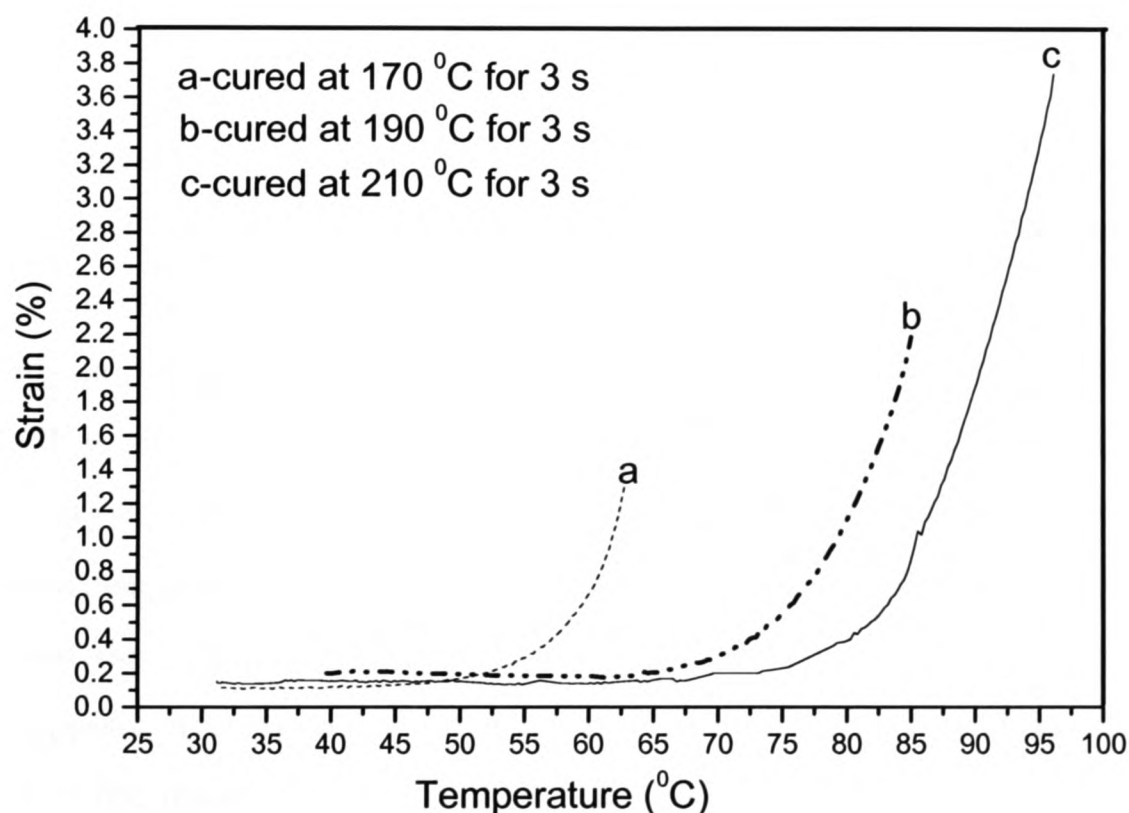


Figure 5-27: The strain (%) of the ACF samples cured at various temperatures for 3 s.

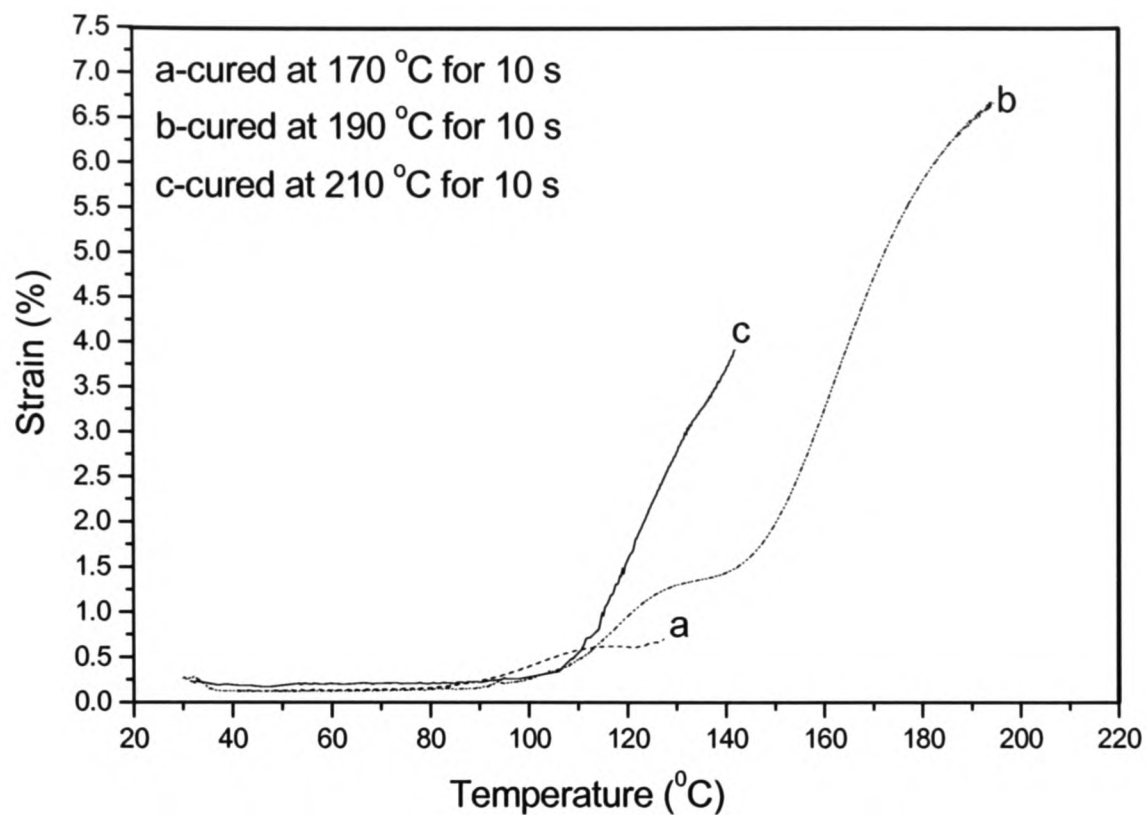


Figure 5-28: The strain (%) of the ACF samples cured at various temperatures for 10 s.

From the above results and discussions it is clear that the bonding temperature and time have great impact on the properties of the ACF. Generally speaking, higher bonding temperatures and longer bonding times are required to achieve higher cross-link density and this leads to an increase in the glass transition temperature of the ACF. However, when the ACF is allowed to cure for a long time at high temperature, the glass transition temperature may decrease rather than increase and the polymeric properties may degrade. This is because the polymeric chain may break and move in the ACF and this allows the transition from the glassy state to the rubbery state to happen at a lower temperature. When this happens, it is difficult for the adhesive matrix to hold the conductive particles in place and as the result the contact areas may not be of good quality. Therefore, both under-curing and over-curing of adhesives have negative impact on the glass transition temperature as well as the physical properties of the ACF. The effects of the bonding temperature on the curing and electrical conduction will be discussed in detail in the following sections.

5.4.3 The Effect of Temperatures on the Curing of ACF

Figure 5-29 shows the curves obtained from the DSC analysis for the ACFs cured at various temperatures. This figure shows the amount of heat released during the temperature ramp. In a DSC experiment, the temperature is usually increased linearly over time [172]. In this work, the temperature ramp rate was chosen as 10 °C/min so that the ACF could melt and the polymer in the adhesives could form cross-links with a proper conformation of the polymer macromolecules with the minimal trapping of excess enthalpy and residual mechanical stress [173].

It was found from the experiment that the onset temperature was 107.10 °C for the uncured ACF. For the ACFs cured at 160, 180, 200, 220 and 240 °C the onset temperatures are 106.19 °C, 104.62 °C, 101.37 °C, 97.30 °C and 96.01 °C respectively. The curves in Figure 5-29 show that initially the heat flow increases due to the low viscosity, then the curves become rather flat up to a certain curing degree, as there is little change in the energy flow into the sample relative to the reference at low temperatures. After that the onset temperatures are reached and the samples begin to melt. At this stage, energy needs to be added to the samples to melt the crystallites and the curves show sharp dips. Since the glass transition temperature (T_g) of the ACF is 130 °C, the heat capacity of the samples changes at this temperature and the heat flow reaches a minimum. For this reason, all curves exhibited a broad exothermic peak at about 130 °C, as shown in Figure 5-29. Moreover, the glass transition is a second order phase transition and appears as a change in the slope of the heating curve, which is endothermic and this affects the curing reactions [174]. As a result, on reaching the glass transition temperature, the reaction between the functional groups decreases dramatically and the local viscosity becomes higher. The areas under the curves shown in the Figure 5-29 are the enthalpy of reaction for the entire event.

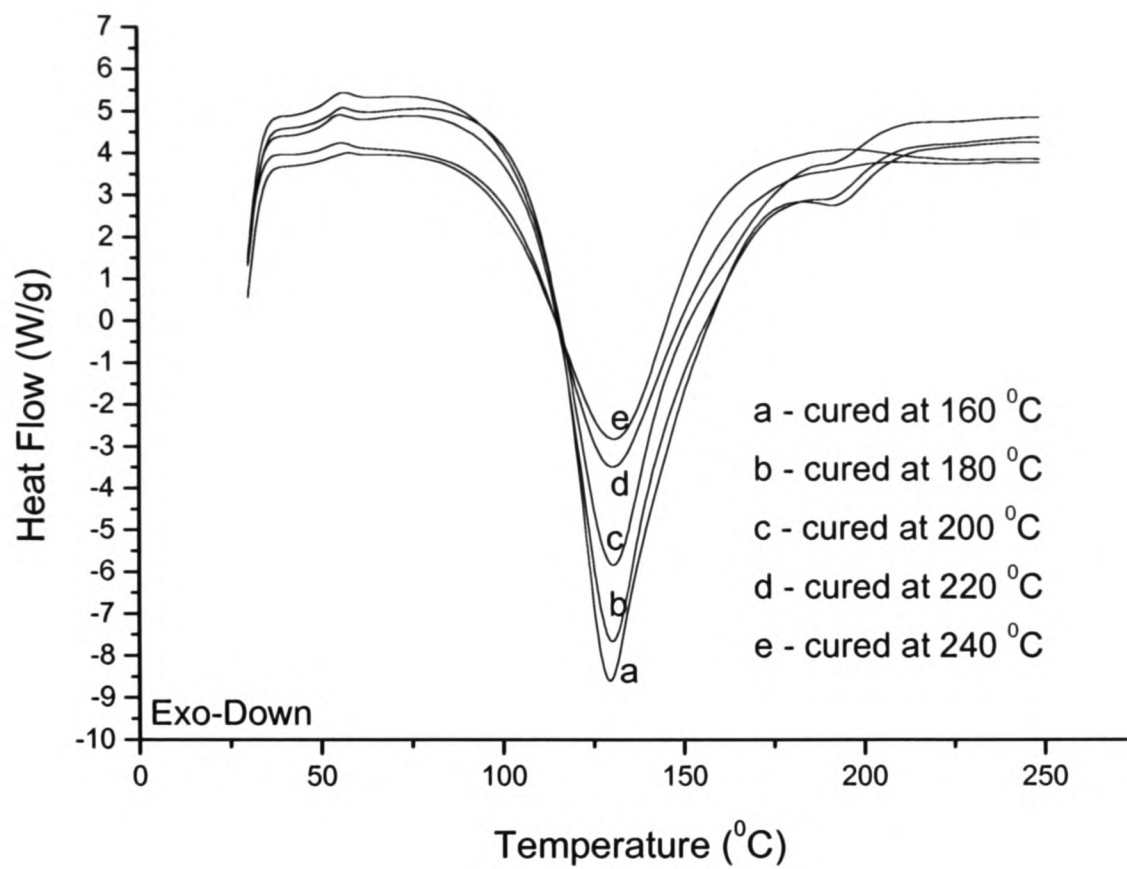


Figure 5-29: DSC scans for ACFs cured at different bonding temperatures.

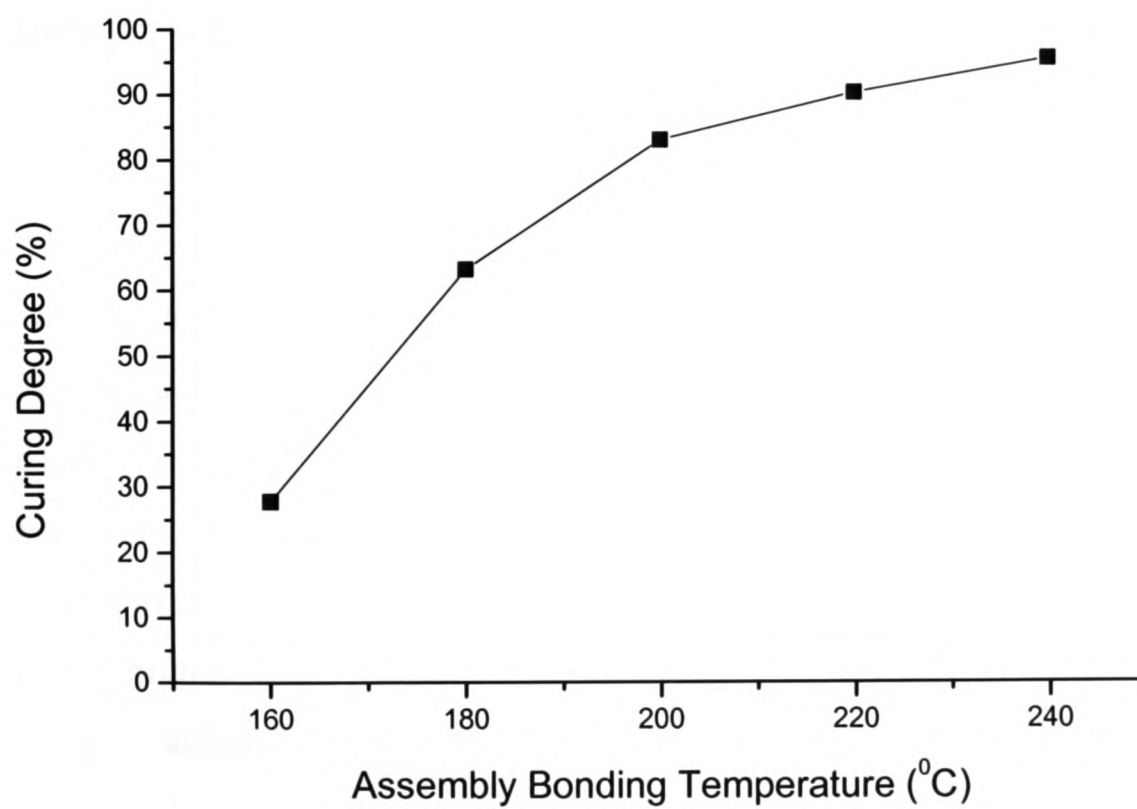


Figure 5-30: Curing degree of ACF samples bonded at different temperatures.

The results from the curing degree measurement using equation (5.1) are shown in Figure 5-30. This figure reveals that 28% of curing can be achieved at a bonding temperature of 160 °C. By raising the bonding temperature to 200 °C, a better curing degree of 83% can be achieved. Bonding at temperatures of 220 °C and 240 °C ACFs can be cured up to 90% and 95% respectively. The curing of ACFs begins with the formation and linear growth of polymer chains in the epoxy resin and soon this polymer chains begin to branch and finally form three-dimensional highly cross-linked chemical networks [158]. A higher bonding temperature provides a higher active energy to initiate and accelerate the cross-linking reaction [175]. Therefore, it can be concluded that the curing of ACFs is largely dependent on the applied bonding temperature and higher bonding temperatures result in better curing of ACFs for a given curing time.

5.4.4 The Effect of Curing on the Performance of ACF Joints after Thermal Ageing

5.4.4.1 Adhesion Strength of the ACF Joints after Thermal Ageing

The properties of ACFs are highly dependent on the bonding parameters such as the bonding pressure, the bonding time, and especially, the bonding temperature. The cross-link density of the ACF significantly affects the ACF's reliability performance [158]. Higher bonding temperatures lead to better cross-linking and a higher degree of curing as discussed earlier. The curing degree plays an important role in the adhesion strength, as shown in Figure 5-31. This figure shows the adhesion strength, characterized by the shear load, for the ACF assembly before and after ageing at 150 °C. It is obvious that, before ageing, there is higher shear strength for the samples bonded at higher bonding temperatures. The adhesion strength increased with the increase in the bonding temperature due to the inter-diffusion and/or reaction between the ACF epoxy and the Polyimide (PI) film [175]. Therefore, a higher bonding temperature would lead to higher adhesion of the ACF to the chip and the substrate, as well as better curing.

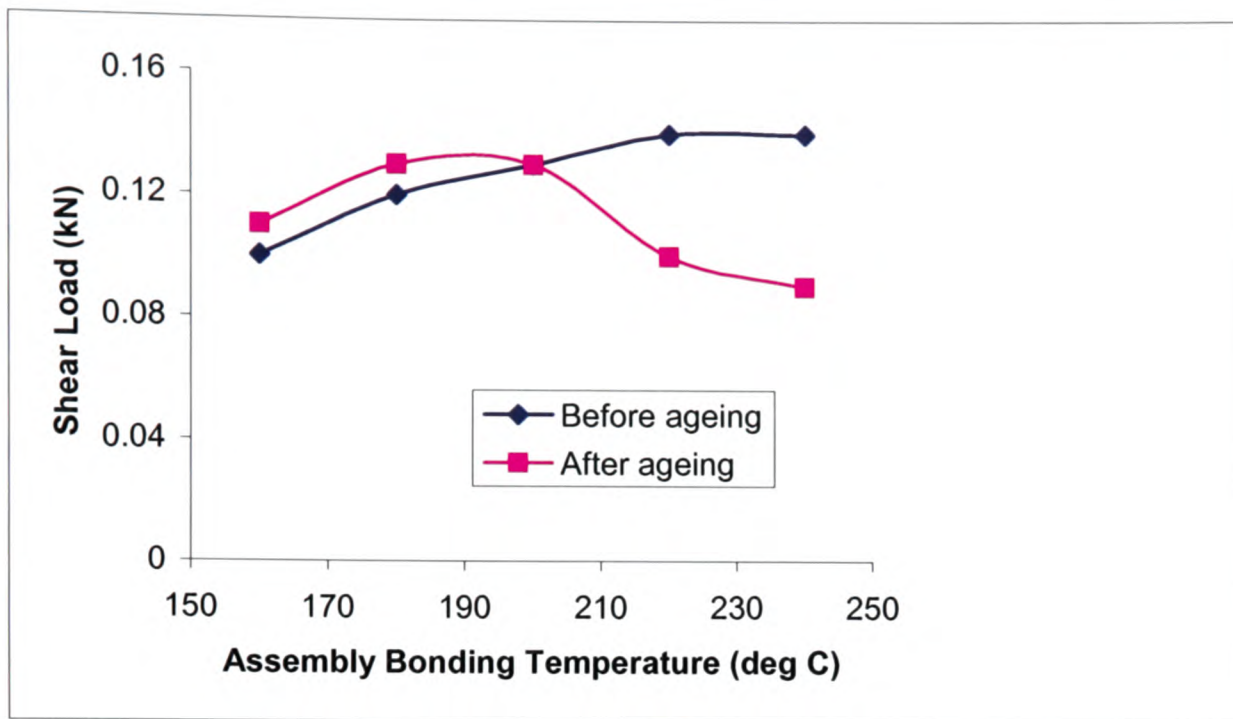


Figure 5-31: Adhesion strength of the ACF assembly before and after thermal ageing.

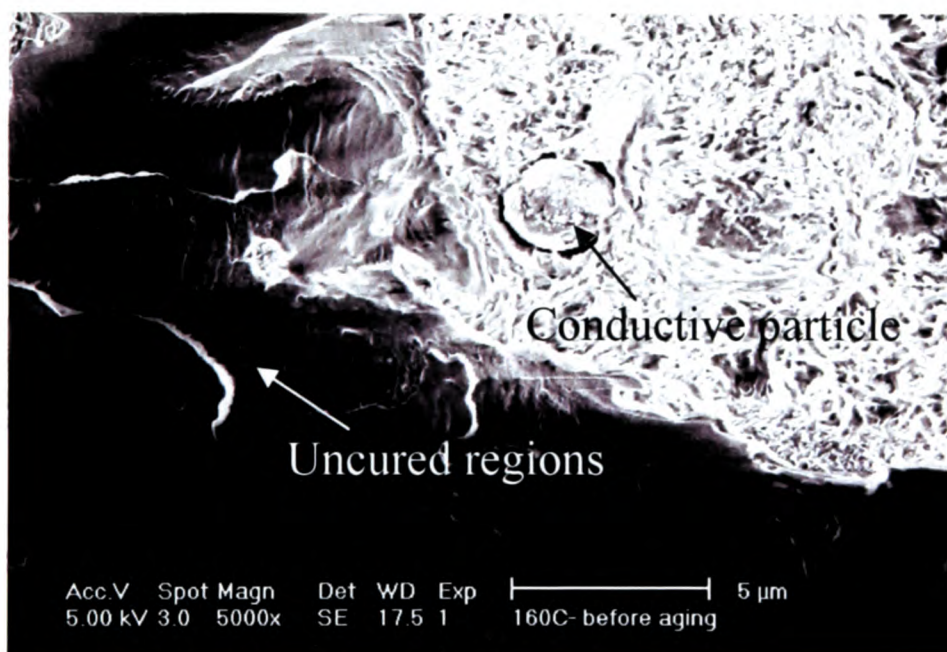


Figure 5-32: SEM image showing uncured regions of the ACF when bonded at 160 °C.

It is interesting that the adhesion strength increased after the thermal ageing treatment for the samples bonded at 160 °C and 180 °C. During the bonding process, the initially non-cross-linked material transforms into a rigid solid due to the irreversible cure reactions. In

this case, the ACF was not fully cured, as shown by the DSC study (Figure 5-29 & 30) and by SEM image shown in Figure 5-32, and might have been further cured while ageing inside the high temperature oven. Though the epoxy based ACF has high specific adhesion to metals, glass, ceramics and polyimide [176], a high cohesive strength along the bond line can only be achieved when the ACF is fully cured. As a result, the adhesion strength increased after thermal ageing due to the further curing of ACF.

In contrast, the sample bonded at 200 °C had no significant change in adhesion strength after thermal ageing. From the curing study, it was found that at 200 °C the ACF can be cured to 83% and this means that any further curing during the ageing treatment was insufficient to affect the adhesion strength. Another interesting finding from this work is that the adhesion strength decreased in an unusual manner for samples bonded at 220 °C and 240 °C after the ageing treatment. This is surprising because the ACF matrix is highly cross-linked yet the adhesion strength could still be reduced due to the over curing of the epoxy. This could be caused by the thermal degradation of polymers and the breakdown of the corresponding molecular networks during the thermal ageing [177]. Moreover, the thermal expansion of highly cross-linked ACF during the ageing treatment at constant high temperature introduces a swelling stress [178] at the chip-ACF and/or ACF-substrate interfaces. This stress may cause delaminations or cracks that could have led to the decrease in the adhesion strength.

5.4.4.2 Contact Resistance of ACF Joints after Thermal Ageing

It has been mentioned earlier that at the beginning of the bonding process of the chip-on-flex assembly, the ACF becomes soft as the bonding temperature is applied. This transformation allows the ACF to flow, which in turn allows the conductive particles to move throughout the ACF joints [179]. Over time, however, three-dimensional cross-linkages form and the ACF becomes hard. At this stage, the conductive particles are no longer free to move. The extent of the cross-linking in the epoxy resins is the curing degree of the ACF [180] and its completeness greatly influences the rigidity and the

Chapter-5: Study of Interconnections formed with Anisotropic Conductive Films

reliability of the ACF. As the curing degree increases, the adhesive shrinks and the conductive particles are deformed as the results of the bonding pressure. This deformation increases the contact area and decreases the contact resistance [181]. Therefore, the curing degree plays an important role in the electrical performance of the ACF assembly.

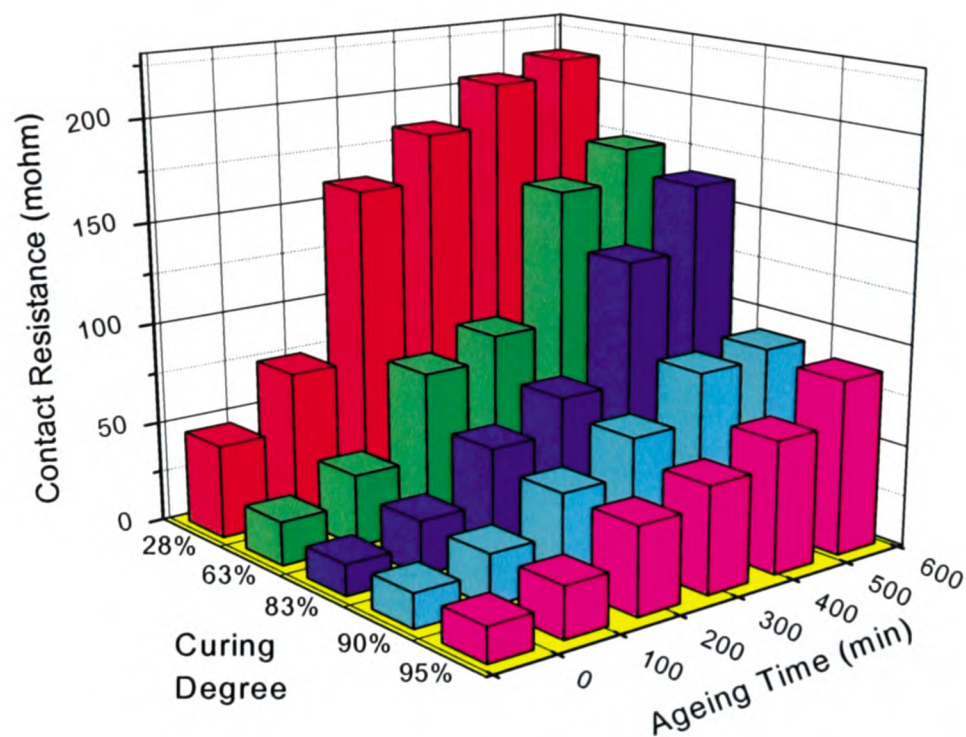


Figure 5-33: Increase in contact resistance of samples which underwent thermal ageing.

Figure 5-33 shows that the contact resistance increases for the samples after the thermal ageing. This figure reveals that for the sample with a curing degree of 28%, the initial contact resistance is relatively high. As the curing degree increases to 83%, the contact resistance decreases. It is interesting to note that ACF assemblies subjected to 90% and 95% curing have increased contact resistance. This may happen due to the breaking of the polymer chains as described earlier. It is evident from this figure that after thermal ageing, the contact resistance increases for all the samples that are bonded at different temperatures. The rate of increase in contact resistance was dramatically higher for the samples bonded at lower temperatures than those with higher curing degrees. For example, the initial contact resistances for the samples bonded at 160 °C and 240 °C were

Chapter-5: Study of Interconnections formed with Anisotropic Conductive Films

46.00 $\mu\Omega$ and 17.23 $\mu\Omega$. After 600 min of thermal ageing these values were measured as 213.65 $\mu\Omega$ and 86.57 $\mu\Omega$. Therefore, a higher bonding temperature and consequent a higher curing degree results in a stronger polymeric chain, higher adhesion strength and a reduced rate of increase in the contact resistance during thermal ageing.

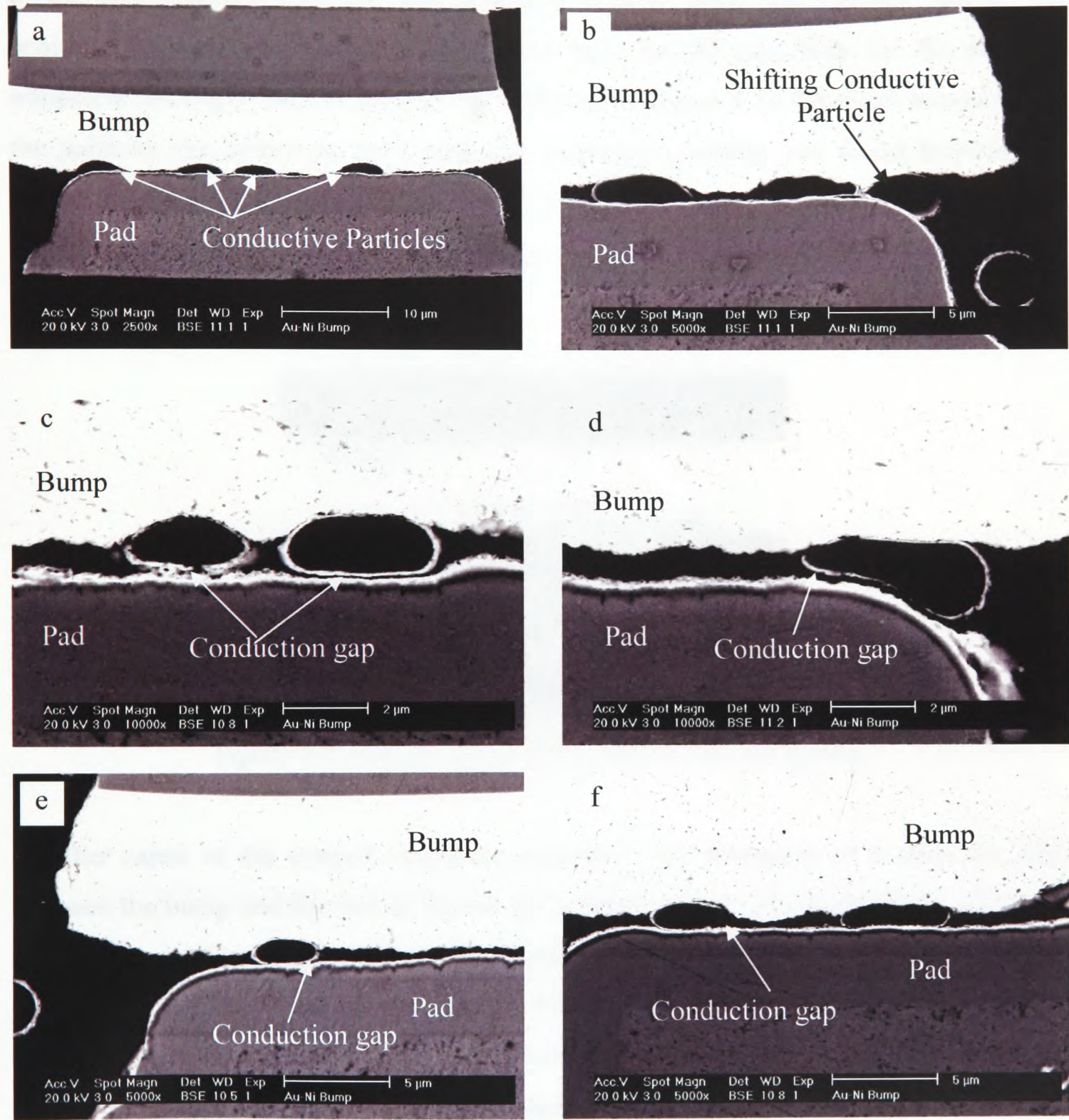


Figure 5-34: SEM images of ACF joints; (a) before thermal ageing and (b-f) after thermal ageing for the samples bonded at (b) 160 °C, (c) 180 °C, (d) 200 °C, (e) 220 °C and (f) 240 °C.

The root causes of the increase in contact resistances after thermal ageing were analyzed through the SEM microstructural images shown in Figure 5-34. Figure 5-34 (a) shows the structure before aging and it can be seen that a sufficient number of conductive particles are located between the bump and the pad. All the particles were trapped leaving no gap at the bump-particle and the particle-pad interfaces. After the thermal ageing, the positions of some conductive particles may have moved especially for the particles trapped at the edges such as the one that is shown in Figure 5-34 (b). Such movement of the particles can create an open joint (no conductive particle was found between the bump and the pad) as shown in the Figure 5-35. As a result, the number of conductive particles in the joint may decrease and this causes the increase of the overall contact resistance.

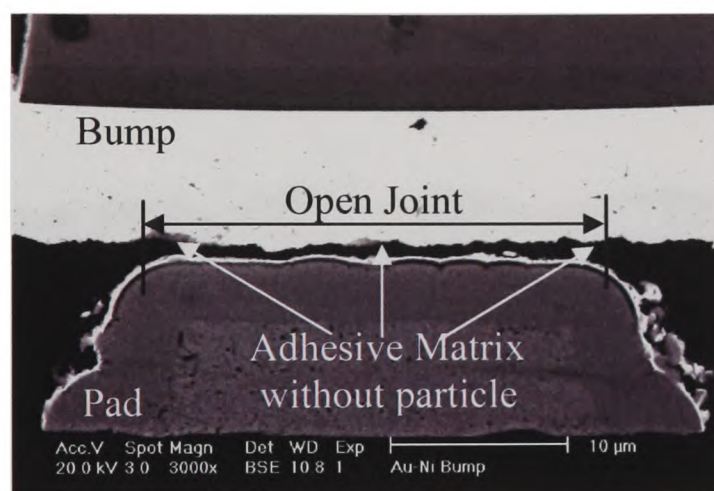


Figure 5-35: Open joint occurred due to thermal ageing.

Another cause of the contact resistance increase is the formation of conduction gaps between the bump and the pad as shown in Figures 5-34 (c) - (f). In the Figures 5-34 (c) and (d), the conduction gaps induced at the particle-pad interfaces for the samples bonded at 180 °C and 200 °C are clearly visible. At these two bonding temperatures the ACF curing degrees are 63% and 83% respectively. Since they are not fully cured, further curing may happen during the ageing treatment. The formation of these conduction gaps could be one of the consequences of this further curing. It is interesting to note that the conduction gaps are less prominent in ACF joints that are 90% and 95% cured (Figure 5-34 e and f). It was stated earlier that the interconnections at the bump-particle and the

particle-pad interfaces do not form with metallurgical reactions. Therefore, a conduction gap can form easily during the ageing treatment. From the adhesion strength study, it was found that a higher degree of curing led to a higher adhesion strength. For this reason, a smaller conduction gap was present in the higher temperature bonded samples than in the lower temperature bonded samples. Another interesting finding was that all the conduction gaps were found at the particle-pad interfaces rather than the bump-particle interfaces (Figures 5-34 c-f). The reason for this is believed to be that the Au-bump is soft and deforms easily which makes the bump-particle interface more resilient to gap formation, while the Cu-pad with Ni-electroplating is stiffer and does not deform as easily as the bump, as shown in Figure 5-36. During the ageing treatment the undeformed and mostly flat surface of the Cu pad helped to induce a gap between the particle and the pad interface.

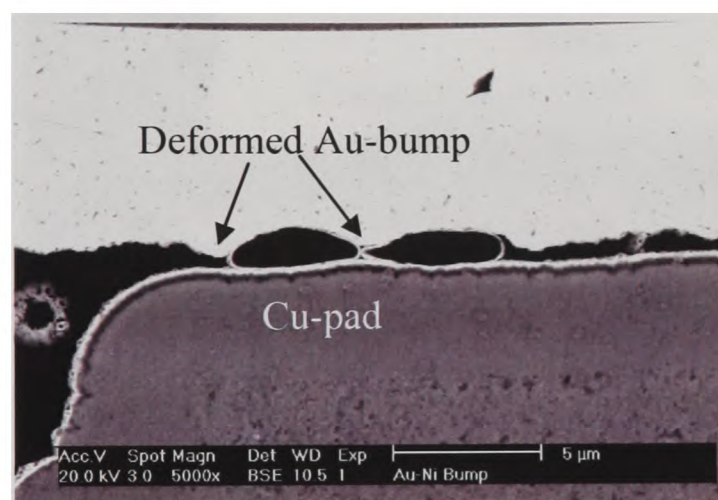


Figure 5-36: SEM image showing deformations of the Au-bump and the conductive particles.

A common cause of conduction gap formation in the ACF joints is the thermal expansion mismatch [182] in the ACF assembly. An ACF joint consists of several materials with different coefficients of thermal expansion (CTE). During thermal ageing the mismatch among the bump, the pad, the particle, and the adhesive matrix is responsible for the conduction gap, as shown in Figure 5-37. Figure 5-37 (a) shows that the bump and the pad were in firm contact without ageing treatment, the conductive particles were deformed and trapped leaving no gap. However, as shown in the Figure 5-37 (b), a gap close to the edge of pad and bump can be seen in the joint with ageing treatment.

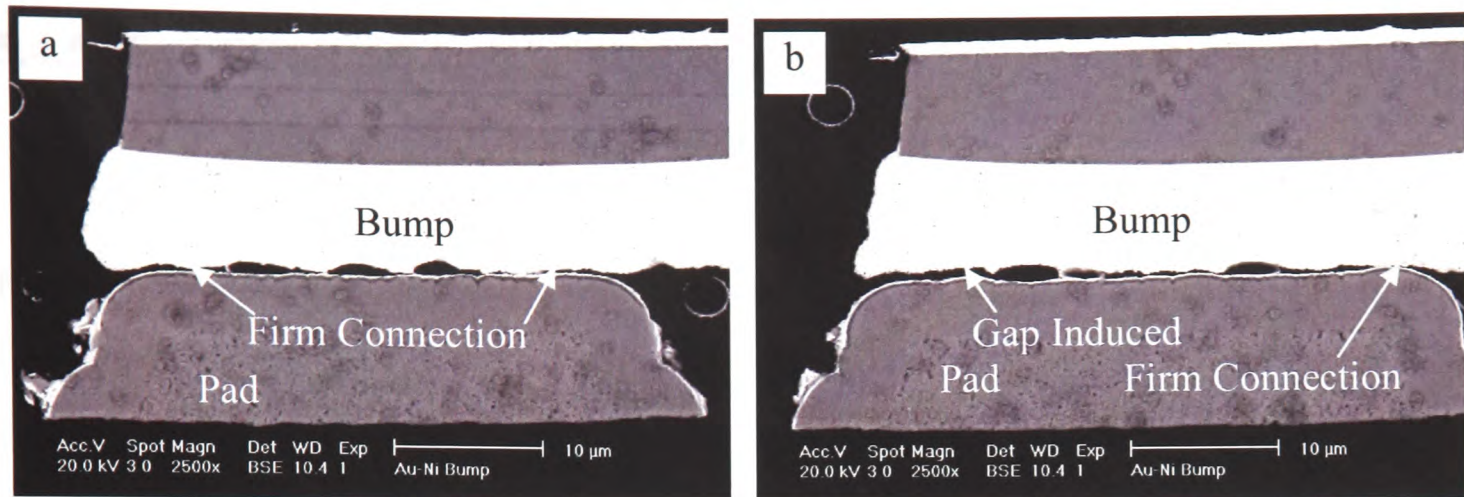


Figure 5-37: ACF interconnection through conductive particles; (a) before thermal ageing, (b) after thermal ageing.

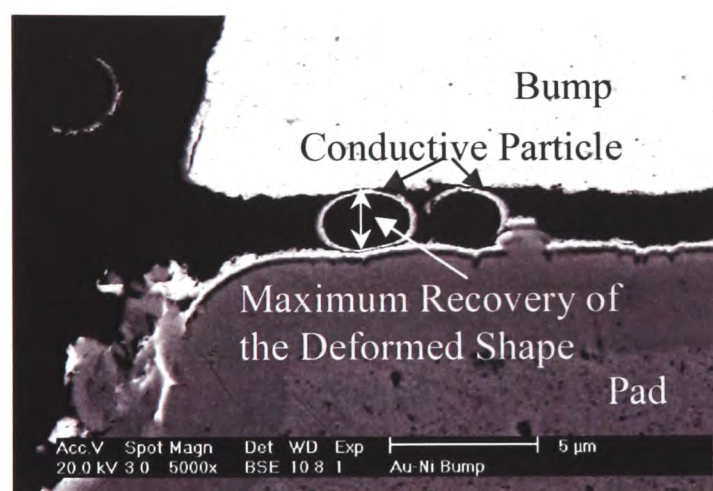


Figure 5-38: Maximum recovery of the deformed particle after thermal ageing.

During the bonding process, conductive particles' shape changes from a sphere to an ovoid as the bonding pressure is applied, and the contact spots at the bump-particle and the particle-pad interfaces spread to make effective contact areas. A larger contact area results in a smaller contact resistance [179][183]. If a deformed particle can find some room between the bump and the pad, it will try to recover its original spherical shape [24] if the particle's deformation is not pure plastic deformation. As a result, the contact area at the bump-particle and particle-pad decreases and contact resistance increases. This contact resistance increase through shape recovery mechanism is difficult to prove in experiment but in Figure 5-38 the nearly spherical shape of the deformed particle suggests that this might be what has happened after the ageing treatment.

5.4.5 The Effect of Ageing Temperature on the Contact Resistance of ACF Joints with Various Curing Degrees

Figure 5-39, 5-40 and 5-41 represent the increase in contact resistances of the flip chip on flex assemblies subjected to thermal ageing at 60, 100 and 140 °C temperatures. The contact resistances increase harshly for the samples that are aged at 140 °C. For all the three ageing temperatures, the contact resistances increase dramatically with time and 28 % cured samples exhibit the worst performance. The tendency in the increase in contact resistance is very high for this sample compared to the highly (83% and 95%) cured samples. For the first two hours of ageing, the increase in contact resistance for both 83% and 95% cured samples is not very significant. However, after two hours, the contact resistances start to increase rapidly for both of these highly cured samples. It should be noted that among the three ACF samples, the 95% cured ACF samples showed the slowest increase in the contact resistance for all thermal ageing conditions.

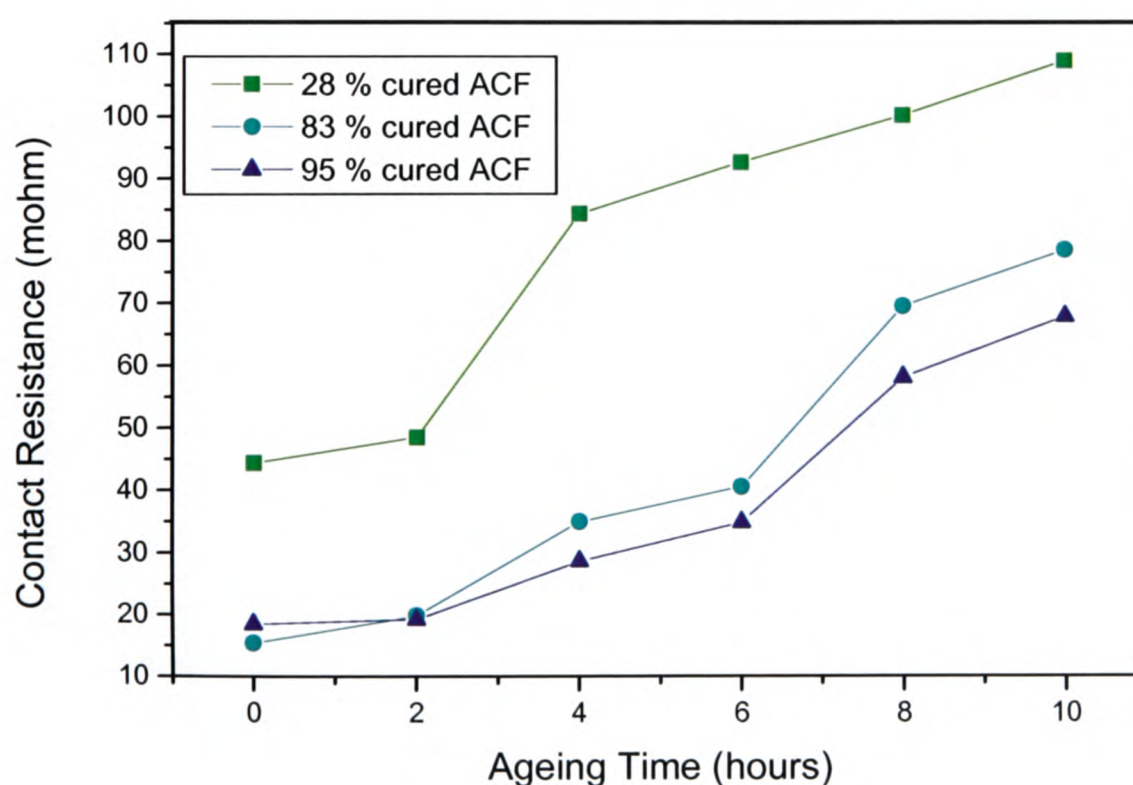


Figure 5-39: Increase in contact resistance of samples underwent ageing at 60 °C.

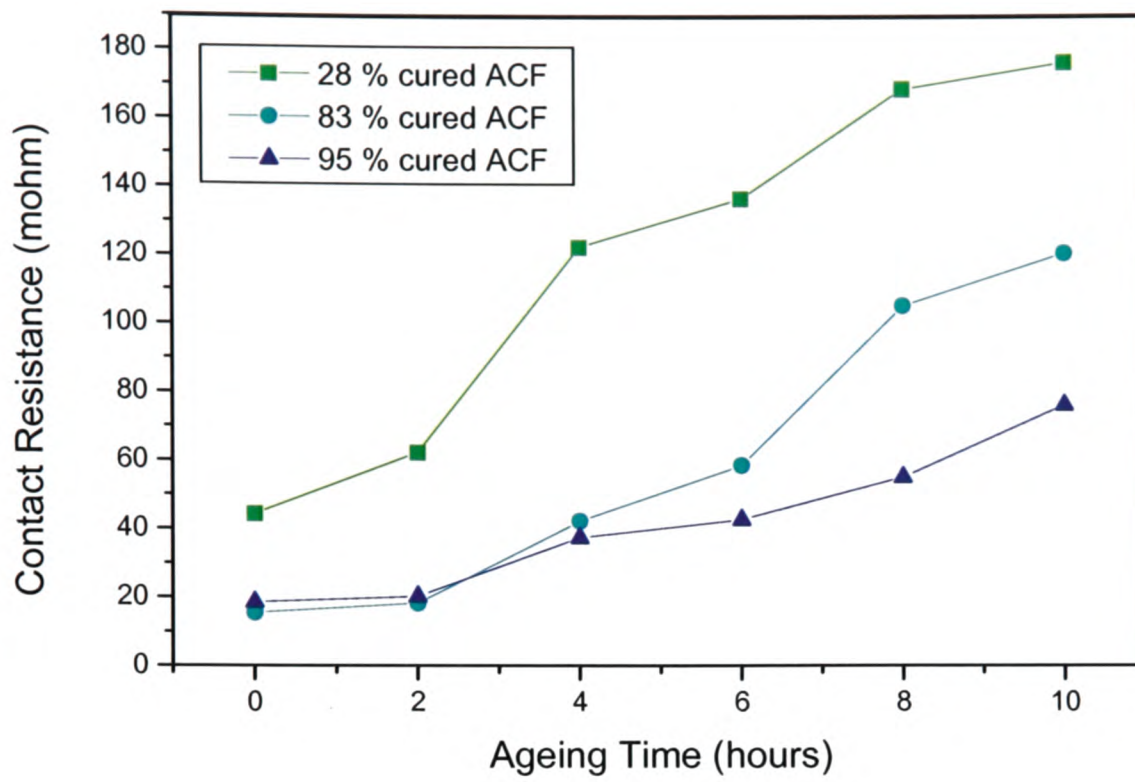


Figure 5-40: Increase in contact resistance of samples underwent ageing at 100 °C.

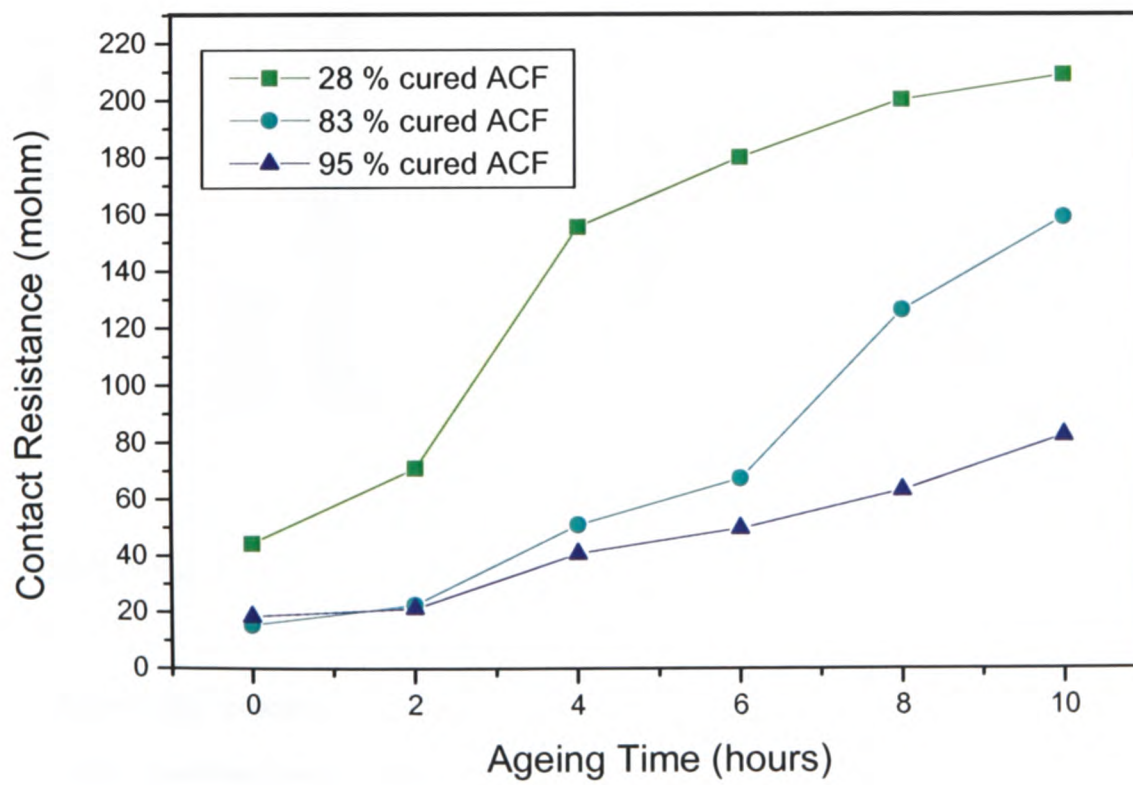


Figure 5-41: Increase in contact resistance of samples underwent ageing at 140 °C.

Compared to the samples aged at 140 °C, the magnitude of the increase in contact resistance is much lower for the samples that are aged at 60 and 100 °C. As it has been described in previous sections, the properties of ACFs change very rapidly above the glass transition temperature T_g . In this case, the ageing temperature of 140 °C is higher than the ACF's T_g (=130 °C). It is, therefore, believed that the physical and the morphological changes to the polymer matrix degrade the bonding strength and this has led to the dramatic increase in the contact resistance. On the other hand, because the ageing temperatures of 60 and 100 °C are far below the T_g , the contact resistance didn't increase as much as it was seen for the ageing temperature of 140 °C. For the samples aged at 60 and 100 °C, the relaxation of the clamping forces provided by the cured adhesive matrix was possibly responsible for the increase in the contact resistance.

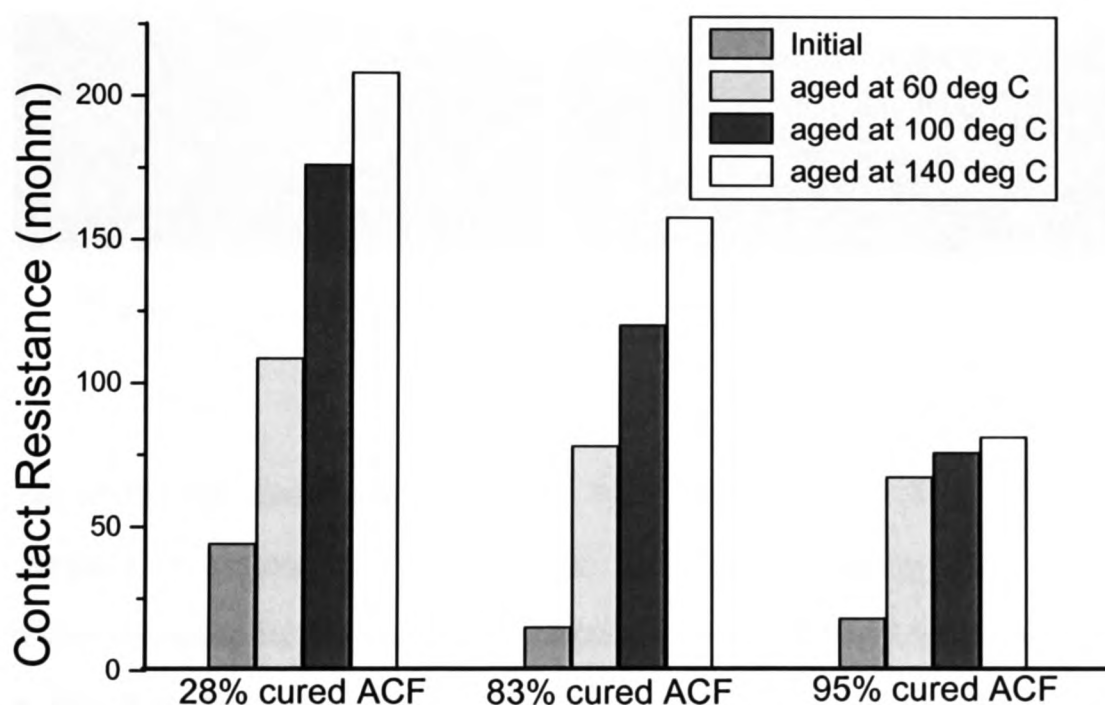


Figure 5-42: Contact resistances after 10 hours of isothermal ageing.

Figure 5-42 shows the contact resistance values of ACFs samples with different curing degrees and aging temperatures. Before ageing, the initial contact resistance was lowest for the 83% cured ACF. For all the three ageing conditions, the increase in the contact resistance of the 95% cured ACF was the lowest. For this highly cured ACF, the

Chapter-5: Study of Interconnections formed with Anisotropic Conductive Films

crosslink density i.e. the number of crosslink monomer units per main chain of that highly cured ACF is very high. The higher the number of crosslink densities, the more rigid the polymer is [184]. Therefore, 95% cured ACF might have protested the further movement of the deformed conductive particles which had helped to lower the increase in the contact resistance. One should bear in mind that although highly cross-linked ACF samples do not show the drastic increase in the contact resistance at a high ageing temperature, the tendency of the polymers to achieve more cross-link densities during a heat treatment may break the polymeric chains. This explains the degradation of the adhesion strength as shown in Figure 5-31.

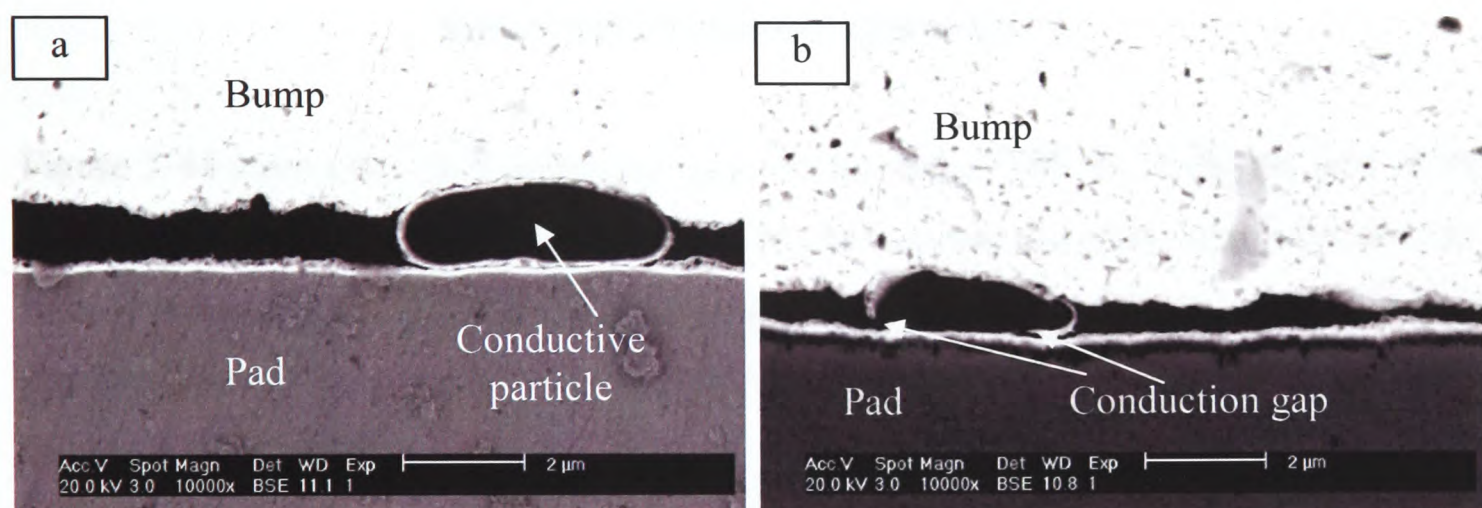


Figure 5-43: ACF joints aged at (a) 60 °C and (b) 100 °C.

Figure 5-43 (a) shows the cross section of the ACF joint aged at 60 °C. It reveals that the conductive particle is almost in contact with the bump and the pad. As a result the magnitude of the increase in the contact resistance at this ageing temperature was not as high as seen for the other two ageing temperatures. Figure 5-43 (b) shows the cross section of the ACF joint aged at 100 °C. The gap between the particle and the pad is clearly visible which indicates a discontinuity of the electrical conduction through the pad and the particle and the bump in the vertical direction. This conduction gap could be the reason behind the dramatic increase in the contact resistance during ageing. It should be noted that the conduction gap in this sample is also found at the particle-pad interface. This observation is consistent with the previous finding shown in Figure 5-34.

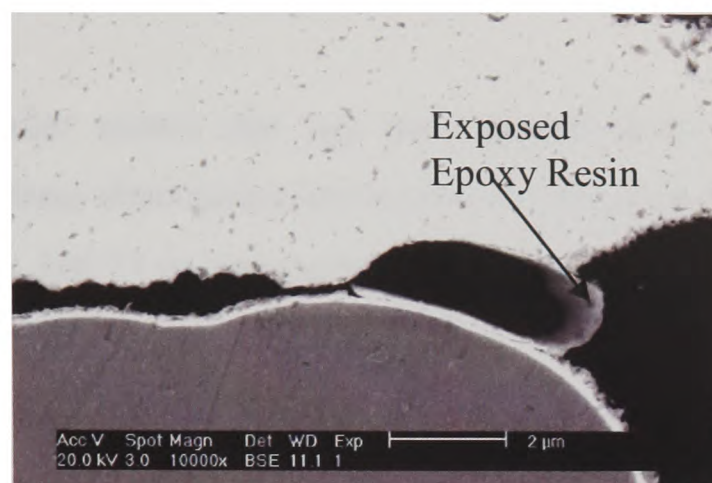


Figure 5-44: ACF joints aged at 140 °C.

Figure 5-44 shows the ACF joints that have been aged at 140 °C. It can be seen in this figure that the metal coating of the particle has broken and the epoxy resin that acts as a core of the conductive particle has come out. It is not clear why this has happened. There are two possible reasons behind this. First, the thermal expansions of the core epoxy might have pushed the metal coatings and second, the thermal expansions of the adhesive matrix might have resulted in too much pressure on the particle. Under the influence of these two forces and if there is enough room around the particle, the deformed core may try to recover its original shape. Therefore, the push in and push back activities might have caused the breaking of the metal coatings and the ‘leaking’ of the core material. Whatever is the reason, the breaking of the metallic part of the conductive particle will result in the discontinuity of the electrical conduction path. This could explain the dramatic increase in the contact resistance as seen in Figure 5-42.

5.4.6 Modelling the Effect of Isothermal Ageing on ACF Joints Delamination

The extensive experimental work on effects of the isothermal ageing on the electrical performances of ACF joints has been described in sections 5.4.4 and 5.4.5. The microstructural analyses shown in those two sections provide the electrical failure modes

Chapter-5: Study of Interconnections formed with Anisotropic Conductive Films

of the ACF joints under thermal load. In this section, a computer modelling analysis of the ageing experiments is described. The computer modelling results can help understand the mechanisms of the electrical failure modes.

The ACF joint computer model that has been described in section 5.3.2 has been analyzed to study the stress distribution in the joint during the thermal aging process. The results for the ageing at 150 °C are shown in Figure 5-45. Figure 5-45 (a) shows the stress generated along x-direction in the cross section of a bump-particle-pad micro joint. It is found that stress concentrates at the round edges of the particle-bump and the particle-pad interfaces. It is evident that the metal coatings of the polymer particle experience very high tensile stresses in the critical regions (as indicated in the figure) whereas the epoxy core of the particle experiences very high compressive stresses in the same regions. Figure 5-45(b) represents the stress values in y-direction and reveals that high stresses can be found at the middle (as indicated in the figure) of the interface between the metal coatings of the particle and the adhesive matrix. The core polymer provides a spherical shape to a conductive particle and the Ni coating on the surface of that polymer sphere provides the electrical conductivity and the thin Au coating around the Ni layer protects from the oxidation. The observed stress concentration along these metallic coatings may cause damage to the coatings. As a consequence, the polymer core may 'leak' into the adhesive matrix as seen in the Figure 5-44. This phenomenon could be one of the main reasons for the increase in the contact resistance during isothermal ageing.

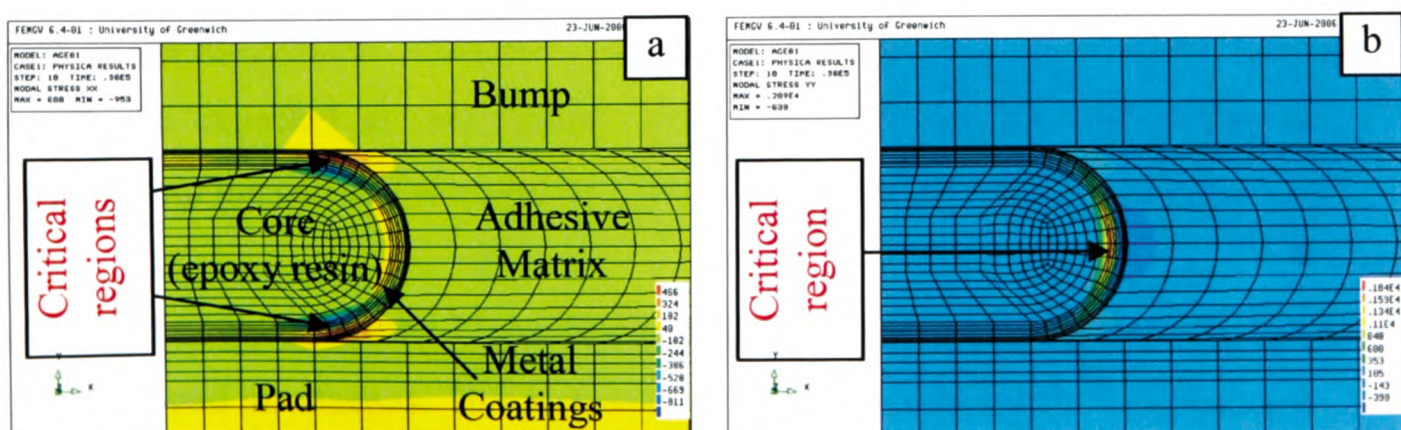


Figure 5-45: Computer modelling shows the ACF joints after isothermal ageing at 150 °C; (a) stress in x-direction; (b) stress in y-direction.

Chapter-5: Study of Interconnections formed with Anisotropic Conductive Films

Figure 5-46 (a) and (b) show the deformation of the conductive particle and the stresses in and around it. It is obvious that the conductive particle has been squeezed and the round edge (as seen in Figure 5-45) has become almost flat. Here, the adhesive matrix has a higher coefficient of thermal expansion (CTE) value compared to all other materials in the ACF joints. Therefore, adhesive matrix expanded more and it is the expansion that has caused the deformation of the particle. It has been described earlier that when the particle is squeezed, the thin metal coatings may burst and the core material may leak out into the adhesive matrix as seen in Figure 5-44.

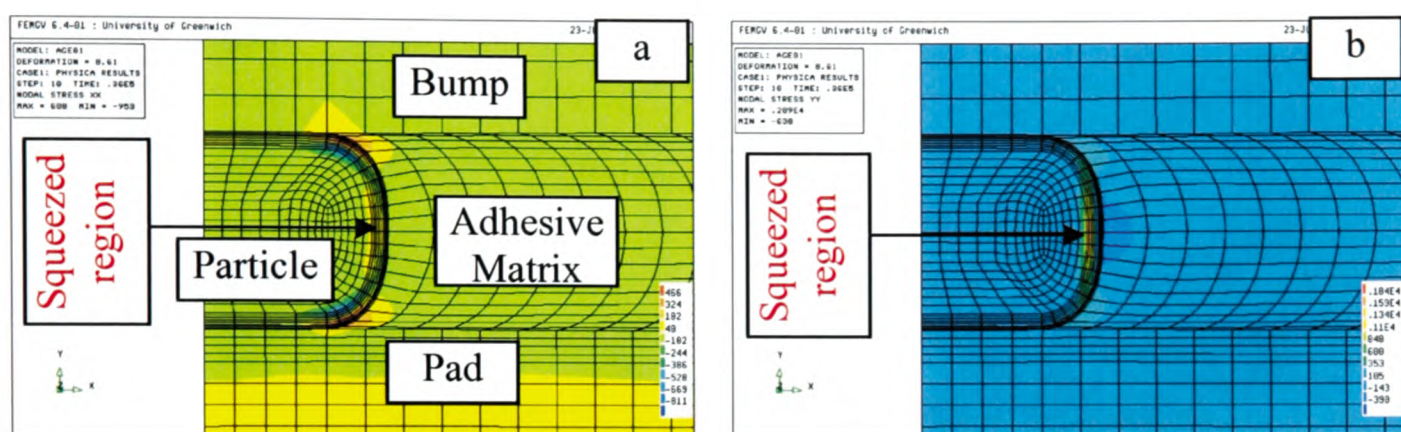


Figure 5-46: Computer modelling shows the ACF joints after isothermal ageing at 150 °C for 10 hours; (a) resultant deformation with stress in x-direction and (b) resultant deformation with stress in y-direction.

Another phenomenon that could be explained through the modelling results is that conduction gaps in ACF joints are always located between the conductive particle and the pad of the substrate as seen in Figures 5-34 and 5-43. The answer could be found in Figure 5-47 that shows the stresses along the particle-pad interfaces. It is seen that all stress components are higher at the edge of the particle-pad interface where adhesive matrix meets the particle. Therefore, subsequent damages and reductions in the adhesion strength are expected at that region. This could lead the conductive particle to be detached from the pad and the adhesive matrix and could generate a conduction gap.

Figure 5-48 reveals that the higher the ageing temperature the stronger the stress along the particle-pad interface is. This is consistent with the observation that the higher ageing temperatures result in more the delaminations along the particle-pad interface. These modelling results are also consistent with the experimental observation that as the contact

resistance increases with the aging temperature rise. Therefore, environment temperature is vital for the electrical and the mechanical reliabilities of ACF joints.

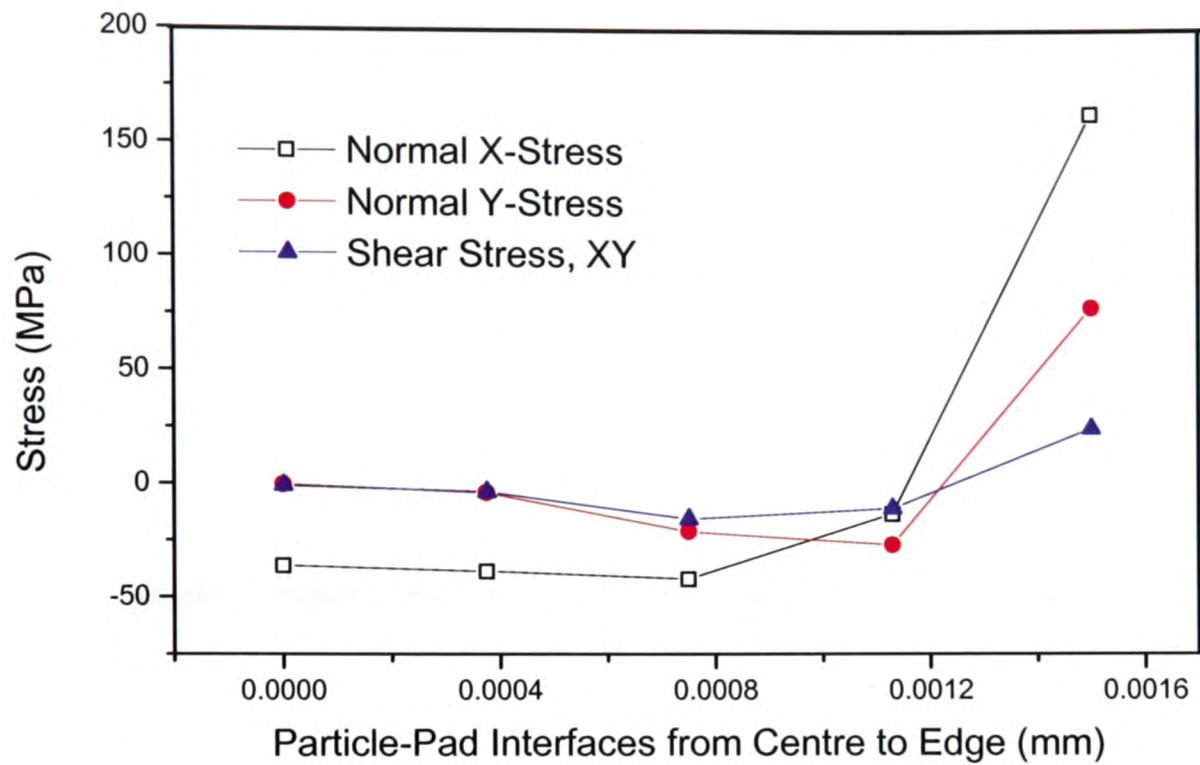


Figure 5-47: Stresses along the particle-pad interface after 10 hours of aging at 150 °C.

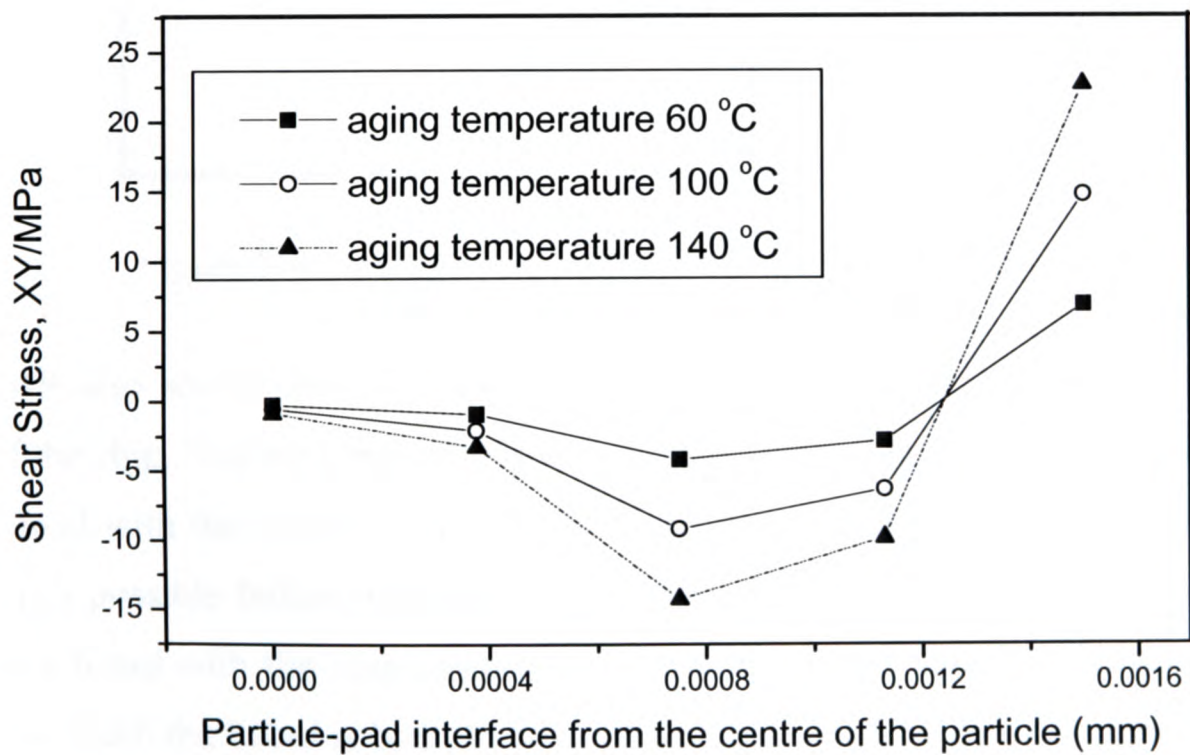


Figure 5-48: Shear stresses along the particle-pad interface at various aging temperatures.

5.4.7 The Effect of Mechanical Loading on the Performance of ACF Joint during 3-point Bending

The ACF-based flip chip assembly under the 3-point bending test condition has been modelled. The deformation of the assembly is shown in Figure 5-49. Different colours represent stress distributions at various parts of the assembly. The load is applied at the centre of the assembly, or to be more precise, at the centre of the FR-4 board. Due to the way the load is applied, the stress in the FR-4 is tensional compressive and in the chip it is tensile. Since the elastic modulus of the silicon chip is much greater than that of the substrate, the chip does not bend as much as the substrate.

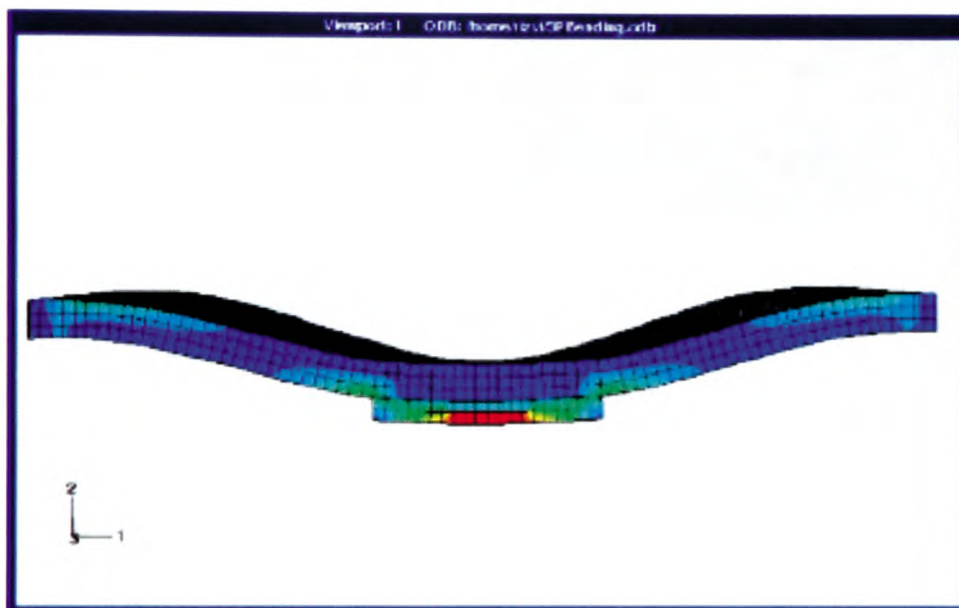


Figure 5-49: Front view of deformed flip chip assembly.

Figure 5-49 also shows that the maximum stress in the assembly can be found at the middle of the chip. The next highest stress is found at the edges of the flip chip where the chip is joined with the substrate through ACF. Because of the high stress in the die, die cracking is a possible failure mechanism. However, as Chengalva MK [185] has pointed out, when a board with flip chip assemblies is bent, it is not possible to crack the die, no matter how much the board is bent. Instead, if the stress is too high at the interface of the package, the crack may initiate in the ACF rather than in the chip. As the stress at both ends of the interconnection is much higher than in the middle, there is a strong possibility

that delamination may start at these regions. The deformation of the ACF from the zoom inner edge view is shown in Figure 5-50. The deformation of ACF is not uniform throughout its length. The deformation is the greatest at the ends. It is also observed that the ACF has been extended in thickness at the end of substrate-ACF-chip joint. The increase of the ACF thickness at the corner of the chip as a function of the applied load was obtained from the computer modelling results and is shown in the Figure 5-51.

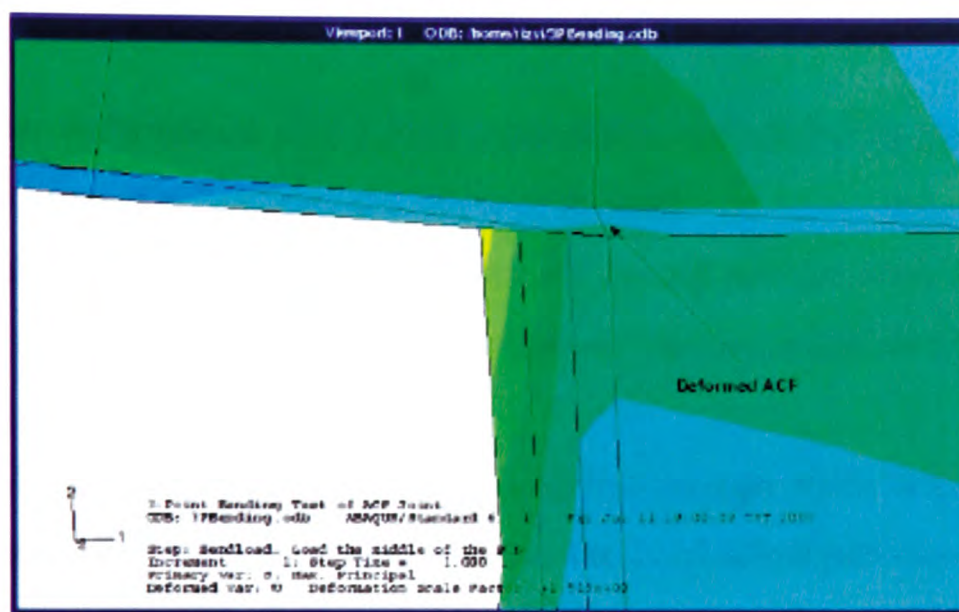


Figure 5-50: Zoom view of deformed ACF (inner edge).

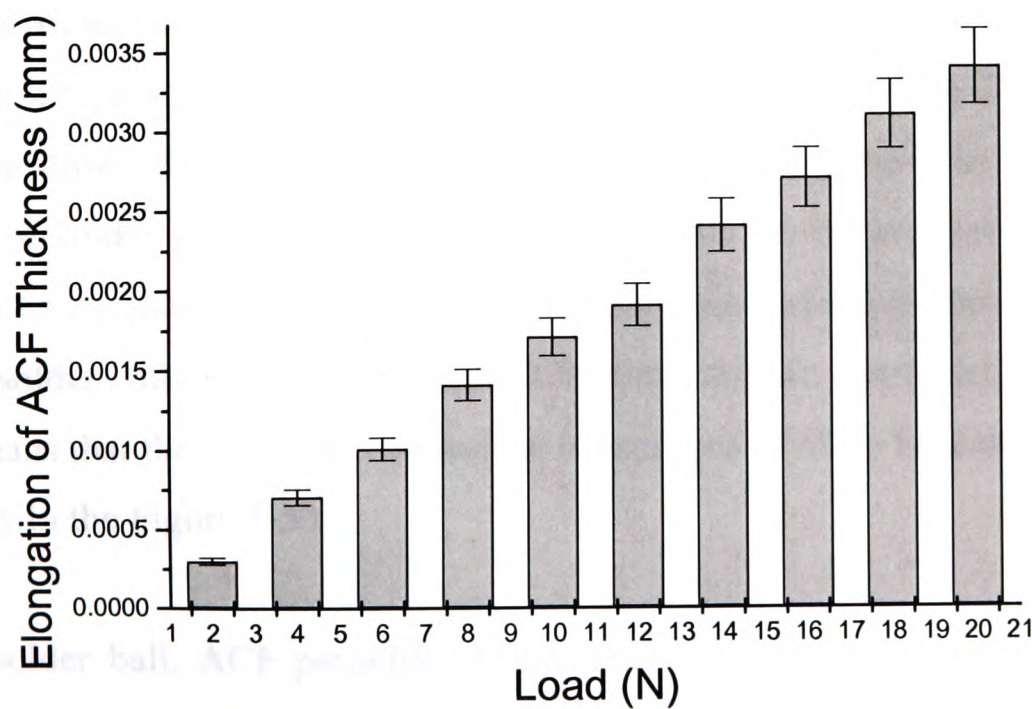


Figure 5-51: Increase in ACF thickness at the corner position of ACF-chip joint.

In this model, the bumps, the particles and the pads are not included in order to simplify the analysis. However, from the modelling results discussed above, it is easy to understand what may happen inside the ACF interconnection when the assembly is bent. Since the substrate bent more severely than the chip, the substrate will try to pull the ACF along with it while the chip will resist this pull. Therefore, the following three interconnect failure mechanisms may exist.

1. The shear deformation of the ACF may cause the conductive particle to lose the physical contact either from the bump or the pad.
2. If the substrate-ACF interfacial adhesion is strong enough, there is a possibility of the pad of the substrate being lifted together with the conductive particles from its original position.
3. If the ACF-chip interfacial adhesion is strong enough, there is a possibility of the pad of the substrate being lifted without the conductive particles. In this case the particles remain on the bump of the chip.

These three possibilities are shown schematically in Figure 5-52 (a), (b) and (c). Because conductive particles only have mechanical contacts with the pad and the bump, these scenarios can all cause problems in the electrical reliability of the ACF joints. This is very different from the situation where solder joints are subject to similar loading conditions. For solder joints, strong metallurgical bonds are formed between solder and metallization on the substrate and chip [186]. When under moderate thermal-mechanical loading, the solder balls become deformed, elongated, but the interfacial contacts are not lost. This means that the electrical connection is kept intact [187]. This situation is shown schematically in the Figure 5-53.

Unlike the solder ball, ACF particles are not metallurgically connected to the pad or bump. When ACF expands, the compressive force that keeps the particle-pad or particle-bump contact will decrease and the particles may recover to their original shape to some extent, i.e. the shape of the deformed particles becomes spherical shape again [47]. When

Chapter-5: Study of Interconnections formed with Anisotropic Conductive Films

this happen the contact area between the particles and the conductive surfaces (either bump or pad) will decrease. This decrease of the contact area will lead to an increase in the contact resistance [188]. The shape recovery is limited by the particle size. The maximum possible recovery of the deformed particle is from its $2\ \mu\text{m}$ deformed height to the original $3.5\ \mu\text{m}$ particle diameter. If the ACF expands more than $1.5\ \mu\text{m}$, gaps may form at the interfaces and this will result in a total loss of electrical contact and this disconnection will lead to the joint become open and no electrical conduction could occur.

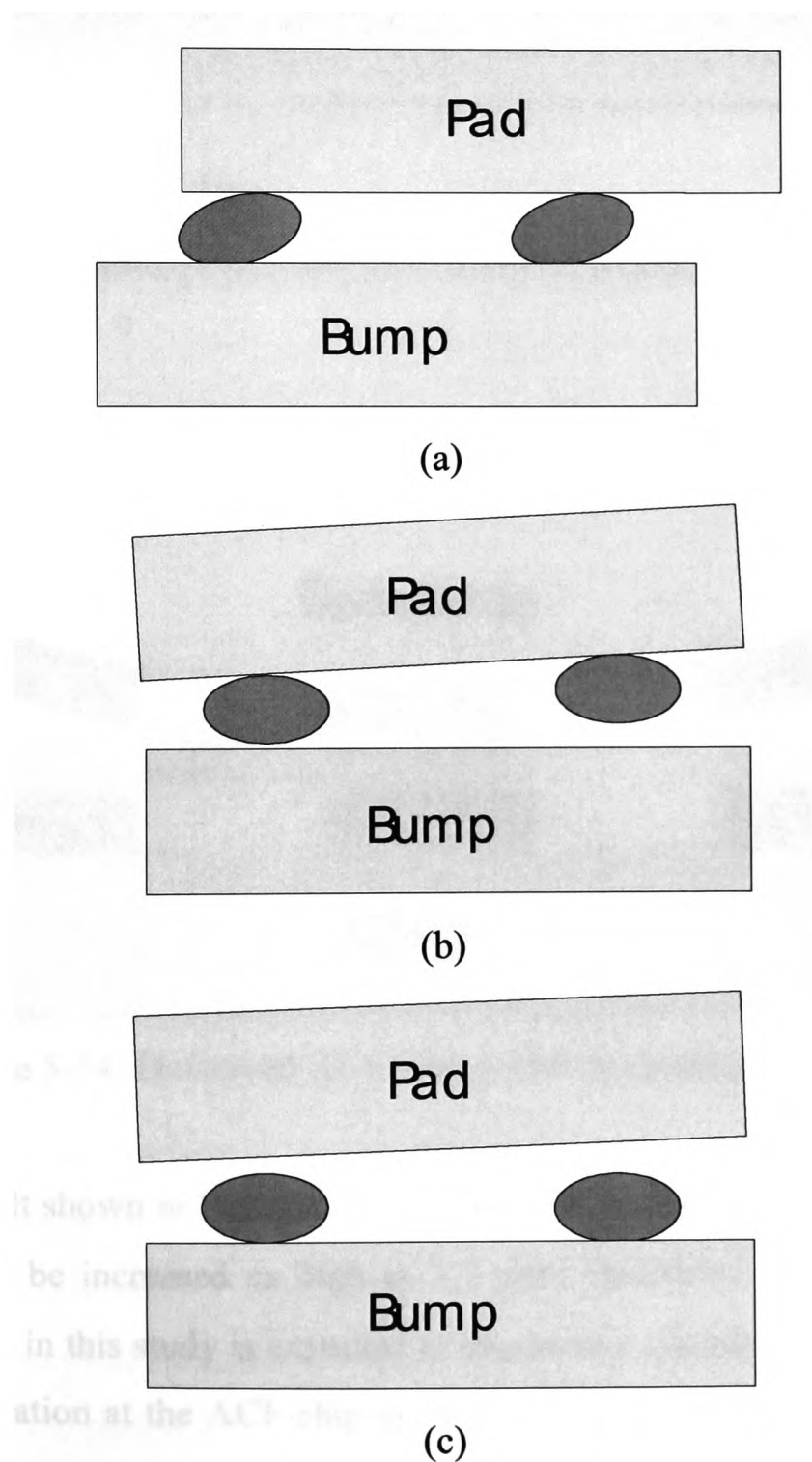


Figure 5-52: The possible three cases of ACF joint failure are shown in (a), (b) and (c).

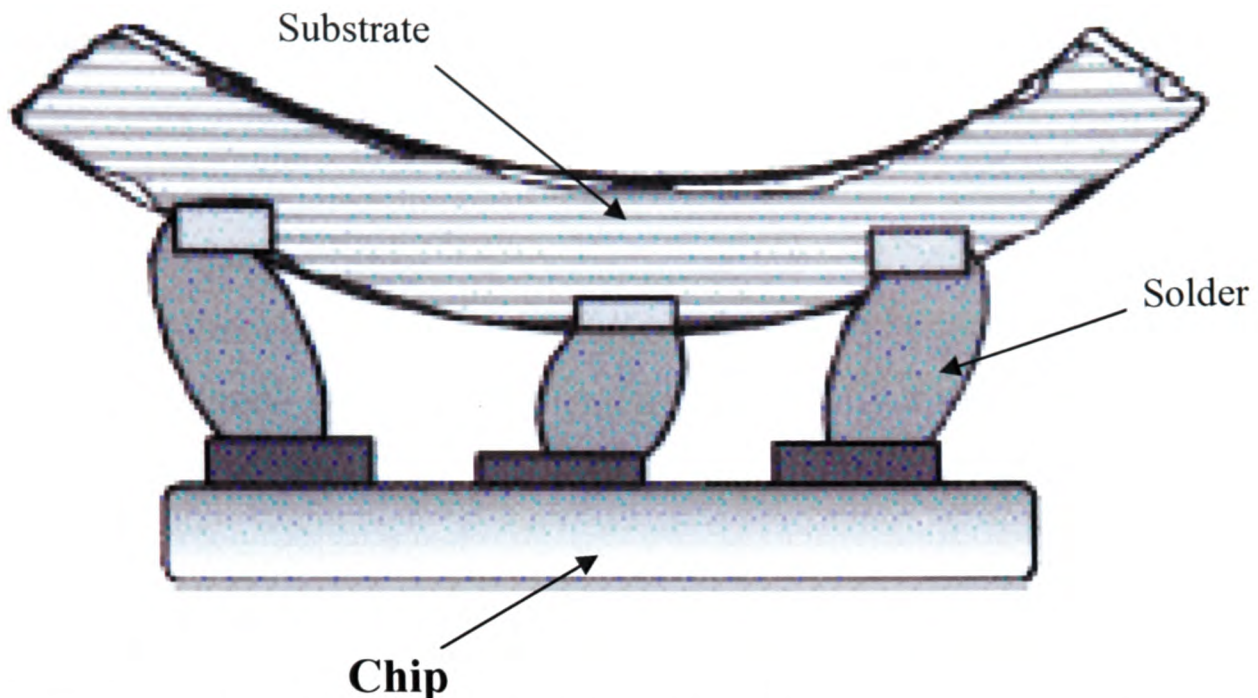


Figure 5-53: Deformed solder joint under mechanical loading [46].

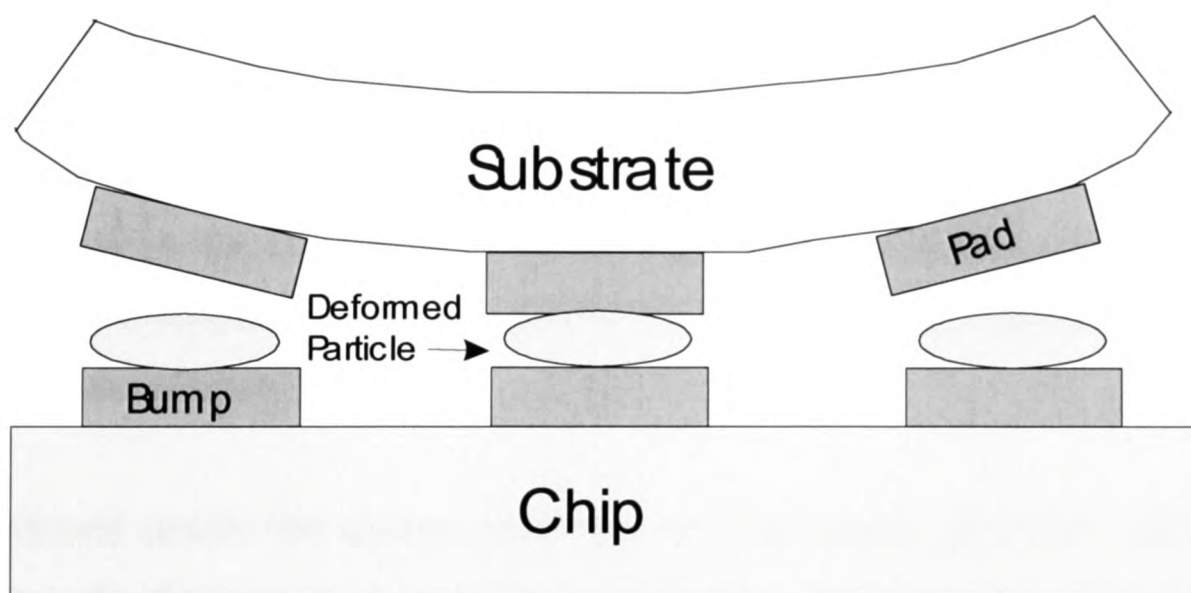


Figure 5-54: Deformed ACF joint under mechanical loading.

The modelling result shown in Figure 5-51 reveals that by applying only a 10 N load, the ACF thickness can be increased as high as 1.7 μm . Therefore, the corner joint of the package considered in this study is expected to experience electrical discontinuity even if there is no delamination at the ACF-chip or ACF/substrate interface. Figure 5-54 shows schematically the phenomenon of the disconnection of the conductive particles at the

Chapter-5: Study of Interconnections formed with Anisotropic Conductive Films

edge of the flip chip assembly. From Figure 5-51, it is also observed that the ACF thickness at the corner is increasing with the increase of the loads. For a particular load, the expansion of the ACF decreases towards the middle of the joint. However, with the increase of loads, the inner joints adjacent to the corner may also fail.

In order to validate the modelling results, an experiment was carried out as depicted in Figure 5-11. Real-time contact resistance under the bending condition was measured with the increase in the applied load. The measured average initial contact resistance was 0.07 ohms. During the test, no significant increase in the contact resistance was found until the load reached 17 N and open joints appeared. However, the first open joints were all found at the corners. With the increase in the applied load, successive open joints were detected from the corner to the middle region. This is consistent with the modelling results that corner joints are more susceptible to failure, and an increase in the load leads to the successive failures of the inner joints. Another finding from the experimental work was that after releasing the load, the contact resistance values of most joints changed back to the initial ones. This supports the above explanations that when the flip chip assembly recovers from bending, the mechanical contact of the conductive particles with the pad or with the bump in the ACF joint can be restored. The load level at which open joints appear observed in the experiment is much higher than it has been predicted in the modelling. This discrepancy may be caused by the inaccurate ACF material data and the simplified computer model geometry.

It was explained earlier that contact resistance may increase at the initial stage of the loading due to the decrease in contact area caused by the elastic recovery of the deformed particles. However, in the experiment, no gradual increase in the contact resistance was detected. Open joints seemed to appear suddenly. One of the possible reasons of this is that the predicted elastic recovery of the conductive particles is not possible for this particular ACF that was used for this study. Elastic recovery of a conductive particle depends on the mechanical properties of the polymeric core of the conductive particles. Thus, if the conductive particles do not expand significantly and the elliptical shapes are kept, even a slight increase in the ACF thickness will make the ACF joint to open. This is

probably why we detected open joints without the gradual increase in the contact resistance. Because the particles did not change their shape, after the bending load was removed and the mechanical contacts were restored, the contact resistance reverted to the initial value. If the real-time contact resistance had increased during the bending test, the value of the contact resistance after the test would have been shifted from its original value. During the test, there must be gaps between the conductive particles and the bump and/or the pad. However, these gaps are difficult to visualize using the normal cross-sectioning technique because this would need the same 3-point bend test fixture during cutting and molding of the sample. As shown in Figure 5-15, cross-sectioning the sample before and after the test the structures look the same.

5.5 Closure

A series of experiments and computer modelling simulations have been carried out to investigate the performance and the behaviour of ACF interconnections under thermal and mechanical loads. Based on the results the following conclusive remarks can be made.

1. Both the computer modelling and the experimental results have demonstrated that the temperature in an ACF joint becomes very close to the required maximum bonding temperature within the first 1 s of bonding time. The higher the bonding temperature the faster the ramp up of temperature is.
2. Dynamic mechanical analysis (DMA) on the ACF samples has revealed that the glass transition temperature of the ACF increases with the increase of bonding time. Rapid changes occur in the physical properties of ACF at temperatures above the glass transition point. When the ACF is cured for a long time at a high temperature, the physical properties may degrade.
3. Differential scanning calorimetric (DSC) studies show that the higher the bonding temperature the more the curing degree of ACF is.
4. The adhesion strength of ACF joint increases as the curing degree increases. However, when the ACF joint undergoes a thermal aging treatment, the adhesion strength increases for the samples bonded at lower temperatures, but decreases for

the samples bonded at higher temperatures. The rate of increase in the contact resistance is dramatically higher for the samples bonded at lower temperatures than for those bonded at higher temperatures. The higher the environment temperature the more severe the electrical failure of the ACF joints is.

5. Computer modelling of the isothermal ageing of ACF joint confirms that the adhesive squeezes conductive particle. This may result in the permanent damage of the outermost conductive metallic layers. Modelling results also show that the magnitudes of the stresses accumulated at the edge of the particle-pad interface where adhesive matrix meets the particle are high. These high stresses could lead to delamination of the interface. As a consequence, the conductive particle could be detached from the pad and from the adhesive matrix and therefore a conduction gap could be generated. These are the possible causes of the increase of the contact resistance of ACF joint during isothermal ageing.
6. Computer modelling of the 3-point bending tests of an ACF-based flip chip assembly reveals that with external mechanical loading, ACF thickness increases at the corners of the chip-ACF joint more than that of the middle position. This causes a gap between the chip and the substrate results in the failure of the mechanical contact among the bump, the conductive particle and the pad. The modelling results predict that by applying only a 10 N load, the ACF thickness can be increased as high as 1.7 μm . Therefore, the corner position of the ACF joint is expected to experience electrical discontinuity even if there is no delamination at the ACF-chip or ACF/substrate interface. Experimentally measured real-time contact resistances during the bending test validate the modelling predictions as the first open joint appears at the corner and proceeds toward the inner joints with the increasing applied load.

Chapter 6

Results Summary and Future Work

6.1 Results Summary

The demands for the miniaturization of the electronic products together with the environmental concerns have led to a tremendous efforts in the industry and the academia to find suitable green interconnect materials that can meet these demands. Lead-free solders have been used for decades without clear understanding of their physical, metallurgical and mechanical properties. As it was discussed in the Chapter 1, poor wettabilities, high consumption of base metallization and high growth rates of the intermetallic compounds (IMCs) at the reactive interfaces are the barriers for the use of lead-free solders in some fields of the electronic packaging. Another interconnection material that is used in the electronic packaging industries is ACF. This material has been used in the cases where the use of solders is not suitable. However, it has some unresolved reliability issues. The electronic products that are assembled using ACFs can only be used in certain conditions because ACFs are highly sensitive to changes in

temperature and humidity level. The purpose of this work is to study the factors that influence the formation of solder and ACF based electronic packaging interconnections and the factors that affect the mechanical and/or electrical reliabilities of these interconnections.

The work on the solder interconnection formation confirms that none of the lead-free solders (SnAgCu, SnAgCuBi, SnCu and SnCuNi) possesses better wettability than that of the conventional SnPb solder. However, the wettability can be improved slightly when a small amount of Bi is added to the SnAgCu and Ni is added to the SnCu lead-free solders. The wettability is highly dependent on the soldering temperature, the type of the flux used and the surface property on which solder wets. An analysis on the microstructures of the wetting interface show that the higher the soldering temperature the faster the consumption of the metallization is. When the reaction temperature is constant, the longer the reaction time the thicker the IMC layer is.

The work on the ACF interconnection formation and reliability shows that the higher the bonding temperature the better the curing of the ACF and the stronger the adhesion strength is. It should be noted that when the ACF is cured for a long time at a high temperature, the physical properties of the ACF may degrade. When an ACF interconnection based electronic product is used in a high temperature environment or is subjected to external bending load, the electrical reliability degrades as the contact resistance increases.

Detailed results and findings of this work have been discussed elaborately in several sections of the Chapter 4 and the Chapter 5. The following is a summary of what have been found about the properties of the two types of electronic packaging interconnections.

6.1.1 Study of Interconnections formed with Lead-free Solder Alloys

The wetting balance tests have been described in Section 4.4.1 for Cu and Ni substrates with NC (no-clean), R (non-activated) and WS (water-soluble) fluxes at 255, 275 and 295 °C to assess the wetting behaviours of Sn-2.8Ag-0.5Cu-1.0Bi, Sn-2.8Ag-0.5Cu, Sn-0.7Cu and Sn-0.7Cu-0.3Ni lead-free solders as well as Sn-37Pb solder. Both the experimental and the modelling results have shown very good agreement. In general, the wettabilities of the lead-free solders are less than that of the SnPb solder. However, adding Bi into the SnAgCu solder and Ni into the SnCu solder can improve the wettability. By increasing the temperature, the contact angle decreases as the thermally induced changes to the molecular structures of flux lower the value of the surface tension γ_{LF} and improves the oxide removal capacity of the flux. The type of flux also plays an important role in solder wettability. For example, the newly developed Sn-2.8Ag-0.5Cu-1.0Bi and Sn-0.7Cu-0.3Ni solders are wettable on Cu and Ni substrates but the wettabilities are strongly dependent on the type of the flux. It has been documented that overall NC-flux is suitable for Cu-substrates whereas WS-flux is suitable for Ni substrates except for Sn-2.8Ag-0.5Cu solder which showed better wettability on Ni substrate with both NC and R-type fluxes. NC-flux possesses the lowest solder-flux surface tension value (370mN/m) among the three fluxes and it has the best wetting performance on Cu substrate. The high fluxing activity of WS-flux provides adequate wetting for Ni substrate. The wettability of Sn-2.8Ag-0.5Cu-1.0Bi solder was found to be slightly higher than that of the SnPb solder at 295 °C when WS flux was used. Non-wetting for both lead and lead-free solders occurred for solders on Ni substrate when R-flux was used. It was thought that this type of flux had resulted in low values of $\gamma_{SF} - \gamma_{SL}$, high contact angles and negative wetting forces. Computer modelling of the wetting balance tests reveal that larger substrate perimeters and smaller immersion depths increase the total wetting force. Contact angle values also have significant effects on the wetting force and the meniscus height. It was also found that an increase in the depth and the radius of the solder bath had no significant effect on the wetting force.

As it has been discussed in Section 4.4.2, higher bath temperature increases the dissolution rate of Cu and Ni in molten solders and also increases the IMC layer thickness at the solder-substrate interface. The consumption of substrate metal and the growth rate of IMCs in the Sn-2.8Ag-0.5Cu solder is a more serious problem than in the Sn-2.8Ag-0.5Cu-1.0Bi solder. Sn-0.7Cu solder dissolves more Cu and Ni in comparison with the Sn-0.7Cu-0.3Ni solder and the former solder also has thicker IMC layer than the latter. All the lead-free solders exhibit a higher consumption rate and a faster dissolution of the substrate compared to the conventional SnPb solder. The computer modelling of the dissolution of the Cu substrate into molten solders predicts the concentration distribution (wt%) of Cu in solders. The analysis also shows that the diffusion of Cu from the substrate is higher in the lead-free solder than in the SnPb solder. An EDX analysis has shown that the predicted copper concentration in solders agrees well with the experimentally measured values.

IMC formation in the Sn-2.8Ag-0.5Cu solder alloy with an additional 1wt% Bi has been investigated for Cu and Ni-substrates during the soldering at 255, 275 and 295 °C. The results are presented in 4.4.2. In Section 4.4.3 the study of the IMCs growth during thermal aging at 150 °C on Cu substrate is discussed. It has been found that immediately after the soldering reaction the IMC layer thickness is comparatively higher for Sn-2.8Ag-0.5Cu solder than that for the Sn-2.8Ag-0.5Cu-1.0Bi solder. For both solders, Cu_6Sn_5 and $(\text{Cu}_{1-x}\text{Ni}_x)_6\text{Sn}_5$ IMCs form with Cu and Ni substrates respectively. The thicknesses of the IMC layers at the interfaces and the grain sizes of those IMCs in the bulk of the solders increase with the aging time due to the continuous diffusions of the substrate materials into the solders. Since the dissolution of Ni into the solders are low compared to that of Cu (Figures 4-21, 4-22, 4-23), the growth rate of the IMC layer on Ni is also less compared to that on Cu. It has been found that an addition of 1wt% Bi into the Sn-2.8Ag-0.5Cu solder slows the nucleation rate of Cu_6Sn_5 and Ag_3Sn IMCs in the solder matrix as well as in the solder-substrate interface during the isothermal aging. A significant increase in the IMC layer thickness during the isothermal aging is noticed for both solders and the rate of increase is lower for the Bi containing Sn-2.8Ag-0.5Cu solder. After aging for different length of time, relatively rough IMC layer is observed in

Sn-2.8Ag-0.5Cu solder than in the Sn-2.8Ag-0.5Cu-1.0Bi solder. High interfacial reaction rate and high Cu dissolution rate of this Sn-2.8Ag-0.5Cu solder/substrate combination is thought to be the reason of this roughness. The growth rate constant of the IMC layer is calculated for Sn-2.8Ag-0.5Cu solder as $2.21 \times 10^{-17} \text{ m}^2/\text{s}$ whereas the addition of 1wt%Bi into Sn-2.8Ag-0.5Cu solder lowers this value to $1.91 \times 10^{-17} \text{ m}^2/\text{s}$. It can be concluded that a small amount (like 1 wt%) of Bi can be added into the SnAgCu solder to reduce the melting temperature, the growth rate of IMCs and the consumption of Cu.

The effects of adding 0.3wt% Ni into the Sn-0.7Cu solder on the growth of the IMC layer has also been investigated in Section 4.4.2 for wetting and in Sections 4.4.3 for isothermal aging. The growth behaviours of the IMC layers during the wetting on Cu and Ni substrates have been studied at temperatures of 255, 275 and 295 °C. The solid state aging has been performed at 150 °C for the samples soldered with Cu substrate at 255 °C. It has been found that the addition of Ni changes the composition of the IMCs that are formed at the solder-Cu interfaces and also in the bulk of the solder matrix during the wetting reaction. The Cu_6Sn_5 compound has formed in the Sn-0.7Cu solder whereas $(\text{CuNi})_6\text{Sn}_5$ has formed in the Sn-0.7Cu-0.3Ni solder. A very small increase in the growth rate of the IMC layer has been observed with the increase in the soldering temperature. For both solders, $(\text{Cu}_{1-x}\text{Ni}_x)_6\text{Sn}_5$ IMCs have formed with the Ni substrate. The formation of this type of compound may be due to the slow diffusion of Ni from the Ni substrate which had led to the production of the faster reaction species of $(\text{Cu}_{1-x}\text{Ni}_x)_6\text{Sn}_5$ compounds, rather than Ni_3Sn_4 . In this case, the solder matrix itself has supplied both Sn and Cu to react with Ni to form this kind of ternary compound. Over the aging time, the IMC layer thicknesses of both solders increased significantly on the Cu substrate. Compared to the Sn-0.7Cu solder, the Ni-containing solder exhibited lower growth rate of the IMC layer during the wetting and during the first two days of aging. However, the thickness of IMC layer increased dramatically after six days of aging and eventually exceeded the IMC layer thickness of the Sn-0.7Cu/Cu soldering system. A thin layer of Cu_3Sn formed between the Cu_6Sn_5 layer and the Cu substrate after 10 days of aging for the Sn-0.7Cu/Cu soldering system. In this soldering system, the thickness of this Cu_3Sn

IMC layer increased after 14 days of aging. However, this Cu_3Sn layer was totally absent in the Ni containing Sn-0.7Cu solder system. It is believed that the formation of the Cu_3Sn layer is the consequence of the limited supply of Sn at the solder/copper substrate interface through the existing IMC layer. The growth of the IMC layer for both solders is diffusion-controlled. The IMC layer growth rate constants for Sn-0.7Cu and Sn-0.7Cu-0.3Ni solders have been calculated as $1.41 \times 10^{-17} \text{ m}^2/\text{s}$ and $1.89 \times 10^{-17} \text{ m}^2/\text{s}$ respectively. It can be concluded that an addition of 0.3wt% Ni to the Sn-0.7Cu solder slightly decreases the IMC thickness after soldering but it increases the growth rate during aging. The effect of the excessive growth of the IMC layer on the reliability of electronic packaging assembly will be investigated through computer modelling in future work.

6.1.2 Study of Interconnections formed with Anisotropic Conductive Films

The measurement of the temperature in ACF during bonding has been described in Section 5.4.1. Both the computer modelling and the experimental results have revealed that the temperature in the ACF can get very close to the required bonding temperature within the first 1 second of the bonding process. Therefore, ACF gets enough time to be cured properly if the bonding time is long enough. It has also been noticed that the higher the bonding temperature the faster the ramp up of temperature in the ACF is.

A Dynamic Mechanical Analysis (DMA) has been carried out to investigate the nature of the changes of the physical properties of ACF for a range of bonding parameters. The method and results are discussed in Section 5.4.2. ACF samples that are pre-cured at 170, 190 or 210 °C for 3, 5 or 10 seconds have been analyzed using a DMA instrument. The results have revealed that the glass transition temperature of the ACF increases with the increase in the bonding time for the bonding temperatures that have been used in this work. For the curing time of 3 and 5 seconds, the maximum glass transition temperature increases with the increase in the bonding temperature, but for the curing time of 10 seconds the maximum glass transition temperature has been observed in the sample which is cured at 190 °C. Based on these results it has been concluded that the suitable

bonding temperature and time for the ACF-based flip chip mounting process are 190 °C and 10 seconds respectively.

The effects of bonding temperatures on the curing of ACF have been investigated in Section 5.4.3. It has been found that a curing degree of 28% can be achieved with a bonding temperature of 160 °C. In order to achieve a 95% curing degree the bonding temperature has to be increased to 240 °C.

Although higher bonding temperature increases the degree of curing of ACF, the studies in section 5.4.2 have shown that higher temperature may cause a deterioration of the physical properties of ACF. Therefore, a further experimental work has been carried out (see Section 5.4.4) to investigate the effect of the curing degrees on the performance of ACF joints before and after thermal ageing. It has been found that higher bonding temperatures not only provide better curing to the ACF but also help to achieve greater adhesion strength, and help to reduce the rate of increase in the contact resistance during thermal ageing. The adhesion strength before ageing increases as the curing degree increases. After the thermal treatment, the adhesion strength increases for the samples bonded at lower temperatures, but decreases for the samples bonded at higher temperatures. The contact resistance increases for all the thermally aged samples (bonded with different temperatures). The rate of increase in the contact resistance is dramatically higher for the samples bonded at lower temperatures than for those bonded at higher temperatures. The change in the contact resistance is thought to be caused by possible further curing of the adhesives, the mobility of the conductive particles, the formation of conduction gaps between the conductive particles and the bumps/pads, and the thermal mismatch in the joint. Although a higher bonding temperature results in a better ACF curing and better electrical performance after thermal ageing, the adhesion strength decreases unexpectedly when the bonding temperatures are over 200 °C. Therefore, further improvement of the ACF is needed to ensure good electrical and mechanical performance of the ACF devices.

The relations between the curing degree and the aging temperatures have been studied in Section 5.4.5. It has been found that a better cured ACF-joint can prevent the increase in the contact resistance for any ageing temperature. The higher the ageing temperature the higher the electrical failure rate is. The formation of conduction gaps between the conductive particles and the pads and damages to the metal coatings of the particle have been identified as the reasons behind the electrical failures during ageing. In order to understand the mechanism for the formation of the conduction gap and the damage in the metal coatings during the isothermal ageing, computer modelling has been carried out and the results are described in Section 5.4.6. The analysis shows that stresses concentrate at the edges of the particle-pad interface where adhesive matrix meets the particle. This could lead subsequent damages and reductions in the adhesion strength in that region and the conductive particle could be detached from the pad and the adhesive matrix. As a consequence, a conduction gap can appear. Furthermore, under thermal loading the thermal expansion of the adhesive matrix squeezes the conductive particle and damages the metal coatings. It is, therefore, assumed that if an ACF-based electronic component operates in a high temperature aging condition, its electrical and mechanical functionalities will be at risk.

In order to investigate the mechanism of the electrical failures of ACF joints under bending loads, a computer model has been built and analyzed and the results are described in Section 5.4.7. It has been found that under the external bending load, ACF thickness increases at the edges more than at the middle. Because of the higher elastic modulus of the silicon chip, the chip bends much less than ACF and the substrate, and the stresses concentrate at the edges of the ACF-chip joint. There is a possibility that a gap between the chip and the substrate may form and this would damage the mechanical contact between the conductive particle and the bump/pad. Higher bending load would lead to higher number of open joints progressively from the edges to the middle. Experimental measurements of the real-time contact resistance during the bending test also confirm that the first open joint appears at the edge and as load is increased inner joints begin to fail.

6.2 Future work

6.2.1 The Effects of Bonding/Soldering Time

The curing of epoxy polymer based ACF not only depends on the applied temperature but also depends on the duration of the application of the temperature. In order to get a perfect cross-linked polymer structure of the adhesive matrix, enough heat energy should be delivered to the ACF for a sustained period of time. Both the bonding temperature and the bonding time determine whether the ACF is under-cured or over-cured. In this work, the degree of the curing of ACF has been studied for a range of bonding temperatures only. A similar study can be carried out in future for a range of bonding times.

The wetting or the spreading of a solder on a metal surface, the metallurgical reactions and the solder joint integrity to some extent depends on the dwell time at the peak reflow temperature. The growth of an IMC layer depends on the soldering temperature and reaction time. The thickness of an IMC layer is expected to increase with the temperature and soldering time. In this work, the wetting behaviour of solders during a fixed time of 10 seconds has been studied. An extended wetting balance test can be performed in future to study the effect of the soldering time.

6.2.2 The Effects of the Surface Roughness

In the process of ACF interconnection formation, ACF melts and flows as a viscous fluid with the application of the bonding temperature. The flow of the molten ACF distributes the conductive particles in the gaps between the chip and the substrate. There are several factors such as the surface roughness of the substrate and the chip, the number and size of the bumps and the pads and their surface roughness all influence the even distribution of the conductive particles. In the process of solder joint formation, the surface roughness of the soldering areas can play a great role on the spreading of the solder alloys [189]. Good

wetting of the molten solder on a metal surface improves the solder joint integrity. Further study can be carried out in the future to measure the surface roughness of the substrate and its effect on the spreading of ACF and solder.

6.2.3 Prediction of the Fatigue Life of ACF/Solder Joints under Thermal Loads

When a flip chip assembly is exposed to cyclic thermal loading, cyclic stress and strain develops in the joints due to the CTE mismatch of the materials in the flip chip assembly. Over time, cracks will initiate and propagate along the bond-line. In recent years there has been lots of research work on the fatigue crack growth in solder joints but the effect of IMCs is not well understood yet. For ACF joints, not much work has been carried out on the fatigue yet. These problems can be dealt with in future work using computer modelling and experimental techniques.

6.2.4 Numerical Modelling of the Growth Kinetics of IMC Layers

During the wetting reaction of a solder with a metallic substrate, IMC layers form at the interfaces. It is believed that the diffusion of metal atoms is responsible for the formation of that IMC layer. This diffusion process is a continuous process at any temperature but it is most prominent when the temperature is high. The IMCs formation plays a very important role in solder joint reliability. In future research work, the growth of the IMC layer thickness over time should be studied.

Publications

International peer reviewed **JOURNAL** articles published from this PhD work:

1. "Study of anisotropic conductive adhesive joint behavior under 3-point bending", **M.J. Rizvi**, Y.C. Chan, C. Bailey & H. Lu, *Microelectronics Reliability*, vol. 45, no. 3-4, 2005, pp 589-596.
2. "The effect of curing on the performance of ACF bonded chip-on-flex assemblies after thermal ageing", **M.J. Rizvi**, Y.C. Chan, C. Bailey, H. Lu & A. Sharif, *Soldering & Surface Mount Technology Journal*, vol. 17, no.2, 2005, pp. 40-48.
3. "Wetting and reaction of Sn-2.8Ag-0.5Cu-1.0Bi solder with Cu and Ni substrates", **M.J. Rizvi**, Y.C. Chan, C. Bailey, H. Lu, M.N. Islam & B.Y.Wu, *Journal of Electronic Materials*, vol. 34, no. 8, 2005, pp. 1115-1122.
4. "Effect of adding 1wt% Bi into the Sn-2.8Ag-0.5Cu solder alloy on the intermetallic formations with Cu-substrate during soldering and isothermal aging", **M.J. Rizvi**, Y.C. Chan, C. Bailey, H. Lu and M.N. Islam, *Journal of Alloys and Compounds*, vol. 407, no. 1-2, 2006, pp. 208-214.
5. "Effect of adding 0.3wt% Ni into the Sn-0.7wt%Cu solder-Part I: Wetting Behavior on Cu and Ni substrates", **M.J. Rizvi**, C. Bailey, Y.C. Chan & H. Lu, *Journal of Alloys and Compounds*, vol. 438, no. 1-2, 2007, pp. 116-121.

6. "Effect of adding 0.3 wt% Ni into the Sn-0.7wt%Cu solder-Part II: Growth of intermetallic layer with Cu during wetting and aging", **M.J. Rizvi**, C. Bailey, Y.C. Chan, M.N. Islam & H. Lu, Journal of Alloys and Compounds, vol. 438, no. 1-2, 2007, pp. 122-128.
7. "Role of bonding time and temperature on the physical properties of coupled anisotropic conductive-nonconductive adhesive film for flip chip on glass technology", **M.J. Rizvi**, H. Lu, C. Bailey, Y.C. Chan, M.Y. Lee & C.H. Pang, Microelectronic Engineering, vol. 85, no. 1, 2008, pp. 238-244.

International peer reviewed **CONFERENCE** article published from this PhD work:

8. "Comparative wetting behavior of Sn-0.7Cu and Sn-0.7Cu-0.3Ni solders on Cu and Ni substrates", **M.J. Rizvi**, C. Bailey, Y.C. Chan & H. Lu, 1st Electronics System Integration Technology Conference (ESTC), Dresden, Germany, September 5th -7th, 2006, pp. 145-151.

International peer reviewed **JOURNAL** and **CONFERENCE** articles published during this PhD candidature:

9. "Dissolution of electroless Ni metallization by lead-free solder alloys", A. Sharif, Y.C. Chan, M.N. Islam & **M.J. Rizvi**, Journal of Alloys and compounds, vol. 388, no. 1, 2005, pp 75-82.
10. "Effect of 9 wt% in addition to Sn3.5Ag0.5Cu solder on the interfacial reaction with the Au/NiP metallization on Cu pads, M.N. Islam, Y.C. Chan, A. Sharif & **M.J. Rizvi**, Journal of Alloys and compounds, vol. 396, no. 1-2, 2005, pp. 217-223.
11. "Investigations of interfacial reactions of Sn-Zn based and Sn-Ag-Cu lead-free solder alloys as replacement for Sn-Pb solder", M.N. Islam, Y.C. Chan, **M.J. Rizvi** & W. Jillek, Journal of Alloys and compounds, vol. 400, no. 1-2, 2005, pp. 136-144.
12. "Effects of thermal cycling profiles on the performance of Chip-on-Flex assembly using anisotropic conductive films", **M.J. Rizvi**, C. Bailey, Y.C. Chan & H. Lu, Proceedings of the tenth Intersociety Conference on Thermal and Thermomechanical Phenomena in Electronic Systems, (ITherm 2006), Sheraton San Diego Hotel and Marina, San Diego, CA, USA, May30-June 2, 2006, pp. 855-860.

13. "Modeling the effect of lead-free soldering on flexible substrate", **M.J. Rizvi**, C.Y. Yin and C. Bailey, Proceedings of 8th International Conference on Electronic Materials and Packaging, Hong Kong, China, 11-14 December, 2006, pp. 653-657.
14. "Performance and reliability of flexible substrates when subjected to lead-free processing", **M.J. Rizvi**, C.Y. Yin, C. Bailey and H. Lu, 16th European Microelectronics and Packaging Conference (EMPC-2007), Oulu, Finland, 17-20 June, 2007, pp.
15. "Thermal-mechanical analysis of flexible substrates during lead-free solder reflow", C.Y. Yin, **M.J. Rizvi**, H. Lu & C. Bailey, 1st Electronics System Integration Technology Conference (ESTC), Dresden, Germany, September 5th -7th, 2006, pp. 1007-1011.
16. "Application of modelling for predicting the behavior of polymers and adhesives in microelectronic and photonic devices", C. Bailey, **M.J. Rizvi**, C. Yin, H. Lu and S. Stoyanov, 6th International IEEE Conference on Polymers and Adhesives in Microelectronics and Photonics, Miraikan, Odaiba-Tokyo, Japan, January 15-18, 2007, pp. 240-244.
17. "Modelling the reliability of components on flexible substrates", **J. Rizvi**, C. Yin, C. Bailey & H. Lu, Proceedings of ASME/Pacific Rim Technical Conference and Exhibition on Packaging and Integration of Electronic and Photonic Systems, MEMS, and NEMS, InterPACK'07, Westin Bayshore Resort and Marina, Vancouver, BC, Canada, July 8-12, 2007, pp.1-6.

Bibliography

- [1] J.H. Lau, “Low cost flip chip technologies for DCA, WLCSP and PBGA assemblies”, McGraw-Hill, New York, pp. 2.
- [2] C.A. Harper, “Electronic Packaging & Interconnection Handbook”, McGraw-Hill, New York, 2nd edition, 1997, pp. xi.
- [3] <http://www.prc.gatech.edu/academics/elpkg/pdf/module1.pdf#search='electronic%20packaging'>
- [4] <http://www.eleceng.adelaide.edu.au/Personal/alsarawi/node4.html>
- [5] F.N. Sinnadurai, “Handbook of microelectronics packaging and interconnection technologies”, Electrochemical Publications, Scotland, 1985, pp. 1-3.
- [6] J.H. Lau and Y.H. Pau, “Solder joint reliability of BGA, CSP, Flip Chip, and Fine Pitch SMT assemblies”, McGraw-Hill, New York, 1997, pp. 4.
- [7] <http://extra.ivf.se/ngl/>
- [8] http://ap.pennnet.com/Articles/Article_Display.cfm?Section=Archives&Subsection=Display&ARTICLE_ID=207746
- [9] http://www.lsilogic.com/files/docs/marketing_docs/asic/wafer-level-packaging_pb.pdf#search='Wafer%20Level%20Packaging'

- [10] http://www.spil.com.tw/products/?u=1*2
- [11] J.W. Jang, D.R. Frear, T.Y. Lee and K.N. Tu, Morphology of interfacial reaction between lead-free solders and electroless Ni-P under bump metallization, *Journal of Applied Physics*, vol. 88, 2000, pp.6359-6363.
- [12] Y. Ding, C.Q. Wang, L.M. Yu and B.H. Sur, Aging effects on fracture behavior of 63Sn37Pb eutectic solder during tensile tests under the SEM, *Materials Science and Engineering A*, vol. 384, no. 1-2, 2004, pp. 314-323.
- [13] D. Li, C.Q. Liu and P.P. Conway, Characteristics of intermetallics and micromechanical properties during thermal ageing Sn-Ag-Cu flip chip solder interconnects, *Materials Science and Engineering A*, vol. 391, no.1-2, 2005, pp.95-103.
- [14] S. Wiese, F. Feustel and E. Meusel, Characterisation of constitutive behaviour of SnAg, SnAgCu and SnPb solders in flip chip joint, *Sensors and Actuators A*, vol. 99, no. 1-2, 2002, pp.188-193.
- [15] S.W. Yoon, W.K. Choi and H.M. Lee, Interfacial reaction between Sn-1Bi-5In-9Zn solder and Cu substrate, *Scripta Materialia*, vol. 40, no. 3, 1999, pp.327-332.
- [16] http://www.hc-sc.gc.ca/iyh-vsv/environ/lead-plomb_e.html
- [17] <http://sis.nlm.nih.gov/enviro/lead.html>
- [18] <http://www.pb-free.info/>
- [19] http://www.smta.org/files/SMTAI04_opening_ceremony_leadfree.pdf#search='Solder%20Trends%20and%20Leadfree%20Soldering%20Issues
- [20] http://www.fu.sav.sk/rq/projects/elfnet/docs/ELFNET_STATUS_REPORT_2004.PDF#search='Problems%20for%20leadfree%20implementation
- [21] D.A. Fazekas, 11th Annual Electronics Manufacturing Seminar Proc. China Lake, CA, NWC TP 6789, pp. 75-85.
- [22] J.W. Kim and S.B. Jung, Effect of bonding force on the reliability of the flip chip packages employing anisotropic conductive film with reflow process, *Mat. Sci. & Engg. A*, vol. 452-453, 2007, pp. 267-272.
- [23] Y.C. Lin, X. Chen, H.J. Zhang and Z.P. Wang, Effects of hygrothermal aging on epoxy-based anisotropic conductive film, *Materials Letters*, vol. 60, no. 24, 2006, pp. 2958-2963.
- [24] M.J. Rizvi, Y.C. Chan, C. Bailey & H. Lu, Study of anisotropic conductive

- adhesive joint behavior under 3-point bending, *Microelectronics Reliability*, vol. 45, no. 3-4, 2005, pp 589-596.
- [25] M.J. Rizvi, Y.C. Chan, C. Bailey, H. Lu & A. Sharif, The effect of curing on the performance of ACF bonded chip-on-flex assemblies after thermal ageing, *Soldering & Surface Mount Technology Journal*, vol. 17, no.2, 2005, pp. 40-48.
- [26] M.J. Rizvi, Y.C. Chan, C. Bailey, H. Lu, M.N. Islam & B.Y.Wu, Wetting and reaction of Sn-2.8Ag-0.5Cu-1.0Bi solder with Cu and Ni substrates, *Journal of Electronic Materials*, vol. 34, no. 8, 2005, pp. 1115-1122.
- [27] M.J. Rizvi, Y.C. Chan, C. Bailey, H. Lu and M.N. Islam, Effect of adding 1wt% Bi into the Sn-2.8Ag-0.5Cu solder alloy on the intermetallic formations with Cu-substrate during soldering and isothermal aging, *Journal of Alloys and Compounds*, vol. 407, no. 1-2, 2006, pp. 208-214.
- [28] M.J. Rizvi, C. Bailey, Y.C. Chan & H. Lu, Effect of adding 0.3wt% Ni into the Sn-0.7wt%Cu solder-Part I: Wetting Behavior on Cu and Ni substrates, *Journal of Alloys and Compounds*, vol. 438, no. 1-2, 2007, pp. 116-121.
- [29] M.J. Rizvi, C. Bailey, Y.C. Chan, M.N. Islam & H. Lu, Effect of adding 0.3 wt% Ni into the Sn-0.7wt%Cu solder-Part II: Growth of intermetallic layer with Cu during wetting and aging, *Journal of Alloys and Compounds*, vol. 438, no. 1-2, 2007, pp. 122-128.
- [30] M.J. Rizvi, H. Lu, C. Bailey, Y.C. Chan, M.Y. Lee & C.H. Pang, Role of bonding time and temperature on the physical properties of coupled anisotropic conductive-nonconductive adhesive film for flip chip on glass technology, *Microelectronic Engineering*, Article in Press.
- [31] M.J. Rizvi, C. Bailey, Y.C. Chan & H. Lu, Comparative wetting behavior of Sn-0.7Cu and Sn-0.7Cu-0.3Ni solders on Cu and Ni substrates, *Proceedings of 1st Electronics System Integration Technology Conference (ESTC)*, Dresden, Germany, September 5th -7th, 2006, pp. 145-151.
- [32] C. A. Harper, "Electronic materials and processes handbook", 3rd Ed. McGraw-Hill, New York, 2003.
- [33] http://www.matrixusa.us/Technical/tech%20Lead%20Free%20Solder_Chris%20Carabello.pdf
- [34] J. Bath, C. Handwerker and E. Bradley, Research update: Lead-free solder alternatives, *Circuits Assembly*, May, 2000, pp. 31-40.
- [35] ANSI/IPC-T-50E Standard, 1992, "Terms and definitions for interconnecting and packaging electronic circuits", Institute for Interconnecting and Packaging
-

Electronic Circuits.

- [36] R. J. K. Wassink, "Soldering in Electronics", Electrochemical Publications Ltd., 2nd ed., 1989.
- [37] D. Frear, H. Morgan, S. Burchett and J. Lau, "The mechanics of solder alloy interconnects", Chapman & Hall, ITP International Thomson Publishing, New York, 1994.
- [38] F. G. Yost, F. M. Hosking and D. R. Frear, "The mechanics of solder alloy wetting and spreading", Van Nostrand Reinhold, New York, 1993.
- [39] D. R. Kitchen, Physics of die attach interfaces, 18th annual proceedings of reliability physics, 1980, pp. 312-317.
- [40] E. Herr, T Frey, R. Schlegel, A. Stuck and R. Zehringer, Substrate to base solder joint reliability in high power IGBT modules, *Microelectronics and Reliability* 37 (10/11), 1997, pp. 1719-1722.
- [41] L. Chiampolini, M. Ciappa, P. Malberti, P. Regli and W. Fichtner, Modelling thermal effects of large contiguous voids in solder joints, *Microelectronics Journal*, 30, 1999, pp. 1115-1123.
- [42] Z. Tang and F. G. Shi, Effects of pre-existing voids on electromigration failure of flip chip solder bumps, *Microelectronics Journal*, 32, 2001, pp. 605-613.
- [43] Y. H. Lin, Y. C. Hu, C. M. Tsai, C. R. Kao and K. N. Tu, In situ observation of the void formation-and-propagation mechanism in solder joints under current-stressing, *Acta Materialia*, vol. 53, 2005, pp. 2029-2035.
- [44] M. Yunus, K. Srihari, J. M. Pitarresi and A. Primavera, Effect of voids on the reliability of BGA/CSP solder joints, *Microelectronics Reliability*, vol. 43, 2003, pp. 2077-2086.
- [45] D. S. Kim, Q. Yu and T. Shibutani, Effect of void formation on thermal fatigue reliability of lead-free solder joints, *Proc. of IEEE Inter Society Conference on Thermal Phenomena*, 2004, pp. 325-329.
- [46] W. Casey, Reduction of voiding in eutectic ball grid array solder joints, *Soldering and Surface Mount Technology*, vol. 11, no. 2, 1999, pp. 12-16.
- [47] J. Liu, "Conductive adhesives for electronics packaging", Electrochemical Publications Ltd, London, 1999.
- [48] D. Wojciechowski, J. Vanfleteren, E. Reese and H-W. Hagedorn, Electroconductive adhesives for high density package and flip chip

- interconnections, *Microelectronics Reliability*, vol. 40, 2000, pp. 1215-1226.
- [49] M. Mundlein and J. Nicolics, Electrical resistance modelling of isotropically conductive adhesive joints, *Proc. of 28th IEEE Int. Spring Seminar on Electronics Technology*, 2005, pp. 128-133.
- [50] W.S. Kwon, K.W. Jang, K.W. Paik, M.J. Yim and J. S. Hwang, High reliable non- conductive adhesives for flip chip Interconnections, *Proc. of IEEE Int. Symposium on Electronic Materials and Packaging*, 2001, pp. 34-38.
- [51] L. Li and J. E. Morris, Curing of isotropic electrically conductive adhesives, *Conductive adhesives for electronics packaging* edited by J. Liu, Electrochemical Publications Ltd, London, 1999.
- [52] http://www.sciencedaily.com/encyclopedia/Computer_simulation/
- [53] W Jung, J. H. Lau, and Y. H. Pao, Non-linear analysis of full-matrix and perimeter-arrayed plastic ball grid array solder joints, ASME paper, ASME Winter Annual Meeting, November, 1966. *Cross reference*: J. H. Lau and Y. H. Pao, "Solder joint reliability of BGA, CSP, Flip Chip, and fine Pitch SMT Assemblies", *Electronic Packaging and Interconnection Series*, McGraw-Hill, New York, 1997.
- [54] P. M. Hall, Force, moments and displacements during thermal chamber cycling of leadless ceramic chip carriers surface mounted to printed wiring boards, *IEEE Trans. Comp. Hybrids. Manuf. Technol.*, vol. 7, no. 4, 1984, pp. 314-327.
- [55] J. S. Corbin, Finite element analysis of solder ball connect structural design optimization, *IBM Journal of Research and Development*, vol. 37, 1993, pp.585-596.
- [56] M. P. Rodriguez and N. Y. A. Shamma, Finite element simulation of thermal fatigue in multilayer structures: thermal and mechanical approach, *Microelectronics Reliability*, vol. 41, 2001, pp. 517-523.
- [57] J. T. Mottram and C. T. Shaw, "Using Finite Elements in Mechanical Design, McGraw-Hill, London, 1996.
- [58] G. Dhatt and G. Touzot, "The finite element method displayed", John Wiley and Sons, Chichester, 1984.
- [59] <http://www.ansys.com/>
- [60] <http://www.abaqus.com/>
- [61] <http://www.algor.com/>

- [62] <http://www.mscsoftware.com/products/marc.cfm>
- [63] <http://www.mscsoftware.com/>
- [64] <http://www.femlab.com/>
- [65] <http://www.flomerics.com/flotherm/>
- [66] <http://www.fluent.com/software/index.htm>
- [67] <http://www.susqu.edu/facstaff/b/brakke/evolver/>
- [68] PHYSICA, <http://www.gre.ac.uk/~physica>
- [69] N.N. Ekere and E.K. Lo, New challenges in solder paste printing, *Journal of Electronics Manufacturing*, vol. 1, no. 1, 1991, pp.29-40.
- [70] S.H. Mannan, N.N. Ekere, I. Ismail and M.A. Currie, Flow processes in solder paste during stencil printing for SMT assembly, *Journal of Mat. Scie: Mats. in Elecs.*, vol. 6, no. 1, 1995, pp.34-42.
- [71] C. Bailey, H. Lu, G. Glinski, D. Wheeler, P. Hamilton, M. Hendriksen and B. Smith, Using computer models to identify optimal conditions for flip chip assembly and reliability, *Soldering and Surface Mount Technology*, vol. 28, no. 1, 2001, pp.14-20.
- [72] D.A. He, N.N. Ekere, B. Salam, D. Rajkumar and G. Jackson, Monte Carlo study of solder paste microstructure and ultra-fine-pitch stencil printing, *Journal of Mat. Scie: Mats. in Elecs.*, vol. 14, 2003, pp.501-506.
- [73] S.H. Mannan, D. Wheeler, D.A. Hutt, D.C. Whalley, P.P. Conway and C. Bailey, Solder paste reflow modeling for flip chip assembly, *Proc. of 3rd Electr. Pack. and Tech. Conf. (EPTC)*, 5-7 Dec., 2000, Sheraton Towers, Singapore, pp.103-109.
- [74] K. Yasuda, H. Akamizu, K. Fujimoto and S. Nakata, Evaluation of wettability for microelectronic materials by reflow mode wetting balance test, *Proc. of IEEE/CPMT Int. Electr. Manu. Tech. Symp.*, 2000, pp. 247-252.
- [75] J.A. Warren, W.J. Boettinger and A.R. Roosen, Modeling reactive wetting, *Acta mater.*, vol. 46, no. 9, 1998, pp.3247-3264.
- [76] K. S. Kim, K. Suganuma, J. M. Kim and C. W. Hwang, The observation and simulation of Sn-Ag-Cu solder solidification in chip scale packaging, *JOM*, vol. 56, no. 6, 2004, pp. 39-43.

- [77] X. Zhang, E. H. Wong, C. Lee, T. C. Chai, Y. Ma, P. S. Teo, D. Pinjala and S. Sampath, Thermo-mechanical finite element analysis in a multichip build up substrate based package design, *Microelectronics Reliability*, vol. 44, 2004, pp. 611-619.
- [78] J.H.L. Pang, D.Y.R. Chong and T.H. Low, Thermal cycling analysis of flip chip solder joint reliability, *IEEE Trans. on Comp. and Pack. Tech.*, vol. 24, no. 4, 2001, pp.705-712.
- [79] K. Hirohata, N. Kawamura, M. Mukai, T. Kawakami, H. Aoki and K. Takahashi, Mechanical fatigue test method for chip/underfill delamination in flip chip packages, *IEEE Trans. on Elec. Pack. Manu.*, vol. 25, no. 3, 2002, pp.217-222.
- [80] Z. Zhong and P.K. Yip, Finite element analysis of a three-dimensional package, *Soldering and Surface Mount Technology*, vol. 15, no. 1, 2003, pp.21-25.
- [81] M.Y. Tsai, W.C. Chiang, T. M. Liu and G. H. Hsu, Thermal deformation measurements and predictions of MAP-BGA electronic packages, *Microelectronics Reliability*, vol. 46, 2006, pp.476-486.
- [82] C.M.L. Wu, J. Liu and N.H. Yeung, The effects of bump height on the reliability of ACF in flip chip, *Soldering and Surface Mount Technology*, vol. 13, no.1, 2001, pp. 25-30.
- [83] M.J. Yim and K.W. Paik, Design and understanding of anisotropic conductive films (ACFs) for LCD packaging, *IEEE Trans. on Comp. Pack. and Manu. Tech.*, vol. 21, no. 2, 1998, pp. 226-234.
- [84] J.W. Kim, W.C. Moon and S.B. Jung, Effects of bonding pressure on the thermo-mechanical reliability of ACF interconnection, *Microelectronic Engineering*, vol. 83, 2006, pp. 2335-2340.
- [85] L.k. Teh, E. Anto, C.C. Wong, S.G. Mhaisalkar, E.H. Wong, P.S. Teo and Z. Chen, Development and reliability of non-conductive adhesive flip-chip packages, *Thin Solid Flms*, vol. 462-463, 2004, pp. 446-453.
- [86] L.H. Su, Y.W. Yen, C.C. Lin and S.W. Chen, Interfacial reactions in molten Sn-Cu and Molten In-Cu couples, *Metallurgical and Materials Transactions B*, vol. 28B, 1997, pp. 927-934.
- [87] J. Glazer, *International Materials Review*, vol. 40, 1996, pp.65.
- [88] S.W. Shin and J. Wu, Creep deformation of Sn-3.5Ag-xCu and Sn-3.5Ag-xBi solder joints, *Journal of Electronic Materials*, vol. 34, 2005, pp.188.
- [89] D. Lewis, S. Allen, M. Notis and A. Scotch, Determination of the eutectic

-
- structure in the Ag-Cu-Sn system, *Journal of Electronic materials*, vol. 31, 2002, pp.161.
- [90] L. Qi, J. Zhao, X.M. Wang and L. Wang, The effect of Bi on the IMC growth in Sn-3Ag-0.5Cu solder interface during aging process, *Proc. of Int. Cnf. on the Business of Electronic Product Reliability and Liability*, April 27-30, 2004, Shanghai, China, pp. 42-46.
- [91] H. Takao and H. Hasegawa, Influence of noble metal coating on wettability of Cu substrate by Sn-Ag eutectic solder, *Materials Transactions*, vol. 45, no.3, 2004, pp.747-753.
- [92] C.M.L. Wu, M.L. Huang, J.K.L. Lai and Y.C. Chan, Developing a lead-free solder alloy Sn-Bi-Ag-Cu by mechanical alloying, *J. of Electron. Mater.*, vol. 29, no. 8, 2000, pp.1015-1020.
- [93] L. Ye, Z. H. Lai, J. Liu and A. Tholen, Microstructure investigation of Sn-0.5Cu-3.5Ag and Sn-3.5Ag-0.5Cu-0.5B lead-free solders, *Soldering & Surface Mount Tech.*, vol.13, no. 3, 2001, pp. 16-20.
- [94] A. Sharif and Y.C. Chan, Dissolution kinetics of BGA Sn-Pb and Sn-Ag solders with Cu substrates during reflow, *Materials Science and Engineering B*, vol. 106, no, 2004, pp. 126-131.
- [95] A. Sharif, Y.C. Chan, M.N. Islam & M.J. Rizvi, Dissolution of electroless Ni metallization by lead-free solder alloys, *J. of Alloys and Compounds*, vol. 388, 2005, pp.75-82.
- [96] J.W. Yoon, C.B. Lee and S.B. Jung, Activation energies of intermetallic compound growth at interface between Sn-5Bi-3.5Ag solder and Cu substrate, *Materials Science and Technology*, vol.19, no.8, 2003, pp.1101-1106.
- [97] J. Zhao, L. Qi, X.M. Wang and L. Wang, Influence of Bi on microstructures evolution and mechanical properties in Sn-Ag-Cu lead-free solders, *J. Alloys and Compounds*, vol. 375, no. 1-2, 2004, pp. 196-201.
- [98] J. Zhao, Y. Mutoh, Y. Miyasuita and S.L. Mannan, Fatigue crack growth behavior of Sn-Ag-Cu and Sn-Ag-Cu-Bi lead-free solders, *J. of Electron. Mater.* vol. 31, no.8, 2002, pp 879-886.
- [99] T.E. Ashram and R.M. Shalaby, Effect of rapid solidification and small additions of Zn and Bi on the structure and properties of Sn-Cu eutectic alloy, *Journal of Electronic Materials*, vol. 34, no. 2, 2005, pp. 212-215.
- [100] C.M.L. Wu, D.Q. Yu, C.M.T. Law and L. Wang, Microstructure and mechanical properties of new lead-free Sn-Cu-Re solder alloys, *Journal of Electronic*
-

- Materials, vol. 31, no. 9, 2002, pp. 928-932.
- [101] C.C. Young, J.G. Duh and S.Y. Tsai, Microstructural evolution in the Sn-Cu-Ni and Pb-sn solder joints with Cu and Pt-Ag metallized Al₂O₃ substrate, *Journal of Electronic Materials*, vol. 30, no. 9, 2001, pp. 1241-1248.
- [102] C.B. Lee, S.B. Jung, Y.E. Shin, C.C. Shur, Effect of isothermal aging on ball shear strength in BGA joints with Sn-3.5Ag-0.75Cu solder, *Mater. Trans.* vol. 43, no.8, 2002, pp. 1858-1863.
- [103] H.K. Kim and K.N. Tu, Rate of consumption of Cu in soldering accompanied by ripening, *Applied Physics Letter*, vol. 67, no. 14, 1995, pp. 2002-2004.
- [104] D. Ma, W.D. Wang, and S.K. Lahiri, Scallop formations and dissolution of Cu-Sn intermetallic compound during solder reflow, *Journal of Applied Physics*, vol. 91, no.5, 2002, pp. 3312-3317.
- [105] V.I. Dybkov and O.V. Duchenko, Growth kinetics of compound layers at the nickel-bismuth interface, *Journal of Alloys and Compounds*, vol. 234, no., 1996, pp. 295-300.
- [106] P.L. Tu, Y.C. Chan, K.C. Hung and J.K.L. Lai, Growth kinetics of intermetallic compounds in chip scale package solder joints, *Scripta Mater.*, vol. 44, 2001, pp.317-323.
- [107] K. Zeng and K.N. Tu, Six cases of reliability study of lead-free solder joints in electronic packaging technology, *Mater. Sci. & Engg. R*, vol. 38, 2002, pp.55-105.
- [108] K.N. Tu, F. Ku and T.Y. Lee, Morphological study of solder reaction products in flip chip technology, *J. Electron. Mater.*, vol. 30, no. 9, 2001, pp.1129-1132.
- [109] J.W. Yoon, Y.H. Lee, D.G. Kim, H.B. Kang, S.J. Suh, C.W. Yang, C.B. Lee, J.M. Jung, C.S. Yoo and S.B. Jung, Intermetallic compound layer growth at the interface between Sn-Cu-Ni solder and Cu substrate, *Journal of Alloys and Compounds*, vol. 381, 2004, pp.151-157.
- [110] J.Y. Tsai, Y.C. Hu, C.M. Tsai and C.R. Kao, A study on the reaction between Cu and Sn3.5Ag solder doped with small amounts of Ni, *Journal of Electronic Materials*, vol. 32, no. 11, 2003, pp. 1203-1208.
- [111] F. Guo, S. Choi, J.P. Lucas and K.N. Subramanian, Microstructural characterization of reflowed and isothermally aged Cu and Ag-particulate reinforced Sn-3.5Ag composite solders, *Soldering and Surface Mount Technology*, vol.13, no.1, 2001, pp. 7-18.

- [112] K.N. Tu, T.Y. Lee, J.W. Jang, L. Li, D.R. Frear, K. Zeng and J.K. Kivilahti, Wetting reaction versus solid state aging of eutectic SnPb on Cu, *Journal of Applied Physics*, vol. 89, no. 9, 2001, pp. 4843-4849.
- [113] J.Y. Park, C.S. Kang and J.P. Jung, The analysis of the withdrawal force curve of the wetting curve using 63Sn-37Pb and 96.5Sn-3.5Ag eutectic solders, *J. of Electron. Mater.*, vol. 28, no. 11, 1999, pp.1256-1262.
- [114] E.P. Lopez, P.T. Vianco and J.A. Rejent, Solderability testing of 95.5Sn-3.9Ag-0.6Cu solder oxygen-free high-conductivity copper and Au-Ni-plated kovar, *J. of Electron. Mater.*, vol. 32, no. 4, 2003, pp. 254-260.
- [115] C.M.L. Wu, C.M.T. Law, D.Q. Yu, and L. Wang, The wettability and microstructure of Sn-Zn-RE alloys, *J. of Electron. Mater.*, vol. 32, no. 2, 2003, pp.63-69.
- [116] A. Tuominen, E. Ristolainen and V. Lehtinen, Qualification of flip chip fluxes by wetting balance and surface insulation resistance tests, *Sold. & Surf. Mount Tech*, vol. 11, no. 1, 1999, pp.21-26.
- [117] P.T. Vianco and A.C. Claghorn, Effect of substrate preheating on solderability performance as a guideline for assembly process development Part-1 Baseline analysis, *Sold. & Surf. Mount Tech*, vol. 8, 1996, pp.12.
- [118] V.I. Dybkov, K. Barmak, W. Lengauer and P.Gas, Interfacial interaction of solid nickel with liquid bismuth and Bi-base alloys, *Journal of Alloys and Compounds*, vol. 389, 2005, pp. 61-74.
- [119] S. Mannan and M.P. Clode, Dissolution of solids in contact with liquid solder, *Soldering and Surface Mount Technology*, vol. 16, no. 3, 2004, pp.31-33.
- [120] K.N. Tu and K. Zeng, Tin-lead (SnPb) solder reaction in flip chip technology, *Materials Science & Engineering R*, vol. 34, 2001, pp.1.
- [121] W.C. Luo, C.E. Ho, J.Y. Tsai, Y.L. Lin and C.R. Kao, Solid state reactions between Ni and SnAgCu solders with different Cu concentrations, *Materials Science & Engineering A*, vol. 396, 2005, pp.385.
- [122] H.T. Lee and M.H. Chen, Influence of intermetallic compounds on the adhesive strength of solder joints, *Materials Science and Engineering A*, vol. 333, no. 1-2, 2002, pp.24- 34.
- [123] S.W. Chen, S.W. Lee and M.C. Yip, Mechanical properties and intermetallic compound formation at the Sn/Ni and Sn-0.7wt%Cu/Ni Joints, *Journal of Electronic Materials*, vol. 32, no. 11, 2003, pp.1284-1289.

-
- [124] M.O. Alam, Y.C. Chan and K.N. Tu, Effect of 0.5wt% Cu addition in Sn-3.5Ag solder on the dissolution rate of Cu metallization, *Journal of Applied Physics*, vol. 94, no. 12, 2003, pp. 7904-7909.
- [125] F. Zhang, M. Li, C.C. Chum, K. N. Tu, Influence of substrate metallization on diffusion and reaction at the under-bump metallization/solder interface in flip chip packages, *Journal of Materials Research*, vol. 17, no. 11, 2002, pp. 2757-2760.
- [126] J.Y. Park, C.W. Yang, J.S. Ha, C.U. Kim, E.J. Kwon, S.B. Jung, C.S. Kang, Investigation of Interfacial Reaction Between Sn-Ag Eutectic Solder and Au/Ni/Cu/Ti Thin Film Metallization, *Journal of Electronic Materials*, vol. 30, no. 9, 2001, pp. 1165-1170.
- [127] C. H. Wang, Masters Thesis, National Tsing Hua University, 2002.
- [128] J.W. Yoon, S.W. Kim and S.B. Jung, Interfacial reaction and mechanical properties of eutectic Sn-0.7Cu/Ni BGA solder joints during isothermal long term aging, *Journal of Alloys and Compounds*, vol. 391, no. 1-2, 2005, pp.82-89.
- [129] J.W. Yoon, S.W. Kim, J.M. Koo, D.G. Kim and S.B. Jung, Reliability investigation and interfacial reaction of ball grid array packages using the lead-free Sn-Cu solder, *Journal of Electronic Materials*, vol. 33, no. 10, 2004, pp. 1190-1199.
- [130] J. Crank, "The mathematics of diffusion", 2nd edition, Oxford University Press, Clarendon Press, Oxford, 1975, pp. 2, 32, 36.
- [131] <http://www.people.virginia.edu/~rej/class209/Chapter5cor3.ppt#14>
- [132] P.G. Shewmon, *Diffusion in Solids*, 2nd edition, TMS AIME, Warrendale, PA (1989), *Cross Reference*: D. Gupta, *Diffusion processes in advanced technological materials*, William Andrew Publishing, Norwich, New York, 2005, pp. 5, 6.
- [133] www.matweb.com
- [134] G. Humpston and D.M. Jacobson, *Principles of soldering and brazing*, ASM International, the Materials Information Society, Materials Park, U.S.A., 1993, pp. 83.
- [135] T.Y. Lee, W.J. Choi and K.N. Tu, Morphology, kinetics and thermodynamics of solid state aging of eutectic SnPb and Pb-free solders (Sn-3.5Ag, Sn-3.8Ag-0.7Cu and Sn-0.7Cu) on Cu, *J. of Mater. Res.*, vol. 17, no. 2, 2002, pp. 291-301.
- [136] D.G. Kim and S.B. Jung, Interfacial reactions and growth kinetics for
-

-
- intermetallic compound layer between In-48Sn solder and bare Cu substrate, *J. of Alloys and Compounds*, vol. 386, no. 1-2, 2005, pp.151-156.
- [137] C.Y. Lee and K.L. Lin, Preparation of solder bumps incorporating electroless nickel-boron deposit and investigation on the interfacial interaction behaviour and wetting kinetics, *J. of Mater. Sci. Mater. Electron.*, vol. 8, no. 6, 1997, pp.377-383.
- [138] P.T. Vianco, A.C. Kilgo and R. Grant, Intermetallic compound layer growth by solid state reactions between 58Bi-42Sn solder and copper, *J. Electronic Materials*, vol. 24, no. 10, 1995, pp.1493-1505.
- [139] C. Chen, C.E. Ho, A.H. Lin, G.L. Luo and C.R. Kao, Long-term aging study on the solid state reaction between 58Bi42Sn solder and Ni substrate, *J. Electron. Mater.*, vol. 29, no. 10, 2000, pp.1200-1206.
- [140] J.W. Yoon, C.B. Lee and S.B. Jung, Interfacial reactions between Sn-58 mass % Bi eutectic solder and (Cu, electroless Ni-P/Cu) substrate, *Materials Trans.*, vol. 43, no. 8, 2002, pp.1821-1826.
- [141] P.T. Vianco and J.A. Rejent, Properties of ternary Sn-Ag-Bi solder alloys: Part I- Thermal properties and microstructural analysis, *J. Electron. Mater.*, vol. 28, no. 10, 1999, pp.1127-1137.
- [142] K. H. Prakash and T. Sritharan, Interface reaction between copper and molten tin-lead solders, *Acta Materiala*, vol. 49, no. 13, 2001, pp. 2481-2489.
- [143] T. Laurila, V. Vuorinen and J.K. Kivilahti, Interfacial reactions between lead-free solders and common base materials, *Materials Science and Engineering R*, vol. 49, no. 1-2, 2005, pp.1-60.
- [144] B.J. Lee, N.M. Hwang and H.M. Lee, Prediction of interface reaction products between Cu and various solder alloys by thermodynamic calculation, *Acta Materiala*, vol. 45, no. 5, 1997, pp. 1867-1874.
- [145] E.K. Ohriner, Intermetallic formation in soldered copper-based alloys at 150 degrees to 250 degrees Celsius, *Welding Journal*, July 1987, pp. 191.
- [146] T.T. Mattila and J.K. Kivilahti, Failure mechanisms of lead-free chip scale package interconnections under fast mechanical loading, *Journal of Electronic Materials*, vol. 34, no. 7, 2005, pp. 969-976.
- [147] W.S. Kwon and K.W. Paik, Fundamental understanding of ACF conduction establishment with emphasis on the thermal and mechanical analysis, *Int. Journal of Adhesion & Adhesives*, vol. 24, no. 2, 2004, pp. 135-142.
-

- [148] J.H. Zhang, Y.C. Chan, Z.M. Zeng and Y.W. Chiu, Research on the interfacial reaction between anisotropic conductive film and bumpless die, IEEE Elec. Comp and Tech. Conf. 2002, pp. 1569-1574.
- [149] K. Pinardi, Z. Lai, D. Vogel, Y.L. Kang, J. Liu, S. Liu, R. Haug and M. Willander, Effect of bump height on the strain variation during the thermal cycling test of ACA flip-chip joints, IEEE Trans. on Comp. and Pack. Tech., vol. 23, no. 3, 2000, pp. 447- 451.
- [150] V.A. Chiriac and T.Y.T. Lee, Transient thermal analysis of an ACF package assembly process, IEEE Trans. on Comp. and Pack. Tech., vol. 24, no. 4, 2001, pp. 673-681.
- [151] G. Sarkar, S. Mridha, T.T. Chong, W.Y. Tuck and S.C. Kwan, Flip chip interconnect using anisotropic conductive adhesive, Journal of Mat. Proc. of Tech., vol. 89-90, 1999, pp. 484-490.
- [152] S.C. Tan, Y.C. Chan and Y.W. Chiu and C.W. Tan, Thermal stability performance of anisotropic conductive film at different bonding temperatures, Microelectronics Reliability, vol. 44, no. 3, 2004, pp. 495-503.
- [153] M.J. Yim, K.W. Paik, T.S. Kim and Y.K. Kim, Anisotropic conductive film interconnection for display packaging applications, Proc. of IEEE Elec. Comp. and Tech. Conf. 1998, pp. 1036-1041.
- [154] I. Watanabe, N. Shiozuka, K. Takemura and T. Ohta, Flip chip interconnection technology using anisotropic conductive adhesive films, Flip Chip Technology, edited by J. H. Lau, McGraw Hill, New York; 1996, pp. 301-305.
- [155] K.M. Kim, J.O. Kim, S.G. Kim, K.H. Lee, A.S. Chen, N. Ahmad, N. Dugbartey, M. Karnezos, S. Tam, Y.D. Kweon and R. Pendse, The viability of anisotropic conductive film (ACF) as a flip chip interconnection technology, Proc. of 50th IEEE Elec. Comp. and Tech. Conf., 21-24 May, 2000, pp.1122-1132.
- [156] S.H. Fan and Y.C. Chan, Effect of misalignment on electrical characteristics of ACF joints for flip chip on flex applications, Microelectronics Reliability, vol. 42, no. 7, 2002, pp. 1081-1090.
- [157] Y. Fu, Y. Wang, X. Wang, J. Liu, Z. Lai, G. Chen and M. Willander, Experimental and theoretical characterization of electrical contact in anisotropically conductive adhesive, IEEE Trans. on Advan. Pack., vol. 23, no.1, 2000, pp. 15-21.
- [158] Y.W. Chiu, Y.C. Chan and S.M. Lui, Study of short-circuiting between adjacent joints under electric field effects in fine pitch anisotropic conductive adhesive interconnects, Microelectronics Reliability, vol. 42, 2002, pp. 1945-1951.

- [159] Y.C. Chan and D.Y. Luk, Effects of bonding parameters on the reliability performance of anisotropic conductive adhesive interconnects for flip-chip-on-flex packages assembly I. Different bonding temperature, *Microelectronics Reliability*, vol. 42, 2002, pp. 1185-1194.
- [160] S.X. Wu, C. Zhang, C.P. Yeh, S. Wille and K. Wyatt, Cure kinetics and mechanical properties of conductive adhesive, *Proc. of IEEE Elec. Comp. and Tech. Conf.*, 1997, pp. 550-553.
- [161] P.L. Tu, Y.C. Chan, K.C. Hung and J.K.L. Lai, Comparative study of micro-BGA reliability under bending stress, *IEEE Trans. on Advan. Pack.*, vol. 23, no. 4, 2000, pp. 750-756.
- [162] F. Yu, W. Sang, E. Pang, D. Liu and J. Teng, Stress analysis in silicon die under different type of mechanical loading by finite element method (FEM), *IEEE Trans. on Advan. Pack.*, vol. 25, no. 4, 2002, pp. 522-527.
- [163] D.T. Hsu, H.K. Kim, F.G. Shi, H.Y. Tong, S. Chungpaiboonpatana, C. Davidson and J.M. Adams, Cure behavior of a no flow underfill encapsulant, *Microelectronics International*, vol. 17, no.1, 2000, pp. 22-26.
- [164] J. Lau, C.P. Wong, J.L. Prince and W. Nakayama, *Electronic packaging design, materials process and reliability*, McGraw-hill, New York, 1998, pp. 448-463.
- [165] ASM Assembly Automation Ltd., Kwai Chung, Hong Kong, China.
- [166] R. Dudek, A. Schubert, S. Meinel and B. Michel, Flow characterization and thermo-mechanical response of anisotropic conductive films, *IEEE Trans. Comp. and Pack. Tech.*, vol. 22, no.2, 1999, pp. 177-185.
- [167] N.H. Yeung, Y.C. Chan and C.W. Tan, Effect of bonding force on the conducting particle with different sizes, *Journal of Electronic Packaging*, vol. 125, no. 4, 2003, pp. 624-629.
- [168] P. Marjamaki, T. Reinikainen and J. Kivilahti, Modeling stresses in ultra-thin flip chips, *Proc. of 4th Int. IEEE Conf. on Adh. Joining and Coating Tech. in Elec. Manu*, 18-21 June, 2000, pp-24-27.
- [169] <http://composite.about.com/library/glossary/n/bldef-n3640.htm>
- [170] <http://www.lasalle.edu/academ/chem/ms/polymersRus/Resources/GlassTrans.htm#glass>
- [171] <http://www.chem.vt.edu/chem-dept/marand/chem4634Lecture15c.pdf>

- [172] F. Lapique and K. Redford, Curing effects on viscosity and mechanical properties of a commercial epoxy resin adhesive, *Int. Journal of Adh. and Adh.*, vol. 22, 2002, pp. 337-346.
- [173] G.A. Matzkanin, Nondestructive characterization of heat damage in graphite/epoxy composite: A state of art report, Texas Research Institute, Austin, available online www.ntiac.com/gamsoar.html.
- [174] E.A. Grulke, "Polymer process engineering", Englewood Cliffs, N.J., PTR Prentice Hall, 1994.
- [175] M.A. Uddin, M.O. Alam, Y.C. Chan and H.P. Chan, Adhesion strength and contact resistance of flip chip on flex packages- effect of curing degree of anisotropic conductive film, *Microelectronics Reliability*, vol. 44, no. 3, 2004, pp. 505-514.
- [176] I. Skeist, "Handbook of adhesives", Van Nostrand Reinhold Company, New York, 2nd edition, 1977, pp. 434.
- [177] E. Bormashenko, R. Pogreb and A. Sheshney, Thermal degradation of thermoplastic and thermosetting polymers induced by laser radiation and its study by FTIR spectroscopy, *Polym Degrad Stab*, vol. 72, 2000; pp. 125-131.
- [178] E.H. Wong, K.C. Chan, R. Rajoo and T.B. Lim, The mechanics and impact of hygroscopic swelling of polymer materials in electronic packaging, *Proc. of 50th Elec. Comp. and Tech. Conf.*, 2000, pp. 576-580.
- [179] Y.C. Chan and D.Y. Luk, Effects of bonding parameters on the reliability performance of anisotropic conductive adhesive interconnects for flip-chip-on-flex packages assembly II. Different bonding pressure, *Microelectronics Reliability*, vol. 42, 2002, pp. 1195-1204.
- [180] C.A. May, "Epoxy Resins", New York, Marcel Dekker Inc., 1988.
- [181] A. Seppala, T. Allinniemi and E. Ristolainen, Failure mechanisms of adhesive flip chip joints, *Microelectronics Reliability*, vol. 42, 2002, pp. 1547-1550.
- [182] C.Y. Yin, M.O. Alam, Y.C. Chan, C. Bailey and H. Lu, The effect of reflow process on the contact resistance and reliability of anisotropic conductive film interconnection for flip chip on flex applications, *Microelectronics Reliability*, vol. 43, 2003, pp. 625.
- [183] J. Maattanen, Contact resistance of metal-coated polymer particles used in anisotropically conductive adhesives, *Soldering and Surface Mount Technology*, vol. 15, no. 1, 2003, pp. 12-15

- [184] M.P. Stevens, *Polymer Chemistry*, Oxford University Press, New York, 1990, pp. 99.
- [185] M.K. Chengalva, Flip chip die cracking-A simplified approach utilizing experimentation and simulations, Proc. of 8th IEEE Intersociety Conf. on Thermal and Thermomechanical Phenomena in Electronic Systems, 30 May-1 June, 2002, pp. 876-883.
- [186] J.H. Constable, T. Kache, H. Teichmann, S. Muhle, M.A. Gaynes, Continuous electrical resistance monitoring, pull strength, and fatigue life of isotropically conductive adhesive joints, *IEEE Trans. Comp. and Pack. Tech.* vol. 22, no.2, 1999, pp. 191-199.
- [187] M. Abtewa and G. Selvaduray, Lead-free solders in microelectronics, Reports: A Review journal, *Materials Science and Engineering*, vol. 27, no. 5-6, 2000, pp. 95-141.
- [188] G.B. Dou, Y.C. Chan and J. Liu, Electrical conductive characteristics of anisotropic conductive adhesive particles, *Journal of Electronic Packaging*, vol. 125, no. 4, 2003, pp. 609-616.
- [189] F.G. Yost, J.R. Michael and E.T. Eisenmann, Extensive wetting due to roughness, *Acta Metall. Mater.*, vol. 43, no. 1, 1995, pp. 299-305.